IDENTIFYING LIFE HISTORY TRAITS IN MODERN AND EXTINCT ARCHOSAURS UTILIZING OSTEOHISTOLOGY

By

CHRISTIAN T. HECK

Bachelor of Arts in Telecommunications
Michigan State University
East Lansing, MI
2008

Bachelor of Science in Ecology
Montana State University
Bozeman, MT
2014

Submitted to the Faculty of the
Graduate College of the
Oklahoma State University
in partial fulfillment of
the requirements for
the Degree of
DOCTOR OF PHILOSOPHY
May, 2022

IDENTIFYING LIFE HISTORY TRAITS IN MODERN AND EXTINCT ARCHOSAURS UTILIZING OSTEOHISTOLOGY

Dissertation Approved:

Dr. Holly Ballard

Dissertation Adviser

Dr. Haley O'Brien

Dr. Tom Curtis

Dr. Jarrad Wagner

ACKNOWLEDGEMENTS

First and foremost I thank my entire family for their support as I changed my career path to one in STEM. Thank you to my parents, Tom and Donna, and my sister Devon for being pillars that I could lean on in times of need.

I thank my advisor, colleague, and most importantly, friend Holly Ballard for always being a guiding light. I cannot count the number of times a simple meeting or game night turned my emotional state completely around. I would not have survived this program if it weren't for your constant support. I thank the members of my graduate committee, Haley O'Brien, Jarrad Wagner, and Tom Curtis for their support and guidance. I thank Haley O'Brien again for making me a better statistician and for further instilling in me a level of self-confidence I lacked before. I thank the entire staff and faculty at Oklahoma State University – Center for Health Sciences, including Nedra Wilson, the late Ken Miller, Paul Gignac, Kent Smith, Anne Weil, Ian Browne for welcoming me into the program and being incredible teachers and mentors.

Thank you to all the wonderful OSU-CHS graduate students who entered my life and changed it for the better, I truly cannot imagine a life without you all in it. Thank you to Leigha Lynch, Todd Green, Amie Francis, Gwyneth Volkmann, Zinar Simsek, Nathan Ong, and David Kay for always being there to commiserate and welcome my complaints with open ears. Thank you to the incredible friends I met in Tulsa who kept me afloat through the good and bad times including Ethan and Haley Voelkers, Tyler Sluss, Tom Ballard, Rick and Melinda Wilson, and the entire Tulsa running community.

Thank you to the volunteers at Museum of the Rockies and the Vertebrate Paleontology lab at OSU-CHS, and Ballard lab field crews for all their hard work excavating Maiasaura specimens. Every scientist owes a debt of gratitude to volunteers and I am no exception. Thank you to John Scannella, Bob Harmon, Ellen Therese-Lamm, Lee Hall, Carrie, and Amy Atwater for all their hard work at MOR, stimulating paleo conversations, training, and for allowing me to explore collections to develop my dissertation. Thank you to Jack Horner for changing my life with his mentorship and his advisement.

Finally, I would like to thank my best friend and partner Celine Cortes. Celine, seeing you is the best part of my day and easily lifts me out of the quicksand. I love you. This could potentially age poorly. I also thank my unofficial emotional support animals: Buddy, Happy, Zeus, Prof, Cilantro, and Basil. You all will never know how important you were to my mental health these past seven years.

This research was funded primarily by the Ballard Lab, a Jurassic Foundation grant, an SVP Jackson School of Geosciences Student Member travel grant, and departmental funds from OSU-CHS Biomedical Sciences. I would like to give one final thank you to everyone who has entered my life these past seven years. Every experience has shaped who I am today for the better.

Name: CHRISTIAN T. HECK

Date of Degree: MAY, 2022

Title of Study: IDENTIFYING LIFE HISTORY TRAITS IN MODERN AND EXTINCT ARCHOSAURS UTILIZING OSTEOHISTOLOGY

Major Field: BIOMEDICAL SCIENCES

Abstract: Interpreting dinosaur life history traits is reliant upon data from modern taxa and large, ontogenetically variable dinosaur samples. Recent advances in the study of osteohistology have increased our understanding of dinosaur life histories, although aspects of dinosaur biology remain unresolved due to an absence of foundational studies and low dinosaur taxon sample sizes. The purpose of this dissertation is to investigate bone cortical signals of life history traits and behavior in modern and extinct archosaurs. Osteohistological data can then be used to further bolster examinations of bone response to changes in loading regimes in dinosaur long bones.

Bone cortices of the North Island Brown Kiwi (*Apteryx mantelli*) and American Alligator (*Alligator mississippiensis*) are examined for cortical signals of sexual dimorphism. Aves and some non-avian dinosaurs form medullary tissue as a calcium reservoir for egg laying, while alligators mobilize calcium from cortical bone. Medullary tissue is found in the female kiwi but not in the male kiwi or alligator sample. Intracortical signals of egg laying are absent in both kiwi and alligators. Extinct archosaur sex cannot be determined from intracortical signals and, instead, continue to rely on the presence of medullary tissue.

Next, bone growth in *Maiasaura* (Dinosauria: Hadrosauridae) humeri is examined and compared to growth in tibiae. Cortical growth marks are counted in each humerus (n=47) and used to construct growth curves and survivorship curves. Humerus growth is best represented by a monomolecular growth curve, similar to tibiae. Likewise, survivorship data shows high mortality in first year *Maiasaura* and mature adults, both mortality trends are similar to those derived from tibiae. *Maiasaura* humeri are reliable for interpreting life history traits in *Maiasaura* and, likely, hadrosaur dinosaurs in general.

Finally, *Maiasaura* age data and humerus bone geometry is used to infer ontogenetic changes in forelimb loading regimes. Regressions of humerus micro- and macro-morphology do not support changes in loading regimes associated with locomotor habit shifts. Age data is used to test separate age groupings, and juvenile regressions also do not support shifts in forelimb function. The results further suggest locomotor shifts did not occur in hadrosaurs.

TABLE OF CONTENTS

Chapter Page

Chapter Page

LIST OF TABLES

Table Page

LIST OF FIGURES

Figure Page

Figure Page

CHAPTER I

INTRODUCTION

Investigations into non-avian dinosaur (hereafter simply 'dinosaur') biology historically focused on anatomy (e.g. Currie 1985), biomechanics (e.g. Thulborn 1982), phylogeny (e.g. Salgado et al. 1997), and extinction (e.g. Russell and Tucker 1971). These studies built a foundation onto which more complex examinations of dinosaur life histories could be developed. Life history traits include size at birth, age and size at sexual and skeletal maturity, mortality schedules, and population dynamics (Stearns 1992). All organisms possess unique combinations of these traits that affect fitness in response to external stimuli (Stearns 1992). Defining life history traits in dinosaurs provides vital information into processes of natural selection and further clarifies the evolution of life history traits in dinosaurs (Padian and Stein 2013). However, dinosaurian life histories remain largely unresolved, despite recent advancements in the study of dinosaur growth and physiology (see Padian et al. 2013, Bailleul et al. 2019, Padian and Woodward 2021 and references therein).

Osteohistology, the study of bone at the microscopic level, is a major driver in advancing dinosaur life history information (Bailleul et al. 2019, Padian and Woodward 2021). The microstructure of bone is influenced by four general factors: ontogeny, phylogeny, mechanics, and environment (Horner et al. 1999, 2000, de Ricqlès et al. 2001, Padian et al. 2001, Padian 2013). Examination of dinosaurian bone microstructure informs our understanding of dinosaur growth rates, survivorship, population structure, pathology, locomotion, and evolution (e.g.

Padian and Lamm 2013, Cubo et al. 2015, Woodward et al. 2015). Paleobiological inferences rely on the study of dinosaur osteohistology and application of actualistic rationale, or uniformitarianism, whereby, a structure found in extinct taxa is assumed to have the same function function as the same structure in modern animals (Padian 2013, Cubo et al. 2015). True modern analogues for dinosaurs may not exist in respect to certain traits (size, metabolism, growth rate, etc.), but examining bone growth dynamics in extant vertebrates still remains essential in using actualistic rationale for interpreting dinosaur bone microstructure (Witmer 1995, Bailleul 2019 and references therein).

Pioneering studies, such as de Ricqlès (1980), used bone vascularity to assess relative growth rates in dinosaurs, by applying the results from an earlier study relating bone growth rate and vascularity in extant animals (Amprino 1947). The relationship between bone vascularity and bone growth rate was further corroborated by studies on modern aves (Castanet et al. 2000, de Margerie et al. 2002). Vascular canal orientation and density is also used to assess relative growth in dinosaurs and other extinct taxa (e.g. Horner et al. 2000, Hübner 2012) (Fig. 1). Castanet et al. (2000) injected modern ratites with fluorescent markers and further confirmed, quantitatively, that increases in vascular density correlate with increased growth rate. Castanet et al. (2000) also determined bone with sub-reticular and longitudinal canals grew at significantly lower rates than bone with reticular or laminar canals. Additionally, radially oriented vascular canals are associated with high rates of appositional growth (Fig. 1), typically found in fast growing juveniles and in pathological bone (de Margerie et al. 2004, Montes et al. 2007, Cubo et al. 2015, Jentgen-Ceschino et al. 2020).

Mineralized collagen fibers deposited by osteoblasts surround the vascular canals and comprise the tissue matrix of bone (Hancox 1972). As with vascular canal orientation, collagen fiber orientation is used to infer relative growth rates (Francillon-Vieillot et al. 1990) (Fig. 2). Collagen

fibers of woven-fibered bone are highly disorganized and are arranged randomly. Woven bone is strongly associated with rapid growth as seen in many juvenile dinosaurs (e.g. Horner et al. 1999, 2000, Woodward et al. 2015, Curry-Rogers and Kulik 2018) (Fig. 2). Fibrolamellar bone (or woven-parallel complex *sensu* Stein and Prondvai 2014) is woven collagen fibers with embedded primary osteons (Francillon-Vieillot et al. 1990) (Fig. 2). Deposition rate of fibrolamellar bone (FLB) has a broad range because vascular canal orientation can vary and gradate (Huttenlocker et al. 2013). Parallel-fibered bone is composed of loosely oriented collagen fibers and is deposited slower than woven bone (Fig. 2). Lastly, collagen fibers are highly organized and deposited slowly in lamellar bone (Francillon-Vieillot et al. 1990) (Fig. 2). Lamellar bone often forms concentric lamellae in osteons, trabeculae, endosteal bone, and outer cortices in skeletally mature vertebrates (Huttenlocker et al. 2013). Tissue organization is often used to assess relative growth rate in dinosaurs rather than absolute, in part due to overlapping rates of deposition between tissue types in modern taxa (de Margerie et al. 2002). The reluctance to quantify growth based on tissue type is also due to the gradational nature of tissue organizations (e.g. collagen fibers less organized than typical parallel-fibered bone, but more organized than woven).

Collagen organization and vascularity are also influenced by biomechanics. Laminar FLB is found in wing bones of birds and pterosaurs, indicating a relationship between torsion and tissue type (de Ricqlès et al. 2000, de Margerie 2002, 2006). Vascular canal orientation in the laminar FLB is primarily circular in regions torsionally loaded, while oblique and radial canals are prevalent in regions experiencing habitual bending (de Margerie 2002, 2006, Skedros et al. 2003, but see Skedros and Doutré 2019). Studies on mammalian bone mechanics and microstructure further support correlations between principle stresses and collagen and vascular orientation (Petrtýl et al. 1996, Kalmey and Lovejoy 2002, Skedros et al. 2009, 2011). Macrostructural traits, such as bone compaction, have been used to infer dinosaur locomotor traits, but biomechanical

influences on dinosaur bone microstructure are not well understood (e.g. Zhao et al. 2013, Ibrahim et al. 2014).

Absolute age and growth rate can be determined by analyzing annual growth marks within bone cortices (Padian 2013, Huttenlocker et al. 2013) (Fig. 3). Lines of arrested growth (LAGs) are hyper-mineralized lines reflecting annual cessation or slowing of growth coinciding with harsher seasons (Peabody 1961, Köhler et al. 2012). LAGs are well-studied and annual deposition has been confirmed in multiple groups of vertebrates (Fig. 3). For example, Köhler et al. (2012) found annually deposited LAGs in the bone cortex of extant ruminants, regardless of climate regime. LAGs can be deposited in a variety of skeletal elements, but Woodward et al. (2014) found LAG counts varied between bones of the same *Alligator mississippiensis* individual (also see Cullen et al. 2014).

Preservation of growth marks in a given element is dependent on growth rate, extent of medullary cavity expansion, cortical drift, and secondary remodeling (Padian et al. 2016). Growth rates vary intraskeletally and interspecifically. For example, sauropods have extremely high growth rates early in ontogeny and do not appear to form LAGs early in life. Major weight-bearing elements, such as tibiae and femora, have thicker cortical walls and undergo less remodeling, thus, preserving the most LAGs in dinosaurs (Werning 2012, Padian et al. 2013). However, Lemnell (1974) concluded that limb bones contained more accurate LAG counts for modern mammals, but Klevezal (1996) suggested LAG counts in mandibles are more accurate for aging. Stein and Sander (2009) also showed that larger limb bones in dinosaurs typically contain the best record of LAGs. Limb bone use for LAG counts is further corroborated by numerous histological studies (e.g. Horner et al. 1999, 2000, Hübner 2012).

Dinosaur age assessment is vital data for determining life history traits. Chinsamy (1993) was the first to utilize LAGs for constructing dinosaur growth rates. LAGs in *Massospondylus* femora

were counted and used to track femoral growth, yearly apposition, and timing of maturity. Erickson and colleagues expanded the use of growth marks to quantitatively assess life history traits of dinosaurs (Erickson and Tumanova 2000, Erickson et al. 2001, 2004, 2007, 2009). Erickson et al. (2001) modelled growth for six dinosaur taxa: *Shuvuuia deserti*, *Psittacosaurus mongoliensis, Syntarsus rhodesiensis, Massospondylus carinatus, Maiasaura peeblesorum,* and *Apatosaurus excelsus*, and found growth curves to be sigmoidal, often with an extended juvenile stage. Erickson et al. (2004, 2007, 2009) continued growth curve modelling for a multitude of taxa, including the theropod dinosaurs *Tyrannosaurus rex, Gorgosaurus libratus, Albertosaurus sarcophagus, Daspletosaurus torosus*, *Oviraptor philoceratops*, *Deinonychus antirrhopus*, Troodontidae nov. sp., *Citipati osmolskae, Troodon formosus,* and the ceratopsian *Psittacosaurus lujiatunensis*. Bybee et al. (2006) applied growth curve modelling to *Allosaurus,* and found growth rate to be intermediate to tyrannosaur growth (Erickson et al. 2004). Growth curve modelling has also been applied to sauropods, ceratopsians, and ornithopods (Lehman and Woodward 2008, Erickson and Druckenmiller 2011, Griebeler et al. 2013, Woodward et al. 2015) These studies were instrumental in applying growth curve modeling to extinct dinosaurs, although many of these studies were limited due to specimen accessibility. Woodward et al. (2015) constructed growth curves of *Maiasaura peeblesorum* based on osteohistological examination from only tibiae (n=50). The growth curves show that *Maiasaura* grew rapidly in early ontogeny, reaching sexual maturity at 2-3 years-old and skeletal maturity around 6-8 years-old. Skeletal maturity is determined when spacing between LAGs decreases substantially in a structure termed the external fundamental system (EFS, or OCL *sensu* Ponton et al. 2004; Francillion-Vieillot et al. 1990). Large sample sizes like the *Maiasaura* dataset provide an opportunity to further explore dinosaur life history (Woodward et al. 2015).

The immense progress in understanding dinosaur biology is still hampered by several factors. Obstacles to dinosaur life history interpretations include fossil biases (e.g. preservational biases,

minimal soft tissue fossilization) low sample sizes, minimal temporal and geographical constraint, and absence of modern analogues (e.g. Woodward et al. 2015, Mallon 2017). Individual variation can skew data in studies utilizing limited sample sizes (e.g. Erickson et al. 2001), while specimens separated in time and space are not truly contemporaneous (e.g. Woodruff et al. 2021). Paleontologists must often work with these limitations out of necessity due to the rarity of monodominant mass death assemblages in the fossil record (e.g. Botfalvai et al. 2021). Additionally, large fossil sample sizes are often not accessible for osteohistological evaluation due to the destructive nature of histological sampling (Padian et al. 2013). These obstacles prevent robust understanding of the extent to which bone morphology and histology can aid in biological inferences of extinct dinosaurs. A unique monodominant hadrosaur bonebed provides a means of lessening select obstacles, such as low sample sizes, inherent in studying life history traits in extinct taxa (Woodward et al. 2015).

Maiasaura

A large sample of the non-avian hadrosaur dinosaur *Maiasaura peeblesorum* has been utilized in exploring dinosaur paleobiology due to number of individuals represented, the diverse range of ontogenetic stages present, the limited geologic time averaging of the assemblage, and extensive and ongoing excavation of the *Maiasaura* mass death assemblage (e.g. Schmitt et al. 2014, Woodward et al. 2015). Research dedication to *Maiasaura* has resulted in *Maiasaura* being the most well-studied and understood dinosaur to date, despite a wealth of information yet to be derived from the assemblage. This dissertation seeks to add to the dearth of *Maiasaura* paleobiological data and use the assemblage to test dinosaur limb function hypotheses.

Maiasaura peeblesorum is a hadrosaurid dinosaur (Hadrosauridae: Brachylophosaurinae; Freedman Fowler and Horner 2015) (Fig. 4) that was first described from a collection of nestling skeletal materials and unassociated, but nearby, adult cranial material (Horner and Makela 1979,

Horner 1983, also see Prieto-Marquez and Guenther 2018) from the Willow Creek Anticline from Two Medicine Formation (Late Cretaceous) sediments (Fig. 5). The described nestlings were found in close proximity within an infilled bowl shaped mudstone depression; the infilling sediment of the depression is green mudstone while the surrounding mudstone is brown. The green mudstone likely represents the *Maiasaura* nest that was infilled; green coloration is either due to decaying vegetation in the nest or decaying nestlings (Horner and Makela 1979, Carpenter 1999). The first description of the species and nests presented novel ideas of enhanced parental behavior in non-avian dinosaurs, further progressing associations between non-avian dinosaurs and modern birds (Horner and Gorman 1988).

Maiasaura nests contained eggshell in addition to nestling material. Eggshell association with a dinosaur species is often difficult, but *Maiasaura* represents a rare case in which the species of egg production is assured (Horner and Makela 1979, Horner 1982, Hirsch and Quinn 1990, Mikhailov 1994). *Maiasaura* eggshell fragments are abundant in the Willow Creek Anticline (Horner and Gorman 1988) and are the basis of several examinations of dinosaur eggshell composition and dinosaur reproductive biology and behavior (Horner and Makela 1979, Horner 1982, Hirsch and Quinn 1990, Mikhailov 1994, Mikhailov 1997, Zelenitsky and Hills 1997, Carpenter 1999, Horner 1999, 2000, Weimann et al. 2018, Zhu et al. 2022).

Maiasaura nestling and embryonic long bone epiphyses have been compared to altricial and precocial aves; long bone epiphyses were found to be underdeveloped until *Maiasaura* reached a length of approximately 1.5m (Horner and Weishampel 1988). Thus, nestling long bones suggest *Maiasaura* hatchlings were altricial and cared for by adult individuals until long bones developed for locomotion (Horner and Makela 1979, Horner 1982, 1984, Horner and Weishampel 1988, but see Geist and Jones 1996).

Maiasaura skeletal development has been evaluated extensively. Cranial material was described in early assessments of *Maiasaura* taxonomy, along with reassessments of described material and recent analyses of *Maiasaura* material found outside the Willow Creek Anticline (Horner and Makela 1979, Horner 1983, Prieto-Marquez and Guenther 2018, McFeeters et al. 2021, 2021). *Maiasaura* is named based on cranial features such as the angle of the quadratojugal process, a wide elongate rostrum, and a rostrodorsally projecting nasofrontal crest (Horner and Makela 1979, Horner 1983). *Maiasaura* postcrania have been examined in several studies utilizing a mass death assemblage in the Willow Creek Anticline.

Multiple fossil bearing facies are present in the Willow Creek Anticline (Lorenz and Gavin 1984). The original *Maiasaura* nestling materials were from one of multiple nesting horizons, whereas a separate horizon in the Willow Creek Anticline contains a mass death assemblage of thousands of *Maiasaura* bones ranging in age from juveniles to adults (Lorenz and Gavin 1984, Horner and Gorman 1988) (Fig. 6). The assemblage is unique for a variety reasons and provides paleontologists an avenue for testing hypotheses of dinosaur biology using a large, single taxon, sample.

Prevailing hypotheses on the bonebed origin suggest herds of *Maiasaura* suffered mass death episodes over multiple years (10^{-1} – 10^{1} years) (Schmitt et al. 2014, Woodward et al. 2015). *Maiasaura* remains were then buried or partially buried prior to being transported by a mass sediment flow. The sediment flow disarticulated the skeletal remains and deposited them across 2 km^2 in Northwest Montana, USA. Evidence from bone scavenging marks, weathering, abrasion, and deformation suggests *Maiasaura* bones were exposed for relatively little time prior to burial and transport. Therefore, the minimal time averaging and exposure suggests the bonebed represents the remains from a maximum of 10 years of *Maiasaura* mass death episodes, a relatively small amount of time for such a large dinosaur assemblage (Schmitt et al. 2014).

Unfortunately, *Maiasaura* remains became disarticulated and disassociated during sediment flow-induced transport.

The mass death assemblage is the primary tool for reconstructing ontogenetic changes in *Maiasaura* biology. *Maiasaura* elements from the assemblage have been used to compare sequence heterochrony across Iguanodontia (Guenther 2009) in addition to specific comparisons of long bone development within hadrosaurids (Guenther 2014). *Maiasaura* bone growth was also examined at the microstructural scale to make inferences of dinosaur physiology (e.g. Horner et al. 2000, Woodward et al. 2015, Woodward 2020). The assemblage also produced study of biomechanically adaptive bone microstructure; two tibiae were described as having pathological bone growth in response to fibular failure (Cubo et al. 2015) after comparisons to modern taxa pathology.

Dilkes (2000) used the extant phylogenetic bracket and the assemblage to reconstruct *Maiasaura* forelimb and hindlimb myology through ontogeny. Myological changes in *Maiasaura* ontogeny suggest a locomotor habit change from bipedal to quadrupedal. A locomotor shift hypothesis was later tested with, and supported by, *Maiasaura* appendicular morphological data (Dilkes 2001). However, Dilkes (2000, 20001) studies did not have the benefit of histologically aging each measured specimen. Disassociation and disarticulation of the assemblage prevents direct intraskeletal inferences without histological aging each bone. Cubo et al. (2015) histologically examined pathological tibiae and reported abnormal bone deposition in two tibiae, a juvenile and adult, was likely the result fibular failure and biomechanical adaptation in the tibia in response. The direction of abnormal bone growth in each tibiae was consistent with the direction predicted for bipedal juveniles and quadrupedal adults, further supporting an ontogenetic locomotor shift in *Maiasaura*.

Finally, the mass death assemblage provided adequate sample sizes to evaluate *Maiasaura* growth rates and population dynamics. Annual cortical growth marks are used to determine age at death and annual growth through ontogeny (e.g. de Buffrénil et al. 2021). Erickson et al. (2001) tested hypotheses of dinosaur growth trends using *Maiasaura*, though Erickson et al. (2001) used a very limited *Maiasaura* sample. Woodward et al. (2015) sampled 50 *Maiasaura* tibiae to construct statistically significant growth curves and survivorship curves. The more extensive sampling in Woodward et al (2015) resulted in different growth curves than previously produced, further emphasizing the importance of large samples in dinosaur studies.

The ever-growing *Maiasaura* sample can be used to further explore dinosaur life history traits. In this dissertation, I utilize the large sample of *Maiasaura* and the extant phylogenetic bracket to determine the utility of osteohistology in archosaur life history interpretation. Thus, the objectives of the dissertation are to explore intracortical biomechanical signals of the hypothesized *Maiasaura* locomotor shift, compare growth rates and demographics between *Maiasaura* hindlimb and forelimb elements, and investigate cortical signals of sexual dimorphism in the extant phylogenetic bracket. The results here can be used as a foundation for further examination of dinosaur life history traits.

Chapter Summaries

To begin, chapter II tests methodological assumptions of osteohistological bone processing product efficacy. Modern and fossil bone undergo different steps in processing for histological analyses. Modern undecalcified tissue is fixed in formalin, dehydrated in step-wise ethanol solutions, and cleared prior to embedding in epoxy resin (Heck et al. 2020). Fossil bone, on the other hand, is not chemically treated prior to embedding in polyester resin (Lamm 2013, Heck et al. 2020). Anecdotal evidence suggests high priced epoxy resin is of higher quality than low cost polyester resin and results in better thin section structural integrity. Resin choice appears to be

directly associated with unfounded assumptions of resultant thin-section quality and slide thickness requirements for modern tissue. Higher costs can be detrimental to underfunded institutions and prohibit necessary research. In this chapter I test polyester and epoxy resin efficacy in modern and fossil hard tissues to establish quantifiable data on thin-section integrity and broad applicability of polyester resin in osteohistological studies. The results of this chapter shape histological methodology in chapters III – V.

Dinosaur paleobiological inferences are built on observed biology of modern aves and crocodylians (i.e. the extant phylogenetic bracket (Witmer 1994)). Chapters III and IV focus on descriptions and exploratory analyses of sexual dimorphism in the North Island Brown Kiwi (*Apteryx mantelli*) and American alligator (*Alligator mississippiensis*). Chapter III is the most thorough intraskeletal description of kiwi bone microstructure (Heck et al. 2021), and utilizes a male and female kiwi of known age. Age data of both specimens allows direct comparisons of cortical growth marks and age at death for each specimen.

Chapter IV examines quantifiable cortical characters in a sample of male and female alligators (*A. mississippiensis*). Reproductive biology in egg-laying tetrapods, such as dinosaurs, necessitates mobilization or consumption of excess calcium for egg shell formation. Previous studies suggest cortical bone is resorbed in female alligators for calcium mobilization, although evidence also suggests alligator osteoderms serve as calcium reservoirs. Resorption of cortical bone for egg-laying would be reflected in bone cortical area and remodeling. I test for quantifiable differences between male and female alligator cortical bone signals of resorption using captive raised alligators of known age and a sample of wild alligators of unknown age.

Chapters VI and VII are examinations of ontogenetic shifts in *Maiasaura* forelimb function. Assessment of functional shifts requires an understanding of ontogenetic changes in bone microstructure and aging of sampled *Maiasaura* humeri. Results from chapters III and IV indicate

cortical signals of sex are likely absent in dinosaurs and, thus, biomechanical signals would not be impacted by sex. Additionally, fossil species growth rates and demographies are often inferred from multiple skeletal elements. In chapter V, I histologically describe bone growth and age markers in a large sample of *Maiasaura* humeri to assess humerus growth and *Maiasaura* survivorship. Intracortical growth marks allow for age-based analyses of humeri morphology in Chapters VI and VII.

Chapter VI reassesses changes in *Maiasaura* humerus macromorphology and limb scaling through ontogeny. An ontogenetic locomotor shift from bipedalism to quadrupedalism is hypothesized for *Maiasaura*. A shift to quadrupedalism would introduce loading and muscle-initiated tensional forces to forelimb elements. Introduced forces would likely result in a bone growth response. Here, I evaluate gross morphological changes in *Maiasaura* humeri to assess signals of locomotor change. I also utilize humerus age data from Chapter V and tibia age data from Woodward et al. (2015) to model forelimb and hindlimb growth in ontogeny to further evaluate skeletal changes and potential locomotor shifts.

Finally, in Chapter VII I examine ontogenetic changes in humerus bone geometry through *Maiasaura* ontogeny. Bone growth responds to introduced forces and a locomotor shift should be detected in humerus cortical geometry. Therefore, I evaluate changes in cortical area, medullary cavity area, cortical thickness, and remodeling extent in *Maiasaura* humeri through ontogeny to further test the locomotor shift hypothesis. Age data from Chapter V is used to test age groupings separately in both Chapter VI and VII.

Figures

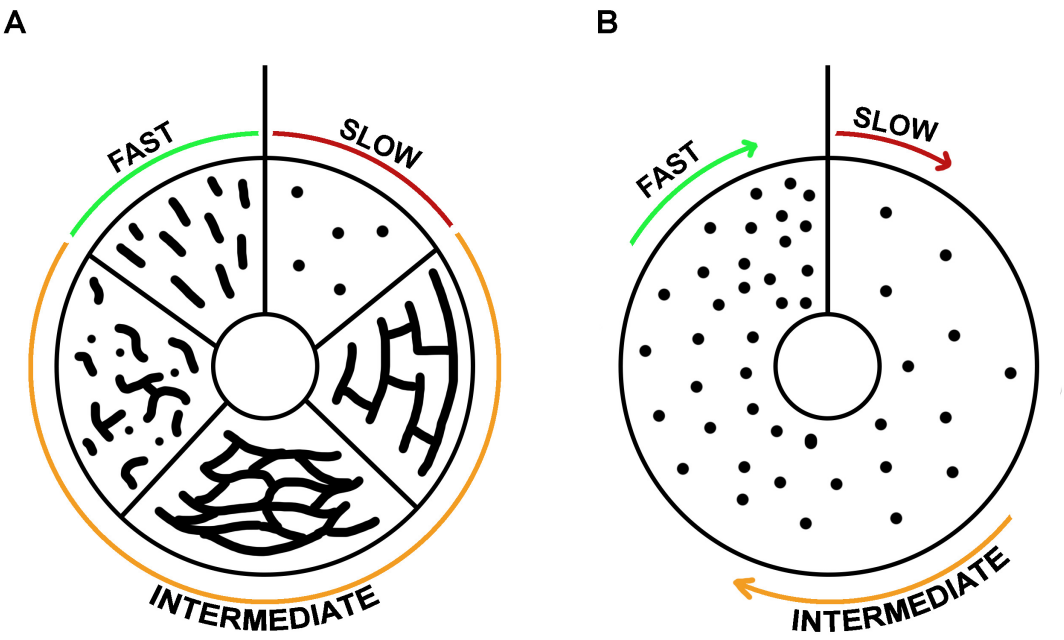

Figure 1. Simplified diagrams showing relationship between (A) vascular orientation and (B) vascular density to growth rate. (A) vascular orientations (clockwise): longitudinal, laminar, plexiform, reticular, and radial. (B) Increases in vascular density is associated with increasing growth rate.

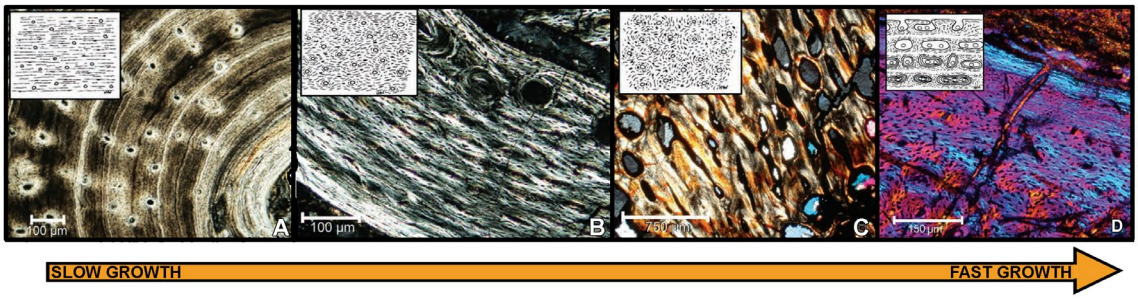

Figure 2. Collagen fiber tissue organization has a direct relationship with relative growth rates. (A) Lamellar bone is slow growing and composed of stacked, plywood bone layers, (B) parallel-fibered bone is deposited faster and is found in a variety of primary tissues, (C) woven tissue is deposited at a high rate, (D) woven-parallel complex tissue is also deposited rapidly. Modified from Huttenlocker et al. 2013.

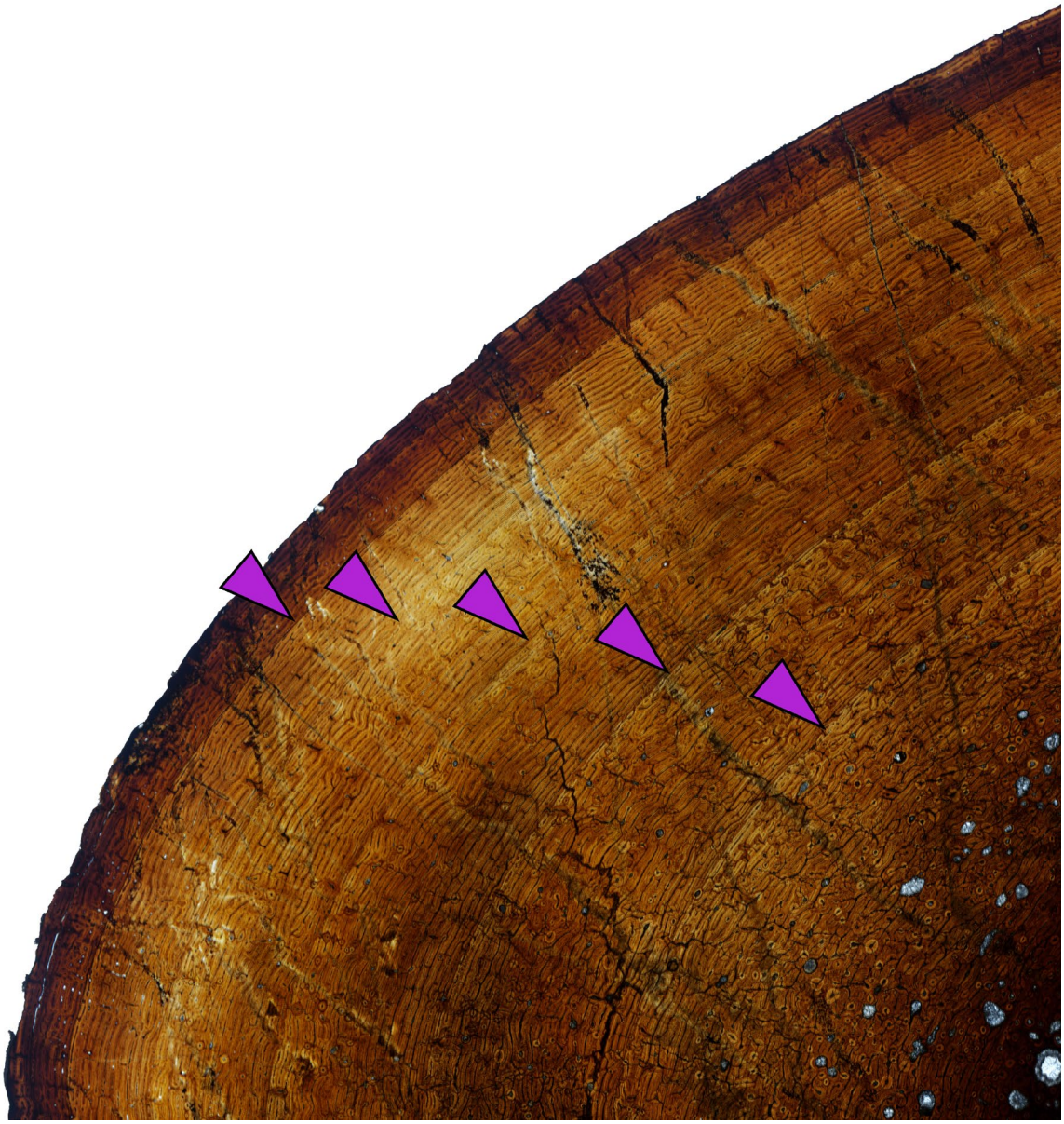

Figure 3. *Maiasaura peeblesorum* humerus cross section. Cyclical growth marks (arrows) are formed annually and used to determine age, growth rate, and maturation.

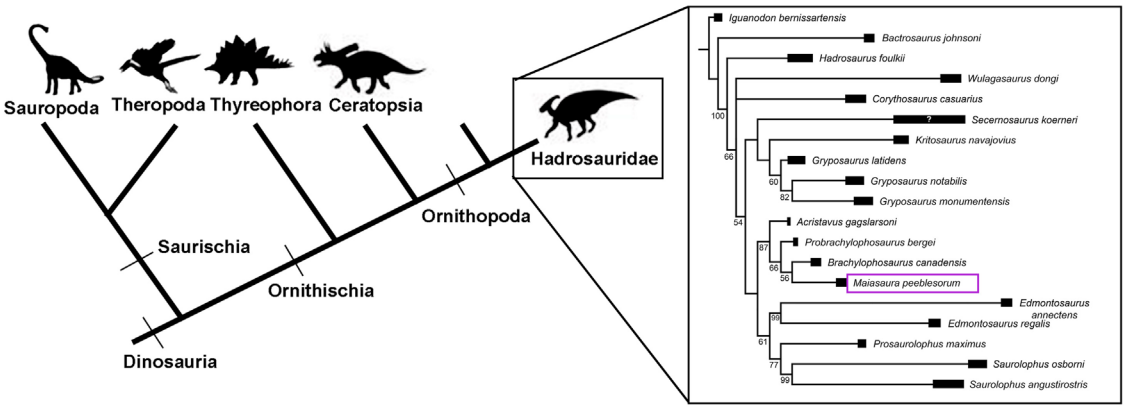

Figure 4. Simplified phylogeny of Dinosauria and expanded relationships within Hadrosauridae (insert). Modified from Maidment and Barrett 2014 and Freedman Fowler and Horner 2015.

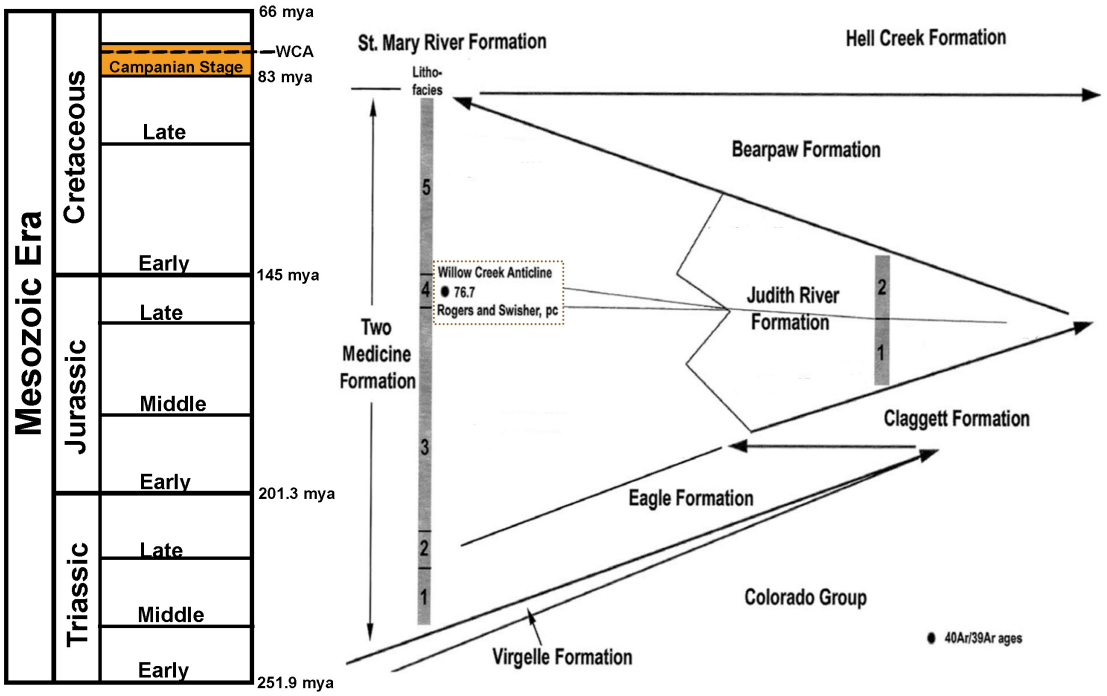

Figure 5. *Maiasaura* specimens are from the Willow Creek Anticline (76.7mya) in the Two Medicine Formation in the Campanian Stage of the Late Cretaceous. Modified from Schmitt et al. 2014.

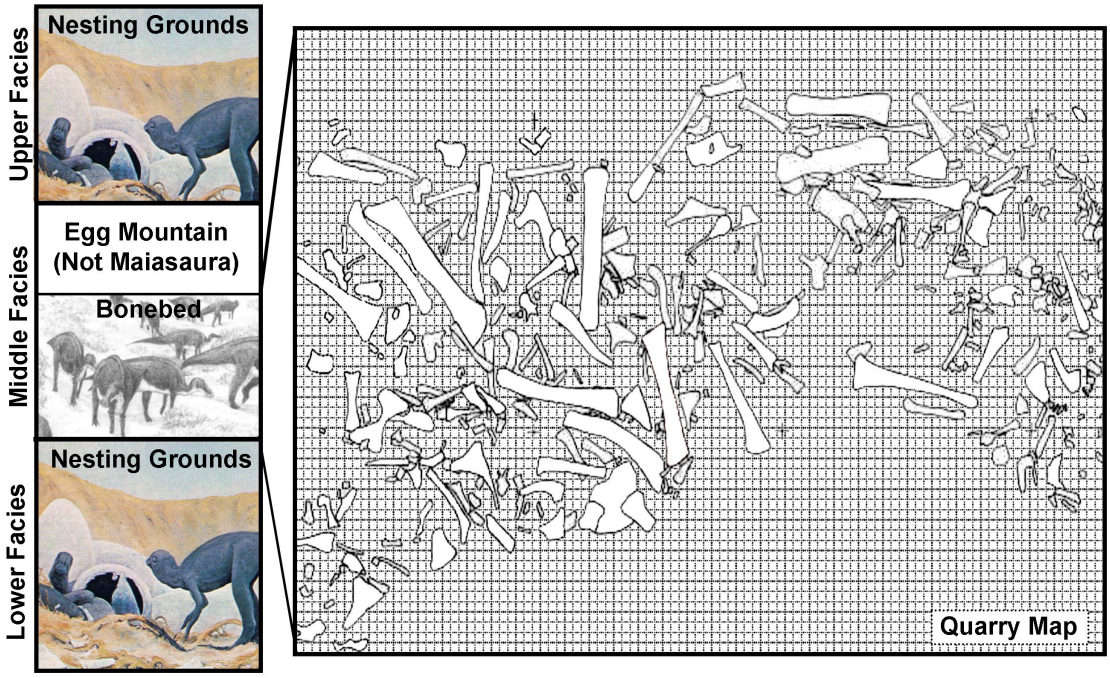

Figure 6. Multiple fossil bearing facies (left) are present in the Willow Creek Anticline. Lower and Upper facies consist of nesting grounds while the Middle facies have the Egg Mountain site and the mass death assemblage of *Maiasaura*. The mass death assemblage consists of disarticulated and disassociated skeletal elements (right). Images from Horner 1984, Horner and Gorman 1988, Varricchio and Horner 1993.

CHAPTER II

POLYESTER OR EPOXY: ASSESSING EMBEDDING PRODUCT EFFICACY IN PALEOHISTOLOGICAL METHODS.

Introduction

Histological examination of bone allows interpretation of relative growth rates, absolute age, pathologies, and life history reconstructions of extinct and extant taxa (Marín-Moratalla et al. 2013, Cubo et al. 2015, Woodward et al. 2015, Calderón et al. 2019). Vertebrate paleontology studies increasingly incorporate osteohistology, or bone histotechniques, for these reasons, with large-sample studies becoming more common. The recognized utility of osteohistology necessitates investigating the cost-effectiveness of consumables involved to reduce expense, especially concerning large sample sizes.

Decalcification of modern hard tissues is necessary for specific staining protocol at the sacrifice of the mineral component (Skinner 2003). However, preparation of hard tissues without decalcification allows for investigation of mineralization patterns and direct comparisons with fossil specimens (Scarano et al. 2003, Skinner 2003, Straehl et al. 2013), as the unmineralized component of bone typically degrades prior to fossilization. Methodology for the preparation of undecalcified hard tissues, also simply termed ‘calcified tissue’, for histological examination varies but generally includes stepwise tissue fixation, dehydration, and clearing prior to specimen embedding in resin, mounting the embedded specimen to a slide with glue, and thin section

polishing (Fig. 7) (An et al. 2003, Schweitzer et al. 2007). Soft tissues in bone, e.g. oils, fats, and the collagen component of bone, are lost during the process of fossilization, thus, preparation of fossil hard tissues does not include the initial chemical treatments of modern hard tissues but still requires embedding in resin for stabilization, mounting, and polishing (Fig. 7) (Chinsamy and Raath 1992, Wilson 1994, Lamm 2013). Embedding, or investing, biological material for histological study was first introduced by Klebs (1869) using paraffin as the embedding medium (Sanderson et al 1988). Over the next century advancements in petrography and biological histology developed, and new methodologies for processing specimens emerged; however, protocol for histological processing of mineralized fossil material in publications was often absent or vague. Mineralized osteohistological studies have since utilized a variety of embedding mediums, with epoxy and polyester resins being common for extant bone and fossil bone respectively. However, choice of fossil and modern hard tissue embedding medium does not appear established on the basis of resin efficacy. Instead, resin selection seems to be personal preference or based off of published corporate technical notes (Ahmed and Vander Voort 2000, 2003). For instance, Chinsamy and Raath (1992) were the first to publish a detailed protocol for their preparation of fossil bone for histological study and utilized epoxy resin for their embedding medium. They state, "…any resin or other rigid, clear mounting medium which does not interfere with the structure or optical properties of the tissues could be used" (Chinsamy and Raath 1992, p. 40). Wilson (1994) also details methods used for preparing fossil bone for histological analysis and lists polyester resin as the preferred embedding medium for fossil bone. Lamm (2013) thoroughly describes the methodology developed at the Museum of the Rockies (Bozeman, MT, USA) for preparation and sectioning of fossil specimens for histological sampling. Lamm (2013) states that small fossils between one millimeter and one centimeter in length benefit from epoxy resin embedding due to the low viscosity of epoxy, which increases resin penetration, but that polyester resin is suitable for larger fossil material.

Resin choice is further compounded by price, with some epoxy resins costing up to 479% that of some polyester resins at the time of this publication. Such expenses can be prohibitive for underfunded researchers and institutions and necessitates determining cost effective alternatives. Here, we investigate the efficacy of polyester and epoxy embedding mediums (of different price points) commonly used in histological studies of fossil bone and modern undecalcified hard tissues to determine the variables requiring higher priced epoxy resins in the event that polyester and epoxy resins are similar in functionality.

Materials and Methods

Materials

Fossil and modern hard tissues were chosen for sampling to test the efficacy of polyester and epoxy resins. The fossils are donated bones, teeth, and fish scales of unknown provenience. Fossil specimens include a turtle femur, two ornithischian dinosaur teeth, gar scale, crocodile scute, and a rib and bone fragment of unknown taxa. Modern bones were either purchased raw from a local grocery store (domestic chicken (*Gallus gallus domesticus*)) or collected as salvage (nine-banded armadillo (*Dasypus novemcinctus*)). Salvage was collected under Oklahoma collecting permits. The chicken humerus, tibia, and femur were sampled as well as both calcanea from the nine-banded armadillo.

Specimen Processing

Fossil material was thoroughly scrubbed with an acetone-soaked brush to remove any consolidants from the bone surface. Intensive exposure to acetone can have deleterious effects on fossil bone, but we did not observe any damage to fossils from acetone washing. Specimens were placed in small silicone containers and vacuum impregnated with either Silmar-41 two-part polyester resin, a commonly manufactured polyester resin, or Buehler Epothin (1 or 2, see Table 1) two-part epoxy resin (Buehler Ltd.). A variety of epoxy and polyester resins are utilized by

osteohistological studies, but the two resins tested here are commonly used in paleohistological embedding (Lamm 2013). Buehler Epothin 1 became unavailable mid-way through the experiment and was replaced by two-part Buehler Epothin 2. We assume there is no major difference in efficacy between Epothin 1 and Epothin 2. Specimen processing then followed standard protocol outlined in Lamm (2013).

All modern bones were processed prior to embedding using modified techniques from An et al. (2003) and Schweitzer et al. (2007) and outlined here. Modern material was soaked in warm water mixed with 1% Tergazyme Enzyme Detergent (Alconox Inc.) to degrade and to ease the removal of soft tissues from the bones. Specimens were air dried and remaining connective tissues and muscle remnants were removed via dissection. Bones were fixed in 10% formalin solution for 2-3 days. Specimens were then dehydrated in step-wise increasing concentrations of ethanol starting at 70% EtOH for 48 hours, followed by 85% EtOH for 48 hours, and finishing in 100% EtOH for 48 hours. Specimens were then cleared in Clear-Advantage Xylene Substitute (Polysciences Inc.) for 2-4 hours and set aside until dry (24-48 hours under a fume hood). Drying specimens after clearing introduces air back into the bone structure, but vacuum embedding replaces the reintroduced air with the embedding resin. Embedding procedure then proceeded as described above for fossil material (see Table 1 for embedding resin type used for each specimen).

One to two thin sections were generated from each embedded specimen (Table 1). A Buehler Isomet 1000 saw (Buehler Ltd.), equipped with a 6” diamond cutoff blade, was used to cut thick wafers of approximately 2.5mm from each embedded specimen block. One side of each wafer was ground on a Buehler Ecomet 4 lapidary grinder/polisher (Buehler Ltd.) using silicon carbide paper from 600 grit to 800 grit. Additionally, one side of the plastic slides was “frosted” using 600 grit silicon carbide paper on the Ecomet 4. Frosting of the wafer and plastic slide permits better adherence when glue is applied. Using 600 grit silicon carbide paper does not create

scratches large enough to affect visibility of the finished section with microscope viewing. Wafers were placed under a fume hood for 24 hours to dry. After drying, wafers were mounted to frosted plastic slides with Starbond cyanoacrylate glue of medium viscocity to form a thin-section slide. Lamm (2013) recommends that polyester embedded specimens be mounted to glass slides using two-part, two-ton epoxy, while epoxy embedded specimens be mounted to plastic slides using cyanoacrylate glue for better adherence. Recent processing of thin sections on glass with two-ton epoxy as the adhesive resulted in artifacts at the microscopic level. Although not visible in plane light, the artifacts appear as tiny birefringent square flakes in cross polarized light (Fig. 8). The presence of birefringent flakes is not isolated to any single brand of two-part epoxy, and are only present in the hardener component (HNW pers. obs.). However, the artifact can be eliminated by reheating the hardener component to 50°C (HNW pers. obs.). Here, we use plastic slides for all specimens because of the much lower cost of plastic slides relative to glass, and apply cyanoacrylate glue to (1) avoid potential visual complications caused by the use of two-ton epoxy and (2) continue following procedure outlined in Lamm (2013). Thin-sections (wafers mounted on slides) were set under a fume hood for 24 hours to cure and were then removed and allowed to cure for an additional 24 hours. Thin-sections were ground and polished using silicon carbide paper of decreasing grit sizes beginning at 320 grit and ending with 800 grit on a lapidary wheel until bone microstructure was visible and identifiable under a polarizing light microscope. Thin-section grinding on the lapidary wheel was controlled by hand and, thus, thin-sections were subjected to slight pressure variation during the grinding process. Slide holders can be used to eliminate pressure variation during lapidary wheel grinding, however, grinding was hand controlled in this study to better simulate low cost thin-section preparation techniques. Thin-sections were further polished by hand with 5µm and 1µm solutions. Osteohistological studies often rely on qualitative descriptions such as that of bone tissue organization and vascular canal organization. Therefore, clarity of tissue organization and visibility between specimens embedded in the two resin types were qualitatively assessed by the authors. Thickness of finished slides was

averaged for each specimen, but a targeted thickness was not set due to differences in transparency of tissue organizations. Differences in resin refractive index were not taken into account when assessing tissue visibility.

Slide Damage Assessment

Two general kinds of damage can occur during grinding and polishing of hard tissues: (1) hard tissue material tearing, or popping, off the slide and (2) complete removal of specimen tissue due to excessive polishing. Lamm (2013) suggests epoxy resin performs better with material requiring extremely low thickness for tissue visibility whereas similar material embedded in polyester resin may succumb to the second type of damage during the grinding and polishing stage. Four specimens used in the study were chosen for further testing the ability of each resin to maintain specimen integrity when polished aggressively. The fossil rib and unknown bone fragment were carefully broken in half using a small hammer, and one half was embedded in Silmar-41 polyester resin and the other half embedded in either Buehler Epothin 1 or Epothin 2 epoxy resin (Table 1). Embedding protocol followed protocol previously stated. Testing each half in a different resin eliminated potential variation in tissue reaction based on mineral density, bone tissue organization, and/or vascular density. Similarly, one fossil tooth and the right nine-banded armadillo calcaneum was embedded in Silmar-41 while a second fossil tooth and the left nine-banded armadillo calcaneum was embedded in Buehler Epothin 2. Specimen processing and thin section preparation followed the previously stated protocol and the resultant thin section slides were polished on a lapidary wheel with 600 grit carbide paper until light could pass through the specimen. Thin sections were then polished further on the lapidary wheel using 800 grit carbide paper until specimen integrity was lost (damage type (1) or (2) as defined previously). Thickness of thin sections at moment of lost integrity was measured using a digital micrometer. Resultant thicknesses were compared between specimens embedded in each resin.

Results

We qualitatively assessed thin-sections produced from specimens embedded in the two resin types, Silmar-41 polyester resin and Buehler Epothin epoxy resins. Assessment included clarity of tissue organization and incurred thin section damage, as described previously. We found no appreciable difference in tissue clarity or visibility between specimens embedded in Buehler Epothin epoxy resin and specimens embedded in Silmar-41 polyester resin (Fig. 9). Additionally, we found no difference in thin-section quality between modern and fossil specimens regardless of resin type. None of the prepared thin-sections exhibited either type of damage prior to tissue organization being visible and identifiable under a polarized light microscope. Final thin section thicknesses ranged from 38µm to 247µm when tissue organization could be identified under a polarized light microscope; averaged thicknesses ranged from 46µm to 237µm (Table 2). Finished, averaged thin-section thickness varied between resin types despite similar tissue visibility with specimens embedded in Buehler Epothin resins ranging from 46µm to 90µm and specimens embedded in Silmar-41 resin ranging from 56µm to 237µm.

We also did not find a difference between thin-section thickness at point of material damage, albeit with a small sample size. Table 2 lists the slide thickness at integrity loss for each specimen. Thickness at integrity loss was well beyond that in which bone microstructure was visible and identifiable in each specimen, and integrity loss resulted in damage type (1) (material tearing or popping off of the slide) (Fig. 10).

Discussion

Our results suggest that polyester resins can be used for embedding undecalcified modern bone and fossilized hard tissues without loss of tissue visibility or embedded material integrity. The finished section thickness did vary between Silmar-41 and Buehler Epothin embedded specimens. On average, epoxy resin embedded specimens had to be ground thinner than polyester embedded

specimens to achieve similar levels of tissue visibility. However, finished section thickness appears more dependent on variation in hard tissue composition rather than resin type. For example, the fossil rib was divided into two parts and each part embedded in a different resin. The average finished section thickness of the polyester resin embedded rib part was 56µm and the epoxy resin embedded rib part was 60µm. Similar trends were observed in the finished slide thicknesses of the divided unknown fossil bone fragment and the two fossil teeth. The gar scale, composed of bone, dentine, and ganoin, was embedded in Silmar-41 resin and finished section thickness was 226µm - 247µm, far thicker than any other finished thin section. Removal of the gar scale section thickness results reduces the polyester resin section thickness range to 38µm - 113µm, closer in range to slides with epoxy resin embedded specimens. Ideally, a future study will embed a fossil gar scale in epoxy resin for comparison of similar specimen material compositions.

Resin type also did not appear to affect tissue visibility with the microscope or thickness at material loss during polishing. Section thickness at moment of material integrity loss was similar between resin types but varied among specimens, similar to results of finished slide thicknesses. This suggests that resin type has no appreciable effect on adherence or material loss at low section thicknesses.

Recently published methodologies for the preparation of undecalcified modern bones and small fossil hard tissues show a preference for the use of epoxy resins as embedding media (Lamm 2013) rather than polyester-based media. In a brief survey of 134 research articles using histological sampling of either fossil bone or undecalcified modern bone (modern bone studies surveyed typically focused on non-primate tetrapods), we found polyester resins were preferably used in fossil studies (41% used a polyester resin, 32% used an epoxy resin, 26% did not use polyester or epoxy or did not specify a resin type) and epoxy resins were preferred for modern undecalcified bone (59% used an epoxy resin, 26% used a polyester resin, 15% did not use

polyester or epoxy or did not specify). Epoxy resins were suggested to improve penetration and bonding of resin to the embedded hard tissue and to prevent material loss at low thin-section thickness. Polyester resins, on the other hand are recommended for larger fossil material (Wilson 1994, Lamm 2013), although several studies have utilized polyester resins for embedding modern undecalcified bone (e.g. Bourdon et al. 2009, Canoville et al. 2019). Our study suggests that the less expensive polyester resins can be used interchangeably with the more expensive epoxy resins, decreasing the costs of histological preparation. However, this is a preliminary study and other variables may affect results including selection of mounting glue, hand pressure during polishing, humidity, room temperature, silicon carbide paper quality, and lab tech experience. In addition, our study focuses on specific resins used in protocol outlined in Lamm (2013) and excludes other commonly used resins (e.g. UV curing glue, Araldite, Technovit, etc.). Our study does not examine the long-term effects of resin types in terms of color changes or changes in brittleness of embedded specimens. Lamm (2013) notes changes in glue color (yellowing) and slide peeling have occurred in a few older specimens (histologically prepared over 24 years ago) in the Museum of the Rockies histology collection. A long-term study is necessary to ensure that resin type does not have a depreciable effect on stored embedded specimens. Lastly, modern specimens sampled were collected and salvaged for the purpose of this study and chemical processing was tightly controlled by the authors. In contrast, modern specimens in museum collections may have a complex and undocumented history of chemical processing. Exposure to atypical chemicals during museum preparation and curation may have deleterious effects on embedding efficacy or long-term integrity of embedded specimens. The current study does not address any potential differences between ‘freshly collected’ modern specimens and modern specimens that have been stored long-term in museum collections, but future researchers should take into account any chemical used on specimens prior to initiating histological processing.

Conclusions

Few studies have focused on product efficacy in paleohistological methods, potentially leading to unnecessary expenses. Epoxy resins are suggested to improve resin penetration, but incur a much larger financial cost relative to polyester resins. In this preliminary study, neither tissue quality under the microscope or integrity of specimen thin sections differed between polyester and epoxy resins. Institutions processing specimens for osteohistological sampling can alleviate some financial strain by utilizing polyester resins. However, long term storage may have negative effects on one resin type more so than another. The results of this study would benefit from an increased sample size and observation of resin embed deterioration over time.

Tables

Table 1. Material histologically sampled using either polyester resin or epoxy resin as the embedding medium.

Resin Type	Specimen Age	Specimen	Element	No. of Sections
Polyester Resin (Silmar-41)	Modern	Domestic Chicken	Humerus	2
			Femur	2
			Tibia	2
		Nine-banded Armadillo	Right Calcaneum*	2
	Fossil	Indet. Turtle	Femur*	2
		Gar	Scale	2
		Indet. Crocodile	Scute	2
		Indet. Ornithopod	Tooth*	2
		Unknown	Rib	2
		Unknown	Fragment*	1
Epoxy Resin	Modern	Nine-banded Armadillo	Left Calcaneum*	2
(Epothin-1)	Fossil	Indet. Turtle	Femur*	1
		Unknown	Rib	1
		Indet. Ceratopsian	Tooth*	2
(Epothin-2)		Unknown	Fragment*	1

Table 2. Slide thickness of each finished thin section and thickness at material loss.

Resin Type	Specimen	Element	Avg. Finished Slide Thickness (µm)	Slide Thickness at Loss (µm)
Polyester Resin (Silmar-41)	Domestic Chicken	Right Humerus	72	-
		Right Femur	61	-
		Right Tibia	100	-
	Nine-banded Armadillo	Right Calcaneum	66	60
	Indet. Turtle	Femur	64	32
	Gar	Scale	237	-
	Indet. Crocodile	Scute	70	-
	Indet. Ornithopod	Tooth	66	45
	Unknown	Rib	56	-
	Unknown	Fragment	80	67
Epoxy Resin (Epothin-1)	Nine-banded Armadillo	Left Calcaneum	78	71
	Indet. Turtle	Femur	46	44
	Unknown	Rib	60	-
	Indet. Ceratopsian	Tooth	81	20
(Epothin-2)	Unknown	Fragment	90	81

Figures

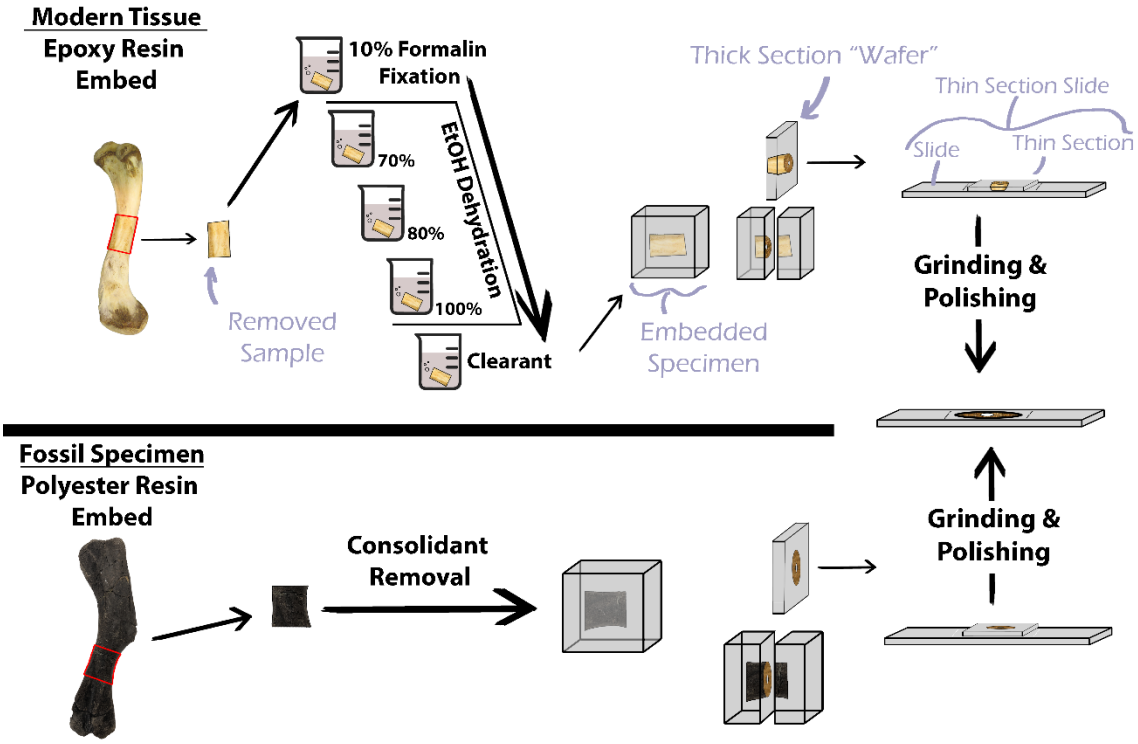

Figure 7. Simplified protocol for osteohistological processing. Modern tissue (top) undergoes chemical processing whereas fossil material (bottom) can be embedded without chemical processing.

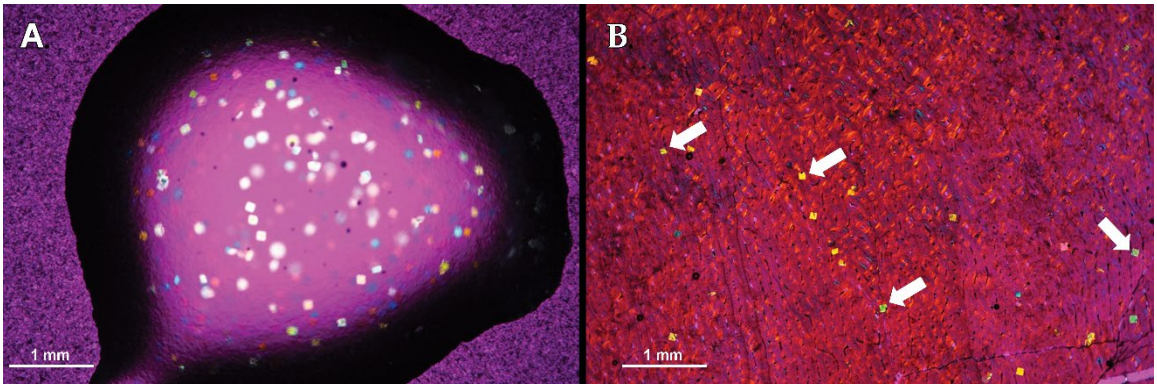

Figure 8. Visual obstructions in the mounting medium 2-ton epoxy resin. The 2-ton epoxy resin is used as a mounting medium for polyester resin embedded specimens to glass slides. (A) A drop of 2-ton epoxy resin imaged showing ‘confetti’ visual obstructions. (B) ‘Confetti’ obstructing tissue visibility in a *Maiasaura* tibia cross-section. Both images taken with a camera mounted to a polarizing light microscope with a ¼ lambda wave plate.

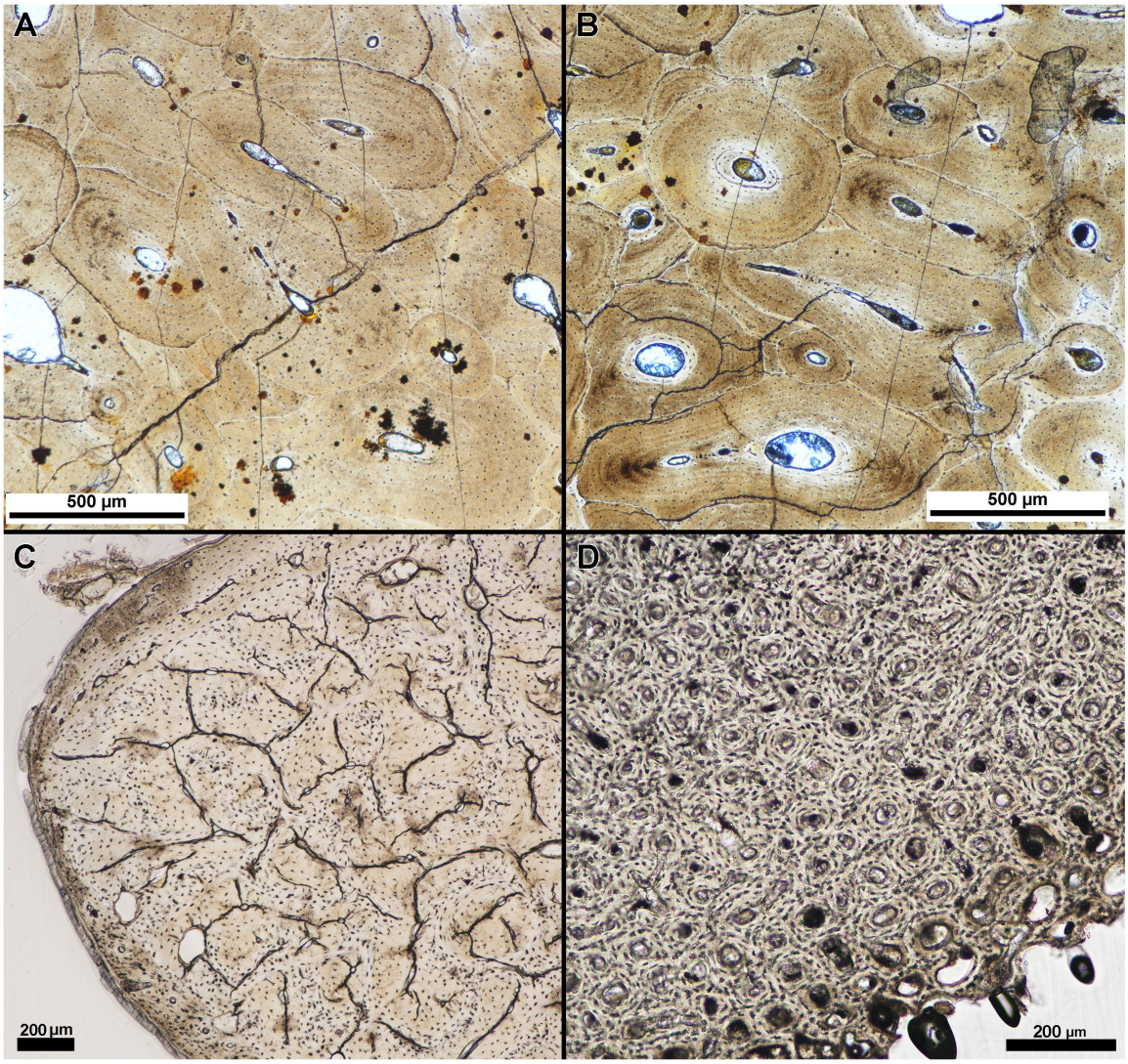

Figure 9. Tissue clarity between polyester and epoxy resin embedded specimens. Separate parts of a fossil rib of an indeterminate taxa were embedded in (A) polyester resin and (B) epoxy resin and the finished sections imaged under linear light with a polarizing light microscope. Tissue clarity, as qualitatively assessed by the authors when viewed with a polarizing light microscope, did not appear to be affected by resin type. (C) Transverse section of the calcaneum of *Dasypus novemcinctus* embedded in polyester resin and (D) transverse section of *Gallus gallus domesticus* humerus embedded in polyester resin. Tissue clarity in modern tissue was not affected by the use of polyester resin.

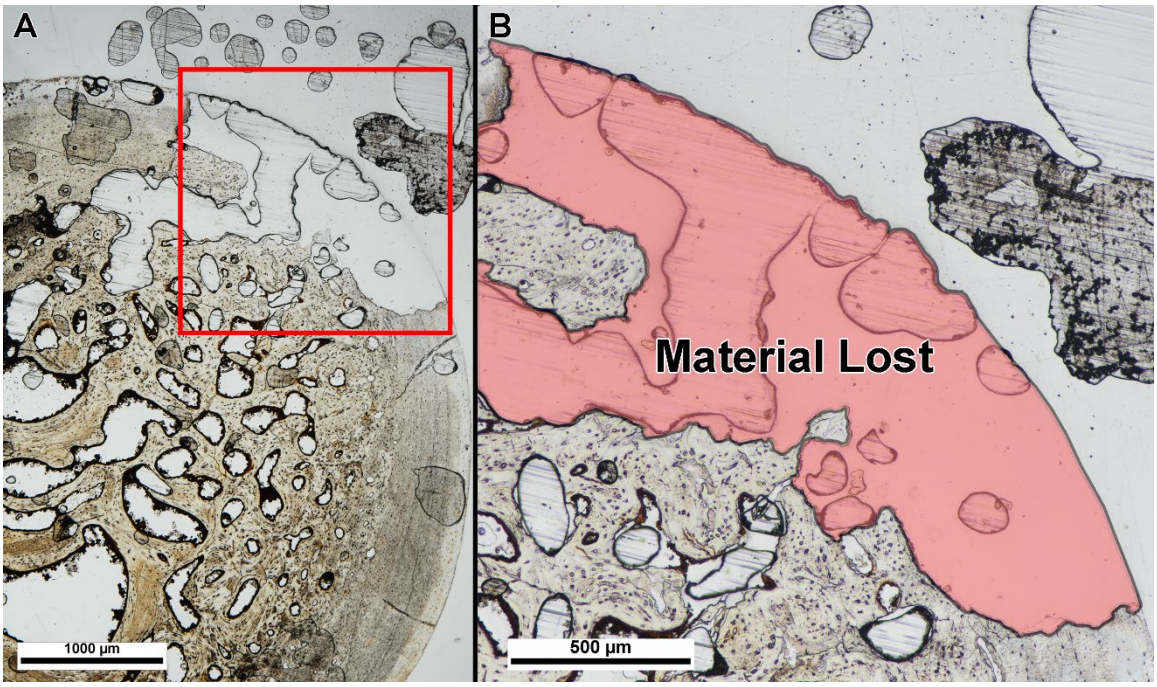

Figure 10. Example of specimen damage incurred during grinding and polishing. (A) Thin section of fossil turtle femur embedded in polyester resin was ground on a lapidary wheel until specimen integrity was lost. (B) Inset of (A) showing region of specimen (red shade) that ripped off of the slide when ground too thin. Image taken under linear polarized light.

CHAPTER III

INTRASKELETAL BONE GROWTH PATTERNS IN THE NORTH ISLAND BROWN KIWI (*APTERYX MANTELLI)*: GROWTH MARK DISCREPANCY AND IMPLICATIONS FOR EXTINCT TAXA.

Introduction

With the importance of applying osteohistology to investigations of extinct vertebrate growth dynamics now firmly established (see Kolb et al. 2015 and Bailleul et al. 2019 for review), further refinements to understanding the relationships between bone biology and life history of present-day vertebrates become increasingly important for permitting more targeted inter- and intra-taxic life history questions using the hard tissue fossil record (Padian and Lamm 2013, Houssaye 2014, Kolb et al. 2015, Bailleul et al. 2019, and references therein). For example, lines of arrested growth (LAGs) form annually within bone cortices of modern vertebrates (e.g. Castanet et al. 2004, Köhler et al. 2012) and, thus, are used to quantify age in extinct vertebrates (e.g. Turvey et al. 2005, Lee and O'Connor 2013, Woodward eet al. 2015). Aging extinct vertebrates enables the study of population dynamics, physiology, and ontogeny (e.g. Erickson et al. 2001, Lee and Werning 2008, Woodward et al. 2015, 2020). However, intraskeletal variation in growth mark counts of modern taxa is rarely examined (e.g. García-Martinez et al. 2011, Woodward et al. 2014, Kolb et al. 2015) and has immediate implications for interpreting and modelling extinct vertebrate growth.

Paleognaths, the sister group to all other modern aves (neognaths), consist of large flightless birds such as the extinct moas and elephant birds, the extinct and extant ostriches, rheas, cassowaries, and emus, and the small tinamous and flightless kiwis (Apterygiformes). Modern aves like kiwis are descendents of non-avian dinosaurs and bone growth characters may conserve phylogenetic signals and be used to reconstruct non-avian dinosaur growth patterns based on bone cortex similarities. Molecular evidence suggests Apterygiformes diversified in response to Pleistocene glaciation and today are comprised of between 5 and 11 species, all of which are at various levels of 'at risk' and declining population sizes (Burbridge et al. 2003, Robertson et al. 2011, Weir et al. 2016). Population decline is a result of several factors including habitat loss, invasive predators, and slow growth rates (McLennan et al. 1996, McLennan et al. 2004, Sales 2005, O'Donnell et al. 2017). Protracted growth (extension of juvenile development phase) in paleognaths is a life history characteristic shared amongst elephant birds, moas, and, despite their small size, kiwis (McLennan et al. 2004, Turvey et al. 2005, Bourdon et al. 2009, de Ricqlès et al. 2016). Slow growth rates, and flightlessness, in kiwis may have developed in response to insular environments lacking major terrestrial predators (Turvey et al. 2005, Bourdon et al. 2009, de Ricqlès et al. 2016). However, slow growth rates in kiwis currently result in prolonged exposure during vulnerable life stages in early ontogeny to invasive terrestrial predators (McLennan et al. 2004). Thus, osteohistological examination can further illuminate growth patterns; information vital for conservation planning and mapping phylogenetic influences on bone growth (e.g. Marín-Moratalla et al. 2013, Legendre et al. 2014). Here, we describe hindlimb and forelimb intraskeletal variation in bone microstructure, including LAG counts, in two North Island brown kiwi (*Apteryx mantelli*) of known age and gender to accomplish several goals:

1) Establish intraskeletal growth mark count variation and potential deviations from known age.

Inferring the ontogenetic age of extinct vertebrates requires consideration of intraskeletal inconsistencies in LAG counts within extant vertebrates. LAGs, and other cyclical growth marks,

represent an annual cessation or slowing of appositional bone growth and are present in vertebrates requiring more than one year to reach adult size (Castanet et al. 1993, Castanet et al. 2004, Köhler et al. 2012). The most complete LAG records in fossils are typically found in long bones, with quantification of maximum annual apposition rates quantified specifically from major weight bearing bones such as the tibia or femur (e.g. Stein and Sander 2009, Padian et al. 2013). However, establishing optimal bones for age and growth rate quantification requires further testing and confirmation in modern taxa (Woodward et al. 2013). Due to variable remodeling rates, LAG counts can vary both intraskeletally and along the length of a single bone, complicating ontogenetic age assessment of extinct taxa given fossil preservation biases, incomplete material, and institutional limitations on "destructive" sampling (e.g. Horner et al. 1999, Hübner 2012, Werning 2012, Cullen et al. 2014). Rates and extent of medullary cavity expansion, cortical drift, and secondary remodeling also vary intraskeletally and are influenced by biomechanical, pathological, physiological, and ecological factors (Enlow 1963, Skedros et al. 2003, Padian 2013, Padian et al. 2016). Therefore, intraskeletal sampling provides insight into the extent of remodeling processes, cortical drift, and ideal sampling locations for aging and assessing growth. A previous report on bone microstructure in several species of kiwi noted the presence of LAGs in femora, tarsometatarsi, and tibiotarsi, and extensive remodeling in tarsometatarsi and tibiotarsi, but precise details of intraskeletal LAG variation were absent (Bourdon et al 2009).

Additionally, the maximum number of LAGs observed in a specimen is often referred to as the 'minimum age at death', recognizing potential discrepancies between maximum LAG counts and actual age (e.g. Kolb et al. 2015). Correlating absolute age and LAG counts is severely understudied due to, in part, insufficient age data in modern vertebrate museum collections. Tracking age in wild individuals requires intense observation, capture-mark-recapture, and tagging: methods that may not be feasible for solitary or scarce taxa. Osteohistology may prove to

be a useful tool in determining absolute age of salvaged kiwi, thus providing essential data for population monitoring and conservation planning. A recent study on wild red deer of known age found cortical growth marks unreliable for accurate aging (Calderón et al. 2019), but growth mark counts correlate with tooth eruption patterns, a well-documented technique for accurate aging in mammals, in captive and wild *Addax nasomaculatis* and *Equus hemionus* (Marín-Moratalla et al. 2013, Nacarino-Meneses et al. 2016). Similar studies are lacking in modern aves, and an alternative aging technique counting periosteal and endosteal lamellae in birds of known age has proven controversial (e.g. Klomp and Furness 1992, Broughton et al. 2002). Sampling captive individuals with extensive life history data, including age at death, is ideal for studying the accuracy of cortical growth marks for aging. Our study tests LAG count accuracy utilizing two captive *A. manetelli* of known age. Establishing ideal bone sampling locations for quantifying age, relative to known age, and growth rates in these brown kiwi specimens will assist targeted bone sampling for establishing baseline life history data vital for conservation planning, as well as to expand the foundational extant bone database so that selection of specific fossil bones for histological analyses is validated.

2) Sex-specific bone microstructure characteristics.

Histological sampling of non-avian dinosaurs (hereafter simply 'dinosaurs') revealed the presence of sex-specific medullary bone in both saurischians and ornithischians (e.g. Schweitzer et al. 2005, Lee and Werning 2008, Hübner 2012, Schweitzer et al. 2016). Medullary bone remains the only character to confirm female sex in dinosaurs despite numerous attempts in identifying sexual dimorphism in dinosaurs (see Mallon 2017 and references therein). Our sample presents the opportunity to analyze differences in cortical bone microstructure between sexes for use in exploring potential sex-specific markers in dinosaur cortical bone. Cortical signals of sex can also assist in identifying sex amongst modern museum specimens or salvaged wild individuals lacking

sex-specific morphological characters, an important utility in using such specimens for assessing wild species population structure and dynamics.

3) Contributions to a broad database of vertebrate bone tissue descriptions.

Life history interpretations from fossil taxa bone microstructure rely on modern bone microstructure descriptions and detailed surveys of modern tissue organization can reveal behavioral correlates to specific bone tissue types (e.g. Padian 2013). For example, recent descriptions of mammalian bone tissue organization suggest a potential link between the presence of secondarily deposited coarse compacted cancellous bone (CCCB) and fossoriality (Legendre and Botha-Brink 2018, Heck et al. 2019). Ecological and life history correlates in tissue organization also lend to conservation planning for related, threatened, or difficult to study species using osteohistological descriptions (Marín-Moratalla et al. 2013, Heck et al. 2019). Moreover, detailed descriptions are important foundational works necessary for future hypothesis testing.

To accomplish these objectives, we provide comprehensive descriptions of tissue organization, vascularity, and growth marks in the appendicular skeleton of the previously undescribed *A. mantelli*. Our study also incorporates forelimb sampling in addition to hindlimb skeletal elements. Finally, the specimens in our sample are of known age and sex, and detailed life history data is available for the female kiwi.

Materials and Methods

Materials

A captive-bred male and female North Island brown kiwi (*Apteryx mantelli*) with recorded life history details were obtained by H.N.W. through arrangements with Kathy Brader, Brown Kiwi Species Survival Program Chairperson for N. Am/EU, and with U.S. Fish and Wildlife Service

import permit number 130066. The male kiwi died of natural causes at the age of 14 years, 4 months. The female died at the age of 5 years, 4 months due to post-egg-laying complications. The female specimen was in the second year of egg production; breeding history was unavailable for the male kiwi. Captive male kiwis typically reach sexual maturity at 2 years and 3 months (Kiwi Captive Management Advisory Committee 2004), therefore, we assume the male kiwi had reached sexual maturity as well. Both specimens were subjected to zoo necropsies and subsequently frozen prior to being shipped to Oklahoma State University – Center for Health Sciences, Tulsa, OK, USA for study. The female kiwi was skeletonized upon arrival whereas the male kiwi was first prepared for diffusible iodine-based contrast-enhanced CT (diceCT) using standard methodology (see Appendix II for complete details) for a separate study. The male kiwi was destained prior to histological processing. Left and right femora, tibiotarsi, tarsometatarsi, humeri, ulnae, and radii from each bird were histologically sampled. Generally, larger weight bearing bones, such as femora, tibiotarsus, and tarsometatarsus, preserve a more complete record of higher apposition rates and can be used to assess annual body mass increases (e.g. Sander and Andrassy 2006, Klein and Sander 2007, Stein and Sander 2009, Campione and Evans 2012, Padian and Lamm 2013). However, very little to no histological descriptions of paleognath forelimb bones have been published. Forelimb histology has previously been examined in ostrich and emu to analyze the correlation of bone tissue organization and absolute growth rates, and, in a separate study, the effects of biomechanical loading on forelimb bone cortices (Castanet et al. 2000, Kuehn et al. 2019). Prior to histological processing, the male kiwi bones were unusually pliable along the longitudinal axis; the mid-diaphyses bent with slight pressure. Preliminary CT scans, prior to iodine-based preparation, suggest diminished mineralization in the male kiwi bones (Pers. Obs. Todd L. Green), but we cannot discount that diceCT preparation or destaining may have had a role in increased pliability (see Early et al. 2020).

Methods

Two serial transverse sections were produced from the mid-diaphysis from limb elements (Fig. 11). The cortices of long bones are thicker at the area of minimum circumference and typically undergo less cortical remodeling relative to the remaining shaft and preserve a more complete record of growth (Sander and Andrassy 2006). Additionally, the occurrence of calcified cartilage, metaphyseal bone, and effects of processes such as trochanters is more limited at the midshaft relative to other regions along the length of the bone; cortical bone growth marks are less likely to be altered at the midshaft than in regions of the metaphysis or muscular processes (Padian et al. 2013). Longitudinal sections were produced from the diaphysis of left femora, tibiotarsi, and tarsometatarsi of both specimens (Fig. 11). Longitudinal sections of forelimb bones were unattainable due to limited material availability from such small bones. Longitudinal sections are used for confirming tissue identifications made from transverse sections (see Stein and Prondvai 2014, Faure-Brac et al. 2019). Specimen chemical processing and ground section preparation followed protocol for extant undecalcified bone in Schweitzer et al. (2007). All sections were stained with toluidine blue at the Woodward Ballard Paleohistology Lab at Oklahoma State University-Center for Health Sciences to enhance contrast of cement lines and LAGs. Bone microstructure descriptions follow standard terminology of Enlow (1963), Francillon-Vieillot et al. (1990), and Huttenlocker et al. (2013) (but see Stein and Prondvai (2014), Prondvai et al. (2014)) and hindlimb myology is derived from McGowan (1979). Figures and additional images available at morphobank.org (P4029).

Results

Osteohistological descriptions are organized by specimen (the female skeleton is described first) to allow for direct comparison of growth mark counts throughout each skeleton.

Female Kiwi

Femur

Tissue that is morphologically consistent with medullary bone (hereafter, simply 'medullary bone') extends into the medullary cavity from the endosteal bone within the female kiwi's left femur (Fig. 12A; see Canoville et al. 2019 for medullary bone description). The endosteal layer of the female kiwi's left femur is composed of a thin band of transversely oriented avascular lamellar tissue, and was undergoing active resorption at the time of the animal's death. The endosteal layer is thickest on the postero-medial side near the attachment region of *M. adductor longus brevis* and thinnest around the antero-medial side. A single spicule of trabecular bone, composed of an outer border of lamellar endosteal tissue around an interior of woven bone, extends into the medullary cavity towards the antero-lateral side from the antero-medial side. The mid-cortex is composed of longitudinally oriented parallel-fibered tissue with regional shifts to transverse orientation and remodeled woven tissue. The remodeled woven tissue with secondary osteons oriented longitudinally and radially composes the cortex on the postero-medial side where the attachment of *M. adductor longus brevis* is located (Fig. 12A). Interestingly, a remodeled woven tissue complex is not present on the postero-lateral side where *M. piriformis pars ilio femoralis* attaches. Instead, the remaining mid-cortex is composed of longitudinally and transversely oriented parallel-fibered tissue. In longitudinal section, the mid-cortex is highly birefringent and osteocyte lacunae are flattened, confirming identifications from transverse views (Fig. 12B). Vascular canals in the mid-cortex are typically simple vascular canals and vascular canals within primary osteons (Fig. 12D); vascular orientation is longitudinal, radial, or reticular. Generally, vascular canals on the medial side have a slight radial tilt, canals are reticular in the deep region of the mid-cortex on the lateral side, and canals elsewhere are longitudinal. LAGs in the mid-cortex are extremely faint and cannot be fully traced around the circumference of the bone due to a lack of contrast. A maximum of three LAGs can be identified postero-medially in the transverse section of the left femur (Fig. 12D), but LAGs could not be identified in the longitudinal section of the same bone (Fig. 12B). The outer cortex of the left femur consists of a thin layer of transversely oriented, low vascular tissue ranging from lamellar to parallel-fibered

around the circumference of the femur (Fig. 12B). Several longitudinal vascular canals are located in the outer cortex (Fig. 12E), which complicates labelling the outer cortex as an external fundamental system (EFS). Instead, the femur of the female kiwi appears to have been actively growing, albeit slowly, as it approached skeletal maturity.

The transverse section of the female kiwi's right femur mostly agrees with tissue and vascular composition described in the left femur. Medullary bone lines the medullary cavity side of endosteal bone and a condensation of tissue forms a crescent shape deep in the medullary cavity (Fig. 12C). The tissue condensation stains partially blue with toluidine blue and is likely a Kastschenko's line (unresorbed mineralized embryonic tissue; see Kastschenko 1881, Haines 1942, Francillon-Vieillot et al. 1990) with medullary bone attached. The medullary bone extends off of the endosteum, contacts, and condenses onto the Kastschenko's line. The Kastschenko's line may simply be a condensation of medullary bone as a Kastschenko's line is unexpected in a nearly skeletally mature individual. This study does not perform the necessary analysis to confirm either explanation. The endosteal layer is thin and displays local regions of lower birefringence in circular polarization, possibly due to collagen fibers oriented perpendicular to plane of section in these darker regions. The medullary border of the endosteal layer displays numerous Howship's Lacunae (Fig. 12C), indicating endosteal resorption was ongoing at the time of death. The endosteal layer is separated from the mid-cortex by a resorption line (Fig. 12G). The mid-cortex is longitudinally oriented parallel-fibered bone, and vascularity is oriented longitudinally, radially, and, rarely, reticularly. The cortex near the *M. adductor longus brevis* attachment site is composed of longitudinally oriented parallel-fibered tissue with few secondary osteons and numerous primary osteons. The muscle attachment site is not as prominent possibly due to slight differences in the location of the section. Maximum LAG count in the transverse section of the right femur is three on the postero-medial side, similar to the left femur. Visibility is higher for a

few LAGs in the right femur under circular polarized light (Fig. 12F), but many of the LAGs remain difficult to discern.

Tibiotarsus

The cortex of the left tibiotarsus has an endosteal layer of transversely oriented, avascular lamellar tissue (Fig. 13A). The medullary border of the endosteal layer was being actively resorbed at the time of death; resorption was concentrated antero-medially. Similar to the right femur, medullary bone extends off of the endosteal layer into the medullary cavity to a potential Kastschenko's line (Fig. 13A, C, D). The endosteal layer is separated from the mid-cortex by a resorption line indicating endosteal resorption of mid-cortical tissue occurred prior to deposition of endosteal lamellar bone. The mid-cortex of the left tibiotarsus is composed of heavily remodeled CCCB (Fig. 13A). Some secondary osteons in the mid-cortex have longitudinally oriented tissue fibers resulting in a darker appearance in circularly polarized light. The mid-cortex of CCCB is thickest on the antero-lateral side and thinnest medially (Fig. 13A). Mid-cortical CCCB is confirmed on the anterior and posterior sides in longitudinal section and appears as large interweaving fiber bundles (Fig. 13C, D). The outer cortex is parallel-fibered tissue with longitudinally oriented simple vascular canals, vascular canals within longitudinally oriented primary osteons, and vascular canals within secondary osteons (Fig. 13E). Additionally, longitudinal sections of the tibiotarsus reveal numerous circumferentially oriented simple vascular canals within the outer cortex (Fig. 13D). Collagen fibers of the outer cortex of parallel-fibered tissue increases in organization towards the periosteal surface; additionally, vascularity within the outer cortex decreases outward towards the periosteal surface. Decreasing vascularity and increasing collagen fiber organization suggests formation of an EFS was in early development in the left tibiotarsus. Within the cortex are up to six possible LAGs (Fig. 13E).

The mid-diaphyseal cortex of the right female tibiotarsus is similar to that of the left tibiotarsus. The medullary bone extends off the endosteal surface to a potential Kastschenko's line, similar to the right femur (Fig. 13B). The endosteal layer is composed of avascular lamellar tissue oriented transversely with few regions of longitudinally oriented lamellar tissue. The mid-cortex is composed of remodeled CCCB and is thin on the medial side (Fig. 13B). The outer cortex is composed of longitudinally oriented parallel-fibered tissue with simple vascular canals oriented longitudinally and vascular canals within longitudinally oriented primary osteons and, rarely, secondary osteons. The outer cortex is likely a developing, or incipient, EFS as in the left tibiotarsus. Very few secondary osteons impede into the outer cortex and, when present, are typically located internally in the outer cortex. Seven LAGs are found on the medial side of the right tibiotarsus (Fig. 13F).

Tarsometatarsus

The mid-diaphysis of the female left tarsometatarsus has an endosteal layer of avascular lamellar tissue oriented transversely (Fig. 14A). Medullary bone extends from the endosteal layer into the medullary cavity (Fig. 14A). Medullary bone is not as prevalent in the tarsometatarsus as in the tibiotarsus or femur. The mid-cortex of the left tarsometatarsus is parallel-fibered tissue of varying organization and orientation with primary osteons and some secondary osteons. The anterior and posterior mid-cortex is composed of longitudinally oriented parallel-fibered tissue as confirmed by longitudinal sampling (Fig. 14A, B). Vascularity in the anterior and posterior mid-cortex is longitudinally oriented simple vascular canals and canals within primary osteons with a few local regions of reticular vascularity. Secondary osteons, when present, are concentrated in the internal regions of the anterior mid-cortex. Tissue organization of the lateral and medial mid-cortex is loosely organized, transversely oriented parallel-fibered bone (Fig. 14A). The lateral-medial axis was not longitudinally sampled and, thus, tissue organization in these regions cannot be confirmed in alternative orientations. Vascularity in the medial and lateral mid-cortex is

primarily longitudinally oriented simple vascular canals and canals within primary osteons in addition to few circumferential canals and secondary osteons. Minimal remodeling has occurred throughout the cortex and secondary osteons, when present, are more prevalent postero-medially and postero-laterally. LAGs are difficult to identify; a total of four LAGs are present in the left tarsometatarsus (Fig. 14F), but are not traceable around the entire circumference. The postero-medial and postero-lateral outer cortex is woven tissue (Fig. 14A), likely formed in response to muscle attachments (e.g. *m. abductor digiti IV* attaches to the postero-lateral corner). The outer cortices at the entheses also contain tissue morphologically consistent with metaplastic hard tissue (sensu Horner et al. 2016; Fig. 14E). Elsewhere, the outer cortex is longitudinally oriented parallel-fibered tissue with few vascular canals oriented longitudinally.

The right tarsometatarsus of the female kiwi was sectioned at the mid-diaphysis and varies slightly from the left tarsometatarsus in terms of mid-cortex tissue organization and vascularity, LAG count, and remodeling. The mid-cortex of the right tarsometatarsus is composed of CCCB and parallel-fibered tissue (Fig. 14C, D). CCCB composes the interior region of the mid-cortex on all sides, but is not present along the entire anterior or posterior sides (Fig. 14C). The posterior mid-cortical vascularity of the right tarsometatarsus is primarily longitudinally oriented vascular canals in primary osteons, similar to the cortex of the left side. However, vascular orientation elsewhere consists of a mix of longitudinal, radial, and reticular canals in primary osteons and very few circumferential vascular canals. Secondary osteon density is higher in the right tarsometatarsus with increased secondary osteons on the anterior and posterior sides. In the right tarsometatarsus, the inner portion of the mid-cortex on the posterior side, where CCCB is absent, has a region of large, longitudinally oriented collagen fibers interrupted by secondary osteons (Fig. 14G). A total of four LAGs are found in the cortex of the right tarsometatarsus.

Humerus

The left and right humeri of the female are similar in tissue organization and vascularity at the mid-diaphysis. The humeri have an endosteal layer of transversely oriented avascular lamellar tissue (Fig. 15A, B). The lamellar tissue was being actively resorbed along its endosteal surface at the time of the animal's death as evidenced by numerous Howship's lacunae along the endosteal surface (Fig. 15B). The mid-cortex is remodeled parallel-fibered tissue with primary tissue fibers oriented transversely. A resorption line separates the endosteal layer and the mid-cortex indicating the endosteal side of the mid-cortex was resorbed prior to deposition of the endosteal lamellar tissue (Fig. 15B). Vascularity in the mid-cortex is longitudinally oriented simple vascular canals and vascular canals within longitudinally oriented primary and secondary osteons. The secondary osteons are large and lamellar fibers are oriented longitudinally (SO appear dark in circularly polarized light and lacunae are round) (Fig.15A). There are four LAGs in the cortex of both humeri (Fig. 15B). The outer cortex of the humeri have avascular longitudinal parallel-fibered tissue in addition to local regions of transversely oriented avascular lamellar tissue.

Radius

The left and right radii of the female kiwi were sectioned at the mid-diaphysis and have an endosteal layer of avascular lamellar tissue that was being resorbed along the endosteal surface (Fig. 15C, D). The mid-cortex of both radii is composed of parallel-fibered tissue primarily oriented transversely, but local shifts to longitudinal orientation occur. Few simple vascular canals oriented longitudinally and obliquely are present in the mid-cortex in addition to few secondary osteons (Fig. 5C). The outer cortex is avascular lamellar tissue that shifts between transverse and longitudinal orientation around the bone and is interpreted as an EFS (Fig 15C). Three LAGs were found in the mid-cortex of both the right and left radii (Fig. 15D).

Ulna

The left and right ulnae have an endosteal layer of avascular, transversely oriented lamellar tissue undergoing resorption on the endosteal surface (Fig. 15E, F). The mid-cortices of both ulnae are composed of remodeled, transversely oriented parallel-fibered tissue (Fig. 15E). A resorption line separates the endosteal lamellar tissue from the mid-cortex in both ulnae. Mid-cortical vascularity is longitudinally oriented simple vascular canals and vascular canals within longitudinally oriented primary and secondary osteons (Fig. 15E, F). The outer cortex of the ulna is EFS of avascular, transversely oriented lamellar tissue with local regions of longitudinal fibers, similar to the outer cortex of the female humeri. The longitudinal fibers are likely components of either parallel-fibered or lamellar tissue, but the ulnae were not longitudinally sectioned to confirm the tissue identification. The outer cortex is separated from the mid-cortex by a resorption line indicating the ulnae had undergone periosteal resorption prior to deposition of the EFS. Four LAGs were found in the outer cortex of both ulnae (Fig. 15F).

Male Kiwi

Femur

The left femur of the male kiwi has a thin endosteal layer of avascular, transversely oriented lamellar tissue (Fig. 16A). The endosteal layer is separated from the mid-cortex by a resorption line (Fig. 16D). The mid-cortex of the left femur is composed of remodeled, transversely oriented parallel-fibered tissue (Fig. 16A, B, D). Remodeling is less extensive in the mid-cortex on the anterior and antero-lateral sides; mid-cortical vascularity is, instead, vascular canals within longitudinally oriented primary osteons. Secondary osteon density in the mid-cortex increases along the medial and lateral side of the femur (Fig. 16E); secondary osteon density peaks on the posterior side of the femur. Longitudinal sections show secondary osteon density also increasing distally on the anterior and posterior sides of the femur (Fig. 16B). Few radial canals are present on the anterior side of the femur. The outer cortex of the left femur is an EFS of avascular

lamellar tissue oriented transversely (Fig. 16D). Few secondary osteons have invaded the outer cortex on the posterior, postero-medial, and postero-lateral sides of the femur (Fig. 16E). A maximum of three LAGs are present in the mid-cortex of the left femur and four additional LAGs are found in the EFS (Fig. 16D).

The right femur of the male kiwi has an endosteal layer of avascular, transverse oriented lamellar tissue separated from the mid-cortex by a resorption line (Fig. 16C). The mid-cortex of the right femur is composed of remodeled parallel-fibered tissue and remodeled CCCB. The collagen fibers of the parallel-fibered tissue are generally oriented transversely with local regions of longitudinal fibers. The interior of the antero-medial mid-cortex is CCCB separated from the external mid-cortical parallel-fibered tissue by a resorption line. Vascular canals within secondary osteons are oriented longitudinally and are most dense on the posterior side within the mid-cortex. Vascular canals within primary osteons are oriented longitudinal, circumferential, and radially throughout the parallel-fibered component of the mid-cortex (Fig. 16F, G). The right femur was cut at the level of a nutrient canal penetrating the cortex at the attachment site of *M. adductor longus brevis* (Fig. 16C). The nutrient canal-attachment site is surrounded by radially oriented, highly organized, parallel-fibered tissue as it penetrates through the cortex toward the medullary cavity, but the region of outer cortex in which the canal passes through is composed of longitudinally oriented lamellar tissue. The posterior edge is also the attachment site of *M. adductor longus et brevis*; tissue organization on the posterior side is likely the result of nutrient canal and muscle attachment site development. The outer cortex of the right femur is an EFS of avascular, transversely oriented lamellar tissue with regional shifts in organization to parallel-fibered tissue. There is a maximum of seven LAGs in the right femur: three LAGs in the mid-cortex and four LAGs within the EFS (Fig. 16F, G).

Tibiotarsus

The mid-diaphysis of the left tibiotarsus has a thin endosteal layer of avascular, transversely oriented lamellar tissue (Fig. 17A). The endosteal layer is separated from the mid-cortex by a resorption line and the mid-cortex is composed of remodeled parallel-fibered tissue; collagen fibers of parallel-fibered tissue is oriented transversely (Fig. 17A, C–E). Vascularity in the mid-cortex consists of vascular canals within longitudinally oriented secondary osteons in addition to vascular canals within longitudinally and circumferentially oriented primary osteons (Fig. 17E). The outer cortex of the left tibiotarsus is an EFS of avascular, transversely oriented parallel-fibered tissue with local regions of lamellar tissue (Fig. 17C-E). Few secondary osteons are present in the EFS. The left tibiotarsus has two LAGs in the mid-cortex and three LAGs within the EFS.

The mid-diaphysis of the right tibiotarsus has a very thin endosteal layer of avascular lamellar tissue with transversely oriented fibers (Fig. 17B, F-G). The endosteal layer is separated from the mid-cortex by a resorption line (Fig. 17F). The mid-cortex of the right tibiotarsus is heavily remodeled, parallel-fibered tissue with longitudinally oriented simple vascular canals and vascular canals within longitudinal primary and secondary osteons (Fig. 17B, F). Remodeling is less extensive on the postero-medial region. Parallel-fibered tissue of the mid-cortex is primarily oriented transversely with regional shifts to longitudinal orientation. The outer cortex is composed of an EFS of avascular, transversely oriented lamellar tissue with little remodeling (Fig. 17B, F); secondary osteons are present in the outer cortex on the antero-medial and lateral sides (Fig. 17G). The right tibiotarsus has three LAGs in the mid-cortex and three additional LAGs in the EFS (Fig. 17F).

Fibula

The right and left fibulae were also sectioned with the male tibiotarsi at the mid-diaphysis level of the tibiotarsi. Both fibulae were entirely remodeled and composed of longitudinally oriented secondary osteons.

Tarsometatarsus

The mid-cortex of the left tarsometatarsus is partially obstructed by unusually darkened regions (Fig. 18A). The obstruction is likely the result of prolonged submersion in formalin solution. Regardless, an endosteal layer of avascular, transversely oriented lamellar tissue is visible but incomplete along the endosteal border of the cortex (Fig. 18A, B). The endosteal layer is thickest on the posterior side of the tarsometatarsus and thinnest on the anterior side. The endosteal layer is separated from the mid-cortex by a resorption line. The mid-cortex, though partially obscured, is heavily remodeled parallel-fibered tissue with longitudinally oriented vascular canals within primary and secondary osteons (Fig. 18A, B). Longitudinal sectioning reveals some variation in osteon orientation, but the majority of osteons are oriented longitudinally (Fig. 18B). The extent of remodeling is difficult to discern due to obstructions, but remodeling appears concentrated on the posterior side. Anteriorly, the mid-cortical parallel-fibered tissue is oriented longitudinally as confirmed by longitudinal sectioning (Fig. 18B). The mid-cortex parallel-fibered tissue is continuous with the outer cortex on the anterior, postero-medial, and postero-lateral sides of the tarsometatarsus. The outer cortex of the medial, lateral, and posterior sides is a thin layer of avascular lamellar tissue with few secondary osteons and is interpreted as an EFS. However, the external portion of the outer cortex of the postero-medial and postero-lateral side appears to have been torn and is absent (Fig. 18A). Obstructions block LAG visibility in the mid-cortex, but a maximum of two LAGs are present in the outer cortex of the left tarsometatarsus on the anterior side (Fig. 18D).

Regions of the endosteal layer and innermost cortex of the right tarsometatarsus are also partially obscured (Fig. 18C). An endosteal layer of avascular, transversely oriented lamellar tissue is present in unobstructed areas and partially visible through the darkened obstruction. The endosteal layer and mid-cortex are separated by a resorption line indicating endosteal resorption of the mid-cortex occurred prior to deposition of the endosteal lamellar tissue. The mid-cortex is remodeled, vascular parallel-fibered tissue oriented transversely (Fig. 18C). Primary parallel-fibered tissue is less remodeled on the lateral and medial sides. Vascular canals of the mid-cortex are contained within longitudinally oriented primary and secondary osteons (Fig. 18E). The outer cortex is parallel-fibered tissue oriented transversely with little remodeling concentrated postero-medially. The outer cortex of the right tarsometatarsus is likely an EFS, though the tissue is less organized than in the left tarsometatarsus. The right tarsometatarsus has one LAG in the mid-cortex and one LAG within the outer cortex (Fig. 18E).

Humerus

The left humerus of the male kiwi was sectioned proximal to the mid-diaphysis, while the right humerus was sectioned at the mid-diaphysis (Fig. 11). Both humeri have an endosteal layer of avascular lamellar tissue showing signs of resorption along the layer's endosteal border (Fig. 19A). The endosteal layer is separated from the mid-cortex by a resorption line (Fig. 19B). The mid-cortex of the humerus is entirely remodeled and, thus, composed of longitudinally oriented secondary osteons (Fig. 19A, B). The outer cortex is avascular lamellar tissue and is separated from the mid-cortex by a resorption line (Fig. 19B). A maximum of four LAGs are present in the outer cortex of the right humerus (Fig. 19B), but LAGs could not be identified in the left humerus.

Ulna/ Radius

Removal of soft tissue from small fragile forelimb elements was difficult due to excess formalin fixation prior to skeletonization. The forearms of the male kiwi were embedded without skeletonizing and sectioned approximately at the mid-diaphysis, but section location could not be visually confirmed due to remaining soft tissues. The right forearm sections contained both the ulna and radius, however, the left forearm sections did not contain either bone. Therefore, we will only describe the right ulna and radius of the male kiwi. The right ulna and radius of the male kiwi are composed entirely of secondary osteons oriented parallel to the long axis of the ulna. LAGs were not visible in either of the male ulnae or radii (Fig. 19C, D).

Discussion

Variation in tissue organization

In general, bone tissue organization is best described as a spectrum from highly unorganized woven tissue to highly organized lamellar tissue, and tissue organization reflects rate of bone deposition (e.g. Amprino 1947, Francillon-Vieillot et al. 1990). In agreement with Bourdon et al. (2009), primary tissue organization in the long bones of the male and female North Island Brown Kiwi is parallel-fibered, interrupted by cyclical growth marks, and with mostly longitudinal vascular canals within primary and secondary osteons. Cortical primary organization increases and cortical vascularity decreases from the innermost cortex to the periosteal surface in both kiwis. Primary osteons within male and female cortices exhibit few lamellae and osteocyte lacunae, potentially fitting loose definitions of 'incipient primary osteons' (Woodward et al. 2014). Neither kiwi exhibited sexually dimorphic cortical tissue organization or vascularity, with the exception of medullary bone within the medullary cavity of female hindlimb elements. Thus, skeletal growth patterns in the kiwi consist of cyclically deposited parallel-fibered tissue with decreasing vascularity through ontogeny, a departure from typical avian bone which consists of uninterrupted, rapidly deposited woven tissue (Bourdon et al. 2009).

Modern and fossil aves are severely under-represented in osteohistological descriptions (Wood and de Pietri 2015). Histological descriptions have been completed for relatively few avian taxa such as Charadriformes (Smith and Clarke 2014), Anseriformes (e.g. Marsà et al. 2019), Sphenisciformes (e.g. Cerda et al. 2015), Paleognaths (e.g. Turvey et al. 2005), and several basal forms such as *Hesperornis* and *Ichthyornis* (Chinsamy et al. 1998, Wilson and Chin 2014). These previous investigations have revealed a shared growth strategy among most ornithurines, including most paleognaths, in which fibrolamellar tissue is rapidly deposited followed by the deposition of an EFS, or outer circumferential layer (OCL), with the attainment of skeletal maturity. However, kiwi bird limb bone growth strays from this general pattern. Instead, appositional growth is much slower throughout the individual's life, as indicated by cyclical parallel-fibered tissue, which is similar to patterns found in some Enantiornithines (e.g. Chinsamy et al. 1995). Similar to most ornithurines, and indeed most vertebrates, skeletal maturity in the kiwi was represented by an EFS (or OCL) of avascular lamellar and parallel-fibered tissue (e.g. Ponton et al. 2004, Woodward et al. 2013). Slow, protracted growth over many years is unique among most ornithurines, and in the kiwi bird is likely due to a combination of 1) the kiwi's low basal metabolism relative to other aves and 2) environmental factors such as limited resources and the historical absence of large predators in New Zealand (McLennan et al. 2004, Bourdon et al. 2009). We review each factor in turn:

1) Bone tissue organization and vascular density/ orientation directly reflect growth rate which is correlated to physiological parameters such as metabolic rates (Amprino 1947). Relatively high growth and metabolic rates in most modern aves results in bone cortices composed of fast growing fibrolamellar tissue (e.g. Turvey et el. 2005). Kiwi have notably lower metabolic rates relative to most modern aves (Calder and Dawson 1978, McNab 1994); lower metabolic rate and lower growth rates result in slower forming parallel-fibered tissue in the kiwi bone cortices. 2) Vertebrates with high growth rates lower certain predation risks based on body size attainment

alone, but high growth rates also require high energetic demands and resource consumption. The kiwi evolved in resource limited environments devoid of large nocturnal predators (Lee et al. 2001, Holdaway et al. 2001). McLennan et al. (2004) suggest the absence of predators allowed kiwi life history to freely develop in order to minimize energy requirements, thus, resulting in protracted growth, extreme precociality, small size, and reduced metabolic rates.

Parallel-fibered tissue in kiwi cortices appears to be a reflection of growth and physiology, but behavior and biomechanical function are also represented in the form of a peculiar tissue type: CCCB. CCCB is formed by osteoblast activity depositing new tissue along the endosteal margins of trabeculae resulting in the infilling of empty space between trabecular struts (Enlow 1963). The overall process of CCCB formation transforms cancellous bone into compact bone and typically occurs during cortical drift. CCCB is a peculiar tissue and has been described in a variety of taxa including armadillos (Heck et al. 2019), aardvarks (Legendre and Botha-Brink 2018), wombats (Walker et al. 2020), rodents (Montoya-Sanhueza and Chinsamy 2017, Garrone et al. 2019), and some non-avian dinosaurs (e.g. Woodward et al. 2018, Avrahami et al. 2019), though some authors note that CCCB is difficult to identify and may be more widespread throughout vertebrate cortical tissue than originally thought (Heck et al. 2019). Nonetheless, CCCB is currently hypothesized to be indicative of fossorial behavior to some degree and has been used to infer fossorial behavior in orodromine non-avian dinosaurs, though the link between behavior and tissue type is complex (Legendre and Botha-Brink 2018, Avrahami et al. 2019). CCCB in the cortices of the kiwi, though sparse and inconsistent in location, provides another example of a link between this particular tissue and fossorial lifestyles; kiwis utilize their hindlimbs in the construction of numerous burrows across their home range and in scratch digging during foraging, similar to behaviors observed in the nine-banded armadillo (Sales 2005).

In addition to influences stated previously, tissue composition in modern birds and some non-avian dinosaurs is also influenced by a sex-specific behavior: egg-laying. Medullary bone is

formed in female birds during the egg-laying cycle as a calcium reservoir, and confirmation of its identification is highly dependent on chemical analyses (Schweitzer et al. 2016). This tissue forms in the medullary cavity of female birds along the endosteal margin of the cortex and is typically woven in organization and highly vascular (e.g. Werning 2018, Canoville et al. 2019). Medullary bone has been identified in some non-avian dinosaurs and is currently the only reliable method of extinct dinosaur sex-determination (Bailleul et al. 2019 and references therein). However, observation of medullary bone in modern or fossil specimens is highly dependent on the timing of an animal's death as medullary bone is resorbed and catabolized for eggshell formation. In the current study, the female kiwi died of complications shortly after an egg-laying event and medullary bone is found in the hindlimb cortices of the female kiwi. The distribution of medullary bone appears to decrease distally among femora, tibiotarsi, and tarsometatarsi and distally within each element as observed in longitudinal sections. Werning (2018) used a candling method to describe the distribution of medullary bone across modern avian groups and described medullary bone in the humerus, femur, and tibiotarsus of the kiwi. Additionally, Canoville et al. (2019) investigated the extent of intraskeletal medullary bone across aves and observed consistent presence of medullary bone in the *Rhea* and Tinamidae ulnae and radii. Medullary bone was not found in the forelimbs of the female kiwi in the current study, and more rigorous chemical processing is necessary to fully describe the presence and intraskeletal distribution of medullary bone in kiwis generally.

LAG Count Variation

Lines of arrested growth are used to assess absolute age, skeletal maturity, and sexual maturity in extant and extinct vertebrates (see Woodward et al. 2013). In turn, aging extinct vertebrates allows further analyses of population structure dynamics, heterochrony, and intraspecific variation of growth rates. Life history reconstruction relies on accurate aging techniques, but processes such as medullary cavity expansion, cortical remodeling, and periosteal resorption can

obliterate cortical growth marks vital for accurate aging (Woodward et al. 2013). Intraskeletal sampling of modern vertebrates of known age is necessary for establishing optimal sampling locations for aging and potential differences between known age and LAG count (e.g. Castanet et al. 2004). Here, North Island Brown Kiwi exhibit intraskeletal variation and LAG count variation in relation to known age (Table 3).

The 14 year-old male kiwi has extensive remodeling, medullary cavity expansion, and periosteal resorption that likely obliterated numerous LAGs in all sampled skeletal elements. Regardless, large, weight-bearing hindlimb elements contain the highest number of observable LAGs: both femora have seven LAGs and tibiotarsi have a maximum of six LAGs. Tarsometatarsi, fibulae, and forelimb elements have higher levels of resorption and remodeling and, thus, have lower LAG counts and are therefore likely unreliable age indicators in older kiwis. The 5 year-old female kiwi has far less remodeling in all skeletal elements. Forelimb and hindlimb elements have 3-4 LAGs, with the exception of 6-7 LAGs in the tibiotarsi. The large disparity in LAG count between the tibiotarsi and other skeletal elements may indicate a delayed onset of extensive cortical remodeling and obliteration of previously formed LAGs in the tibiotarsi, but a more comprehensive ontogenetic sample is required to test this hypothesis.

LAG count varied from known age in both specimens. Remodeling likely obliterated previously deposited LAGs in the male kiwi long bones, but a more extensive ontogenetic series is needed to confirm remodeling processes. Still, a decoupling of age and LAG deposition after attainment of skeletal maturity is supported by our observations of the 14 year-old male kiwi and is consistent with observations of wild red deer (Calderón et al. 2019) and captive mouse lemurs (Castanet et al. 2004). *Apteryx mantelli* skeletal maturation is obtained at approximately 4.5 – 6 years of age followed by low rates of periosteal bone deposition, typically resulting in an EFS (Beale 1985, Beale 1991, Bourdon et al. 2009). LAG counts within the EFS of the 14 year-old male kiwi reach a maximum of four in the mid-diaphysis of the femur; eight to ten LAGs would be expected in

the EFS given tight coupling between age and LAG deposition. The 5 year-old female kiwi also has, generally, lower cortical LAG counts relative to age, likely a result of LAG obliteration due to medullary cavity expansion. Curiously, the female tibiotarsi have 6-7 LAGs: 5-6 within the cortex and one LAG in the EFS. Intraskeletal disparity in LAG counts may also be a reflection of increase resource availability or artificial photoperiodicity (see Castanet et al. 2004) in captivity and not a true representation of wild kiwi growth mark deposition (Prier et al. 2013).

Bone growth marks are formed in correlation to unfavorable seasons or events interrupting normal bone growth (e.g. Köhler et al. 2012, Nacarino-Meneses and Köhler 2018). For example, weaning lines have been observed in bone cortices of some mammals (e.g. Morris 1970, Nacarino-Meneses and Köhler 2018) and hatching lines have similarly been described in reptiles (e.g. Hugi and Sánchez-Villagra 2012), amphibians (e.g. Bruce and Castanet 2006), and archosaurs (e.g. Rogers et al. 2016). Bone growth mark morphology varies and can be a distinct zone of tissue or a distinct hypermineralized line, as in a LAG (see Francillon-Vieillot et al. 1990, Klevezal 1996, Woodward et al. 2013 and references therein). LAGs are typically formed annually (e.g. Castanet et al. 2004, Köhler et al. 2012), though the presence of 'double-LAGs' or 'triple-LAGs' in vertebrate long bone cortices is likely a sign of some developmental plasticity (e.g. Klein et al. 2019). Starck and Chinsamy (2002) examined cortical bone response, including LAG formation, to variable environmental conditions on the Japanese quail (*Coturnix japonica*). The authors implemented food limitations and biomechanical loading to separate experimental groups of *C. japonica*, but neither environmental condition induced the formation of annuli, LAGs, or other growth marks. Excess LAGs in the bone cortices of the kiwi, in addition to the results of Starck and Chinsamy (2002), indicate plasticity in LAG formation is complex and requires further investigation. The innermost growth mark in the female kiwi may be a hatching line explaining the discrepancy between LAG count and actual age. However, the innermost LAG is morphologically similar to other LAGs within the cortex of the tibiotarsi. Alternatively, the

presence of excess LAGs within bone cortices of the female *A. mantelli* could be the cessation of growth correlating with late stages of egg development.

Egg production is a massive undertaking for kiwi; additional energy expenditures equivalent to near 100% of the female kiwi's basal metabolic rate are required during the period of egg production (Prinzinger and Dietz 2002). An average North Island Brown Kiwi weighs approximately 2.2kg and lays an egg around 416g, an egg weight 400% higher than expected relative to body mass (Prinzinger and Dietz 2002, Sales 2005). Egg production and laying results in significant weight loss in female North Island Brown Kiwis (Potter et al. 1996). Appositional bone growth may slow or halt during this period as resources and energy are focused and mobilized for egg production. Formation of a LAG in response to egg-laying would be a sexually dimorphic signal within the bone cortices with potential utility in determining sex in extinct archosaurs. Our current investigations cannot confirm this potential dynamic, but more intensive ontogenetic sampling may resolve such a hypothesis. Regardless, excess number of LAGs in the kiwi cortices is evidence of plasticity in LAG formation, though excess LAGs may be a product of artificial conditions in captive rearing. Studies examining cortical growth marks in wild individuals of known age are necessary to confirm our results, because these findings have widespread implications on previous, and future, skeletochronological analyses in fossil taxa.

Implications for extinct taxa

Growth marks in extinct dinosaurs, both avian and non-avian, are used to assess ontogenetic changes, sexual maturity, and skeletal maturity (see Padian and Lamm 2013, Bailleul et al. 2019 and references therein). Construction of non-avian dinosaur growth curves rely heavily on cortical bone growth marks (e.g. Woodward et al. 2015) and, often, the assumption of minimal intraskeletal variation. Intraskeletal variation has often been ignored as a potential source of error due to (1) a lack of foundational intraskeletal examinations such as this study; (2) the scarcity of

the fossil record; and (3) limitations on specimen availability for histological sampling. For example, Erickson and Tumanova (2000) constructed growth curves for the ceratopsian *Psittacosaurus mongoliensis* using growth marks from fragmented samples of humeri, femora, and tibiae. Potential intraskeletal variation in *P. mongoliensis* would lead to inaccurate growth curves and possibly misleading inferences of other fossil taxa. Here, intraskeletal growth mark variation in the kiwi highlights the need for consistency in skeletal element sampling for quantitative analyses and interpretations.

Numerous intraskeletal examinations of non-avian dinosaur taxa suggest skeletal elements with limited medullary cavity expansion, such as weight-bearing limb bones, contain the highest number of growth marks (e.g. Horner et al. 1999, Cullen et al. 2014). The large hind limb elements of the kiwi contain the highest number of growth marks, similar to growth mark variation found in some mammals (e.g. Sander and Andrassy 2006, García-Martínez et al. 2011) and non-avian dinosaurs (e.g. Horner et al. 1999). The cortex of the kiwi fibulae does not contain any growth marks, is composed entirely of remodeled tissue, and has limited expansion of the medullary cavity. Similarly, non-weight-bearing bones of the forelimb were composed primarily of remodeled tissue and LAG counts lower than those found in the hindlimb elements and support hypotheses stated in Padian et al. (2016), that remodeling in reduced forelimbs is likely a manifestation of metabolic processes rather than a biomechanical response due to minimal usage (Padian et al. 2016). Our findings provide more support for the use of large weight-bearing limb bones in examining skeletochronology of extinct dinosaur taxa.

Skeletal maturity can be assessed histologically by the presence of an EFS lining the outer bone cortex. An EFS is composed of avascular, slowly deposited tissue such as parallel-fibered bone or lamellar bone and is the result of drastic reductions in bone apposition. Cortical primary tissue can transition into an EFS or can be delineated from the outer EFS by a periosteal resorption line. The presence of an EFS within a single bone cortex indicates the attainment of maturation for that

specific bony element. However, each skeletal element has its own ontogenetic trajectory and each bone varies in timing of maturity. Therefore, overall skeletal maturity can only be assessed through the identification of widespread EFS presence throughout an individual's skeleton. The presence of an EFS is vital to our interpretations of extinct organisms' life histories. Histological signals of skeletal maturation have been used to assess the validity of distinct non-avian dinosaur taxa (Woodward et al. 2020), assign specimens to specific species (e.g. Cullen et al. 2020), elucidate intraskeletal variation in somatic maturation (e.g. Woodward et al. 2015), and investigate faunal responses to climatic events such as the cataclysmic Permian-Triassic mass extinctions (e.g. Botha-Brink et al. 2016). Here, an EFS is found in the cortices of all hindlimb bones sampled from the male kiwi, but the forelimb cortices are completely remodeled. Likewise, an EFS is present in the tarsometatarsus, tibiotarsus, and femora of the female kiwi, but is not present in the forelimbs. In all elements with an EFS, the primary cortical tissue transitions into the outer avascular lamellar/ parallel-fibered tissue complex indicative of skeletal maturity. Primary tissue in the female kiwi forelimb elements is PFB with minimal vascularity and little remodeling, characteristics that obscure a transition from typical primary bone growth to skeletal maturity due to their similarity in tissue organization with an EFS. The forelimb elements of the kiwi are extremely small in relation to the kiwi forelimbs due to flightlessness and appositional bone deposition in smaller long bone elements is, in general, slower compared to deposition rates in larger weight bearing elements. Lower apposition rates in small long bones results in tissue organization and vascular densities similar those found in the EFS of larger long bones, thus obscuring the presence of an EFS in smaller long bones.

The interpretations of osteohistological characters in extinct taxa is dependent on observations made of modern species. Further sampling and investigations of modern taxa are necessary to refine our understanding of the evolution of life histories across vertebrates (e.g. Houssaye 2014, Wood and de Pietri 2015). Modern aves present a unique group whose life history characteristics

are applicable in interpreting growth and biology of non-avian dinosaurs in addition to fossil neornithines. The findings of this current study impact the interpretations of cortical growth marks, external fundamental systems, and intraskeletal variation in extinct taxa, but a larger sample of individuals across ontogeny is necessary to confirm and expand upon our results.

Conclusions

Intraskeletal variation in tissue organization, vascularity, and growth mark counts in the North Island Brown Kiwi has been fully described for the first time. The tarsometatarsus, tibiotarsus, femur, humerus, ulna, and radius of a captive raised female kiwi and male kiwi of known age were histologically sampled. Generally, tissue organization reflected the kiwi's low metabolic rates and protracted growth; cortices of hindlimb elements were composed primarily of cyclical parallel-fibered tissue, longitudinal vascular canals, sparse secondary osteons, and local regions of CCCB. The 14-year old male kiwi forelimb cortices exhibited extensive remodeling, obliterating primary tissue and growth marks. Intraskeletal LAG counts in the male kiwi hindlimbs and female kiwi forelimbs and hindlimbs were inconsistent and rarely aligned with known age of each individual. In particular, LAG counts in the female tibiotarsi exceeded the actual age of the individual. We advise caution when using LAGs as age indicators in skeletally mature kiwis, though decoupling of age and LAG deposition may be due, in part, to abnormal resource availability in captivity. This study adds to an increasing extant osteohistological database and serves as a useful comparative tool for the interpretation of growth marks in non-avian dinosaurs.

Tables

Table 3. Counts of lines of arrested growth identified in each skeletal element of the male and female *Apteryx mantelli*.

Skeletal Element	Female (5 years-old)	Male (14 years-old)
Left Femur	3	7
Right Femur	3	7
Left Tibiotarsus	6	5
Right Tibiotarsus	7	6
Left Tarsometatarsus	4	2
Right Tarsometatarsus	4	2
Left Humerus	4	-
Right Humerus	4	4
Left Radius	3	-
Right Radius	3	-
Left Ulna	4	-
Right Ulna	4	-

Figures

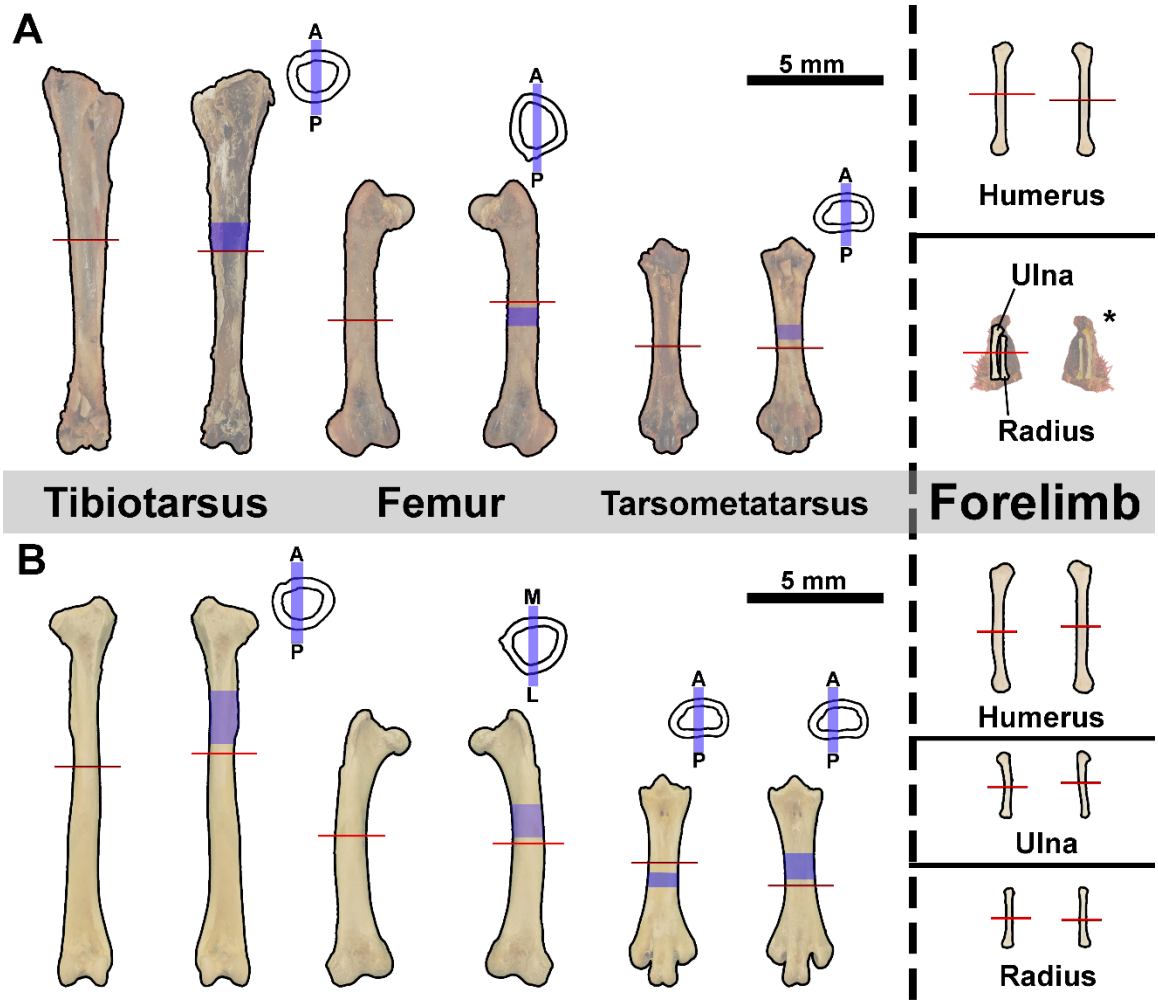

Figure 11. Cut-line locations. Transverse sections (red lines) taken, approximately, from the mid-diaphysis of (A) male kiwi and (B) female kiwi hindlimb and forelimb elements. Longitudinal sections taken from each left hindlimb diaphysis (blue shading). Longitudinal sections were either taken along medial-lateral axis or anterior-posterior (see blue bars on simplified cross-sections).

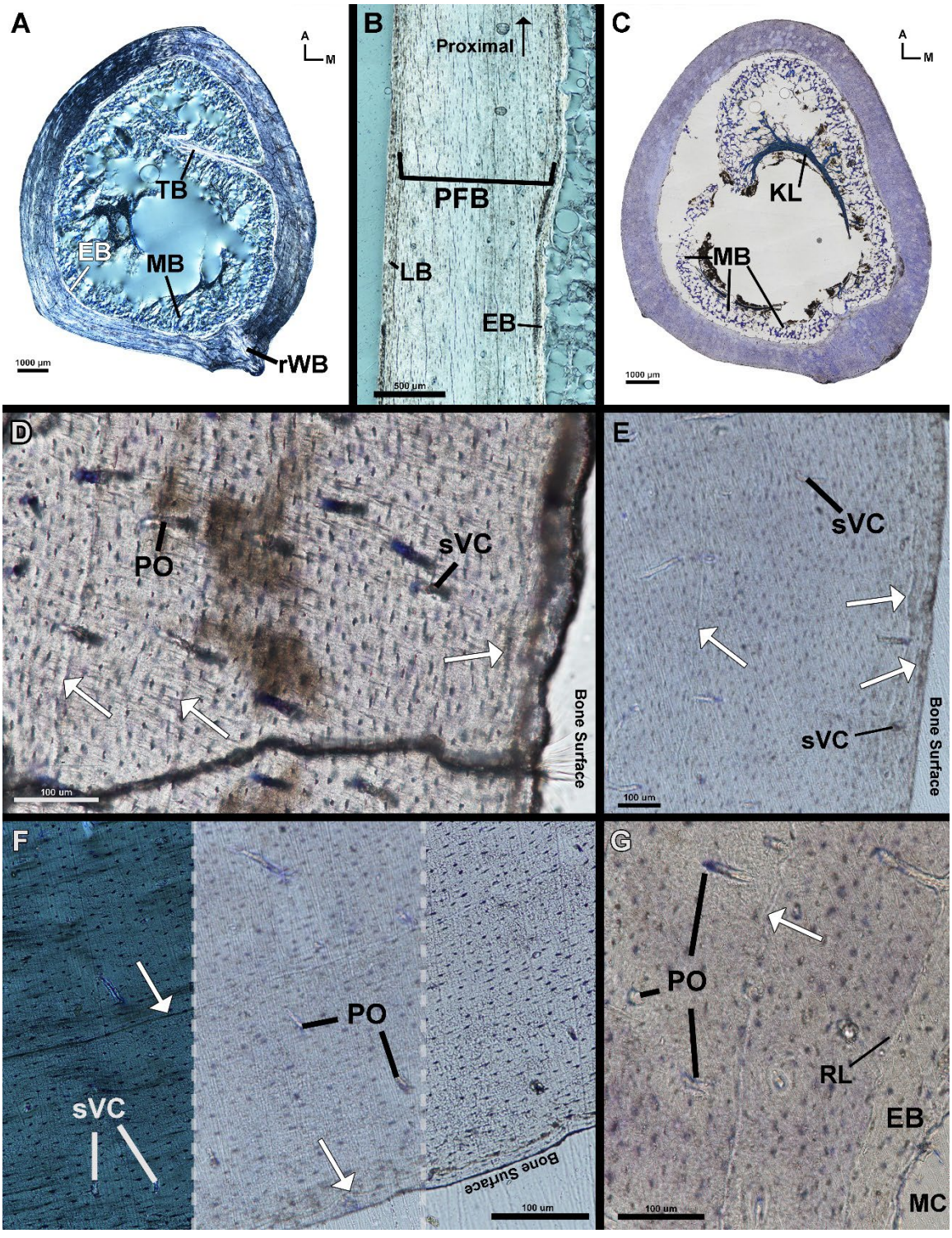

Figure 12. Female kiwi femora microstructure. (A) Transverse section of left femur under circular polarized light showing highly birefringent endosteal lamellar bone and remodeled woven bone in the poster-medial corner. (B) Longitudinal section of left femur medial diaphysis under circular polarized light. Mid-cortical parallel-fibered bone fibers are oriented parallel to section as

indicated by elongated osteocyte lacunae. Osteocyte lacunae of outer cortical, transversely oriented, lamellar bone are plump and rounded. (C) Transverse section of toluidine stained right femur under linear light. Medullary bone extends off endosteal surface and attaches to a crescent shaped Kastschenko's line within medullary cavity. Endosteal resorption is evident from multiple Howship lacunae (insert). (D) Three LAGs (arrows) are present on the medial side of left femur (imaged under linear light). (E) Three LAGs (one in the mid-cortex and two in the outer cortex) on the antero-medial side of the left femur (imaged under linear light). (F) Posterior side of right femur exhibiting LAG contrast under circular polarized light (left), linear light out of focus (center), and linear light in focus (right). (G) Resorption line separates endosteal layer of lamellar bone and mid-cortical parallel-fibered bone. Arrows – LAGs, A – anterior, EB – endosteal bone, HL – Howship Lacunae, KL – Kastschenko's line, LB – lamellar bone, M – medial, mALB – *m. adductor longus brevis* attachment, MB – medullary bone, MC – medullary cavity, mPPF – *m. piriformis pars iliofemoralis* attachment, PFB – parallel-fibered bone, PO – primary osteon, RL – resorption line, rWB – remodeled woven bone, sVC – simple vascular canal, TB – trabeculae.

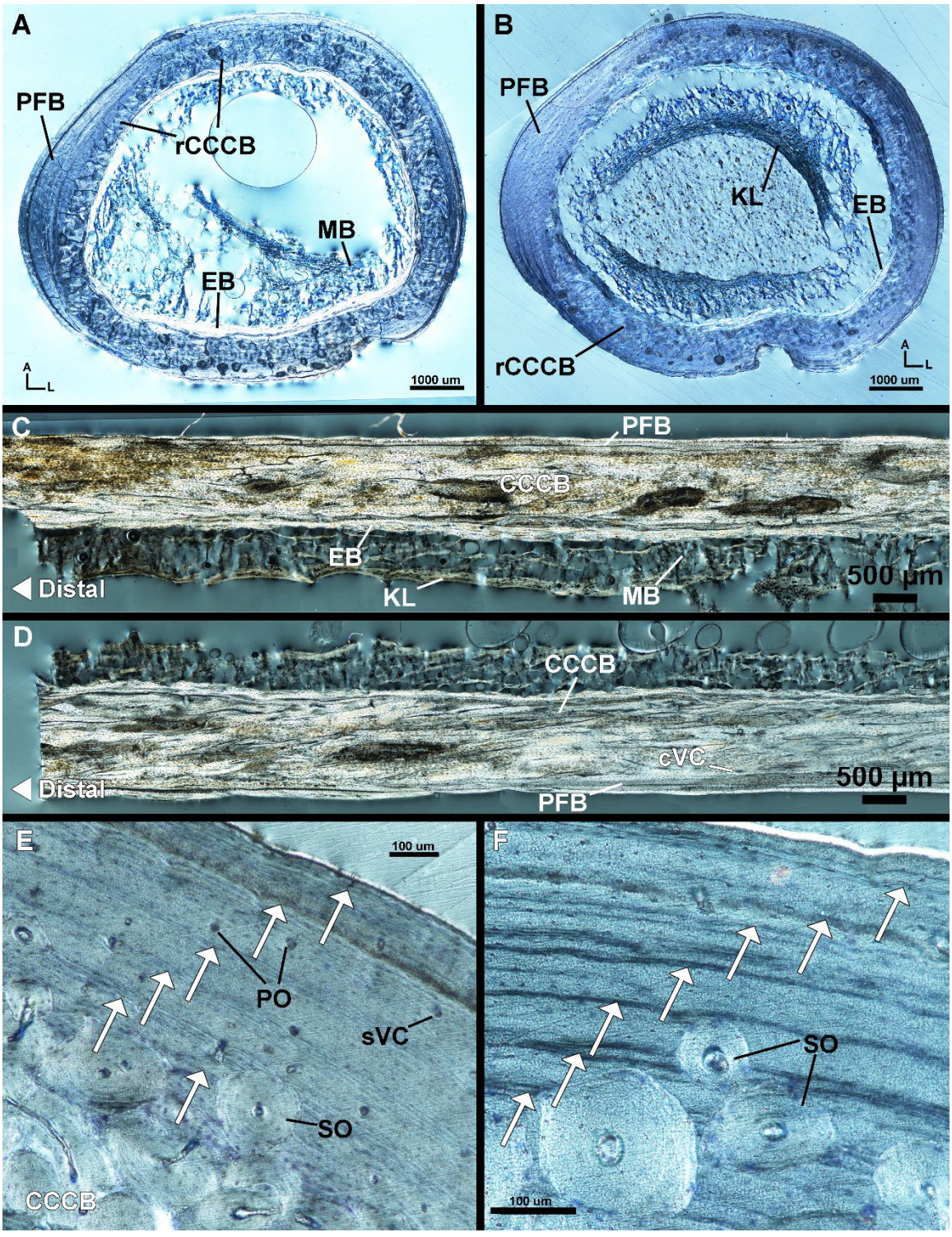

Figure 13. Female kiwi tibiotarsi microstructure. (A) Transverse section of left tibiotarsus under circular polarized light. The cortex is composed of endosteal bone, CCCB, and parallel-fibered bone. (B) Transverse section of right tibiotarsus under circular polarized has similar composition as left tibiotarsus, but with distinct Kastschenko's line within medullary cavity. (C) Longitudinal

section of posterior diaphysis from left tibiotarsus under circular polarized light. (D) Longitudinal section of anterior diaphysis from left tibiotarsus under circular polarized light. (E) Antero-medial corner of left tibiotarsus has inner mid-cortex of CCCB and outer mid-cortex and outer cortex of parallel-fibered bone with five LAGs. (F) Antero-medial corner of left tibiotarsus under circular polarized light has seven LAGs. Arrows – LAGs, A – anterior, CCCB – coarse compacted cancellous bone, cVC – circumferential vascular canal, EB – endosteal bone, KL – Kastschenko's line, L – lateral, MB – medullary bone, PFB – parallel-fibered bone, PO – primary osteon, SO – secondary osteon, sVC – simple vascular canal.

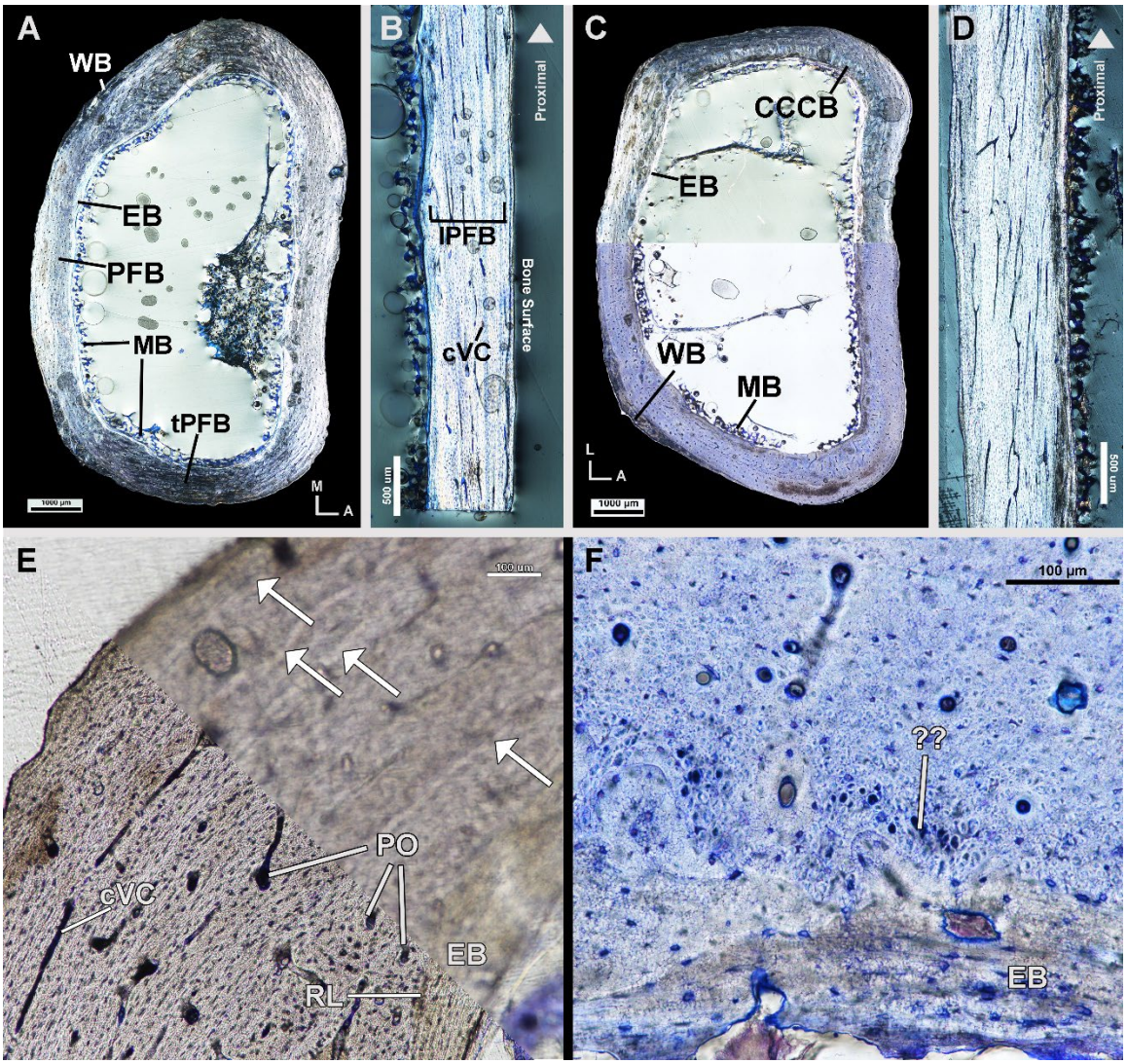

Figure 14. Female kiwi tarsometatarsi microstructure. (A) Transverse section of left tarsometatarsus under circular polarized light showing a cortex of endosteal bone, parallel-fibered bone, and woven bone. (B) Longitudinal section of posterior diaphysis of left tarsometatarsus under circular polarized light with highly birefringent, longitudinally oriented, parallel0fibered bone. (C) Transverse section of right tarsometatarsus under circular polarized light (top) and linear polarized light (bottom). Cortex is similar to left tarsometatarsus with the addition of a small patch of CCCB on the antero-lateral side. (D) Longitudinal section of anterior diaphysis of right tarsometatarsus under circular polarized light showing highly birefringent parallel-fibered bone of the mid-cortex. (E) Metaplastic hard tissue is present at entheses in the left tarsometatarsus. (F) Antero-lateral left tarsometatarsus under linear polarized light in focus (bottom) and out of focus (top). Four LAGs are present with increased clarity when viewed out of focus. (G) Inner cortex of posterior right tarsometatarsus, stained with toluidine blue and imaged

under linear polarized light, has large, longitudinal collagen fiber bundles in addition to lamellar endosteal bone and parallel-fibered mid-cortex. Arrows – LAGs, A – anterior, CCCB – coarse compacted cancellous bone, cVC – circumferential vascular canal, EB – endosteal bone, L – lateral, LCF – longitudinal collagen fiber bundles, lPFB – longitudinal parallel-fibered bone, M – medial, MB – medullary bone, MP – metaplastic tissue, PFB – parallel-fibered bone, PO – primary osteon, RL – resorption line, SO – secondary osteon, tPFB – transverse parallel-fibered bone, WB – woven bone.

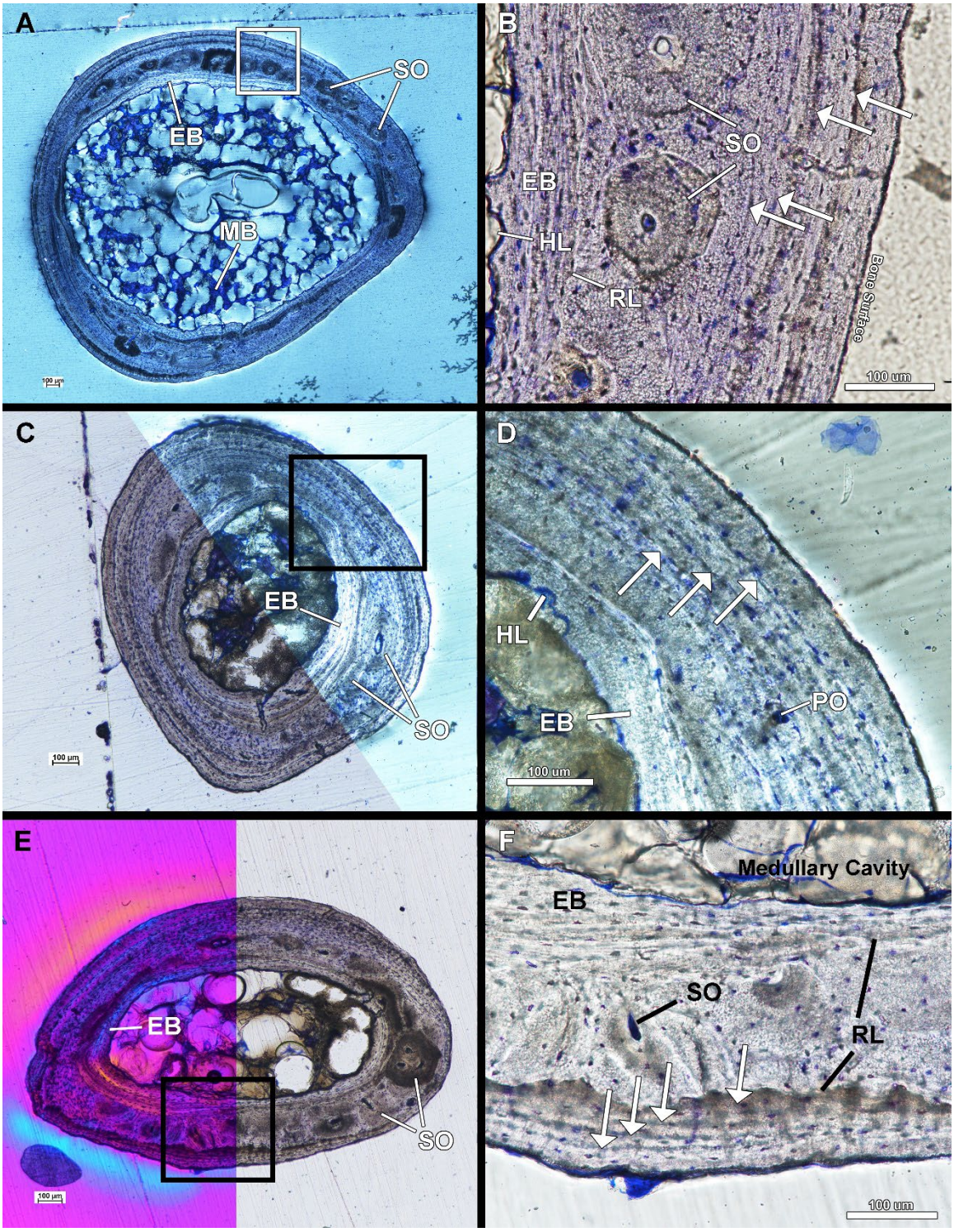

Figure 15. Female kiwi forelimb microstructure. (A) Transverse section of left humerus under circular polarized light showing endosteal lamellar bone, remodeled parallel-fibered bone, and an outer cortex of parallel-fibered bone. (B) Four LAGs are found in the cortex of left humerus under linear polarized light. (C) Transverse section of left radius under linear polarized light

(bottom) and circular polarized light (top). Three LAGs can be found in the cortex of the radius (Imaged under circular polarized light). (E) Transverse section of left ulna under a full lambda waveplate (left) and under linear polarized light (right). (F) The mid-cortex of the left ulna underwent resorption on the endosteal surface and periosteal surface prior to the deposition of endosteal bone and the outer cortex. The outer cortex has four LAGs at the mid-diaphysis. Arrows – LAGs, EB – endosteal bone, HL – Howship lacunae, MB – medullary bone, PO – primary osteon, RL – resorption line, SO – secondary osteon.

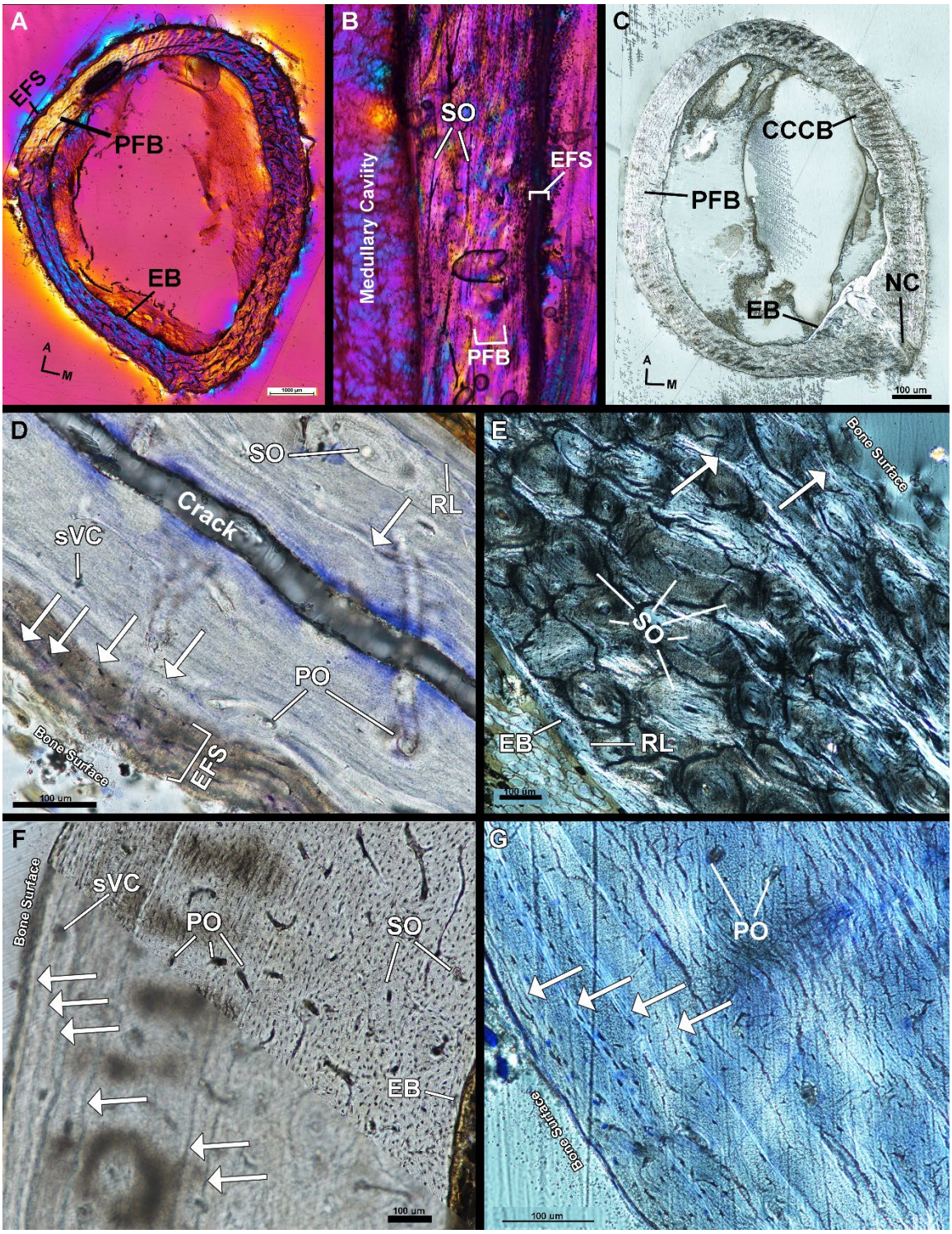

Figure 16. Male kiwi femora microstructure. (A) Transverse section of left femur under polarized light with full lambda waveplate. (B) Longitudinal section of left femur under polarized light with full lambda waveplate showing remodeled parallel-fibered bone in the mid-cortex. (C) Transverse section of right femur under circular polarized light. (D) Lateral side of left femur stained with

toluidine blue and imaged under linear polarized light. Parallel-fibered bone composes the mid-cortex and an EFS forms the outer cortex. A total of five LAGs can be identified on the lateral side. (E) Cortex of left femur on medial side, imaged under circular polarized light, is heavily remodeled and only two LAGs can be located. (F) Antero-lateral side of right femur under linear polarized light out of focus (bottom) and in focus (top). Six total LAGs can be found and have higher contrast when viewed out of focus. (G) Postero-lateral cortex of right femur stained with toluidine blue under circular polarized light. Four LAGs are found in the outer cortex EFS on this side of the femur. A – anterior, Arrows – LAGs, CCCB – coarse compacted cancellous bone, EB – endosteal bone, EFS – external fundamental system, M – medial, NC – nutrient canal, PFB – parallel-fibered bone, PO – primary osteon, RL – resorption line, sVC – simple vascular canal, SO – secondary osteon.

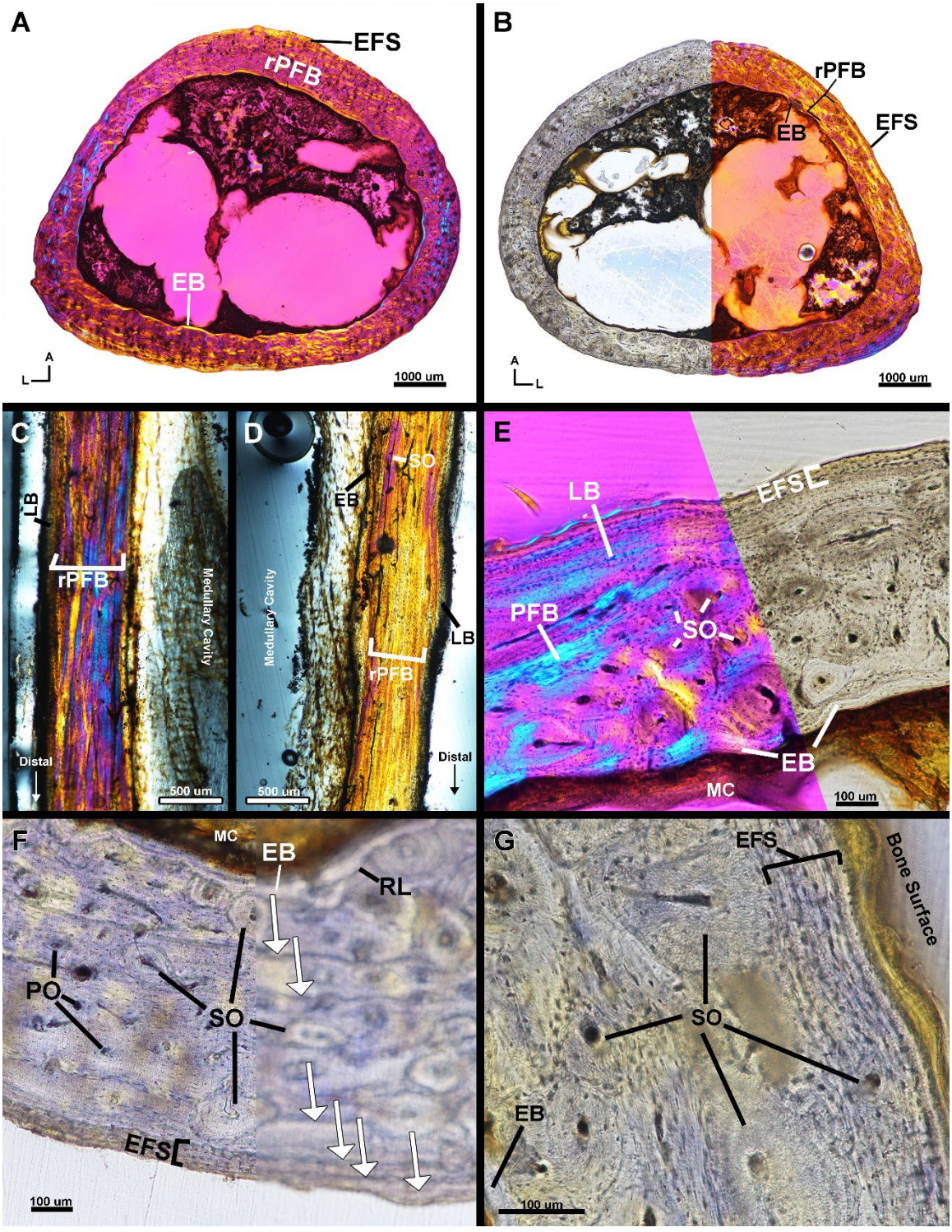

Figure 17. Male kiwi tibiotarsi microstructure. (A) Transverse section of left tibiotarsus under linear polarized light with a full lambda waveplate. (B) Transverse section of right tibiotarsus under linear polarized light without a waveplate (left) and with a full lambda waveplate inserted (right). (C) Longitudinal section of anterior diaphysis of left tibiotarsus under linear polarized

light with full lambda waveplate. (D) Longitudinal section of posterior diaphysis of left tibiotarsus under linear polarized light with full lambda waveplate. (E) Lateral cortex of left tibiotarsus is composed of endosteal bone, remodeled parallel-fibered bone, and an EFS. (F) Posterior cortex of right tibiotarsus under linear polarized light in focus (left) and out of focus (right). Six total LAGs are present on the posterior side in the mid-cortex of remodeled parallel-fibered bone and in the EFS. (G) Lateral side of right femur under linear polarized light showing the heavy remodeling in the mid-cortex and an EFS. A – anterior, Arrows – LAGs, EB – endosteal bone, EFS – external fundamental system, L – lateral, LB – lamellar bone, MC – medullary cavity, PFB – parallel-fibered bone, PO – primary osteon, RL – resorption line, rPFB – remodeled parallel-fibered bone, SO – secondary osteon.

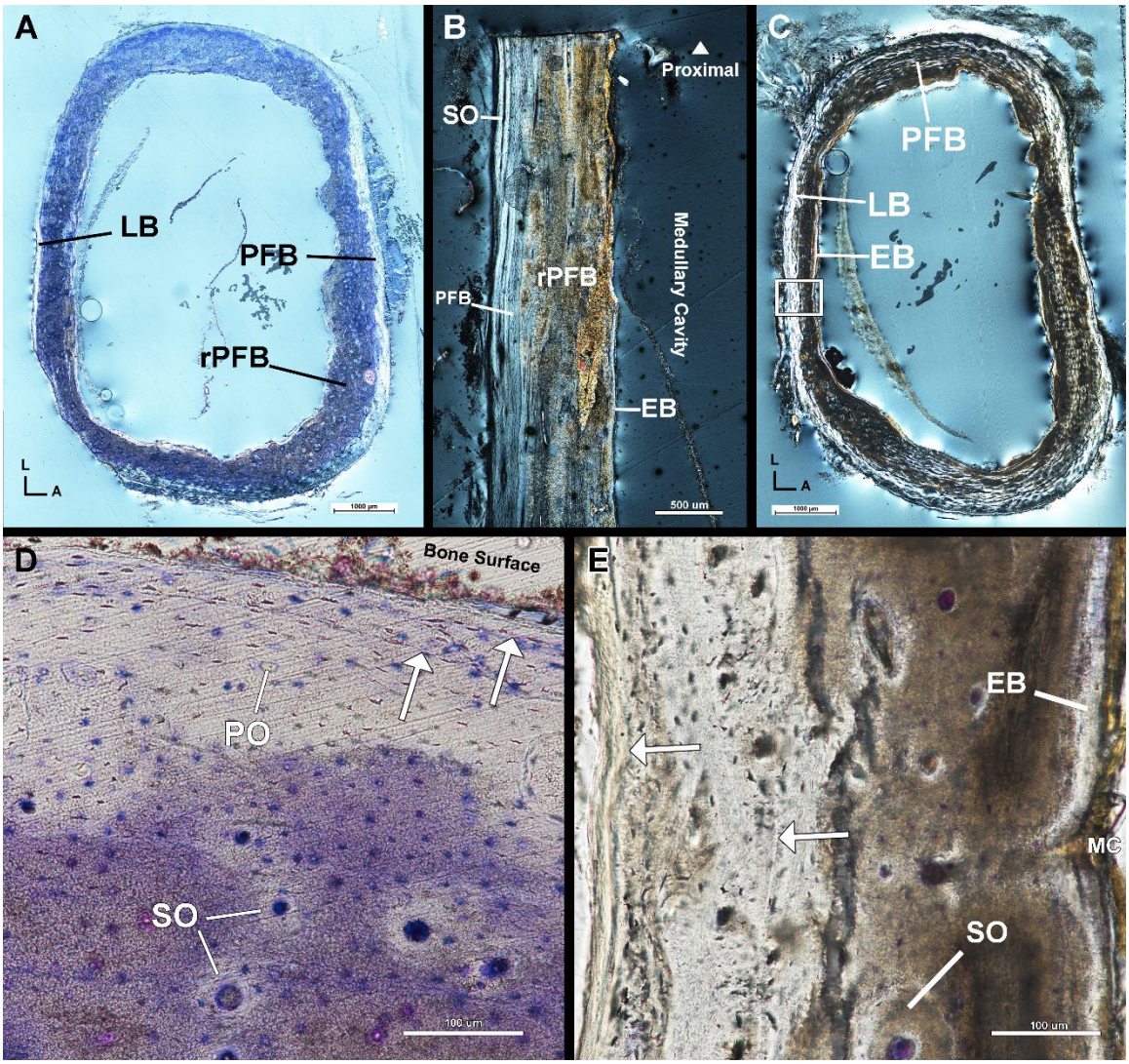

Figure 18. Male kiwi tarsometatarsi microstructure. (A) Transverse section of left tibiotarsus under circular polarized light. Cortex is mostly remodeled parallel-fibered bone and an outer cortex of lamellar and parallel-fibered bone. (B) Longitudinal section of left tarsometatarsus under circular polarized light confirming cortical composition described in transverse section. (C) Transverse section of right tibiotarsus under circular polarized light. (D) Antero-medial corner of left tibiotarsus under linear polarized light. Two LAGs are visible in this region of the left tibiotarsus. (E) Posterior side of right tibiotarsus under linear polarized light showing two LAGs: one in the outer cortex and one in the mid-cortex. A – anterior, Arrows – LAGs, EB – endosteal bone, L – lateral, LB – lamellar bone, MC – medullary cavity, PFB – parallel-fibered bone, PO – primary osteon, rPFB – remodeled parallel-fibered bone, SO – secondary osteon.

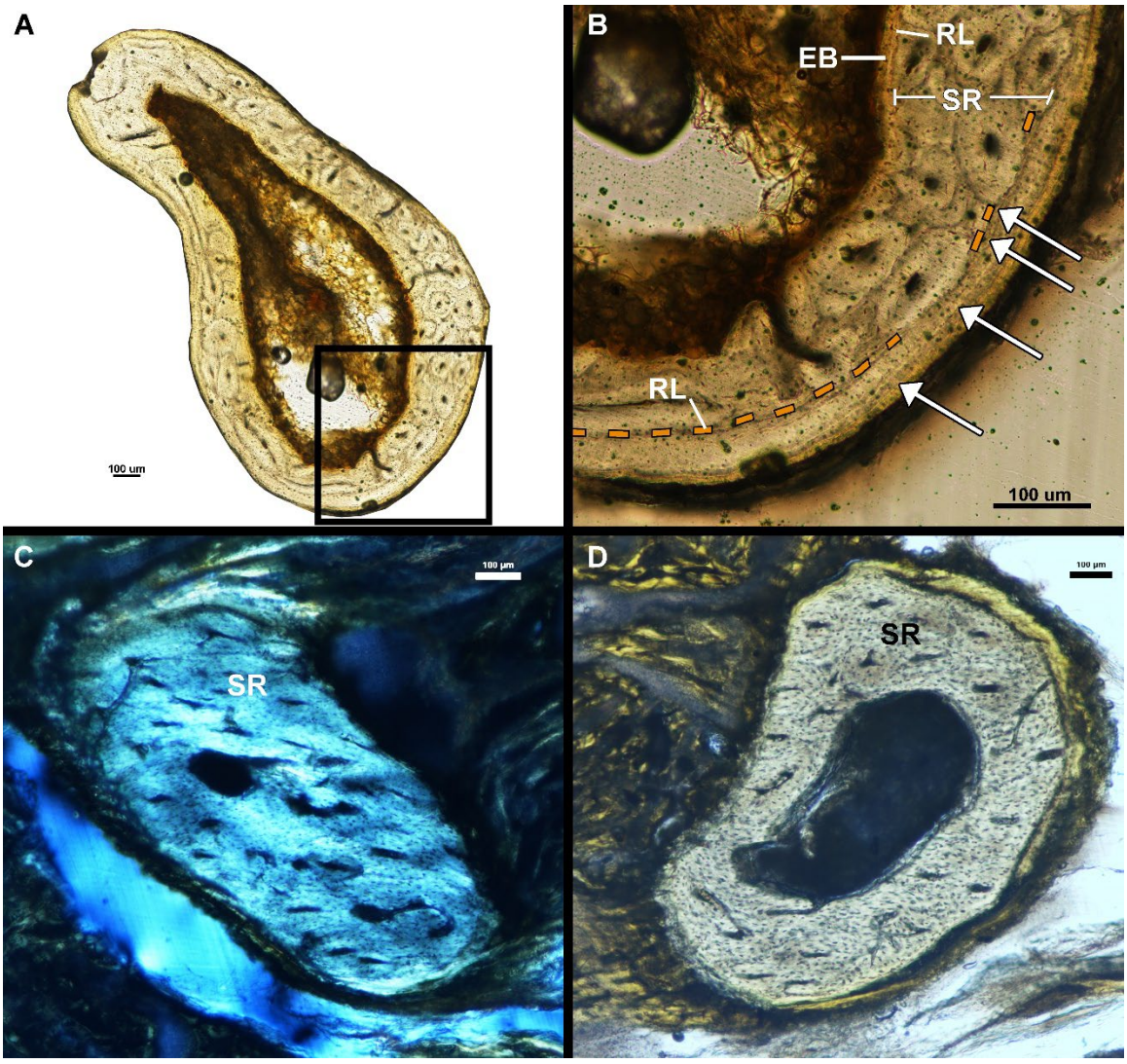

Figure 19. Male kiwi forelimb microstructure. (A) Transverse section of left humerus under linear polarized light. (B) Cortex of left humerus is composed of a thin layer of endosteal lamellar bone, mid-cortex of remodeled bone, and an outer cortex of lamellar bone with four LAGs. (C) Transverse section of left ulna under circular polarized light. Ulna is composed entirely of remodeled tissue. (D) Transverse section of left radius under linear polarized light. Radius is composed entirely of remodeled tissue. Arrows – LAGs, EB – endosteal bone, RL – resorption line, SR – secondary remodeling.

CHAPTER IV

INVESTIGATING INTRACORTICAL REPRODUCTIVE SIGNALS IN THE AMERICAN ALLIGATOR (*ALLIGATOR MISSISSIPPIENSIS*): IMPLICATIONS FOR SEX DETERMINATION IN EXTINCT ARCHOSAURS

Introduction

Sexual dimorphism is widespread throughout the animal kingdom and presents as intraspecific differences in behavior, physiology, or morphology between sexes (Andersson 1994). Dimorphic features can arise from sexual selection as well as selection for species recognition, resulting in fitness increases via changes in mating success, fecundity, growth, foraging success, or viability (Andersson 1994, Saitta et al. 2020). Identification of sexually dimorphic features has extensive utility for vertebrate paleontology as dimorphic characters can infer the sex of an individual fossil specimen, enhance studies on extinct taxon population demographics, and aid in taxonomic referrals (Prieto-Marquez et al. 2007). Because sexually dimorphic behaviors and physiologies cannot be directly observed from the fossil record, paleontologists must rely on morphological sexual dimorphism: the anatomical differences between sexes expressed in reproductive organs, cranial ornamentations, color patterns, tooth shape/ size, and overall body size (Shine 1989).

Thus, examination of morphological characters such as skeletal shape variation (e.g. pelvic width; Prieto-Marquez et al. 2007), cranial ornamentation (e.g. Dodson 1990), presence of medullary tissue (e.g. Schweitzer et al. 2005, Lee and Werning 2008), and body size (e.g. Klein and Sander 2008) for evidence of sexual dimorphism has been the focus of many non-avian dinosaur

(hereafter, simply ‘dinosaur’) studies (Mallon 2017 and references therein). Unfortunately, low sample sizes have contributed to the inability to detect the dinosaur morphological sexual dimorphism hypothesis under rigorous statistical analyses (Mallon 2017, but see Saitta et al. 2020).

Despite this failure, the sexual dimorphism hypothesis is reasonably grounded in the dinosaur extant phylogenetic bracket, comprised of Aves and Crocodylia (Witmer 1995, Hone and Mallon 2017). Reproductive organs aside, species in both groups exhibit a variety of gross morphological dimorphic characters including sexual size dimorphism (SSD). For example, male American alligators (*Alligator mississippiensis*) from South Carolina are 136% larger than females (Wilkinson and Rhodes 1997), North Island Brown Kiwi (*Apteryx mantelli*) females are significantly larger than males (McLennan et al. 2004), and Great Bustard (*Otis tarda*) males weigh approximately 2.5x more than females (Alonso et al. 2009). But despite observed dimorphism, Mallon (2017) found sexual dimorphism statistically undetectable in modern *A. mississippiensis* pelvic measurements and in *Centropus superciliosus* (coucal bird) body mass using mixture modeling. Hone and Mallon (2017) also reported that protracted growth in Crocodylia, a growth pattern shared with dinosaurs and some modern aves, obscures statistically detectable SSD with even relatively moderate sample sizes. While gross skeletal morphological characters appear inadequate in dinosaur sex identification, skeletal microstructural morphology remains largely unexplored for potential sexually dimorphic signals. Specifically, archosaur compact bone micromorphological signals of egg-laying and reproduction (excluding medullary tissue).

Extant crocodylians and avians lay hard-shell eggs, a condition once thought to be plesiomorphic among archosaurs. Recent discovery of soft-shelled egg material in the nests of *Protoceratops* and *Mussaurus* suggests soft-shell eggs are ancestral in Archosauria with hard-shell eggs independently evolving multiple times within the clade (Norell et al. 2020). Regardless, hard

eggshell formation relies on large amounts of labile calcium reserves during the reproductive cycle (Graveland and Berends 1997). In addition to increased calcium uptake during feeding (e.g. Graveland and Drent 1997), modern avians and crocodylians utilize two different strategies for eggshell calcification. Medullary tissue serves as a calcium reservoir for eggshell mineralization in modern female birds and some dinosaurs but is absent in alligators (Elsey and Wink 1986, Schweitzer et al. 2007, Werning 2018, Bailleul et al 2019) (Fig. 20). Alligators appear to utilize osteoderms in eggshell calcification (Dacke et al. 2015). Additionally, Elsey and Wink (1986) observed increases in appendicular bone porosity in egg-laying female alligators. The discovery of soft-shelled ornithischian and sauropod dinosaur eggs (Norell et al. 2020) suggests the possibility that skeletal tissue mobilization for hard eggshell calcification could be the ancestral condition in Archosauria and may have been utilized by some dinosaurs in combination with medullary tissue production, or in isolation (Fig. 21). Here, we investigate potential effects of calcium mobilization during eggshell formation on the bone microstructure of a large sample of male and female *A. mississippiensis* femora for utility in discerning potential morphological sexual dimorphism in dinosaurs and extinct pseudosuchians. Specifically, we test the hypothesis that cortical remodeling and resorption differs between *A. mississippiensis* sexes as a result of calcium mobilization for eggshell formation (Fig. 22).

Materials and Methods

Materials

Alligator mississippiensis eggs were collected in 1972-1973 from wild alligator nesting populations and artificially incubated, hatched, and raised in captivity at the Rockefeller State Wildlife Refuge (RWR) in Grand Chenier, Louisiana for a separate study (Fig. 23). This captive-raised *A. mississippiensis* cohort was to be utilized in examining alligator reproductive biology, and were terminated in their 26th or 27th year of life due to state-level budget limitations (see

Joanen and McNease 1987, Farlow and Britton 2000). Body mass and sex were recorded for most individuals upon termination and femora were removed and skeletonized for a previous study (Farlow et al. 2005). Mean and standard deviation of each sex is recorded in Table 4 (see Appendix III – Table S1 for full measurements).

A. mississippiensis displays higher growth rates and larger size at maturity in captive-raised individuals compared to wild individuals (Elsey et al. 1992). Thus, subperiosteal signals of reproduction in captive-raised individuals may not be representative of true biological signals found in wild populations. A separate sample of wild male (n=6) and wild female (n=6) *A. mississippiensis* were harvested from RWR for a previous study. Femur length, total length, and body mass were recorded for wild specimens by Farlow et al. (2005). Age at death was unknown for all wild specimens. Mean and standard deviation of each sex is recorded in Table 4.

Methods

Mid-diaphyseal transverse petrographic thin-sections of *Alligator* femora (Fig. 24) were prepared at Museum of the Rockies (MOR; Bozeman, MT) prior to the present study. Approximately 1mm wide holes were drilled into the diaphysis of each femur prior to embedding to increase penetration of resin into each femur. Thin-sections of captive-raised male (n=10) and female (n=19) alligator femora were imaged in plane polarized light using a Nikon DS-Ri-2 camera mounted to a Nikon Ni-U Eclipse polarizing microscope at Oklahoma State University – Center for Health Sciences (Tulsa, OK). Composite stitching of femora thin section images was automatically completed by Nikon NIS Elements: Documentation.

Composite images were edited and analyzed further in Adobe Photoshop CC v22.5 and ImageJ 1.53C. Holes drilled into each femur during histological preparation resulted in a sliver of missing cortex in each femur cross section. The missing cortex radiates from the medullary cavity out to the periosteal surface along a straight line. To estimate cortical properties of the entire section,

missing cortical bone in femora cross sections was artificially infilled in Photoshop by duplicating adjacent cortical bone and pasting the duplicated bone into the missing section. Cross section centroid, minimum axis, maximum axis, circumference, cortical area, and total cross section area were determined using the BoneJ plugin for ImageJ (Doube et al. 2010, Schneider et al. 2012, Domander et al. 2021).

Age at first nesting was recorded at 5 years 10 months for captive female *A. mississippiensis* in Louisiana, but wild female *A. mississippiensis* in Louisiana typically reach sexual maturity far later, at 9 years 10 months. (Joanen and McNease 1975, 1987). Regardless, all alligators utilized in this study were well beyond age of sexual maturity (26-27 years at time of termination) and are assumed to have nested multiple times throughout their lives. Wink and Elsey (1986) reported significant differences in bone porosity between egg-laying *Alligator* females and males. Egg-laying female cortical porosity appears to increase through larger and more numerous resorption canals concentrated in the internal cortex, in addition to an expanded medullary cavity (Fig.1 in Wink and Elsey 1986). Medullary cavity expansion in female *A. mississippiensis* may be partially driven by eggshell formation wherein resorption of endosteal cortical bone mobilizes calcium and in turn enlarges the medullary cavity. Medullary cavity area, cortical area, and total cross section area were measured to evaluate cortical porosity differences between male and female alligators (Fig. 25). Total cross section area is the sum of the area of cortical tissue and medullary cavity area in a given cross section (Fig. 25D), while cortical area is restricted to the area encompassed by bone (Fig. 25C). In the current study the variable 'compaction' is defined as the proportion of total section area that is cortical tissue (cortical area/total cross section area).

Wink and Elsey (1986) compared porosity levels between three *Alligator* groups: egg-laying females, non-egg-laying females, and males. Porosity in egg-laying females was significantly different from non-egg-laying females and males, but porosity in non-egg-laying females was not significantly different from males. Thus, female cortical tissue appears to undergo resorption

prior to, or during, eggshell formation, followed by bone deposition within previously resorbed spaces sometime after egg-laying. When resorption cavities are infilled with new bone the resulting structure is a secondary osteon (Fig. 22): concentric layers of lamellar bone tissue surrounding a neurovascular bundle. Secondary osteons are typically associated with bone repair due to biomechanical stresses, pathologies, or simple aging (de Buffrénil and Quilhac 2021). In the current study, we hypothesize that porous bone in female *A. mississippiensis* after egg-laying is infilled with lamellar tissue resulting in increased density in secondary osteons, but resorption cavities and intertrabecular space may remain unfilled after resorption for eggshell formation. Therefore, we measured area of secondarily deposited bone and open, resorbed spaces in the cortices of male and female *A. mississippiensis*. These two measures were summed and termed 'Resorbed Tissue Area' (RT) (Fig. 25). Four transects approximately 1mm wide were used as proxies in each thin section. Each transect extended from the centroid to the periosteal surface. Transects were aligned along the minimum and maximum axes except in specimens where either axis intercepted the missing cortical tissue (Fig. 25B). In these cases, transect orientation was rotated about the centroid until none of the four transects intercepted the strip of missing cortex. RT (mm^2) in each transect was measured using the BoneJ plugin for ImageJ and was divided by total transect area (mm^2) to determine the proportion of resorbed tissue (Doube et al. 2010) (Fig. 26).

Rate of bone growth is reflected in cortical tissue organization, growth marks, and vascularity (de Buffrénil et al. 2021). Preliminary observations of adult *Alligator* femora indicated similar cortical tissue organization regardless of sex and, thus, tissue organization was not included in this analysis. Similarly, zonal bone area between growth marks was not measured. Captive alligators used in this study were of similar age when terminated and had reached skeletal maturity. Skeletal maturity is indicative in transverse cross-sections by the presence of tightly spaced growth marks in the external cortex, an external fundamental system (EFS) (see

Woodward et al. 2011). Growth mark formation in the EFS does not appear to be annual, and growth mark counts in the EFS are thus unreliable indicators of age. Therefore, comparing zonal bone area through our sample set cannot be accomplished due to an inability to match specific yearly growth across the sample.

Data were analyzed by pairwise t-test comparisons between the four groups: captive male (CM), captive female (CF), wild male (WM), and wild female (WF). Additionally, five random subsamples (n=10) were taken without replacement from the captive female sample. T-tests were performed between the female subsamples and the captive male sample to test for sample size effect on t-tests. Data analysis was performed in Microsoft Excel 2016.

Results

Between sex differences

Basic summary statistics are listed in Table 5 for all groups (also see Appendix III – Fig. S1-S4 for visual results). Statistical signals of calcium mobilization from cortical bone is absent in the sample. There was no significant difference ($p<0.05$) in compaction, resorbed tissue proportion, or secondary tissue proportion between males and female alligators within each group (captive and wild). There was a significant difference in perimeter and cortical area between sexes in both groups, congruent with overall size dimorphism in *A. mississippiensis*. Perimeter and cortical area were significantly higher in males compared to females in each group. Out of five captive female subsamples, one subsample was significantly different in resorbed tissue proportion in comparison to captive males.

Captivity vs. wild alligators

There was no significant difference in resorbed tissue proportion, secondary tissue proportion, or compaction between captive and wild alligators within each sex. There was a significant

difference in perimeter and cortical area between captive and wild alligators within each sex. Perimeter and cortical area were significantly higher in captive-raised alligators compared to wild alligators.

Discussion

Reproductive physiology in archosaurs

Extinct and extant dinosaurs and crocodylians lay calcified, hard-shelled megalecithal eggs. Hard-shelled eggs were thought to be a shared ancestral trait between Dinosauria and Crocodylia until recent discovery of soft-shelled dinosaur eggs. Chemical analysis of *Protoceratops* (Dinosauria: Ornithischia) and *Mussaurus* (Dinosauria: Saurischia) nests reveal soft-shelled eggs were ancestral and hard-shelled eggs were secondarily acquired multiple times in Dinosauria (Norell et al. 2020). Evolutionary origins for hard-shelled eggs differ between Dinosauria and Crocodylia, resulting in different approaches to reproductive biology and, specifically, oogenesis (Carpenter 1999).

Egg shelling in aves begins in the uterus and shelling is completed sequentially in which, typically, a single egg is shelled and laid every 24 hours (Sturkie 1965). Clutch size in wild and domestic aves is highly variable, ranging from 1 egg (e.g. *Prionops poliolophus*) up to 20 eggs (*Aepypodius arfakianus*) (Jetz et al. 2008). Number of broods, or clutches, per year is also variable throughout modern aves, and domestic chickens (*Gallus gallus*), for example, can produce approximately 30-40 clutches in a single year (Whitehead 2004).

Crocodylians, on the other hand, shell all eggs *en masse* in the posterior part of the uterus – all eggs are shelled in rapid assembly line fashion prior to egg laying (Carpenter 1999, Schweitzer et al. 2007). Female *A. mississippiensis* can produce a single clutch per year of approximately 35 eggs (Thorbjarnarson 1996), and ovulation and oviposition of the clutch takes approximately 3-3.5 weeks (Joanen and McNease 1989). Clutch size (12-48) and clutch mass (677g – 5644g) vary

throughout Crocodylia and are associated with female body mass (Thorbjarnarson 1996 and references therein).

Eggshell Composition and Production

Hard-shelled, or rigid, eggshells of modern aves and crocodylians are a calcitic biomineral composed primarily of calcium carbonate (Carpenter 1999, Dacke et al. 2015). Egg shelling requires intensive calcium demands: shelling of a single alligator egg uses 3-5g of calcium (Packard and Packard 1989, Lance 2003), while 2.2g of calcium are utilized for shelling a domestic chicken (*Gallus gallus)* egg (Romanoff and Romanoff 1949). The calcium requirements of a single *A. mississippiensis* clutch are 10-20 times less than those for a single clutch of domestic chickens when body mass and clutch size are taken into account (Dacke et al. 2015). However, female alligators require high concentrations of calcium over a much shorter period of time due to simultaneous shelling of the entire clutch (Dacke et al. 2015). Higher concentrations of calcium over a longer period of time in domestic chickens repeats with each additional clutch in a single year.

To meet these high mineral demands, modern aves and crocodylians utilize a combination of dietary and osseous calcium reserves (e.g. Wink and Elsey 1986, Whitehead 2003). Aves form an endosteally derived, heavily mineralized, woven tissue within appendicular and axial skeletal elements, termed 'medullary tissue' (see Canoville et al. 2019 and references therein). Medullary tissue is deposited by osteoblasts in response to increased estrogen levels prior to eggshell formation. Estrogen levels subsequently decline during shelling, and, coupled with rising parathyroid hormone, induce resorption of medullary tissue via osteoclast activity and mobilizing calcium for egg shell formation (Kerschnitzki et al. 2014). Additionally, mobilization of calcium through catabolism of structural bone has been observed in domestic chickens, but medullary

tissue remained the predominant source for egg-shelling calcium in those hens (Whitehead 2004, Whitehead and Fleming 2000).

On the other hand, medullary tissue has not been observed in Crocodylia (Schweitzer et al. 2007). Estradiol injections did not stimulate medullary tissue formation in *Caiman sclerops* or *A. mississippiensis* (Elsey and Wink 1986, Prosser and Suzuki 1968). Schweitzer et al. (2007) did not observe medullary tissue in femoral cross sections of four female *A. mississippiensis,* despite calcified and partially calcified eggs found in the oviducts of two individuals. Additionally, previous osteohistological studies of crocodylian long bones did not describe the presence of medullary tissue (e.g. Rainwater et al. 2021, Woodward et al. 2014, Chinsamy 1993, de Buffrénil et al. 2021 and references therein). In the absence of medullary tissue, structural cortical bone serves as the skeletal calcium reserve for alligator egg shelling (Schweitzer et al. 2007, Dacke et al. 2015).

Crocodylian Calcium Reserves

Structural cortical bone serves as a reproductive calcium reserve in many amniotes unable to develop medullary tissue (e.g. crocodylians (Wink and Elsey 1986), testudines (Edgren 1960), lizards (de Buffrénil and Francillon-Vieillot 2001, Hugi and Sanchez-Villagra 2012), and mammals (Torres et al. 2017, Montoya-Sanhueza et al. 2021)). Wink and Elsey (1986) found significant increases in *A. mississippiensis* femoral porosity among egg-laying females relative to non-egg-laying females and males. Wink et al. (1987) measured femoral robusticity and porosity in female *A. mississippiensis* along seven stages of reproduction. Femoral porosity and robusticity indicated calcium mobilization from femoral cortical bone occurred just prior to oviposition. Increased porosity in alligator femora returned to pre-ovulatory levels 1-2 months after egg laying (Wink et al. 1987). Dacke et al. (2015) proposed labile calcium for eggshell formation in alligators was, in part, derived from osteoderm structural bone. Alligator labile calcium reserves

are derived from multiple skeletal elements (e.g. Wink et al. 1987, Dacke et al. 2015), although widespread intraskeletal analyses of bone mineral density, porosity, or robusticity changes during female reproduction are absent.

Releasing calcium from skeletal tissue requires osteoclast-driven resorption of cortical bone. Increases in alligator femoral porosity during eggshell formation are concentrated in the inner cortex (Wink and Elsey 1986, Wink et al. 1987). Osteoclasts breakdown cortical bone and form pits along bone surfaces and resorption rooms or cavities within the cortex (Pawlina and Ross 2018). Intensive cortical resorption results in osteoporosis and the skeletal element is more susceptible to fracture and failure (e.g. Whitehead 2004). Wink et al. (1987) found increases in bone porosity, through intracortical resorption, in post-ovulatory alligators returned to pre-ovulatory porosity levels 1-2 months after oviposition. Thus, resorption rooms are infilled with new bone in egg-laying female alligators to return porosity to pre-ovulatory levels and stabilize structural integrity of the femur.

The present study did not find a reproductive signal within the cortices of *A. mississippiensis* femora. Compaction, proportion of whole section that is cortical tissue, was not significantly different between male and female alligators within captive and wild groups. Proportion of resorbed tissue and secondary tissue was also not significantly different between male and female alligators within captive and wild groups. Additionally, there was no significant difference in compaction or resorbed tissue proportion between captive and wild males nor between captive and wild females. Cortical signals of egg-laying appear to be unreliable for determining sex in *A. mississippiensis*.

Male and female alligator femora undergo similar rates of bone turnover when femur size is taken into account. Secondarily deposited cortical bone, such as infilling of resorption rooms, does not appear to be useful in sex determination in senescent alligators. Our study also did not find a

significant difference in compaction between sexes. Wink and Elsey (1986) recorded differences in femoral porosity between egg-laying female alligators and both male and non-egg-laying female alligators. The infilling of resorption rooms contributing to porosity should be identifiable and, thus, contribute to our variable 'Resorbed Tissue'. However, our study indicates signals of reproduction to be absent in senescent female alligators, although sample traits and sample size could be contributing factors that affect our ability to detect dimorphic cortical signals.

Sampling Biases

Captive alligators in the current study were all sacrificed at 26-27 years old for a previous project. Alligators in our sample were beyond skeletal maturity and cortical signals of reproduction may have been obscured by age-induced remodeling processes. High growth rates in captive-raised individuals could have resulted in medullary cavity expansion, and erasure of potential dimorphic cortical signals. Reproductive history of female specimens was not available, thus, number of egg-laying years and clutch size was unknown. Lower resorbed tissue proportions and compaction values in captive females could be the result of successive non-egg-laying years. Individuals that may not have an extensive history of egg-laying can affect results in combination with low sample sizes. Testing along an ontogenetic series of specimens with known reproductive histories would be a beneficial step towards unravelling dimorphic signals in alligator bone cortices.

Five captive female subsamples were tested against the captive male sample. One of the five subsamples was significantly different in resorbed tissue proportion between male and female alligators, suggesting a potential sampling effect. Future examination of cortical traits would benefit from larger samples and less discrepancy between male and female sample sizes.

Captive alligator growth and longevity is typically higher than in wild alligators (e.g. Elsey et al. 1992). Thus, captivity status could be a confounding variable in detection of cortical signals of

dimorphism. For example, Meers (2002) found captive crocodylian humeri bone geometry to be more robust than wild alligators. The present study did not find a significant difference in resorbed tissue proportion and compaction between captive and wild male alligators or captive and wild female alligators. This suggests that resource abundance is not a determining factor in either variable. However, the limited wild male and female alligator samples contain individuals of unknown age and reproductive history and are thus limited in their utility.

Conclusions

Identifying sex in extinct archosaurs has proven difficult due, in part, to low sample sizes, preservation biases, and methodology (Mallon 2017, also see Saitta et al. 2020). Confident referral of archosaur specimens to a sex can refine our understanding of archosaurian population dynamics, reproductive strategy, dimorphic growth patterns, and archosaur life history evolution. Thus far, the presence, not absence, of medullary tissue is the only reliable indicator of sex in non-avian dinosaurs. Multiple reproductive strategies were likely utilized throughout Dinosauria, as evident from the presence of soft-shelled eggs in some non-avian dinosaur nests. Therefore, calcium reservoirs for eggshell formation may also be variable throughout Dinosauria and reflect conditions found in modern crocodylians in addition to, and separate from, modern aves. Results of the present study indicate reproductive signals in long bone cortices are not reliable indicators of sex in senescent *A. mississippiensis*, but future study of dimorphic signals would benefit from more extensive sampling and limiting of confounding variables. If present in senescent non-avian dinosaurs, utilization of structural bone as a calcium reserve is undetectable based on the current study.

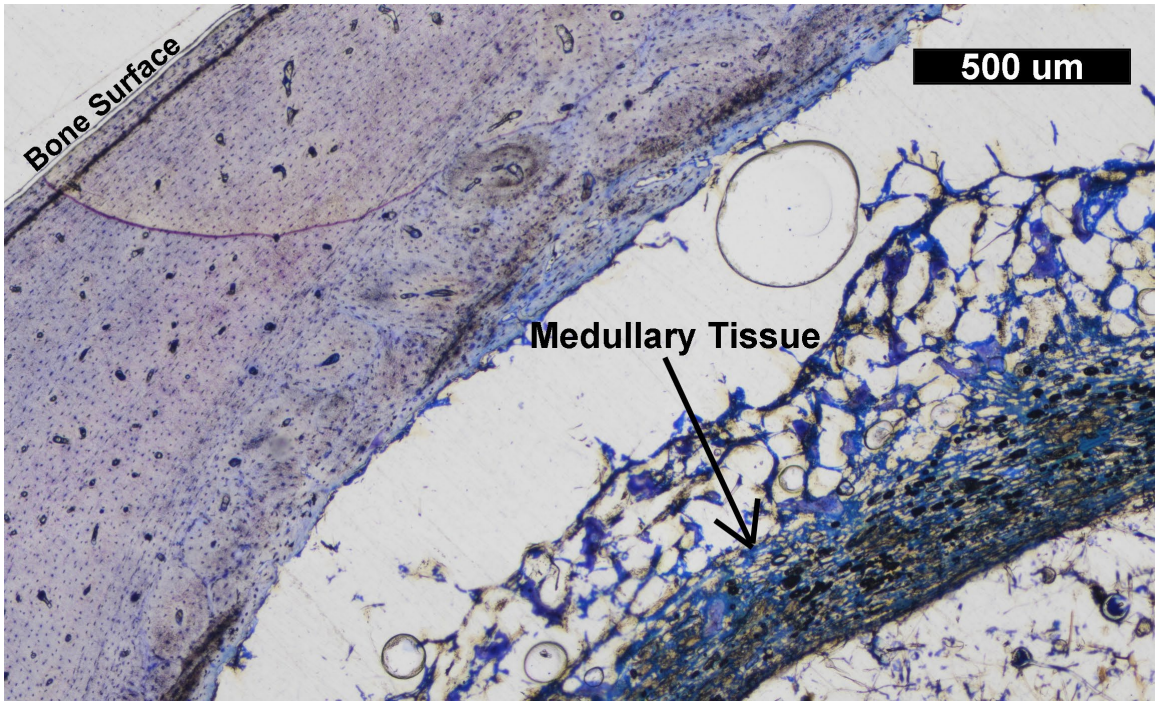

Figure 20. Modern aves and some non-avian dinosaurs utilize medullary tissue for excess calcium needs in eggshell formation.

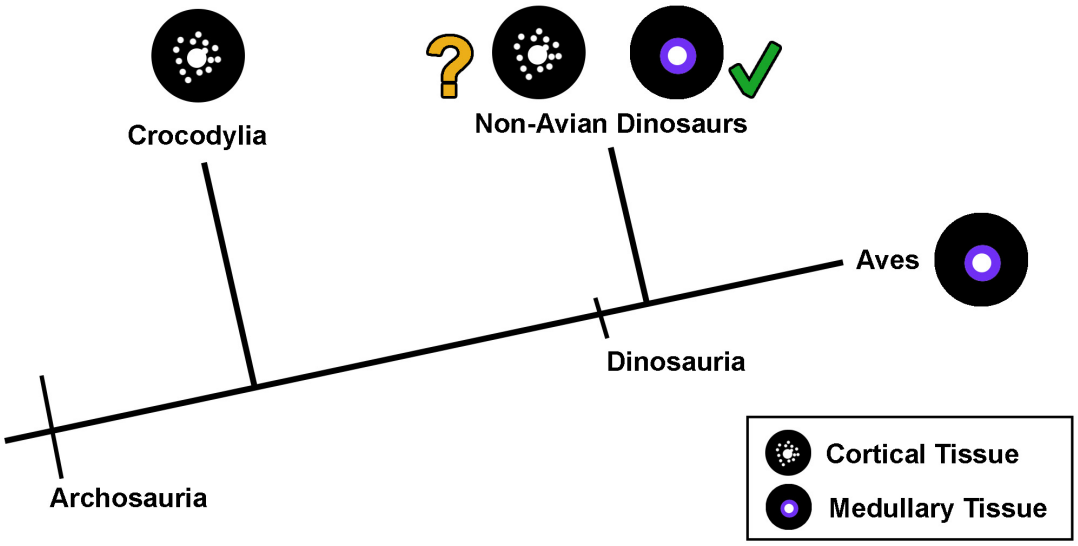

Figure 21. Simplified archosaur phylogeny. Medullary tissue has been found in few dinosaur species but cortical resorption for calcium mobilization has yet to be investigated thoroughly in non-avian dinosaurs.

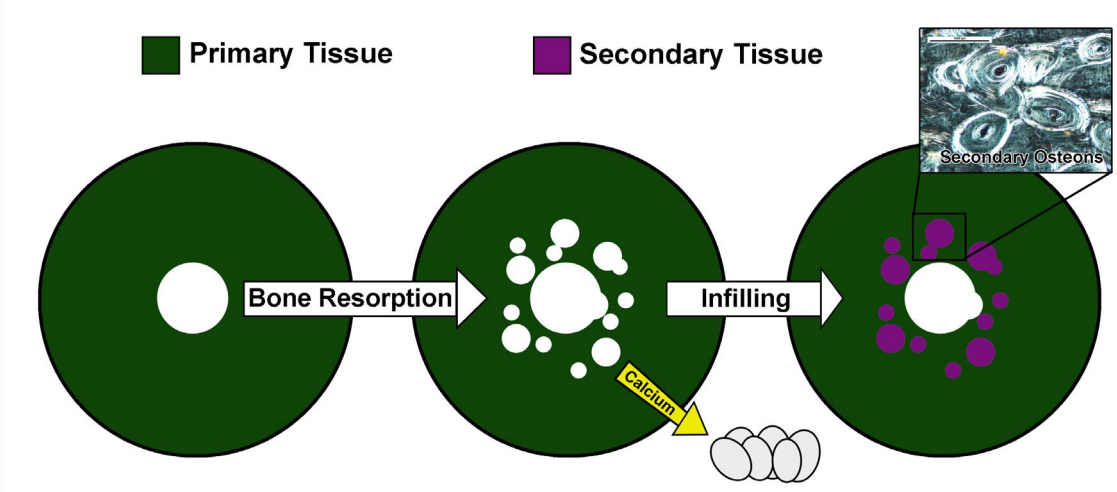

Figure 22. Hypothesized impact of cortical bone resorption for calcium mobilization on cortical bone microstructure. Resorbed bone will be infilled and result in identifiable secondary tissue structures.

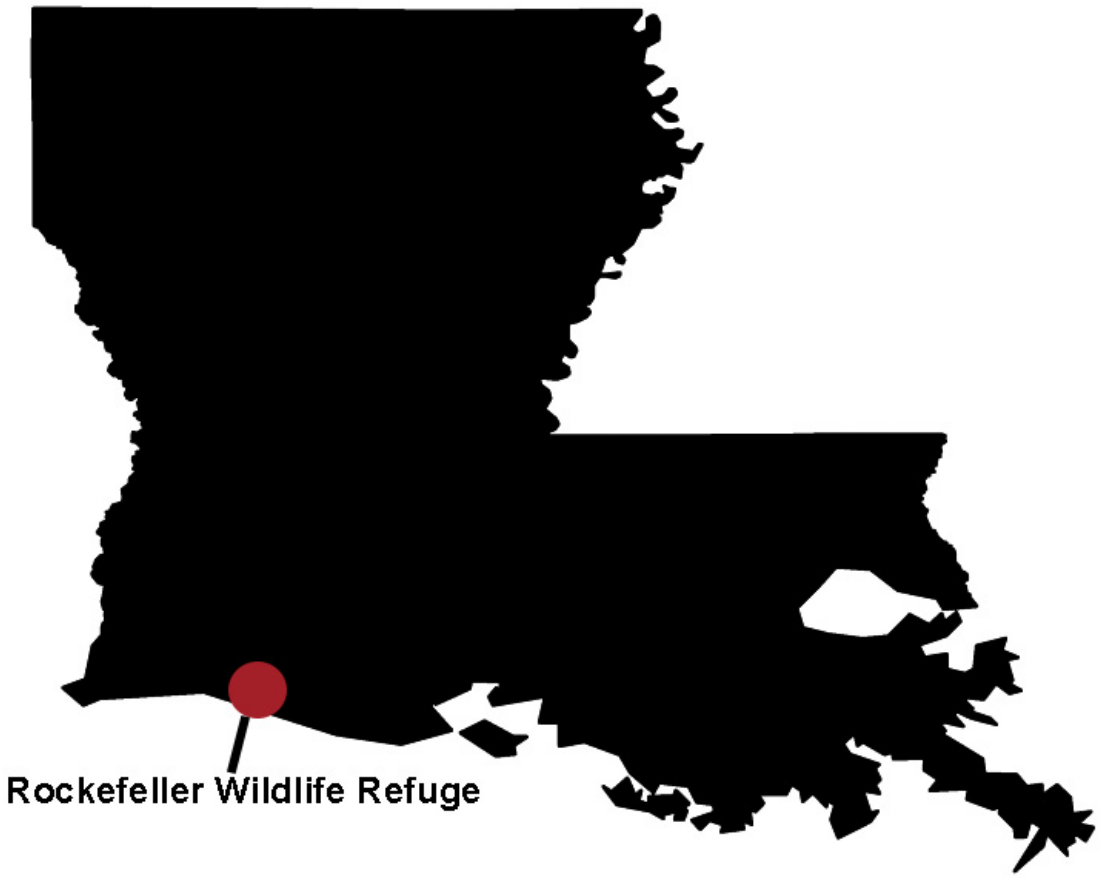

Figure 23. Alligator specimens originated from Rockefeller Wildlife Refuge in Southwest Louisiana.

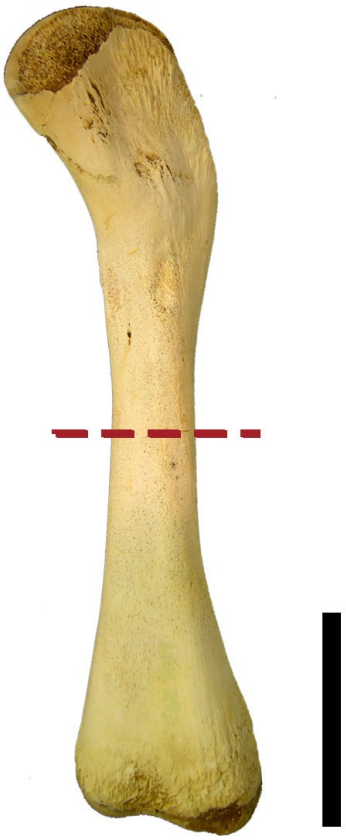

Figure 24. Transect sections were removed from the mid-diaphysis of *A. mississippiensis* femora.

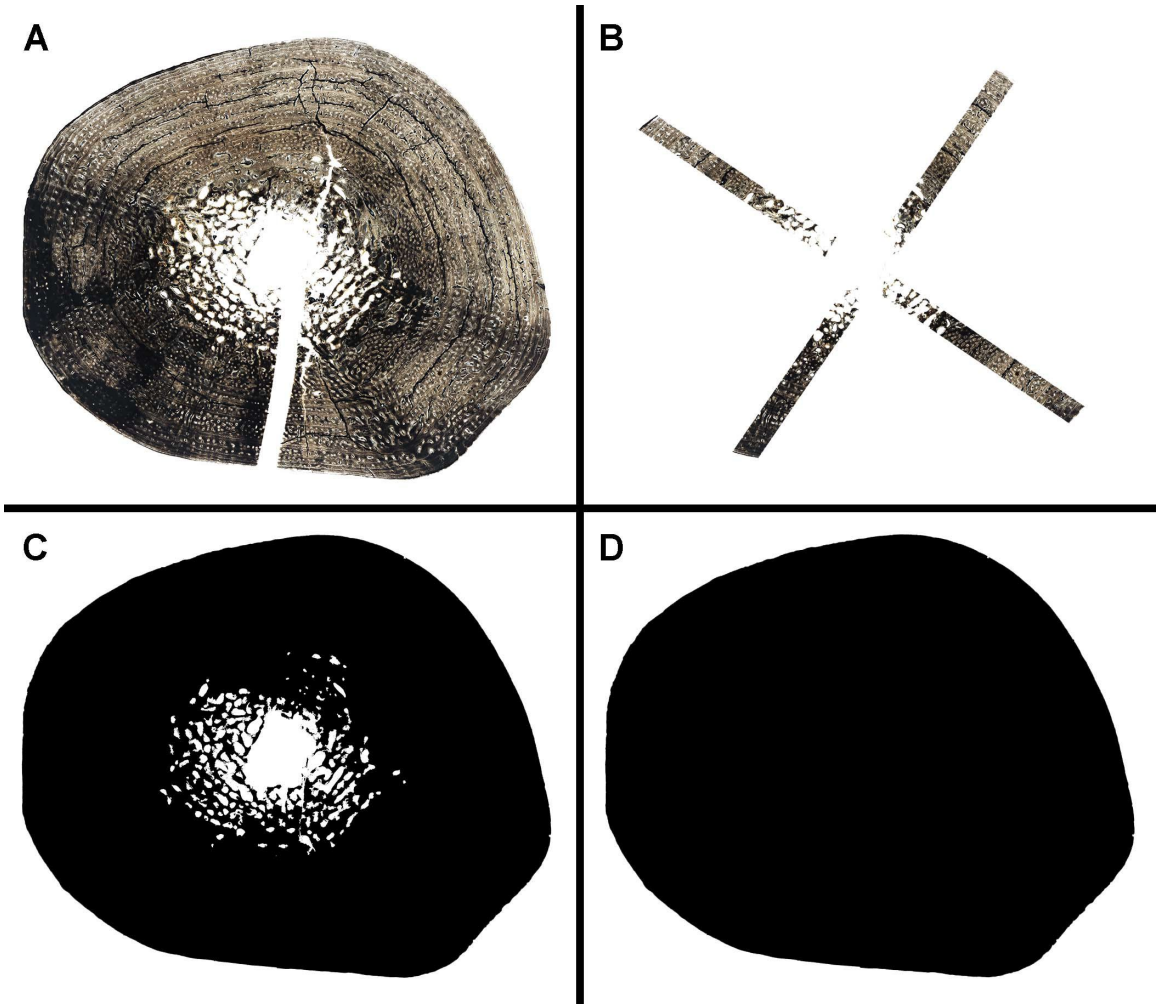

Figure 25. (A) Full *Alligator* femora cross-section. Missing cortex was infilled with surrounding cortical copies. (B) 1mm wide transects were examined for resorbed tissue measurements. (C) Cortical silhouette displaying cortical area (black) and medullary cavity area (inner white). (D) Full cross section area used for compaction measurements.

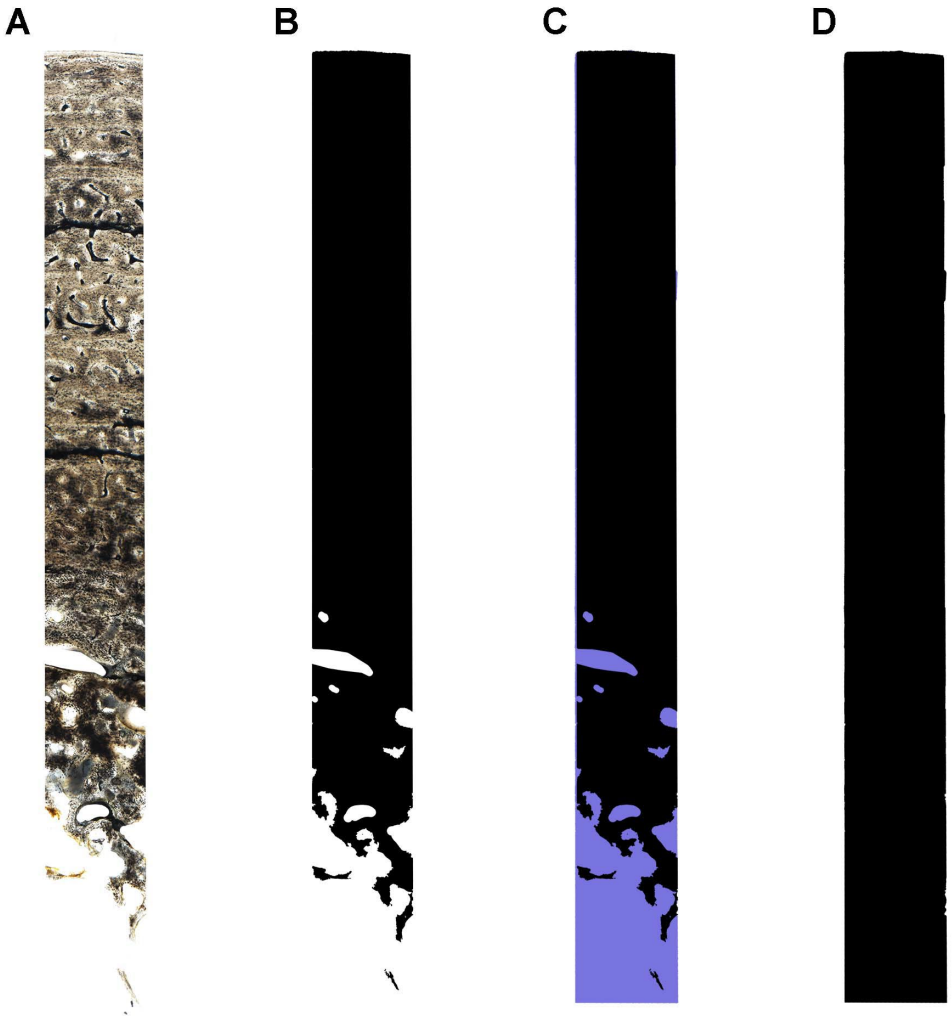

Figure 26. Transect measurements. (A) Full unedited transect. (B) Cortical area. (C) Cortical area (black) and resorbed tissue area (purple). (D) Full transect area.

Tables

Table 4. Mean gross morphological measurements of sampled alligators.

	Captive Female (n=19)	Captive Male (n=10)	Wild Male (n=6)	Wild Female (n=6)
Femur Length (mm)	185.5 ± 10.6	240.4 ± 30.6	160.7 ± 30	125.1 ± 35.5
Total Length (mm)	2725.2 ± 193.8	3601 ± 514.7	2293.6 ± 996.2	1822.4 ± 511.9
Body Mass (kg)	85.6 ± 25.3	229.1 ± 85.6	42.7 ± 25.7	21.8 ± 11.6

Table 5. Alligator femoral microstructure characters (mean ± standard deviation).

	N	Compaction	Resorbed Tissue Proportion	Secondary Tissue Proportion	Cortical Area (mm^2)[J¥]	Perimeter (mm)[J¥]
Captive Male	10	0.924 ± 0.015	0.359 ± 0.031	0.155 ± 0.027	595.135 ± 129.35	99.201 ± 9.121
Captive Female	19	0.918 ± 0.019	0.372 ± 0.045	0.171 ± 0.038	309.043 ± 47.77	71.383 ± 6.477
Wild Male	6	0.919 ± 0.020	0.311 ± 0.060	0.073 ± 0.027	224.264 ± 93.903	59.357 ± 13.104
Wild Female	6	0.904 ± 0.033	0.336 ± 0.048	0.069 ± 0..056	112.65 ± 51.000	44.097 ± 14.400

[J] - Significant difference between sexes within both groups ($p < 0.05$)

[¥] - Significant difference between captive and wild samples within each sex ($p < 0.05$)

CHAPTER V

MAIASAURA PEEBLESORUM HUMERUS GROWTH AND PALEODEMOGRAPHICS: A CASE STUDY IN FORELIMB AND HINDLIMB DIMORPHISM IN NON-AVIAN DINOSAURS

Introduction

Taxonomic paleobiological inferences depend upon life history interpretations involving growth rate, timing of sexual and somatic maturity, and population structure (Stearns 1992) using the fossil record and appropriate modern analogues. Although the direct observation of life history and species' ecology of fossil and extinct taxa is impossible, osteohistology permits analysis of individual bone growth and age (see Padian and Lamm 2013, de Buffrénil et al. 2021 and references therein). Annually deposited growth marks within vertebrate bone cortices are used to construct growth curves, survivorship curves, and life tables, and are utilized extensively in inferring non-avian dinosaur life history (e.g. Erickson 2005, Bybee et al. 2006, Woodward et al. 2015, Cullen et al. 2021). However, an understanding of non-avian dinosaur biology is often based on low sample sizes or samples that are unconstrained temporally, geographically, or intraskeletally.

Population dynamics (e.g. survivorship, mortality rates, age structure) have been assessed for relatively few non-avian dinosaurs. Erickson et al. (2006) constructed life tables, survivorship curves, and growth curves for the tyrannosaurid *Albertosaurus sarcophagus* using growth mark counts in a small sample (n=6) of fibulae and metatarsalia. Longevity derived from the small

histological sample was used to interpolate age in 16 *A. sarcophagus* from a single bonebed and construct a survivorship curve. Erickson et al. (2010) updated the *A. sarcophagus* life tables and survivorship curves with four additional specimens, though age of the additional specimens was determined by interpolation and not through histological analysis. Similarly, Erickson et al. (2006) constructed survivorship curves for the tyrannosaurids *Tyrannosaurus rex, Gorgosaurus libratus,* and *Daspletosaurus* using growth mark counts in small samples (n=7, n=5, n=3 for *T. rex, G. libratus,* and *Daspletosaurus* respectively) to interpolate age in other specimens of the same species. Erickson et al. (2009) histologically aged 24 *Psittacosaurus lujiatunensis* and used the longevity data to estimate age in 56 additional specimens; growth curves, survivorship curves, and life tables were then constructed. These novel studies utilized available material to analyze non-avian dinosaur paleobiology in innovative ways, but the robusticity of resulting inferences are limited by small histological sample sizes and incongruence in skeletal element sampled.

Examination of *M. peeblesorum* paleobiology by Woodward et al. (2015) was the first histological approach to constructing non-avian dinosaur survivorship and growth curves using a sufficiently large sample size of a single skeletal element (n=50) to produce statistically significant results. Woodward et al. (2015) histologically sampled all 50 tibiae from a single, laterally expansive, minimally time-constrained, monodominant bonebed of *M. peeblesorum* from the Willow Creek Anticline in Montana, USA. The Willow Creek Anticline *M. peeblesorum* mass death assemblage has been utilized to explore ontogenetic shifts in posture, intraskeletal micromorphology, biomechanically adaptive bone growth, and taphonomic processes (Varricchio and Horner 1993, Horner et al. 2000, Dilkes 2000, 2001, Schmitt et al. 2014, Cubo et al. 2015, Woodward et al. 2015, Woodward 2019). Histological aging of the tibia sample revealed a right skewed assemblage in which the majority of individuals were less than one-year-old (Woodward et al. 2015). Similar to Erickson et al. (2006, 2009, 2010), the *M. peeblesorum* survivorship curve was convex after high juvenile mortality; *M. peeblesorum* tibiae showed rises in mortality from

ages 0-1, 2-3, and 8-10 (Woodward et al. 2015). However, these results may be subject to fossil biases within the assemblage due to specific skeletal element preservation. Here, a large sample of *M. peeblesorum* humeri (n=47) from the Willow Creek Anticline death assemblage are histologically assessed to 1) describe ontogenetic changes in *M. peeblesorum* humeri bone growth; 2) quantify humerus growth and evaluate modeling curves in a hadrosaur dinosaur using a sufficiently large sample; and 3) compare paleodemographic data derived from humeri with that of tibiae to increase single or multi-element usage precision in paleobiological inferences.

Materials and Methods

All specimens used in this study are housed at Museum of the Rockies (MOR), Bozeman, MT (specimen MOR 748, MOR 005). *M. peeblesorum* humeri (n=47) sampled in this study were collected from a single, laterally expansive bonebed in the Two Medicine Formation (Upper Cretaceous) sediments at the Willow Creek Anticline in Teton County, Montana, USA (Schmitt et al. 2014). The anticline consists of multiple facies including a troodon nesting horizon, multiple *M.* peeblesorum nesting horizons, and a separate *M. peeblesorum* mass death bonebed (Lorenz and Gavin 1984). The bonebed consists of disarticulated and disassociated bones attributable primarily to hadrosaurs, although few theropod and unidentifiable bones are present (Varricchio and Horner 1993, Schmitt et al. 2014). Hadrosaur bones identifiable down to species are attributable to *M. peeblesorum* (Schmitt et al. 2014); growth curves of tibiae from the bonebed further support a single taxon, monodominant composition (Woodward et al. 2015).

Taphonomy, skeletal composition, and survivorship curves suggest the *M. peeblesorum* assemblage is the result of multiple catastrophic mass-death events with little geologic time-averaging (Schmitt et al. 2014, Woodward et al. 2015). Analyses of tibiae (Varricchio and Horner 1993, Woodward et al. 2015), humeri, and femora (Varricchio and Horner 1993) revealed high mortality rates in <1 year-olds, decreased mortality in late juveniles and subadults, and ending

with increased mortality in adults due to senescence (B1 survivorship curve) (Woodward et al. 2015). High mortality rates in <1 year-old *M. peeblesorum* could be due to age-specific events such as drought or disease, thus, the assemblage is likely catastrophic in origin but attritional in composition (Woodward et al. 2015). Survivorship curves from Woodward et al (2015) are derived from the methodology of Steinsaltz and Orzack (2011) which assumes stationary age distributions within a population over time. Recent analysis suggests the *M. peeblesorum* population was increasing substantially over time (Griebeler 2021), though general inferences of survivorship remain consistent with Woodward et al. (2015).

Forty-seven *M. peeblesorum* humeri across an ontogenetic series were sampled for the present study (Fig. 27). Larger sample sizes limit effects of individual variation on paleobiological inferences. Perinatal material has not been identified in the mass death assemblage, thus *M. peeblesorum* nestling (YPM-PU 22400) measurements from Prieto-Marquez and Guenther (2018) were used to establish baseline measurements for regression and growth analyses. For sampling, *M. peeblesorum* humeri with relatively intact diaphyses were selected; the humeral diaphysis of *M. peeblesorum* is defined as the cylindrical shaft distal to the delto-pectoral crest and proximal to the distal epiphysis (Fig. 28). Prior to sampling, the minimum circumference of each humerus was identified and measured using fabric tape. Generally, humeri from the assemblage are subjected to crushing, deformation, and fracture during initial sediment transport and subsequent burial and uplift (Fig. 27). Initial least circumference measurements did not account for taphonomic distortion. Total length was measured from the dorsal edge of the proximal articulation to the distal boundary of the distal condyles along a straight line in complete or near-complete specimens (n=17). Fracturing, erosion, and compression often resulted in partial loss of the deltopectoral crest (n=16), complete loss of the deltopectoral crest (n=10), and/or loss of condyles (n=9).

Linear regressions between humerus total length and least circumference were performed in Microsoft Xcel 2003 using complete specimens (n=17) to determine relationship between length and circumference and estimate length in incomplete specimens (n=30). The sample of complete specimens (n=17) encompassed the entire range of humerus lengths (206mm – 575mm) and age (<1 – 19 years-old; see below). Regressions were performed on 1) length and circumference prior to histological sampling (using fabric tape) and 2) length and cross-section circumference of histological sections (using BoneJ plugin for ImageJ; Doube et al. 2010, Schneider et al. 2012, Domander et al. 2021) after retrodeformation. Both regressions were run with and without nestling measurements by Prieto-Marquez and Guenther (2018) as the baseline, anchoring data point (Table 6). Incomplete specimen lengths were interpolated from retrodeformed least circumference using best fit linear regression (highest R^2).

The diaphysis of each humerus was removed about the region of minimal, or least, circumference (Fig. 28). The diaphysis was selected due to 1) diaphyses of long bones typically preserve the most complete record of growth (Padian et al. 2013) and 2) humerus bone morphology proximal to the diaphysis is strongly affected by muscle attachments and biomechanical signals (e.g. Dilkes 2000). Diaphyses were removed using hammer and chisel along pre-existing fractures or using a tile saw when pre-existing breaks were absent. All diaphyses were molded and casted prior to histological processing to preserve morphological data following protocol of Lamm (2013). Diaphyseal bone samples were embedded in Silmar-41 polyester resin using MEKP as a catalyst resulting in a resin embedded bone block. A ~3.0 mm transverse section from each embedded diaphysis was removed from the region of minimum circumference. The transverse section was processed, mounted, and polished using standard petrographic thin-sectioning protocols (Lamm 2013). Thin-sections were examined using a Ni-U Eclipse polarized transmitted light microscope. Images of thin-sections were taken using a Nikon DS-Ri-2 camera mounted to a Nikon Ni-U Eclipse polarizing microscope and composite stitching of full-size scans was performed

automatically by Nikon NIS Elements: Documentation. Thin-section processing and imaging was performed at the Woodward Ballard Paleohistology Lab on the Oklahoma State University – Center for Health Sciences campus (Tulsa, OK).

Post-burial deformation is common in humeri and distorts measures of circumference, medullary cavity area, cortical area, and growth marks (e.g. lines of arrested growth (LAGs)). Deformation in cross sections presents as compression, crushing, fracturing, and missing cortical bone. Medial-lateral compression was most common in humerus diaphyses (n=30). Full cross-section images of deformed humeri were retrodeformed manually using Adobe Photoshop CC 22.5 (Fig. 29). Retrodeformation was completed by lining up growth marks, vascular canals, tissue type transitions, and infilling of missing cortex (Wosik et al. 2020).

Osteohistological descriptions follow terminology of Francillon-Vieillot et al. (1990) with the exception of fibrolamellar bone. Fibrolamellar bone is a complex of woven fibered tissue and parallel-fibered tissue with primary osteons (vascular canals within circumferential lamellae). Early descriptions of fibrolamellar bone implied composition was primarily woven-fibered tissue with less parallel-fibered tissue. Here, we follow descriptions and terminology by Stein and Prondvai (2014) and Prondvai et al. (2014) in which bone tissue composition consists primarily of more organized parallel-fibered and lamellar tissue with less woven-fibered tissue. Thus, we use the term ‘woven-parallel complex’ for cortical bone composed of woven scaffolding perforated with primary osteons in which lamellae are parallel-fibered or lamellar tissue.

LAGs are typically thin, black lines continuous around the circumference of the bone. LAGs are formed annually from complete or near-complete cessations of periosteal bone apposition and are typically reliable age indicators (e.g. Castanet et al. 2004, Köhler et al. 2012; but see Schucht et al. 2021, Heck et al. 2021). Therefore, LAGs represent circumference and shape of the periosteal surface during growth arrest in that particular year. The distance between successive LAGs (i.e.

zonal bone) represents a full year of cortical apposition and growth, although duration of growth hiatus resulting in a LAG is unknown. For example, American alligator (*Alligator mississippiensis*) growth in northern regions (e.g. North Carolina, USA) is inhibited by low temperatures for approximately 6 months, whereas alligator growth in warmer southern regions of Louisiana, USA and Florida, USA are not restricted for significant durations of time (e.g. Lance 2003).

LAGs can be obliterated by medullary cavity expansion, periosteal erosion, and bone remodeling leading to intraskeletal LAG count variation (e.g. Cullen et al. 2020, Heck et al. 2021). Additional evidence suggests a de-coupling of age and LAG formation after the attainment of skeletal maturity in some tetrapods (e.g. Castanet et al. 2004, Calderón et al. 2019). After skeletal maturity, LAGs continue to form with minimal tissue deposition between each LAG. This results in a stacking of tightly spaced LAGs near the periosteal surface termed an external fundamental system. LAGs were traced manually in each humerus cross-section in Adobe Photoshop CC 22.5. Gaps in data due to periosteal erosion, remodeling, and fractures were estimated to construct a full circumference. LAG circumference and cortical area bounded by each LAG was quantified using the BoneJ plugin for ImageJ (Doube et al. 2010, Schneider et al. 2012, Domander et al. 2021).

Annual bone apposition in a single individual is the amount of cortical bone deposited between successive LAGs. Full cross-section geometric centroid, major axis, and minor axis were determined using the BoneJ plugin for ImageJ (Doube et al. 2010, Schneider et al. 2012, Domander et al. 2021). Distance from centroid to each LAG along the major and minor axes was quantified in ImageJ. Inner LAG distance was subtracted from distance to successive LAG on each axis for single year apposition. The four distances (2 along major axis, 2 along minor axis) were averaged for each year to determine annual apposition. Daily apposition rates were

calculated for 365 days of bone growth and 275 days of bone growth (i.e. 90-day growth hiatus) for direct comparison with previous studies (Köhler et al. 2012, Woodward et al. 2015).

Humeri with at least 3 traceable cortical LAGs (n=20) were used to model ontogenetic cortical apposition in *M. peeblesorum* humeri following protocol modified from Lee and O'Connor (2013) and Cooper et al. (2008) (see Woodward et al. 2015). Individual humerus circumference growth was analyzed with Monomolecular, Von Bertalanffy, Gompertz, Logistic, and Linear modeling. Best fit models are used to evaluate growth trends within a single skeletal element or individual body mass. For example, Linear models indicate consistent growth through ontogeny, whereas Logistic, Gompertz, Von Bertalanffy, and Monomolecular express variable growth and life history event timing. Logistic models best fit organisms with delayed onset of rapid juvenile growth and slightly elongated timing of skeletal maturity. Monomolecular and Gompertz models best fit organisms with rapid growth through early ontogeny, elevated growth rates during sexual maturity and faster attainment of skeletal maturity relative to other models. AIC_c values for each model were averaged across the entire modeled sample to determine best fit. Goodness of fit was determined by lowest AIC_c and mean residual standard error. The best fit model was then used to produce a mean growth curve of humerus circumference by age. Confidence intervals (95%) were established for the mean growth curve using mean residual standard errors. Unlike tibiae, LAGs in humeri were not preserved throughout ontogeny and were obliterated through extensive cortical remodeling and medullary cavity expansion in older individuals (Woodward et al. 2015; but see Wosik et al. 2020). The number of missing LAGs within humeri cortices was manually determined using the best fit growth model as a guide. Missing LAGs and observed LAGs were totaled to estimate age at death.

Survivorship curves were modeled using age at death estimations derived from *M. peeblesorum* humerus LAG counts and growth curve analysis. Survivorship curve modelling, mean annual mortality rates, and significant mortality differences between age groupings followed protocol

outlined in Woodward et al. (2015) utilizing methods from Steinsaltz and Orzack (2011). Confidence intervals (95% CI) of mortality ratios for each age group determined significant decreases in mortality between age groupings as outlined in Woodward et al. (2015).

Terminology used to describe age classes and groupings is inconsistent across non-avian dinosaur literature. Age group nomenclature often uses vague terms such as 'juvenile', 'subadult', and 'adult'. In agreement with Griffin et al. (2021), we avoid usage of such nomenclature and instead use more informative numerical age ranges.

Results

Ontogenetic changes in bone microstructure

The fifteen smallest specimens in the sample (i.e. those with smallest minimum circumference) lacked annual growth marks (LAGs) and are considered <1 years-old. The *M. peeblesorum* <1 year-olds have humerus cortices composed of woven-parallel tissue complexes. Vascular orientation is reticular in the deep cortex and transitions to laminar orientation in the outer cortex (Fig. 30A). The extent of reticular vascular canals is dependent on region of the cross section; reticular canals are more prevalent on the anterior side of the cortex. Laminar vascularity is dominated by circumferential rows of longitudinal canals interconnected with circumferential canals and few radial anastomoses. Large resorption cavities are present near the medullary cavity indicating medullary cavity expansion was occurring at time of death in this group (Fig. 30B). Cortical remodeling is typically focused postero-laterally near the endosteal surface (e.g. H2 – H5) and extends around the entire medullary cavity in the innermost cortex (e.g. H13-H14).

LAGs are present in larger humeri cortices (minimum circumference > 113mm) and are similar in morphology to those described in Horner et al (2000) and Woodward et al. (2015) (Fig. 30C). Reticular fibrolamellar tissue transitions to laminar fibrolamellar tissue prior to the first LAG. Humeri with more than one LAG are generally plexiform, laminar, or sub-laminar woven-parallel

tissue complexes with local regions of reticular vascularity. Vascular orientation shifts primarily to circumferential rows of longitudinally oriented primary osteons in specimens >7 years old. Woodward et al. (2015) described shifts in vascular orientation within yearly growth in *M. peeblesorum* tibiae; vasculature was reticular immediately following LAGs (starting with the second LAG) and then shifted to laminar and plexiform vascularity. Distinct patterns of vascular shifts are not present in humeri cross sections. Local vascular shifts occur but are not consistent within a specimen or between specimens.

Secondary osteons are present in nearly all humeri cortices. Remodeling in <1 year-olds is initially isolated to the postero-lateral innermost cortex before spreading throughout the inner cortex. Secondary osteons are present evenly around the inner cortex of humeri between 1 and 3 years old. Remodeling expands outward toward the periosteal surface in individuals >4 years old. Remodeling and medullary cavity expansion obliterate primary cortical tissue and innermost LAGs in older individuals. Missing LAGs in the inner cortex was common in larger humeri, and a maximum of three LAGs in two individual humeri (H42, H44) were obliterated from remodeling and medullary cavity expansion. In contrast to the largely open medullary cavity in the tibiae, resorptive processes and secondary tissue deposition maintain an extensive network of trabeculae within the medullary cavity of all humeri; trabeculae are composed of a woven tissue core surrounded by secondarily deposited lamellar tissue.

LAG spacing is typically tighter on the lateral and medial sides of the cortex and spacing increases on the anterior side. Qualitative identification of an EFS is difficult due to LAG spacing variation. An external fundamental system is characterized by tightly spaced LAGs, parallel-fibered or lamellar bone tissue, and reduced vascularity (e.g. Horner et al. 1999, Ponton et al. 2004). Using these criteria, seven humeri have a definitive EFS (H34, H37, H38, H39, H41, H44, H47) and three additional humeri have an incipient EFS (H28, H35, H40).

Growth curve analysis

Three or more LAGs were identified in twenty-four humeri, but remodeling, compression, and/or fracturing prevented accurate LAG tracings in five humeri (H24, H30, H35, H36, H41). Thus, nineteen humeri were used to evaluate humerus circumference growth. Overall humerus circumference growth was best described by a monomolecular model (lowest AIC_c), similar to tibiae (Woodward et al. 2015). Humerus circumference is variable by age, and individual growth curves can extend above and below the mean growth curve (Fig. 32).

Daily apposition rates were calculated for humeri containing at least one LAG (n=32). However, fracturing, compression, and remodeling in three humeri (H30, H35, H41) prevented accurate apposition calculations. Average daily apposition rate is highest in the first year of growth (40.67 μm/day) and decreases by 75% in year 2 (9.92 μm/day) (Table 7). Average daily apposition rate continues to decrease after the second year, although year to year changes in average daily apposition rate are minimal (-2.39 μm/day – 0.37 μm/day).

Survivorship

Growth curve modeling revealed sampled humeri encompass a thorough ontogenetic series; *M. peeblesorum* ages not represented include 9-year-olds, 13-14 year-olds, and 16-18 year-olds. All un-represented ages are those predicted to be skeletally mature by growth curve analysis (Fig. 31). Survivorship curve calculation revealed three distinct age groups based on mortality rate: 0-1 years-old, 2-8 years-old, and ≥9 years-old (Figure 33). Mortality is highest in skeletally mature individuals 9 years and older (29%), followed by ≤ 1 year-olds (24%) and 2-8 year-olds (13%) (Fig. 33).

Regression analysis

Four linear regressions were performed to analyze the relationship between humerus length and least circumference using complete/ near-complete specimens (n=17): 1) gross morphological circumference (GMC) and length (Fig. 34A), 2) GMC and length including nestling GMC (circumference = 27.3mm, length = 76.3mm per Prieto-Marquez and Guenther 2018) (Fig. 34B), 3) retrodeformed circumference (RDC) and length (Fig. 34C), 4) RDC and length including nestling GMC (Fig. 34D). Correlation was highest in the relationship between RDC and length including nestling GMC (R^2=0.9861) followed by RDC and length (R^2=0.9805), GMC and length including nestling GMC (R^2=0.9715), and GMC and length (R^2=0.9589). Lengths of incomplete humeri (n=30) were interpolated from the 'RDC and length including nestling GMC' linear regression (y=2.661x – 5.4214).

Humerus length ranged from 205mm – 580mm and was variable within and between age groups. <1 year-old humerus length did not overlap with other age groups (205mm – 303mm), while overlap occurs within ages 1-3 (334mm – 407mm) and within ages ≥4 (426mm – 580mm). Individual variation in humeri lengths is highest in ages 4 (426mm – 545mm), 8 (460mm – 575mm), and 7 (463mm – 565mm). Additionally, the oldest individual in the sample (H39) was not the longest humerus, although the longest humerus (H44) was also skeletally mature.

M. peeblesorum humeri are aged using number of LAGs within each cortex and adjusted using the above growth curve analysis. However, humeri with four LAGs that are nearing a fifth year (but lack a fifth LAG) would still be categorized as 4-years-old at time of death. LAG circumference is thus a more appropriate data point than cross section circumference. Thus, *M. peeblesorum* humeri with LAGs are used to bolster the humerus length data with longitudinal sampling (Figure 35). Each LAG circumference is used to interpolate humerus length at that particular age using the above linear regression. Humerus length in <1 year-old *Maiasaura* overlaps with year 1 humeri after longitudinal data sampling. Humerus length increases sharply

between years 1 and 5 and growth slows until reaching horizontal asymptotic growth between years 7 and 9.

Discussion

Collagen fiber organization and vascular canal orientation reflect apposition rates in bone cortices. High growth rates are associated with woven fibered tissue complexes, and lamellar tissue is the result of low apposition rates (e.g. Castanet et al. 2000, de Margerie et al. 2002). Similarly, radial vascular canals are associated with high growth rates and longitudinal canals with low growth rates, but growth rates overlap between vascular orientations (Castanet et al. 1996, 2000, de Margerie et al. 2002, 2004) (Table 8, Fig. 36). Early *M. peeblesorum* humerus growth is characterized by woven-parallel tissue with reticular vascularization. Reticular vascularization shifts to laminar vascularity prior to the first LAG and continues as plexiform and laminar vascularity through ontogeny with local regions of sub-laminar and reticular vascularity. Apposition is highest in the first year of growth in *M. peeblesorum* humeri, consistent with previous measures of high growth rate associated with reticular vascularization (e.g. Castanet et al. 2000).

Cortical bone in *Maiasaura* humeri shares general characteristics with previously described *Maiasaura* long bone diaphyses (see Horner et al. 2000, Woodward et al. 2015). Woven-parallel bone (sensu fibrolamellar; see Francillon-Vieillot et al. 1990) is described throughout the skeleton of *Maiasaura* (Horner et al. 2000, Woodward et al. 2015). Vascularity in tibiae cortices is reticular or laminar in younger individuals before shifting to plexiform vascularization, similar to humeri (Woodward et al. 2015). Woodward et al. (2015) also note vascular shifts in young of the year and within zonal bone of tibiae. Local increases in vascularity prior to the first LAG in tibiae are not annual markers and are generally isolated to the posterior side of the cortex (Woodward 2019). A narrow region of decreased vascular density is present in the inner cortices of five <1

year-old humeri, but the region of reduced vascularization is not consistent around the cortex. Vascular decline may be an artifact of compression or increased mineralization within vascular canals and not a true biological signal. However, vascular reduction may also be a non-cyclical growth mark recording the timing of young departing the nest, akin to a weaning line in mammals (e.g. Nacarino-Meneses and Köhler 2018). Sampling nestling humeri would clarify the presence or absence of analogous vascular rings and their biological significance.

Zonal bone in *Maiasaura* tibiae undergo a shift in vascular orientation after the second LAG; reticular vascular canals are present immediately after each LAG and vascular canals then quickly shift to laminar or plexiform orientation. This pattern repeats in each zone and is most prevalent on the posterior side of the tibia cortex. Such shifts in vascular canal orientation are not present in *Maiasaura* humeri. Instead, humeri are primarily composed of laminar and sub-laminar vascularity within zonal bone and local shifts to reticular vascular canals do not reveal consistent patterns. Higher apposition rates, such as those in tibiae, are more likely to reflect external stimuli (e.g. environment, resource limitations, biomechanics). For example, fast growing, juvenile, cortical bone is more responsive to experimental mechanical loading than slow growing, adult cortical bone (Pearson and Lieberman 2004). The absence of annual vascular shifts in humeri is likely due to lower cortical apposition rates in *Maiasaura* humeri relative to tibiae.

Cortical remodeling is extensive throughout humerus ontogeny unlike minimal remodeling in tibiae (Woodward et al. 2015). Secondary osteons begin to proliferate in <1 year-old humeri and eventually obliterate multiple LAGs in older individuals. Trabeculae extend across and throughout the medullary cavity in humeri but are limited in tibiae. Remodeling and trabeculae in humeri may be a signal of biomechanical shifts due to ontogenetic locomotor transitions. Dilkes (2000, 2001) and Geunther (2014) noted ontogenetic allometric changes in humerus morphology. Dilkes (2001) suggested morphological changes were due to a change in locomotion from bipedal juveniles to quadrupedal adults. Indeed, increases in appendicular mechanical loading results in

directional proliferation of cortical remodeling along axes of introduced strain (e.g. Bentolila et al. 1998). Quantification of cortical remodeling would aid in identifying the potential presence of intracortical signals of mechanical loading.

However, cortical remodeling does not occur only in response to biomechanical stimuli. Cortical remodeling is a vital ontogenetic process for the repair of cortical bone (e.g. Burr et al. 1985), and the presence of remodeled bone is likely due to a multitude of factors including age, biomechanics, phylogeny, and environment. Padian et al. (2016) presented an alternative hypothesis to explain intraskeletal variation in bone remodeling: bone metabolism and resource cycling relative to individual bone growth. Simply, remodeling is more extensive in smaller bones (e.g. humeri) due to excess resources that are not put toward periosteal cortical apposition, whereas remodeling is limited in larger bones (e.g. tibiae) because resources are primarily devoted toward periosteal apposition. Remodeling trends in *Maiasaura* humeri and tibiae are consistent with the metabolic-growth rate hypothesis, though the metabolic hypothesis does not preclude other influences on cortical remodeling, such as biomechanical loading. A more thorough and quantitative approach to humerus micromorphological changes through ontogeny would add more resolution to the locomotor shift hypothesis.

Woven-parallel complexes have been found in a variety of vertebrate long bone cortices including non-avian dinosaurs (Baielleul et al. 2019 and references therein), aves (e.g. Atterholt and Woodward 2021), mammals (e.g. Kolb et al. 2015 and references therein), and crocodylomorphs (e.g. Tumarkin-Deratzian 2007, Klein et al. 2009, Woodward et al. 2014). Woven-parallel tissue complexes with reticular, laminar, and/or plexiform vascularity is a common component of hadrosaur long bone cortices (e.g. Fowler and Horner 2015, Bertozzo et al. 2017) and is likely a physiological tool to achieve substantial body sizes rapidly in large-bodied dinosaurs. Woodward et al. (2015) noted the continued presence of woven-parallel complexes in adult *Maiasaura* tibiae despite drastic declines in apposition rate and zonal bone

thickness. Similar trends are present in *Maiasaura* humeri and are either the result of increased time of growth hiatus/cessation (see Woodward et al. 2015) or extreme growth rate plasticity of woven-parallel complexes (e.g. de Margerie et al. 2002).

Cortical apposition in *Maiasaura* humeri is highest in the first year (40.67 μm/day) of growth and drastically decreases in year 2 (9.92 μm/day) and beyond (Table 9). Second year daily apposition rate in the humerus is a 76% decrease and third year daily apposition rate (8.53 μm/day) is a 79% decrease from first year apposition rates. Average daily apposition rate decreases by 96% in the fifth year relative to average daily apposition rates from the first year of growth. Average daily apposition rates in the *Maiasaura* tibiae show similar decreases relative to apposition rates in the first year: 67% decrease in daily apposition rates in year 2 and a 79% decrease in year 3. However, decreases in tibia daily apposition rates do not descend by 96% until the sixth year of growth. Slight differences in apposition rates between humeri and tibiae is due to overall size differences between the two elements and larger sample size of >1 year-old specimens in the humerus sample. Humeri reach skeletal maturity earlier in ontogeny than tibiae, possibly due to the smaller size of humeri throughout ontogeny. Alternatively, heterochrony divergence between the two elements could reflect limb scaling patterns as a result of locomotor shifts. A locomotor shift in the first year of life would necessitate high humerus growth rates to account for center of mass shifts and introduced mechanical loading. Humerus growth then slows rapidly after reaching a size that allows for efficient quadrupedal locomotion. Investigating the locomotor shift hypothesis would benefit from detailed analyses of limb scaling patterns in *Maiasaura*, although the disarticulated and disassociated nature of the *Maiasaura* bonebed prevents direct limb bone comparisons.

Growth curves of age and minimum circumference were constructed for individual humeri containing three or more LAGs and had minimum deformation (n=19). Individual growth curves were used to model a mean growth curve with 95% confidence intervals, similar to methods of

Woodward et al. (2015). Circumference growth in both humeri and tibiae are best explained by a monomolecular model despite differences in sample sizes between the two studies. The results of the current study, utilizing a large sample of humeri, confirms growth curve results from tibiae (Woodward et al. 2015) and shows growth in *Maiasaura* humeri follow similar monomolecular curve patterns as tibiae.

Survivorship curves and life history tables provide a means to better understand the paleobiology of extinct populations. However, previous attempts to construct non-avian dinosaur survivorship curves, with the exception of *Maiasaura* (Woodward et al. 2015), were limited by low sample sizes, mixed skeletal element analysis, and minimal histological confirmations of animal age. Individual, cross-sectional growth curves of *Maiasaura* humeri and tibiae display individual variation in both length and circumference; variation that can shift demographic inferences in the absence of histological aging. Woodward et al. (2015) was the first study to utilize more than thirty specimens of the same element (with age determined by histology) to construct survivorship curves. Presently, this is only the second study to age 30 or more specimens using osteohistology to infer paleodemographics of a single extinct population.

General patterns of mortality are similar between data derived from *Maiasaura* tibiae and humeri. Survivorship curves from both skeletal elements are similarly sigmoidal with relatively high mortality in juveniles and adult individuals. Mortality rate per year led to similar age groupings based on significant differences between age mortality: 0-1 years-old, 2-8 years-old, and >9 years-old. There is also a significant increase in mortality between ages 2 and 3 in both *Maiasaura* tibiae and humeri. However, only one of the three age groupings had numerically similar mortality rates between humeri and tibiae: mortality rate in the 3-8 years-old age grouping was similar between both skeletal elements (12.7%). Mortality rates in the ≥9 years-old grouping was higher in tibiae (44.4%) than humeri (29.3%) and mortality rates in the 0-1 years-old age grouping was significantly higher in tibiae (89.9%) than humeri (24.1%).

Large scale analyses of non-avian dinosaur survivorship often result in sigmoidal (B1) survivorship curves (Erickson et al. 2006, 2009, 2010, Woodward et al. 2015, but see Weon 2015 and Griebeler 2021). Traditionally, sigmoidal (B1) survivorship curves were best exemplified by Deevey (1947) in which populations remained stable until high mortality due to senescence (e.g. humans). However, we accept the revised definition of type 1 survivorship curves in which mortality is high in juveniles, stabilizes in sub-adults, and increases again in elder individuals (Hill et al. 2021).

High mortality in juveniles is common in non-avian dinosaur survivorship profiles (e.g. Erickson et al. 2006, Woodward et al. 2015) and resembles survivorship observed in extant r-selected taxa (e.g. Roe deer (Putman et al. 1996)). We hypothesize that <1 year-old humeri in our sample originate from individuals that died during their first unfavorable season, in agreement with Woodward et al. (2015).

Specific risk factors (i.e. predation, drought, disease) place pressures on individuals to attain certain minimum sizes early in life. For example, a capture-monitoring study of female white-tailed deer (*Odocoileus virginianus*) found that overwinter mortality decreased 4.3% with each additional kilogram of body mass (Kautz et al. 2020). *Maiasaura* <1 years-old in the bonebed may not have reached a large enough body mass to reduce or eliminate such risks. LAG circumference can be used as a simple approach to preliminary investigations into body size attainment and death. Average humeral circumference of year 1 LAGs is 100.6mm (n=20) with median circumference of 100.2mm. Only five of the fifteen <1 year-old humeri have a circumference exceeding 101mm. Five individuals that perished during the third year of life (n=6) were below the average LAG 3 circumference (154.7mm) and median LAG 3 circumference (157.9mm). Low sample sizes in other age groups prevent further preliminary analysis of individual size and mortality. Nonetheless, the unfavorable season and event resulting

in *Maiasaura* mass death have had a disproportionate impact on smaller individuals within <1 year-old and 3 year-old age groups.

Juvenile over-representation in the *Maiasaura* bonebed (Varricchio and Horner 1993, Woodward et al. 2015) (Fig. 37) is consistent with previously described hadrosaur population compositions (e.g. Brinkman 2014, Fondevilla et al. 2018, Wosik et al. 2020). However, individuals in the 2-4 years-old age range are often under-represented in assemblages (e.g. Horner et al. 2000, Woodward et al. 2015, Wosik et al. 2020, Holland et al. 2021) and may be the result of age-specific survivorship (Woodward et al. 2015) or age segregation (e.g. Holland et al. 2021). *Maiasaura* tibiae lacked individuals 1-2 years-old and 3-4 years-old (Woodward et al. 2015). All individual ages ≤8 years-old are represented in the *Maiasaura* humerus sample. Thus, absence of specific age groupings in previous *Maiasaura* studies is likely an artifact of taphonomic bias.

Scavenging can result in bone modification and transport (Sala and Arsuaga 2018), thus, altering demographic interpretations of bonebeds. Modern studies indicate scavenging is size-biased: smaller specimens are more likely to be scavenged and transported (Behrensmeyer et al. 1979). Capaldo and Peters (1995) found loose correlation between scavenged skeletal element and marrow potential in drowned wildebeests. Wildebeest tibiae have high marrow content and were underrepresented in skeletal inventories of drowned individuals. Indeed, some carnivores show preference for marrow-rich bones under experimental conditions (Marean et al. 1992). Fewer adult *Maiasaura* tibiae are represented in the death assemblage relative to adult humeri, a pattern similar to that of modern Wildebeest. However, evidence of scavenging of *Maiasaura* remains, prior to sediment flow transport, was minimal (Schmitt et al. 2014), and juvenile overrepresentation supports limited influence of scavenging.

Alternatively, age composition differences between *Maiasaura* humeri and tibiae may relate to element sorting and transport. The *Maiasaura* death assemblage location is the result of a mass

sediment flow transporting buried and unburied *Maiasaura* remains (Schmitt et al. 2014). Transport distance is reliant upon skeletal element articulation and element size (e.g. Aslan and Behrensmeyer 1996, Coard 1999, Moore and Varricchio 2018). Smaller skeletal elements are more likely to be relocated in fluvial systems (Aslan and Behrensmeyer 1996) and smaller elements are transported a greater distance with increased sorting. *Maiasaura* skeletal elements originate from multiple excavation sites across the death assemblage at the Willow Creek Anticline (Schmitt et al. 2014), and bone size composition of each site may be dependent on distance from debris flow center. Differences in age profiles between *Maiasaura* humeri and tibiae may simply reflect excavation biases along the assemblage due to sorting differences in which smaller humeri are transported further than similarly aged, but larger, tibiae.

Preservation and collecting biases impact paleobiological inferences by artificial alteration of collection composition. The *Maiasaura* mass death assemblage has been extensively and thoroughly excavated for over 40 years (Horner and Gorman 1988) and potential collecting biases are likely minimal. On the other hand, mortality rates in humeri may be impacted by preservation bias. *Maiasaura* tibiae undergo little medullary cavity expansion and, thus, have thick cortices at the minimum circumference (Horner et al. 2000, Woodward et al. 2015). Thicker cortices provide stability and prevent, to a degree, deformation about the diaphysis in larger limb bones. Medullary cavity expansion is greater in humeri and deformation is more extreme relative to tibiae (pers. obs.). Deformation and fracturing about the minimum circumference prevents histological aging and such specimens were not included in the current study. Deformed and fractured specimens could be aged using relative size comparisons to the aged sample to bolster survivorship data and provide more accurate insight into *Maiasaura* life history.

Insight into extinct taxa demography is affected by taphonomic biases, collection biases, and sample size. The *Maiasaura* mass death assemblage is a unique bonebed that can be utilized to test and ground truth paleobiological assumptions using a sample size sufficient for producing

statistically significant results. The bonebed has limitations due to the disarticulated and disassociated nature of *Maiasaura* skeletal material (e.g. Varricchio and Horner 1993), similar to numerous other non-avian dinosaur bonebeds (e.g. Snyder et al. 2020). Skeletal material disassociation prevents direct observations of aging, ontogeny, and scaling between elements. The present study assumes LAG counts between humeri and tibiae are similar as has been shown in previous intraskeletal studies (e.g. Woodward et al. 2014), although evidence of intraskeletal growth mark count and spacing variability has been described in some extinct and extant tetrapods (e.g. Cullen et al. 2014, Heck et al. 2021). Intraskeletal osteohistological examination of an articulated *Maiasaura* would add credence to our results and interpretations.

Conclusions

Previous attempts at inferring life history traits were reliant upon low sample sizes and mixed element analyses due to specimen availability, fossil biases, and trophic biases (e.g. Erickson et al. 2006). The current study suggests humeri and tibiae are valid for analyzing broad patterns of survivorship in non-avian dinosaur populations. However, differences in humerus mortality rates within early juvenile (0-1 years-old) and adult (≥9 years-old) age groupings warrant caution in mixed element sampling. Further demographic analyses of the *Maiasaura* assemblage should focus on single long bone element testing (e.g. femora, ulnae, radii) for comparison with results derived from humeri and tibiae data. Additionally, modern studies focused on osteohistological life history reconstructions are essential for clarifying intraskeletal variation in life history signals.

Figures

Figure 27. Subset of sampled *Maiasaura* humeri displaying varying degrees of fracturing, missing cortex, and compression. Shaded regions are estimated area of missing cortex.

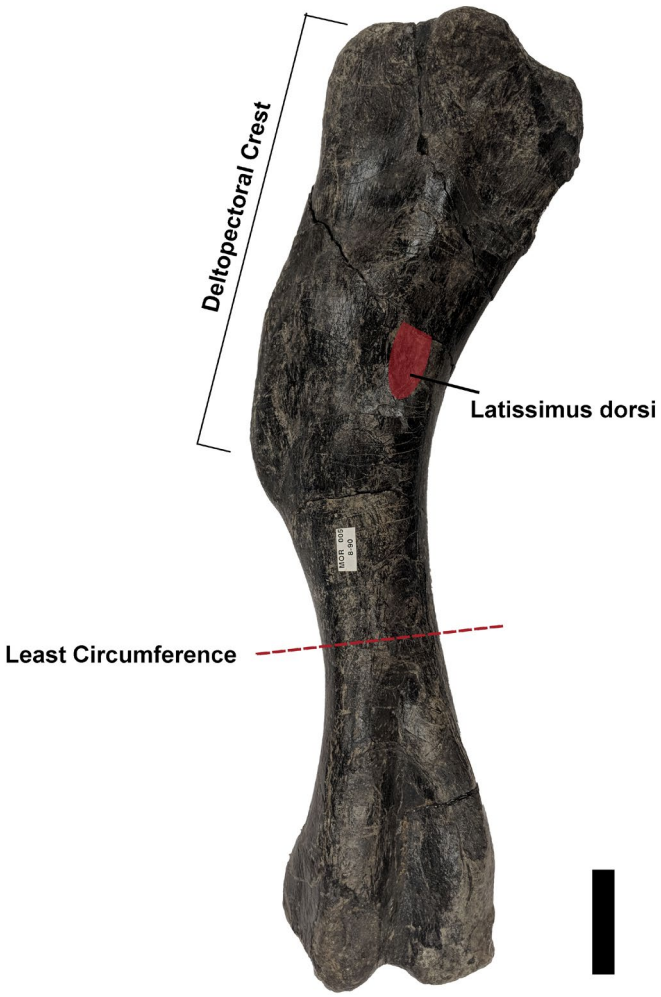

Figure 28. *Maiasaura* humerus anatomy. Transverse sections were removed from the least circumference, distal to the deltopectoral crest.

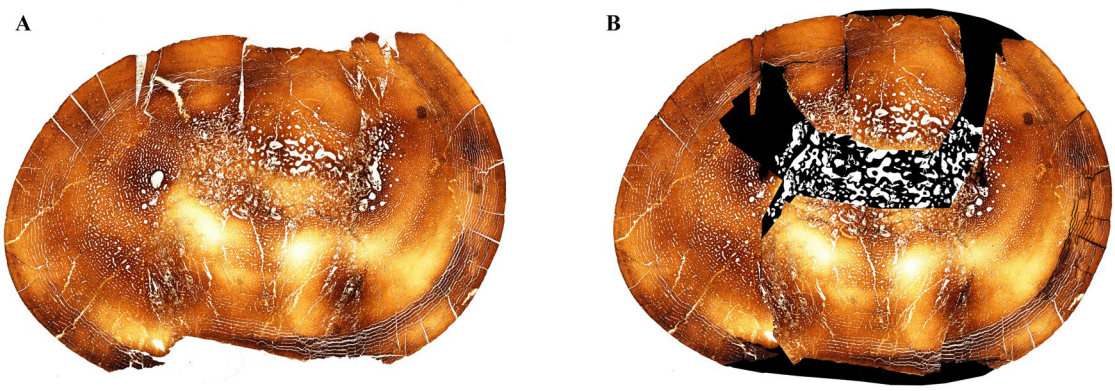

Figure 29. Compressed specimens (left) were retrodeformed (right) for more accurate measurements of perimeter, cortical area, and medullary cavity area. Missing cortex was estimated.

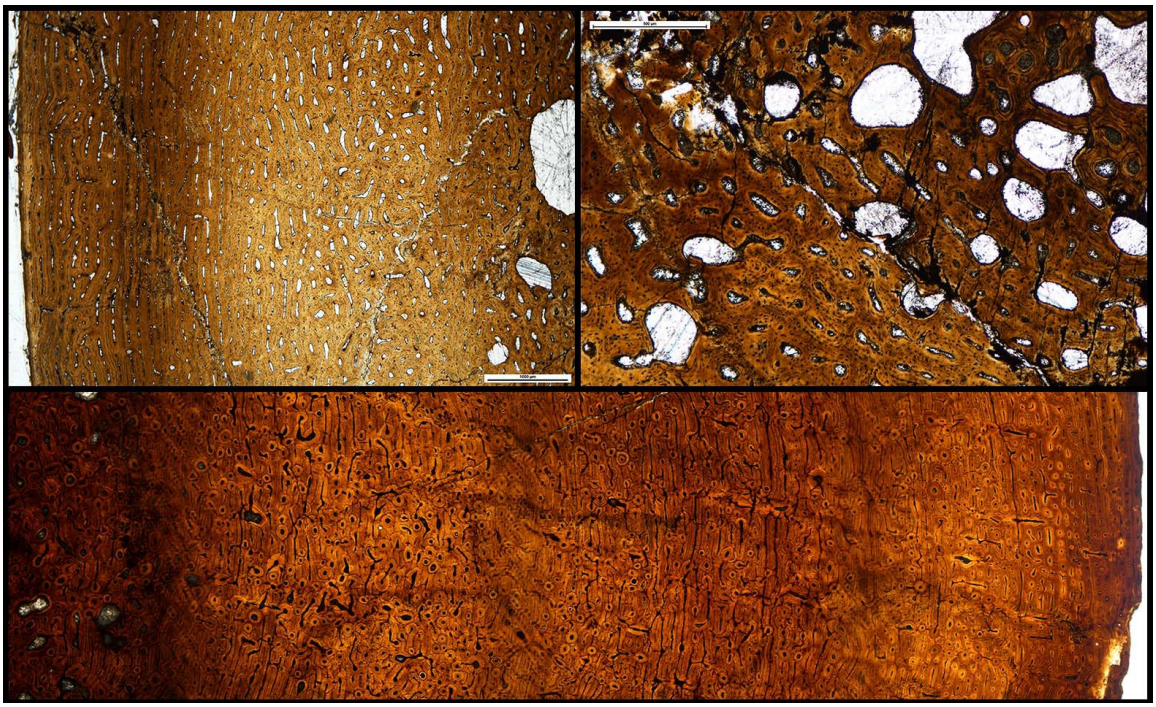

Figure 30. Cortical composition of juvenile *Maiasaura* (A, B) and adult *Maiasaura* (C). (A) Juvenile *Maiasaura* show reticular vascular orientation in the deep cortex before transitioning to laminar or sub-plexiform vascular orientation in the outer cortex. (B) Cortical resorption is present in juvenile *Maiasaura* and infilling of resorption cavities is also ongoing. (C) Adult *Maiasaura* show laminar, reticular, and plexiform vascular orientation along with cortical growth marks.

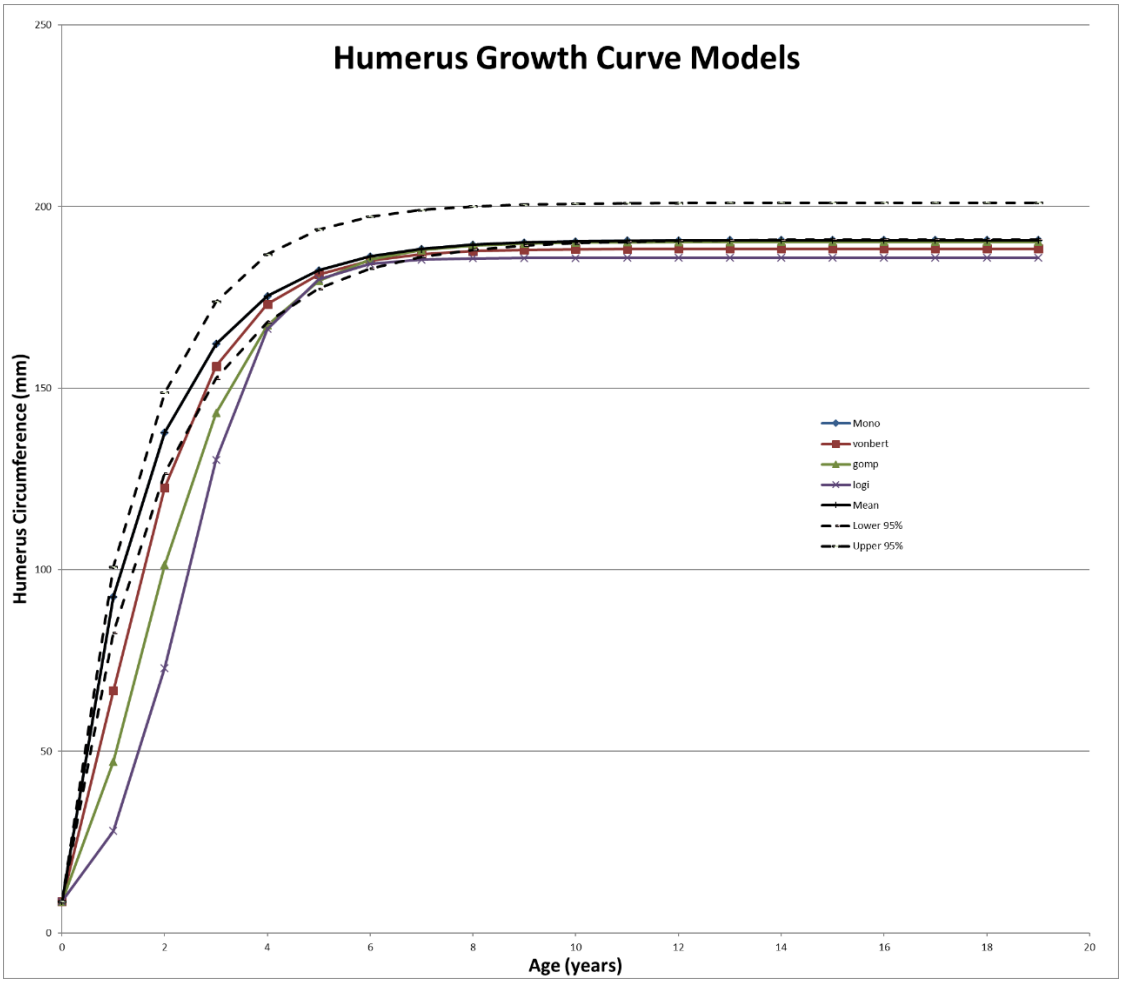

Figure 31. Annual growth marks were used to construct growth curves and models were assessed by AIC_c score. *Maiasaura* humerus growth was best fit with a monomolecular model.

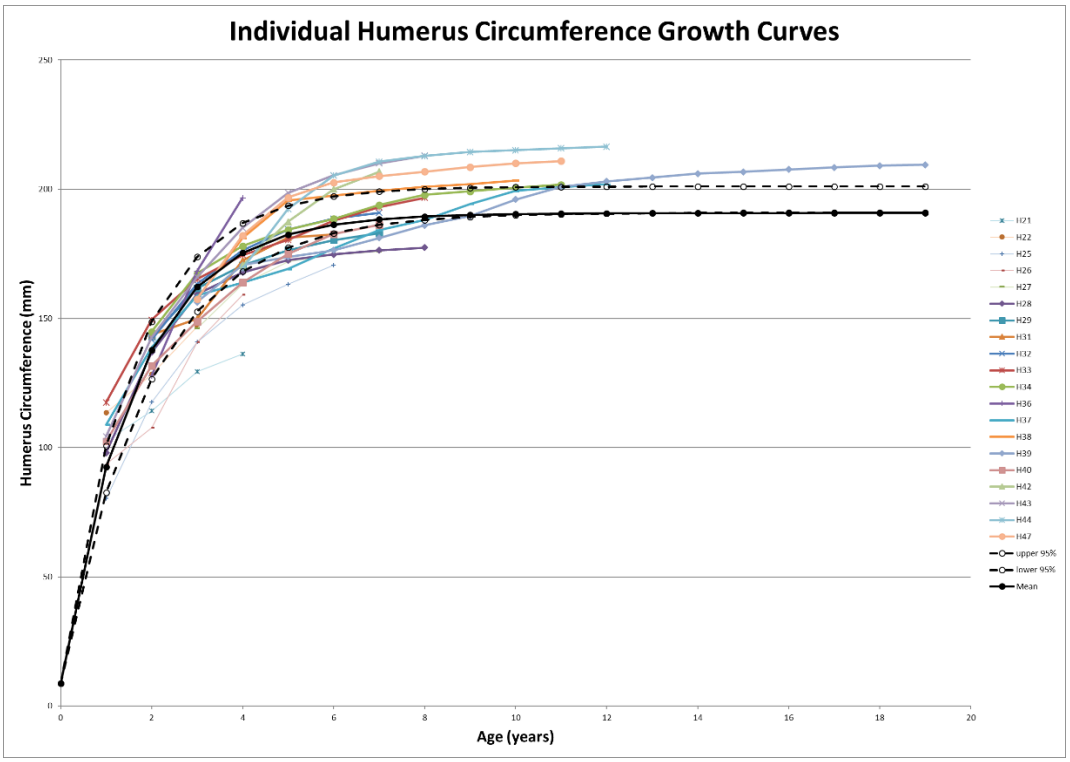

Figure 32. Individual *Maiasaura* humerus growth based on cortical growth marks with hatchling data as an anchor point. *Maiasaura* humeri displayed individual growth variation.

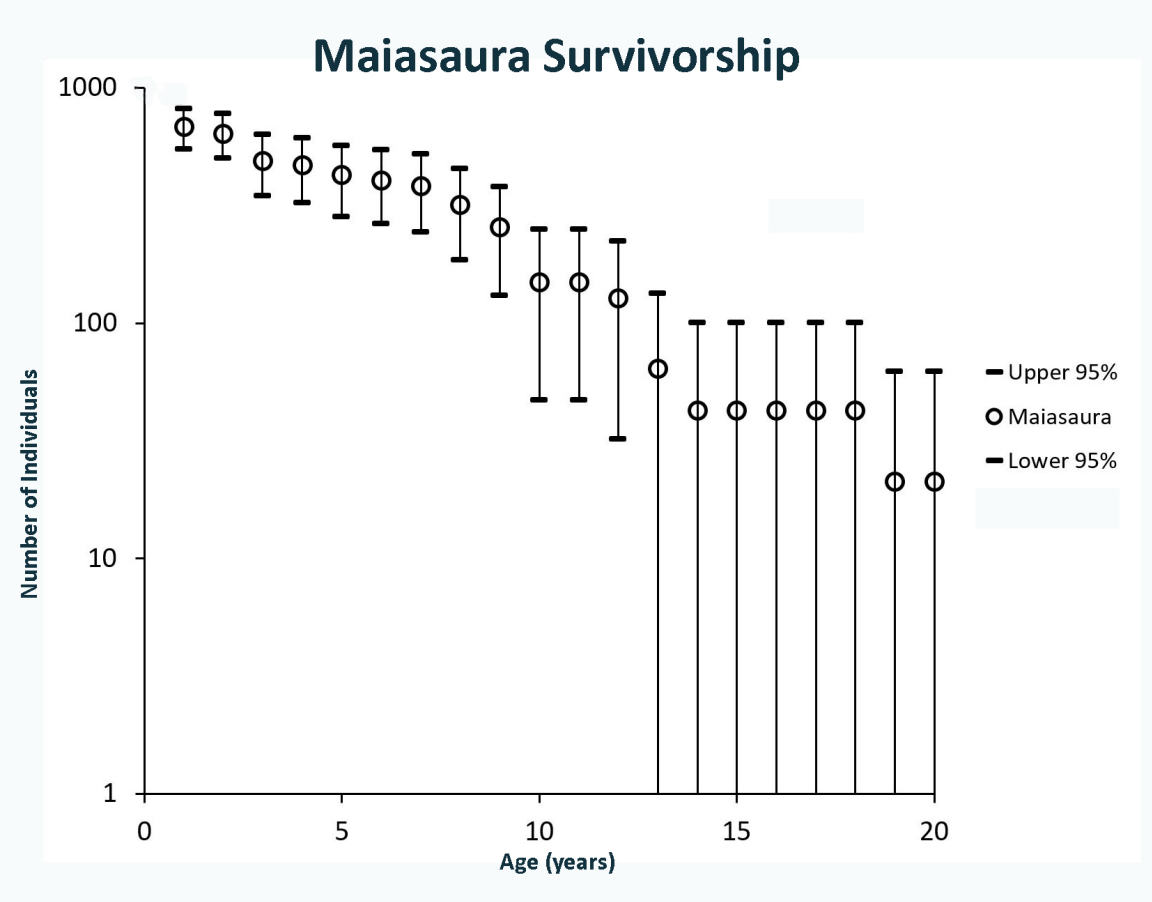

Figure 33. *Maiasaura* survivorship based on cortical growth marks and growth curve modeling. Mortality is highest in older specimens (>9 years-old) and young of the year juveniles.

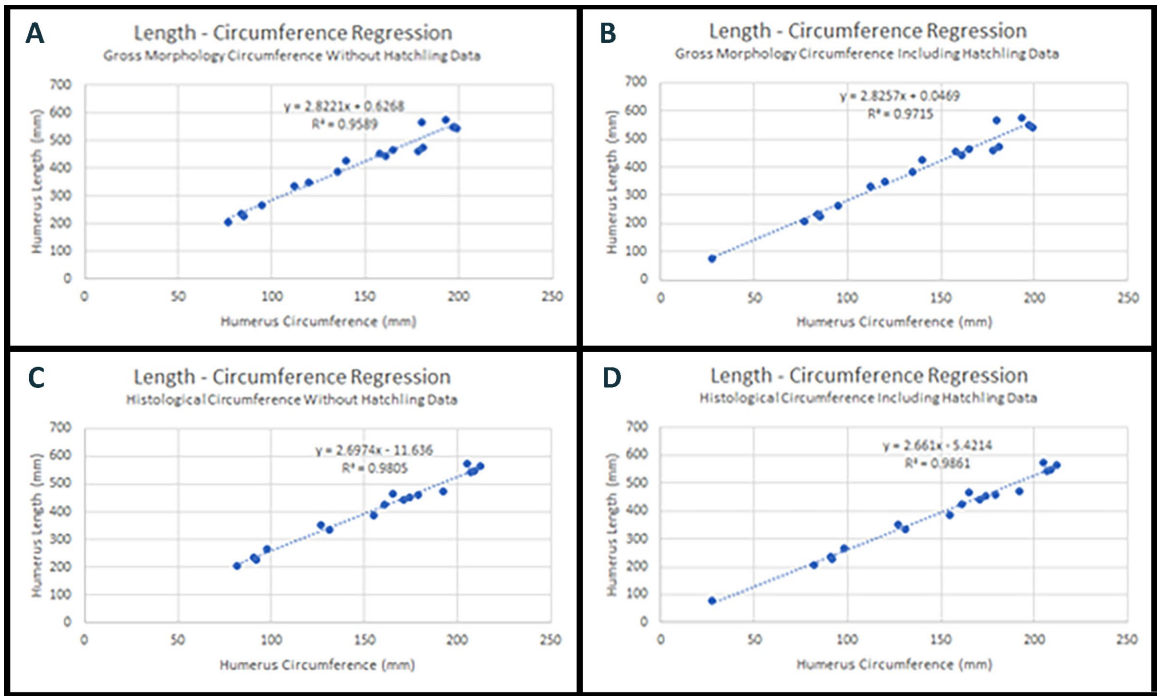

Figure 34. Linear regressions of humerus length and circumference. (A) Regression using gross morphology circumference as measured with fabric tape without hatchling data and (B) with hatchling data. (C) Regression using retrodeformed cross-sections for circumference measurements without hatchling data and (D) with hatchling data.

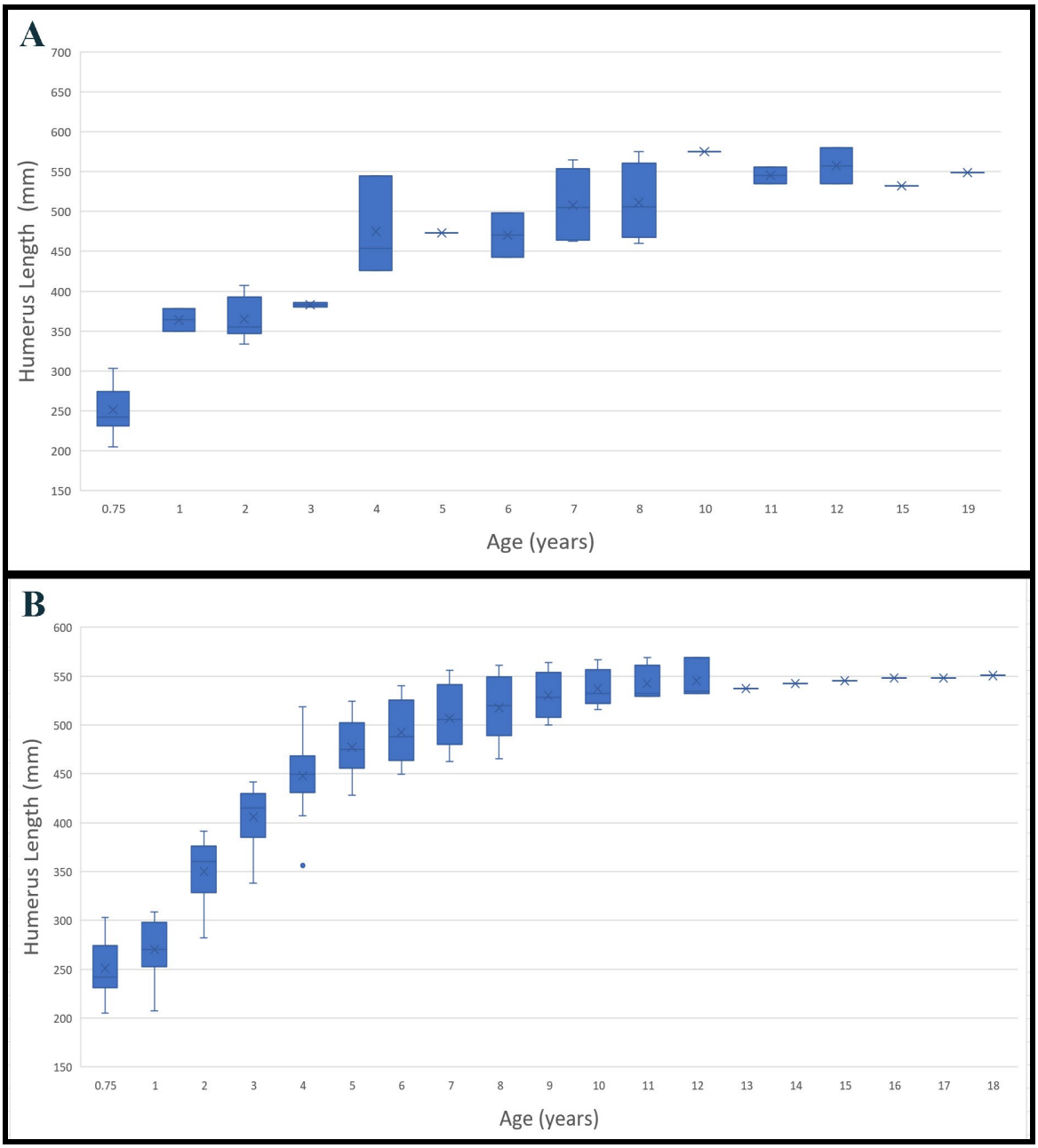

Figure 35. Humerus length with age as determined by (A) outer bone circumference and (B) longitudinal LAG circumference. Length was determined using regressions (above).

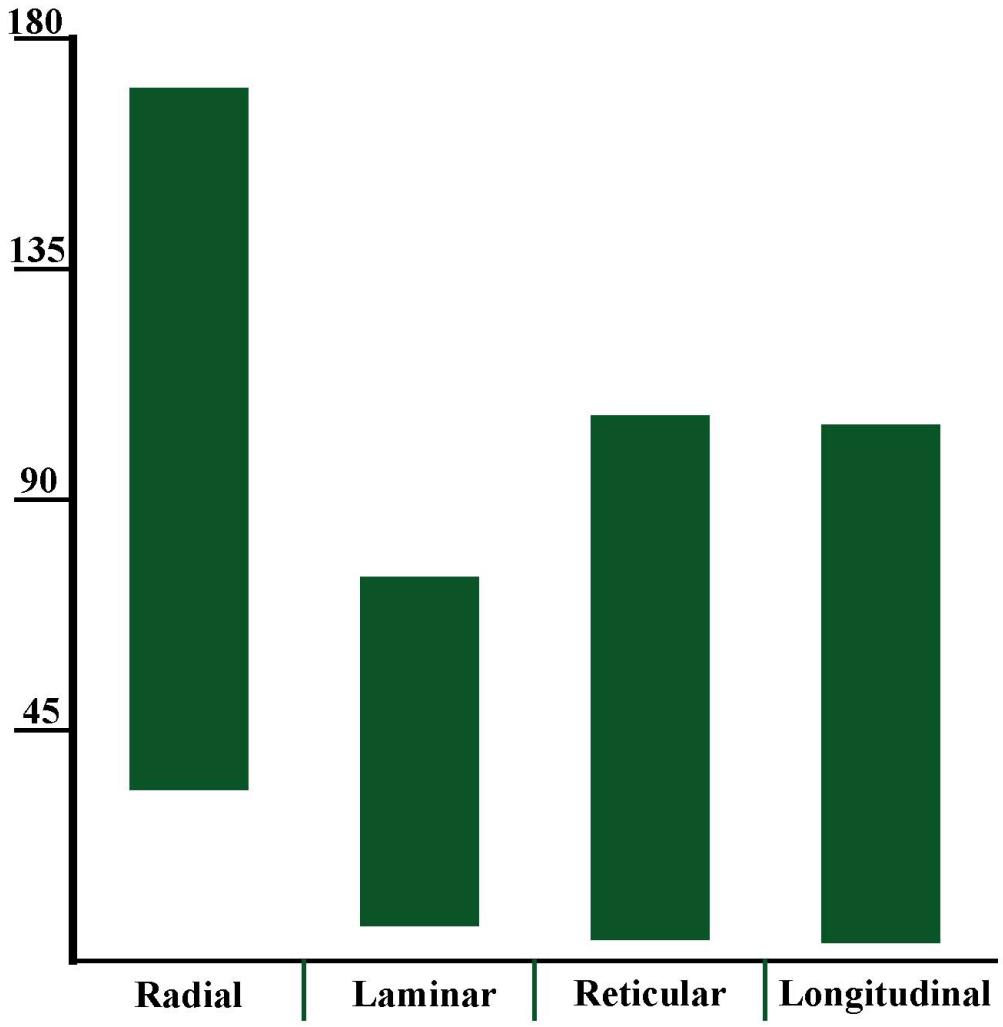

Figure 36. Vascular canal orientation and apposition rate overlap within woven-parallel tissue complexes. Data derived from Castanet et al. 2000, de Margerie et al. 2002, 2004.

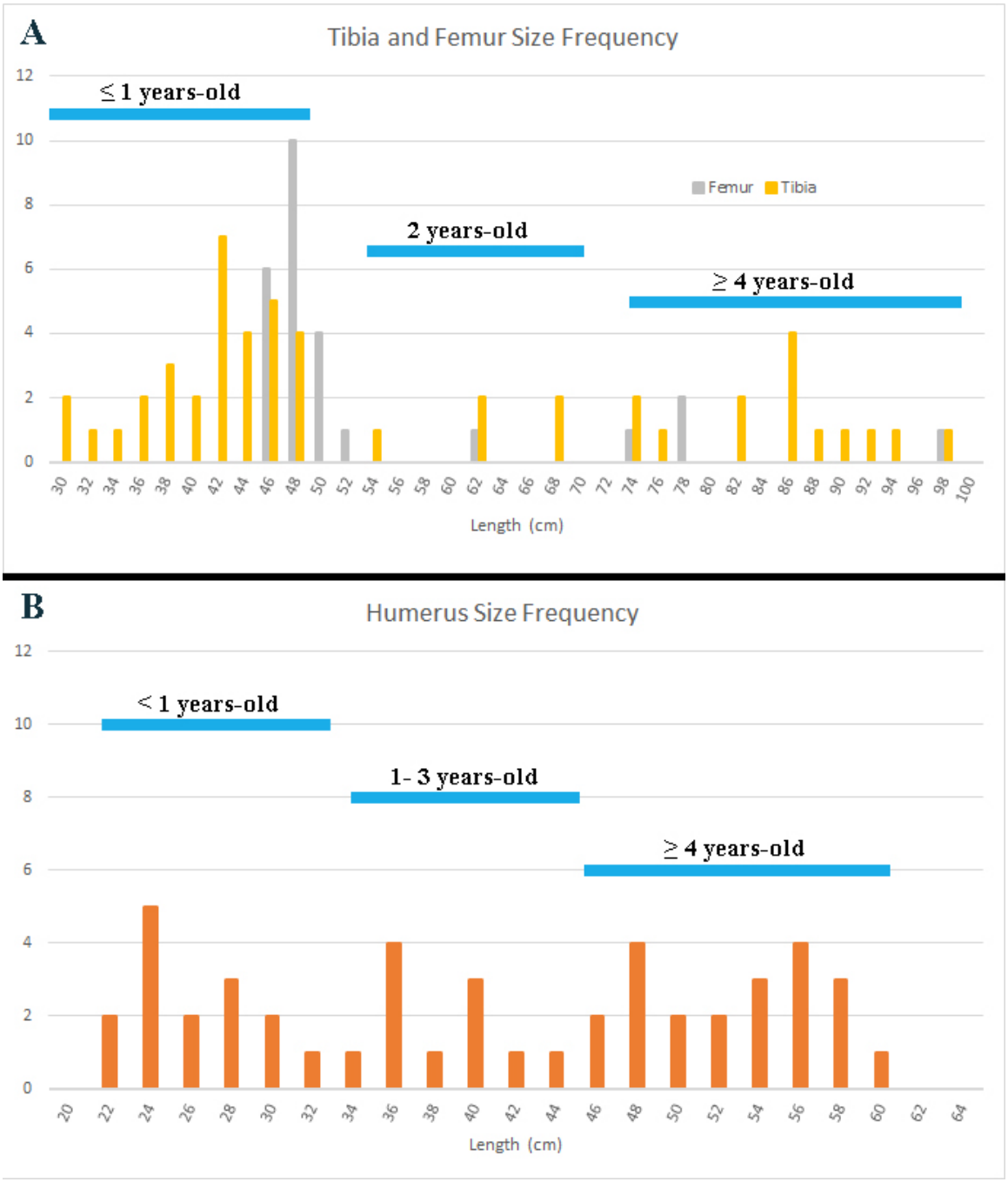

Figure 37. Frequencies of long bones found in the Willow Creek Anticline based on total length. (A) Tibiae and femora frequency and tibia age derived from Varricchio and Horner 1993, Woodward et al. 2015. (B) Humeri frequency as aged in the present study.

Table 6. Length and circumferences of complete specimens used in linear regressions for length interpolations of incomplete specimens.

Humerus Code	Macro Least Circumference (mm)	Total Length (mm)	Cross Section Circumference (mm)
H1	77	206	82
H3	84	235	91
H7	85	226	92
H11	95	265	98
H14	112	334	131
H20	135	385	155
H21	140	426	161
H23	120	350	127
H25	161	443	171
H26	158	454	174
H28	178	460	179
H30	181	473	192
H35	165	465	165
H38	193	575	205
H39	197	549	209
H40	180	565	212
H42	199	542	207
Hatchling	27.3	76.3	-

Table 7. Average daily apposition rates in *Maiasaura* humeri. Apposition rates are determined by zonal bone thickness between successive LAGs. Conventional apposition rate refers to 365-day growth period (continuous growth). 90-day growth hiatus in congruent with ungulate data (Köhler et al. 2012) and assumes a 90-day hiatus during unfavorable season.

		Conventional apposition rate		90 day growth hiatus	
	n	Mean Apposition Rate (micrometers/ day)	Standard Deviation	Mean Apposition Rate (micrometers/ day)	Standard Deviation
LAG1	19	40.67	4.33	53.38	7.02
LAG2	17	9.92	4.21	13.17	5.58
LAG3	14	8.53	2.97	11.31	3.94
LAG4	17	6.42	2.81	8.52	3.73
LAG5	16	4.03	2.26	5.35	3
LAG6	16	2.18	1.67	3.15	1.87
LAG7	13	1.57	0.78	2.16	1.03
LAG8	10	1.3	0.7	1.73	0.92
LAG9	6	1.08	0.86	1.44	1.15
LAG10	6	1.17	0.97	1.55	1.29
LAG11	5	0.73	0.62	0.97	0.83
LAG12	3	0.44	0.33	0.58	0.44
LAG13	1	0.81	0	1.07	0
LAG14	1	0.6	0	0.8	0
LAG15	1	0.24	0	0.32	0
LAG16	1	0.23	0	0.31	0
LAG17	1	0.41	0	0.55	0
LAG18	1	0.02	0	0.03	0
LAG19	1	0.12	0	0.16	0

Table 8. Recorded apposition rates within long bones of sampled aves showing overlap in apposition rates associated with vascular canal orientation. All vascular orientations refer to vascularity within woven-parallel complexes. Data from Castanet et al. 2000, de Margerie et al. 2002, de Margerie et al. 2004.

	Mallard	Emu	Ostrich	Penguin
Humerus				
Radial	-	-	-	100 (45-165)
Laminar	19.2 (7.1-62)	-	20 (Range NA)	24.4 (10-46)
Reticular	12.8 (4.5-66.2)	9.5 (8.1-11)	12.4 (10.1-15.5)	84.7 (48-110)
Longitudinal	21.5 (4.7-54.5)	7.4 (5.5-9.2)	7.8 (6.4-9.2)	47.4 (32-60)
Femur				
Radial	-	-	-	113 (76-171)
Laminar	19.2 (7.1-62)	30.3 (18.1-58.1)	24.2 (13.4-35.9)	36.8 (12-72)
Reticular	12.8 (4.5-66.2)	53.5 (29.8-89.4)	33.8 (13.3-39.6)	52.8 (21-101)
Longitudinal	21.5 (4.7-54.5)	-	4.2	61.5 (30-91)
Tibiotarsus				
Radial	-	-	-	86.8 (34-135)
Laminar	19.2 (7.1-62)	33.5 (31.5-35.5)	31.9 (22.5-34.9)	30.6 (17-60)
Reticular	12.8 (4.5-66.2)	30.1 (11.7-55)	38.9 (35.8-42)	39 (30-48)
Longitudinal	21.5 (4.7-54.5)	-	7.8	54.2 (15-105)
Total Range				
Radial	-	-	-	34-171
Laminar	7.1-62	18.1-58.1	13.4-35.9	10-72
Reticular	4.5-66.2	8.1-89.4	10.1-42	21-110
Longitudinal	4.7-54.5	5.5-9.2	4.2-9.2	15-105

Table 9. Humerus and tibia apposition rates and yearly changes in growth. Tibia data from Woodward et al. 2015.

	Humerus *n*	Humerus Mean Apposition Rate (um/day)	% change relative to year 1	Tibia *n*	Tibia Mean Apposition Rate (um/day)	% change relative to year 1
LAG 1	19	40.67	-	9	65.1	-
LAG 2	17	9.92	-76%	9	21.4	-67%
LAG 3	14	8.53	-79%	5	13.7	-79%
LAG 4	17	6.42	-84%	4	6.9	-89%
LAG 5	16	4.03	-90%	4	5.9	-91%
LAG 6	16	2.18	-95%	3	2.9	-96%
LAG 7	13	1.57	-96%	2	5.8	-91%
LAG 8	10	1.3	-97%	1	2.4	-96%
LAG 9	6	1.08	-97%	1	2.6	-96%
LAG 10	6	1.17	-98%	0		
LAG 11	5	0.73	-99%	0		
LAG 12	3	0.44	-98%	0		
LAG 13	1	0.81	-99%	0		
LAG 14	1	0.6	-99%	0		
LAG 15	1	0.24	-99%	0		

CHAPTER VI

LIMB SCALING AND HUMERUS MORPHOLOGY: TESTING THE LOCOMOTOR SHIFT HYPOTHESIS IN *MAIASAURA PEEBLESORUM*

Introduction

Non-avian dinosaurs (hereafter, simply 'dinosaurs') exhibited varying degrees of quadrupedal and bipedal locomotion (Barrett and Maidment 2017), with evolutionary shifts in locomotor posture (e.g. bipedal to quadrupedal) occurring numerous times across dinosaur clades (Maidment and Barrett 2014, Barrett and Maidment 2017) including Sauropodomorpha, Thyreophora, Ceratopsia, and Ornithopoda. The evolution from bipedal to quadrupedal locomotion in tetrapods is proposed to occur by numerous morphological adaptations to the axial and appendicular musculoskeletal system (Maidment and Barrett 2012, 2014, Maidment et al. 2012). However, whether locomotor shifts in dinosaur taxa also occurred over ontogeny remains unresolved. This is due in part because 1) osteological correlates of bipedalism and quadrupedalism are not as apparent when characterizing ontogenetic locomotor shifts in dinosaurs, and 2) gaps in the ontogenetic fossil record of taxa result in an inability to identify potential osteological correlates indicative of locomotor shift, and 3) limited sample sizes of fossil taxa restrict confident identification of morphological changes as biomechanical in origin. Here, we use a large limb bone sample to evaluate morphological signals of locomotion and directly test the ontogenetic locomotor shift hypothesis in the hadrosaur dinosaur *Maiasaura*

peeblesorum.

Morphological correlates of locomotion

Both the appendicular and axial skeleton of tetrapods exhibit morphological adaptations for either quadrupedal or bipedal locomotion (e.g. Maidment and Barrett 2011, Klinkhamer et al. 2018, Morschhauser et al. 2018, Slowiak et al. 2019). Axial skeleton correlates typically center on vertebral morphology while the appendicular skeleton of tetrapods contains a suite of adaptations for locomotion. Long bone shape and structure is influenced, in part, by biomechanical forces within the organism's phylogenetic constraints (Currey 2002). Locomotion applies stress and strain to limb bones and bone growth response coincides with musculoskeletal functions (e.g. development of muscle attachments) (Turner 1998). Bones also respond dynamically to locomotor habits to maximize biomechanical advantage and safety factors, minimize mass, and dissipate bending stresses (Biewener 1983, 2005, Biewener and Tayler 1986, Bertram and Biewener 1992). However, long bone morphology can also be influenced by other behaviors such as scratch-digging and forelimb use in foraging (e.g. Kilbourne and Hutchinson 2019). Nonetheless, forelimb bone morphology in quadrupedal dinosaurs reflects forelimb myology and leverage during locomotion as well as weight bearing forces acting on bone development (Biewener 1983, Hutchinson 2021 for review). An allometric bone response is assumed for heterochronic quadrupedal shifts in dinosaur locomotor function due to extreme increases in forelimb loading (e.g. Lanyon 1996, DIlkes 2001, Currey 2014).

In addition, Maidment and Barrett (2014) assessed osteological correlates of quadrupedalism in ornithischian dinosaurs and found that reduction of the fourth trochanter and femur length less than tibia length were both strongly correlated with quadrupedal locomotion. Additionally, forelimb length relative to hindlimb length showed some correlation with locomotion, although the authors recognize the ambiguity could be a result of insufficient sample sizes. Further analysis

of ornithischian locomotion revealed that gait and body size were strong influences on appendicular morphology. While derived ceratopsians (e.g. chasmosaurines) and thyreophorans are unambiguous obligate quadrupedal ornithischians, assessment of hadrosaur morphology suggests a facultative quadrupedal locomotor habit (Butler and Barrett 2012, Barrett and Maidment 2017)

Dinosaur Ontogenetic Locomotor Shifts

Ontogenetic shifts in locomotor posture are rare within tetrapods, most notably occurring within *Homo sapiens* as quadrupedal juveniles shift to bipedality. Within Dinosauria, ontogenetic locomotor shifts have been proposed for several taxa of ornithopods (e.g. *Maiasaura peeblesorum* (Dilkes 2000, 2001), *Iguanodon bernissartensis* (Norman 1980), *Dryosaurus lettowvorbecki* (Heinrich et al. 1993)), sauropodomorphs (e.g. *Massospondylus carinatus* (Reisz et al. 2005, 2010), *Mussaurus patagonicus* (Otero et al. 2019)), and early ceratopsians (e.g. *Psittacosaurus lujiatenensis* (Zhao et al. 2013)). *M. carinatus, M. patagonicus, P. lujiatenensis,* and *D. lettowvorbecki* have all been proposed to undergo a shift from quadrupedal juveniles to bipedal adults while *Maiasaura* and *I. bernissartensis* undergo a shift from bipedal juveniles to quadrupedal adults. Proposals of ontogenetic locomotor shifts in these taxa have been based on morphological assessments of forelimb and hindlimb elements and limb scaling patterns. However, evaluations of postural change in these taxa are often hampered by low sample sizes, inadequate methodology, or inconsideration of individual variation. Recent analyses have rejected ontogenetic locomotor shifts in most taxa, but sample size continues to limit thorough testing (e.g. Neenan et al. 2018, Chapelle et al. 2019).

A Case Study Using Maiasaura

A large collection of skeletal remains from a monodominant mass death assemblage of *Maiasaura* has been utilized to test dinosaur paleobiological inferences. Dilkes (2000) partially

reconstructed the hindlimb and forelimb myology of *Maiasaura* using muscle scarring on studied elements within an ontogenetic and phylogenetic framework. Muscle attachments for forelimb contractors and pectoral muscles appeared to increase with positive allometry through ontogeny. Dilkes (2001) continued to investigate ontogenetic changes in *Maiasaura*, this time focusing on appendicular osteological features such as second moment of area and linear measurements of individual boney elements. Ontogenetic changes within the appendicular skeleton of *Maiasaura* seemed to indicate a shift in function occurred in forelimb elements. Dilkes (2000, 2001) hypothesized an ontogenetic shift from bipedal juveniles to quadrupedal adults occurred in *Maiasaura* (Fig. 38). However, recent analysis of tetrapod forelimb and hundlimb robusticity rejected the *Maiasaura* locomotor shift hypothesis, though the sample of *Maiasaura* was extremely small (n=2) (Chapelle et al. 2019).

Here, we independently assess the hypothesis of an ontogenetic locomotor shift in *Maiasaura* by combining an evaluation of ontogenetic morphological changes in humeri through ontogeny and limb scaling patterns between humeri and tibiae. Morphological changes in the humerus during a locomotor shift should reflect increases in limb retractor muscle attachments, thus, allometric increases in the deltopectoral crest and proximal humerus. Our study differs from Dilkes (2001) in that we benefit from twenty additional years of specimen collection (increase sample size) and all humeri examined have been histologically sampled in order to assign absolute age for better precision in ontogenetic stage assignment.

Materials and Methods

Materials

Maiasaura humeri and tibiae used in this study were collected from Late Cretaceous Two Medicine Formation sediments in the Willow Creek Anticline of Teton County, Montana. *Maiasaura* fossils have been excavated from multiple horizons over the past 40 years by

Princeton University, Montana State University, and Oklahoma State University field crews and are housed at Museum of the Rockies, Bozeman, MT. Perinatal specimens were excavated from nesting horizons of the Willow Creek Anticline, while all other *Maiasaura* specimens were from three localities (TM-003, TM-151, TM-158) of a single, monodominant, mass death bonebed (Schmitt et al. 2014). The mass death assemblage is composed of thousands of disarticulated and disassociated *Maiasaura* skeletal materials. Taphonomic evidence suggests the bonebed is the result of a mass sediment flow which mobilized surface level and partially buried *Maiasaura* skeletal remains. Skeletal weathering patterns indicate remains accumulated over 0.1-10 years prior to sediment flow mobilization (Schmitt et al. 2014).

Recent osteohistological aging of *Maiasaura* tibiae and humeri confirm previous assessments of population dynamics and assemblage composition (Varricchio and Horner 1993, Woodward et al. 2015, Heck Ch. V). *Maiasaura* aged 0-15 years-old are represented in humeri and tibiae, although juvenile (0-1 years-old) representation is higher in tibiae and 1-4 year-olds have higher representation in humeri. Assemblage demographics and survivorship suggest the bonebed is the result of multiple mass death episodes (Schmitt et al. 2014, Woodward et al. 2015). High juvenile and adult mortality is likely due to age-specific survivorship, although under-representation of intermediate ages (2-4 years-old) could be due to age segregation (e.g. Holland et al. 2021, Yoon et al. 2021, Pol et al. 2021). Perinatal specimens are not present in the bonebed and are derived from separate nesting horizons within the Willow Creek Anticline (Lorenz and Gavin 1984). *Maiasaura* remains the most well-understood dinosaur due to the extensive skeletal material from the mass death assemblage and nesting horizons of the Willow Creek Anticline.

Here, we utilize the *Maiasaura* dataset to examine biomechanical shifts in function of hindlimb and forelimb skeletal elements. *Maiasaura* was previously suggested to undergo a locomotor shift in early ontogeny from bipedal to quadrupedal (Dilkes 2001). Morphometrics of *Maiasaura* limb bones show numerous ontogenetic changes supporting locomotor shifts (e.g. weight-bearing

adaptations in the manus, increased humerus robustness, decreased resistance to bending stresses in tibae and femora) (Dilkes 2001). Guenther (2014) noted slight ontogenetic changes in *Maiasaura* limbs such as humerus length shortening relative to pectoral girdle size, fourth trochanter extension, and widening of proximal and distal tibiae ends. However, previous examinations did not account for individual variation. *Maiasaura* bonebed material is disarticulated and disassociated, preventing direct measures of intraskeletal growth. For example, Guenther (2014) examined ontogenetic changes in *Maiasaura* forelimb and hindlimb elements by grouping individual bones by size into 'growth stages'. Length range was provided for each element including humeri (9mm – 276mm) and tibiae (12mm – 564mm). Recent osteohistological aging and growth curve analysis of *Maiasaura* humeri and tibiae reveal maximum lengths of 276mm (humerus) and 564mm (tibia) are likely from individuals <1 years-old and 2 years-old, respectively (Woodward et al. 2015, Heck Ch. V). Comparisons between these elements are, therefore, imprecise due to the rapid growth of *Maiasaura* in the first 3-4 years of life.

Previous histological analyses of *Maiasaura* tibiae and humeri measured individual bone growth rates and age at death. Woodward et al. (2015) and Heck (Ch. V) used cortical growth marks at the mid-diaphysis of tibiae (n=50) and humeri (n=47) to construct growth curves and retrocalculate missing LAGs (but see Wosik et al. 2020). Growth curves of both skeletal elements were best fit by a monomolecular model. Linear regressions in both elements showed tight correlation and high predictive power between length and minimum circumference. Here, we utilize this histological data to more accurately measure *Maiasaura* humerus bone growth and limb scaling through ontogeny.

Methods

Humerus measurements

Ten morphometric distances on the humerus were measured for direct comparison with Dilkes (2001) (Fig. 39). Humeri in the sample have been deformed, fractured, and compressed from taphonomic processes, specifically along the diaphysis. Heck (Ch. V) examined relationships between humerus length and minimum circumference and found retrodeformed histological cross sections resulted in more accurate circumference measurements. Gross morphological measures of minimum circumference do not take deformation into account and can result in error. Therefore, the present study uses minimum circumference derived from retrodeformed cross sections instead of gross morphological measurements.

Heck (Ch. V) found tight linear correlation between humerus cross section circumference and humerus length in a sample of complete humeri (n=17). Correlation between circumference and length increased with the addition of perinatal material. Length in incomplete humeri was interpolated using linear regressions of humerus circumference and length. Here, raw length measures of complete humeri and interpolated length measures from linear regressions are used for incomplete humeri.

Linear distances between humerus bone landmarks account for the remaining eight measurements and are numbered 1-8 (Fig. 39). All eight measurements were straight lines between two points and did not account for bone topography. Measurement 1 is the distance from the dorsal aspect of the anterior delto-pectoral crest down to the ventral inflection of the crest toward the diaphysis. Measurements 2, 3, 5, and 8 also use the inflection point as a landmark. Measurement 3 is the distance from the inflection point of the crest diagonally to the distal most point of the lateral condyle. Measurement 8 is similar to 3, but measurement 8 is the vertical line distance from the inflection to the distal most point of the lateral condyle. Three measures (2, 4, 6) are associated with muscle scarring on the postero-lateral aspect of the humerus. The muscle scar is typically a nodule of rugose bone and is the attachment of muscle lattisimus dorsi (Dilkes 2000). Measurement 5 is a variation of measurement 8 in Dilkes (2001). Measurement 5 is the width of

the lateral aspect of the humerus at the distal point of the delto-pectoral crest. A majority of humeri (n=30) were in states of fracture, compression, or missing cortex and not all measurements could be completed on each specimen.

Five measurements incorporate the deltopectoral crest and are used to measure changes in forelimb musculature (Fig. 39). Myological reconstructions of dinosaurs are derived from phylogenetic bracketing, and forelimb reconstruction is derived primarily from crocodylians (Witmer 1995, Dilkes 2000). Dilkes (2000) utilized the extant phylogenetic bracket to infer the myology of *Maiasaura*. The proximal humerus in *Maiasaura* serves as an attachment for forelimb retractors (e.g. *m. lattissumus dorsi*), protractors (e.g. *m.deltoides clavicularis*) and stabilizers (e.g. *m. deltoides scapularis*), muscles essential for crocodilian quadrupedal locomotion. Therefore, deltopectoral changes in *Maiasaura* can be used to infer shifts in mechanical advantages of muscles incorporated during quadrupedal locomotion.

All measures were natural log transformed to normalize distributions and meet required statistical assumptions. Ordinary least squares (OLS) regressions were performed in R version 4.1.0 (R Development Core Team 2022) to evaluate growth in all measurements relative to humerus circumference and length (Kilmer and Rodriguez 2017). A relationship was considered allometric if the confidence intervals of slope did not include 1 and the relationship had a significantly low p-value (<0.05).

Humerus measurements of *Maiasaura* aged 0-3 years-old were also regressed in a separate analysis without adult data to test for juvenile specific changes in morphology. *Maiasaura* growth rates are highest in the first three years of life and sexual maturity is hypothesized to occur at 3 years-old (Woodward et al. 2015). Measurements in 0-3 year-old Maiasaura humeri were regressed using OLS in R version 4.1.0 in addition to regressions of the full size range of humeri.

Limb Scaling with Monomolecular Modeling

Histological aging of tibiae and humeri allow for analyzing limb scaling in disassociated skeletal material. Ideally, scaling would compare two zeugopodial elements or two stylopodial elements, but *Maiasaura* femora, ulnae, and radii have not been histologically assessed to the degree in which growth curve modeling has been performed. One-to-one growth mark pairing of humeri and tibiae was not possible due to differences in age representation within each sample. For example, Woodward et al. (2015) found 31 <1 year-old tibiae and zero 1 year-old tibiae, while Heck (Ch. IV) recorded 15 <1 year-old humeri and two 1 year-old humeri. Growth curves were used to compare tibiae and humerus growth due to discrepancies in age representation in tibiae and humeri samples. Models were previously fit to tibiae and humeri growth curves using LAG circumference and LAG count (age at death). Best fit models for curves were determined using AIC_c scores and mean residual standard error. Growth curves for tibiae and humeri were best fit with a monomolecular model. Monomolecular models from Woodward et al. (2015) and Heck (Ch. IV) were used to determine humerus and tibia circumference at each given age. Element length was calculated using linear regressions between circumference and length (see above). Lengths and circumferences were natural log transformed to meet statistical assumptions of normal distribution. Tibia and humerus length and circumference at each age were paired and OLS regressions performed in R version 4.1.0.

Limb Scaling in Juveniles (0-3 years-old)

Growth curve modeling is constructed using elements with ≥3 traceable cortical growth marks and does not incorporate juvenile data. Apposition rates in *Maiasaura* tibiae and humeri are highest in the first three years of life and changes in limb dimensions were likely more prominent during the first three years of development. However, age is typically determined by counting cortical growth marks and <1 year-olds do not have reliable cortical growth markers. Here, age estimation in <1 year-olds is calculated with proportion of maximum circumference. Circumferences in <1 year-old *Maiasaura* humeri and tibiae is variable and represents growth

since birth. Circumference differences between humeri or tibiae is due to differences in timing of hatching or differences in growth rates. Qualitative assessments of bone cortices note similarities in tissue organization and vascular orientation between <1 year-olds. Therefore, we assume differences in circumference in <1 year-olds is the result of timing of hatch and larger individuals hatched earlier and are older. This oversimplification allows for modeling individual bone growth between 0-3 years and directly comparing forelimb and hindlimb growth. The largest <1 year-old humerus and tibia circumferences were assigned an age of 0.95 years-old. Circumferences of remaining humeri and tibiae were divided by the maximum circumference to attain an estimated age.

Maximum apposition after the last recorded LAG in each successive age group was similarly assigned a proportion of #LAGs.95 (e.g. 1.95 years-old, 2.95 years-old). This method then only accounts for the past year of growth to assign ages. Humerus and tibia circumferences were then plotted with age and best fit models (based on R^2) were determined in Microsoft Xcel 2003. Logarithmic models fit tibia and humerus growth curves best and resulting equations were used to calculate circumference at given age. Calculated circumferences were then used to determine length using linear regressions (see above). All data was natural log transformed and OLS regressions were performed in R version 4.1.0. Allometry was determined by regression slope and confident intervals.

Results

Humerus morphology

Nine comparisons describe the growth of the humerus through *Maiasaura* ontogeny (Table 10, S13 for raw data, Fig. 40-42A). Six measurements are well-correlated with both humerus length and circumference (R^2>0.85). Five measurements have a negative allometric relationship with humerus length and humerus circumference. All five negative allometric measurements are

associated with the proximal humerus. Measurement 5 has a negative relationship with humerus length (m=0.442; n=28) and circumference (m=0.426), but has a low F-statistic (20.53) and R^2 (0.4319). Three measurements maintain an isometric relationship with humerus length and circumference. Humerus circumference has a positive relationship (m= 1.03) with humerus length.

Comparisons within 0-3 year-old humeri are not as well correlated due to lower sample sizes (Table 11, Fig. 42B). Only one measurement (measurement 2) has a negative relationship with humerus length and humerus circumference when regressions are limited to ages 0-3. Humerus circumference has an isometric relationship (m=1.04) with humerus length within the 0-3 year age group, though humerus length has a weak negative allometric relationship with humerus circumference. All other measurements are considered isometric.

Limb scaling

Two approaches were performed to evaluate the relationship between *Maiasaura* humerus and tibia growth. Four measurements describe growth between humeri and tibiae. The monomolecular model revealed tibia length has a positive allometric relationship (m=1.091) to humerus length (Table 12, S14 for raw data). The remaining three comparisons (humerus length:tibia circumference; tibia length:humerus circumference; humerus circumference:tibia circumference) maintain isometric relationships. Additionally, evaluation of isolated tibia growth using the monomolecular model reveal tibia circumference grew with negative allometry relative to tibia length (m=0.924). Humerus circumference maintains positive allometry (m=1.033) relative to humerus length using monomolecular modeling.

The second approach to evaluating limb scaling centered on estimating element age using relative apposition. Four measurements describe growth between humeri and tibiae, and all four measurements result in positive humerus growth relative to tibia growth (Table 13, S15 for raw

data). Tibia length (m=0.978) and tibia circumference (m=0.925) have a negative allometric relationship with humerus length. Humerus circumference has a positive allometric relationship (m=1.039) with tibia length, and tibia circumference has a negative allometric relationship (m=0.910) with humerus circumference. Additionally, tibia circumference has a negative allometric relationship (m=0.946) with tibia length, and humerus circumference has a positive allometric relationship (m=1.016) with humerus length.

Limb scaling of isolated ages 0-3 years-old was analyzed using the second approach (Table 13). Relationships using the entire ontogenetic range are maintained in the juvenile subsample with two exceptions: tibia circumference and humerus circumference relative to humerus length. Tibia circumference has a positive relationship (m=1.02) to humerus length, and humerus circumference has a negative relationship (m=0.908) with humerus length in juveniles.

Discussion

Limb bones are loaded as beams and undergo compressive and tensile forces during terrestrial locomotion (McGowan 1999). Forces encountered during locomotion are curtailed by limb bone position, shape, and cortical geometry (e.g. Biewener 1983, 2005, Gatesy and Biewener 1991, Robling et al. 2002, Song et al. 2019). For example, graviportal tetrapod limbs are positioned as columns and bending and torsional stresses are minimized (Carrano 1998, Houssaye et al. 2016), while limb bones of cursorial animals, such as *Maiasaura*, are loaded as inclined beams, undergo a variety of bending and torsional stresses during locomotion, and minimize ground reaction forces through cortical geometry, bone curvature, and holding limbs in a more upright posture (Bertram and Biewener 1988, Biewener 1989, Carrano 1998, McGowan 1999). Cortical bone can adjust to forces encountered during locomotion by increasing robustness in response to increasing loading regimes (e.g. Gross et al. 1997, Lieberman et al. 2001), such as locomotion change.

However, bone response timing may not directly align with the timing of ontogenetically novel functions.

Morphology and locomotion

Locomotor shifts from bipedal juveniles to quadrupedal adults may introduce ground reaction forces and increase muscle strain in forelimb skeletal elements early in ontogeny during development (Biewener 1989; Fig. 43). However, bone response in this scenario remains theoretical because extant animal models of a bipedal to quadrupedal shift are non-existent and only *Homo sapiens* exhibit protracted quadrupedal and bipedal stages of locomotion. Nonetheless, several species of dinosaurs are hypothesized to undergo a locomotor shift including *Maiasaura peeblesorum* (Dilkes 2001). *Maiasaura* undergo several key morphological developments through ontogeny supporting a locomotor shift hypothesis: united metacarpals in the manus with hyperextendable joints, enlargement of forelimb protractor lever arms, and increased robusticity of the humerus (Dilkes 2001, Kilbourne and Makovicky 2010). Myological reconstructions also support shifts in *Maiasaura* locomotion. The muscle attachment site of *m. latissimus dorsi* expands through *Maiasaura* ontogeny with likely positive allometry (Dilkes 2000). *M. latissimus dorsi* is an important muscle in forelimb retraction during quadrupedal locomotion, and muscle attachment expansion indicates an increase in muscle physiological cross section and usage possibly as a result of increased forelimb loading during a locomotor shift to quadrupedalism (Dilkes 2000, 2001).

Dinosaur myological reconstructions are dependent upon skeletal signals of muscle attachments (e.g. Dilkes 2000, Fearon and Varricchio 2016, Smith 2021) and the extant phylogenetic bracket (Witmer 1995). Bone-muscle interfaces are complex in morphology and highly dependent on the nature of the enthesis composition. Muscles can join to bone directly or indirectly via tendinous or aponeurotic connections. Muscles that attach directly to bone typically leave little

morphological evidence as fibers connect primarily to the bone periosteum. Anchor points of indirect attachments can be strengthened by increasing bone surface area for attachment via expansion of processes, tubercles, and crests or increased surface rugosity. Therefore, expanded attachment sites, such as crests or areas of rugosity, can be used as a proxy for muscle physiological cross section and strength (Deymier-Black et al. 2015, but see Bryant and Seymour 1990). Dilkes (2000) utilized these principles to reconstruct the myology of *Maiasaura* and recorded an ontogenetic expansion of muscle attachments associated with forelimb locomotion. Additionally, DIlkes (2001) quantified positive allometric increases in *Maiasaura* deltopectoral crest length and width through ontogeny. Dilkes (2000, 2001) used the expansion of both the *Maiasaura m. lattisimus dorsi* attachment site (Fig. 44) and deltopectoral crest to suggest an ontogenetic locomotor shift leading to increases in forelimb loading and usage patterns.

The current study finds most measures of the deltopectoral crest to decrease through ontogeny relative to both humerus length and circumference (Fig. 42). Increases in humerus length are instead driven primarily by extensions of the distal half of the humerus. Additionally, a *post hoc* regression analysis revealed crest width (measurement 5) has a negatively allometric relationship (m=0.394; CI=0.142 – 0.647) with crest length (measurement 1) although correlation was low (R^2=0.314). In agreement with previous studies, humerus circumference increases with positive allometry relative to humerus length, albeit weak positive allometry (m=1.026). Increases in humerus robustness have been noted for other ornithopods (e.g. Guenther 2014) and is one of the skeletal changes used to support locomotor shift in *Maiasaura* (Dilkes 2001).

Separate regressions of ≥4 year-old and 0-3 year-old *Maiasaura* humeri show consistently weak positive allometry between humerus circumference and humerus length. Robusticity and intrabone growth may be limited in utility for inferring locomotor habits and may be especially prone to error with low sample sizes, a typical obstacle in dinosaur paleobiology (Brown and

Vavrek 2015). Humerus growth plasticity is more evident in >4 year-old specimens (low correlations between variables), influencing regression analyses.

Increases in long bone robustness have also been noted in quadrupedal crocodylians (e.g. Meers 2002) and the scaling pattern alone may not be indicative of locomotor change. Kilbourne and Makovicky (2012) recorded increased robustness in cetartiodactyl long bones through ontogeny and isometric scaling and decreased robustness in most other mammal long bones through ontogeny. *Giraffa camelopardalis* humeri cranio-caudal diameter scale with positive allometry (increased robustness) through ontogeny relative to humerus length, while radii, metacarpi, femora, tibiae, and metatarsi diameters typically scale isometrically relative to bone length (Van Sittert et al. 2015). Nevertheless, weak positive allometry in humerus circumference throughout *Maiasaura* ontogeny does not support a locomotor shift in early ontogeny.

Limb scaling and locomotion

Locomotor shift, or gait-shift, hypotheses in dinosaurs are founded primarily on allometric study of limb dimensions and scaling (e.g. Kilbourne and Makovicky 2010, Maidment et al. 2012). Generally, bipedal taxa have longer hindlimbs relative to quadrupedal animals in combination with shifting center of mass (Maidment et al. 2014). Shifts between quadrupedalism and bipedalism should be reflected in forelimb to hindlimb ratios and comparative growth rates through ontogeny (Bishop et al. 2020). There is strong evidence that *Mussaurus patagonicus*, a sauropodomorph dinosaur, underwent an ontogenetic locomotor shift from quadrupedal juveniles to bipedal adults (Otero et al. 2017, 2019, Chapelle et al. 2019). *M. patagonicus* forelimb-hindlimb ratio drastically changes through ontogeny: 0.76 forelimb/hindlimb ratio in juveniles to 0.55 forelimb/hindlimb ratio in adults (Otero et al. 2019). Similarly, *Psittacosaurus lujiatunensis* likely underwent a quadrupedal to bipedal locomotor shift, supported by juvenile forelimb/ hindlimb ratios of 0.84 that decrease to 0.61 in adult specimens (Zhao et al. 2013).

Intrabone and intraskeletal allometric scaling efficacy in inferring locomotion is complicated by confounding variables such as ecology and environment. Quadrupedal crocodylian limbs scaled with allometry and isometry, and allometry was not a consequence of locomotor shifts (Livingston et al. 2009, Iijima and Kubo 2019). Allometric limb scaling also occurs in a variety of mammals in response to behavior amid stable locomotor habits (e.g. Fariña and Vizcaíno 1997, Lammers and German 2002, Samuels and Van Valkenburgh 2008). A recent comprehensive analysis of extant and extinct amniotes suggests humerus-to-femur robusticity is a better predictor of locomotion than limb length scaling (McPhee et al. 2018, Chapelle et al. 2019). However, extreme limb scaling patterns (e.g. *P. lujiatunensis* and *M. patagonicus*) can shed light on locomotor habits in the absence of stylopodial robusticity comparisons (Zhao et al. 2013, Otero et al. 2019).

Limb scaling analyses of *Maiasaura* were previously unattainable due to the disarticulated and disassociated nature of the bonebed. Few articulated *Maiasaura* specimens have been excavated elsewhere (e.g. nestlings, ROMVP 44770) and allometric scaling of small sample sizes are prone to error (Brown and Vavrek 2015). Histological aging of *Maiasaura* tibiae (Woodward et al. 2015) and humeri (Chapter V) permit scaling assessments of forelimb and hindlimb elements. A locomotor shift from bipedal juveniles to quadrupedal adults is expected to result in an increase in forelimb-to-hindlimb length ratios (positive allometric growth in humeri relative to tibiae; Fig. 45). *Maiasaura* limb scaling trends are model dependent. Monomolecular modeling resulted in weak positive allometry in both tibia length and humerus circumference relative to humerus length and a negative allometric relationship between tibia circumference and tibia length. Increases in humerus robusticity and decreases in tibiae robusticity broadly supports forelimb functioning in locomotion and a cranial shift in center of mass reducing hindlimb ground reaction forces. However, tibiae outgrowing humeri through ontogeny is the condition found in dinosaurs

shifting locomotion from quadrupedal-to-bipedal (e.g. *M. patagonicus* and *P. lujiatunensis*; (Zhao et al. 2013, Otero et al. 2019)).

Logarithmic modeling better accounts for individual skeletal variation within 0-3 years-old. Logarithmic modeling of the entire ontogeny resulted in regressions of positive allometry between humerus circumference and humerus length, similar to results from direct individual measurements and monomolecular modeling. Similarly, tibiae circumference has a negative allometric relationship with tibia length. However, tibia length is negatively allometric in relation to humerus length, as predicted for bipedal to quadrupedal locomotion shifts.

Juvenile (0-3 years-old) *Maiasaura* limb scaling is generally similar to >3 year-old trends using the logarithmic regression method. Tibia length remains negatively allometric in relation to humerus length in both age groupings. On the other hand, humerus circumference is negatively allometric with humerus length in 0-3 year-old *Maiasaura* and positively allometric in >3 year-old individuals. According to logarithmic modeling, *Maiasaura* humeri length increased at a faster rate than tibia length and humerus circumference, as is predicted for a bipedal to quadrupedal locomotor shift.

Each method of analysis presents conflicting information on ontogenetic locomotor shifts in *Maiasaura.* Intrabone measurements show increase in humerus length without increasing deltopectoral crest robustness. Increasing deltopectoral crest and proximal humerus dimensions increase muscle attachment sites and, thus, would suggest an increase in forelimb muscle function during a locomotor shift to quadrupedalism. Tibia length through ontogeny, as determined by monomolecular modeling, increases at a faster rate than humerus length and tibia circumference. Hindlimb length increases relative to forelimbs is evidence of locomotor shifts to bipedalism. Logarithmic regressions result in humerus length increases at a faster rate than tibia length, opposite of monomolecular measures and evidence of shifts to quadrupedalism. Lastly, humerus

circumference increases at a faster rate than humerus length in all three analyses. Locomotor shifts to quadrupedalism would likely result in increased forelimb robustness to maintain safety factors in response to increased weight-bearing stress.

Previous tests of locomotor shifts in dinosaurs relied on skeletal changes through ontogeny. *P. lujiatunensis* and *M. patagonicus* hindlimbs rapidly outgrew forelimbs through ontogeny as center of mass shifted caudally and locomotor habit shifted to bipedalism. Alternatively, Wosik et al. (2018) inferred quadrupedalism throughout *Edmontosaurus* ontogeny due to isometric growth between hindlimb and forelimb elements. *Maiasaura* locomotor shifts were based, in part, upon intrabone and intraskeletal scaling, but disassociated skeletal elements add a layer of complexity in reducing effects of individual variation and growth plasticity. Previous analyses of *Maiasaura* locomotion lacked histological aging, preventing locomotor analyses within specific age groupings.

Our gross morphology results suggest a complicated relationship in *Maiasaura* skeletal growth and locomotor habit interpretations. Intrabone measurements of humeri are not overtly indicative of a locomotor shift, but sample sizes and increased variation in late ontogeny may be affecting our interpretations. Bolstering the juvenile sample may clarify potential signals of biomechanical function, and future study would benefit greatly from the inclusion of nestling data. Limb scaling also provided mixed inferences based on the method used to estimate limb dimensions at given ages. Monomolecular modeling is constructed using >3 year-old specimens and is likely over-simplifying early growth when locomotor shifts would have occurred. Logarithmic modeling generalizes element growth and is inversely affected by individual variation. Despite the limitations, logarithmic growth revealed a potential signal of locomotor shift when comparing age groupings, although allometric trends weak. Gross morphological investigations of locomotor shifts are limited and investigations into *Maiasaura* bone micromorphology may reveal stronger

signals of biomechanically adapting bone. Investigating directional bone growth and remodeling during *Maiasaura* ontogeny could clarify the locomotor gait change hypothesis.

Figures

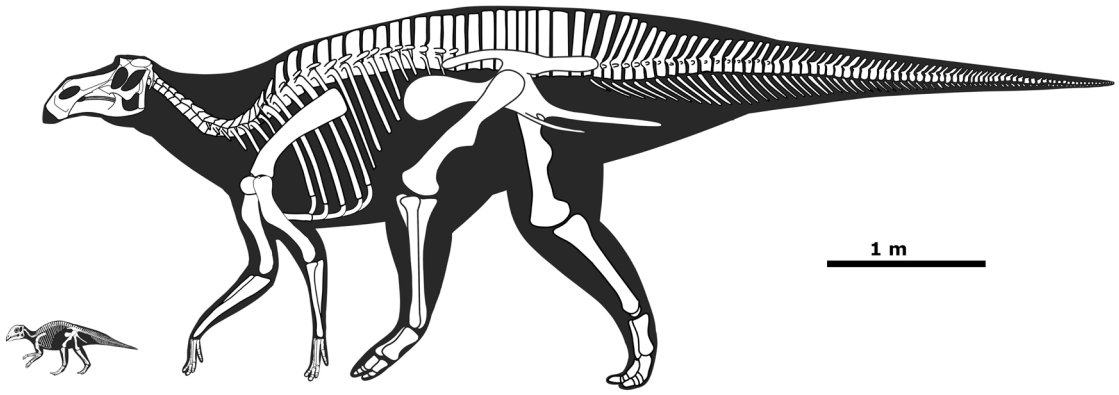

Figure 38. Proposed locomotor shift of bipedal juveniles to quadrupedal adults in *Maiasaura* .

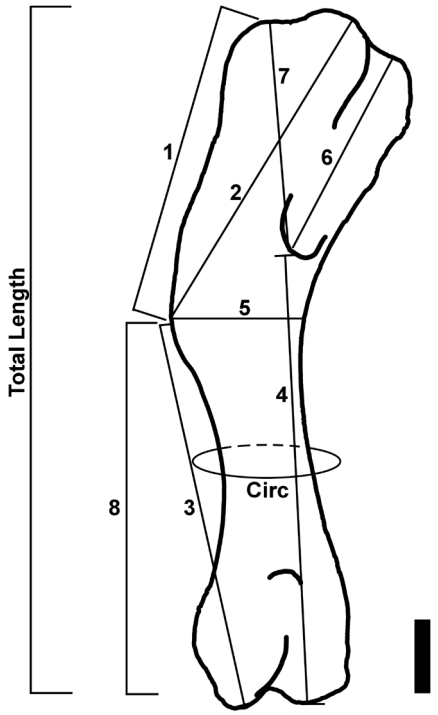

Figure 39. Linear measurements taken on each *Maiasaura* humerus. Measurements were regressed to both Total Length and Circumference (Circ).

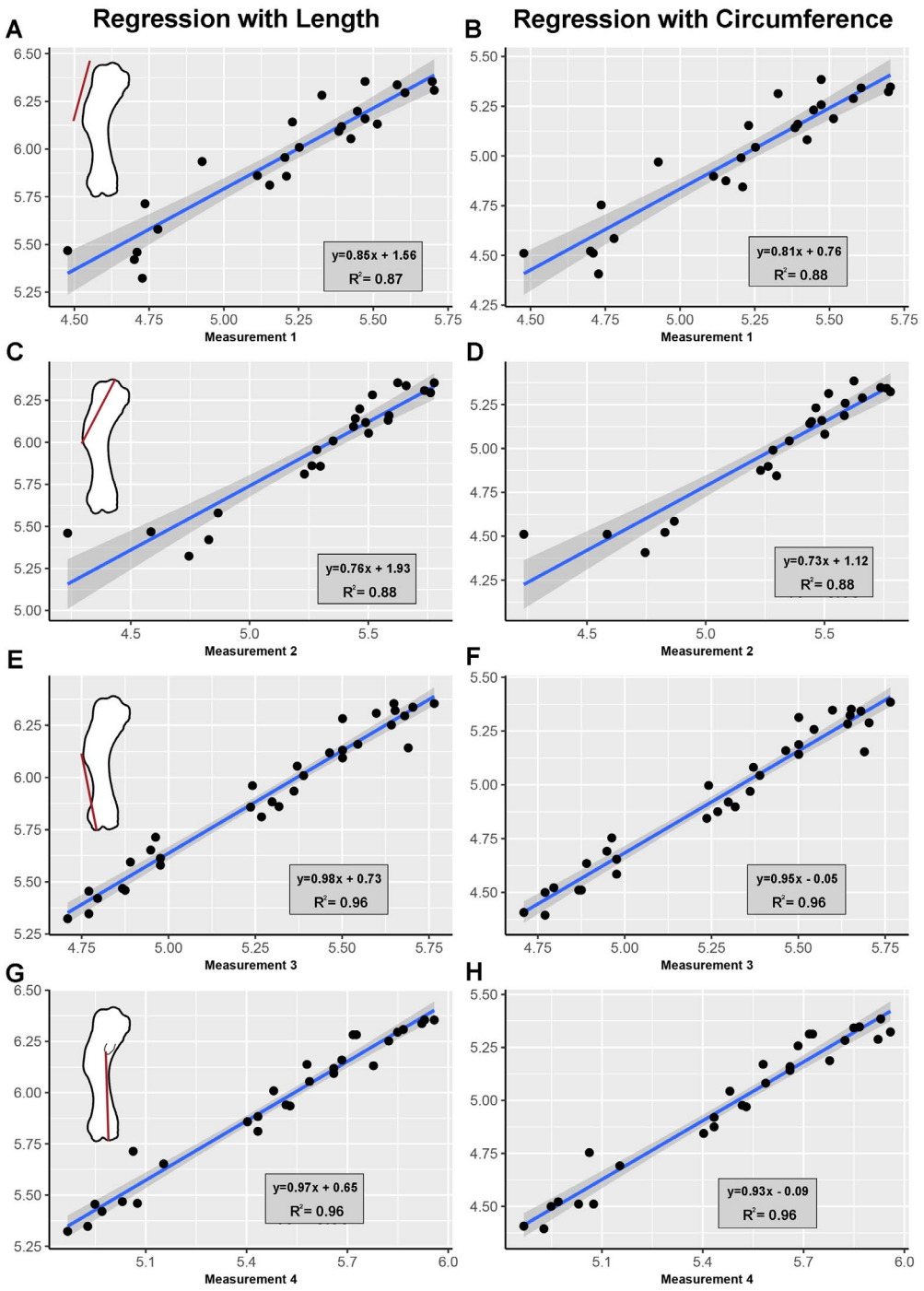

Figure 40. Regressions of measurements 1-4 to (A, C, E, G) humerus length and (B, D, F, H) humerus circumference. All measures were natural log-transformed.

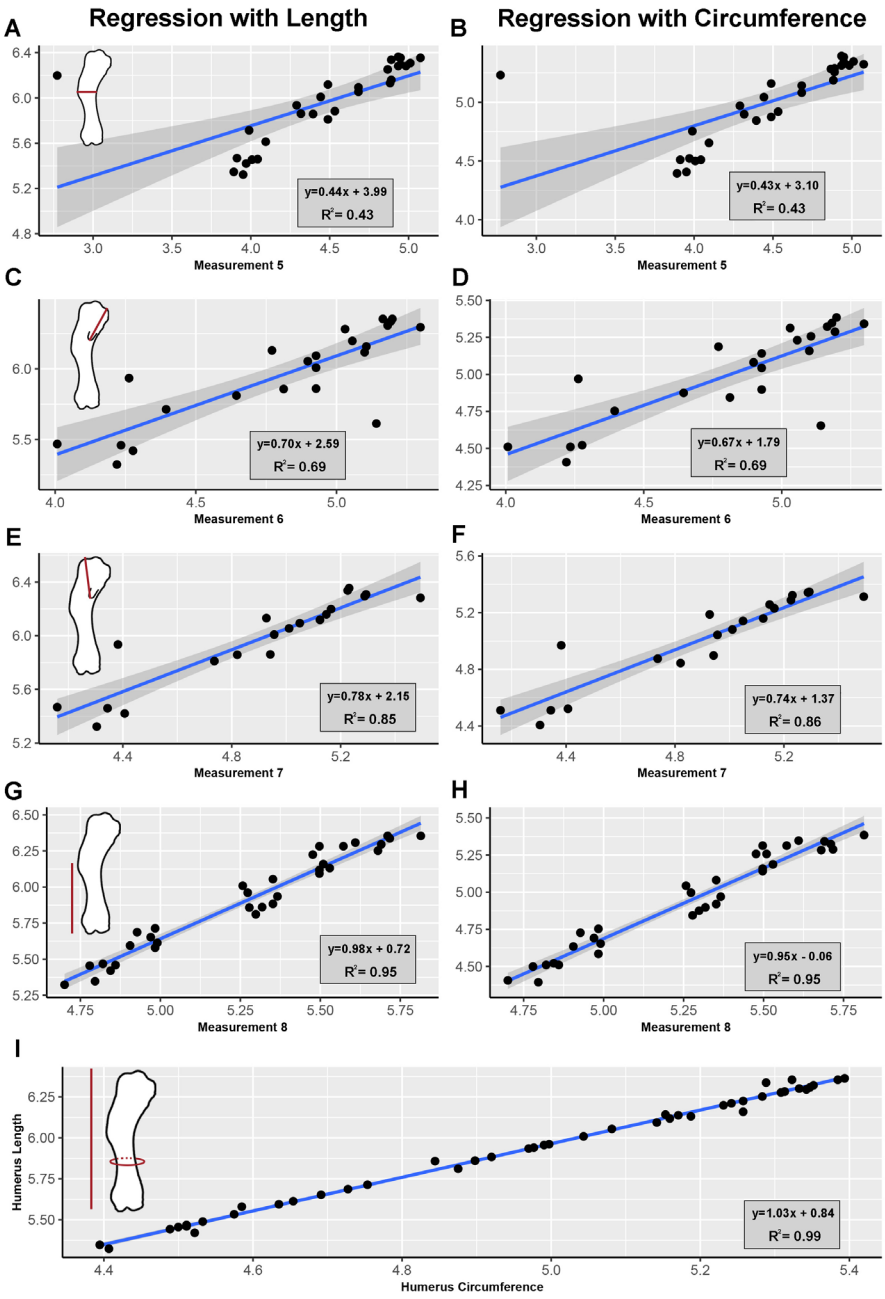

Figure 41. Regressions of measurements 5-8 to (A, C, E, G) humerus length and (B, D, F, H) humerus circumference. (I) Regression of humerus length to humerus circumference. All measures were natural log-transformed.

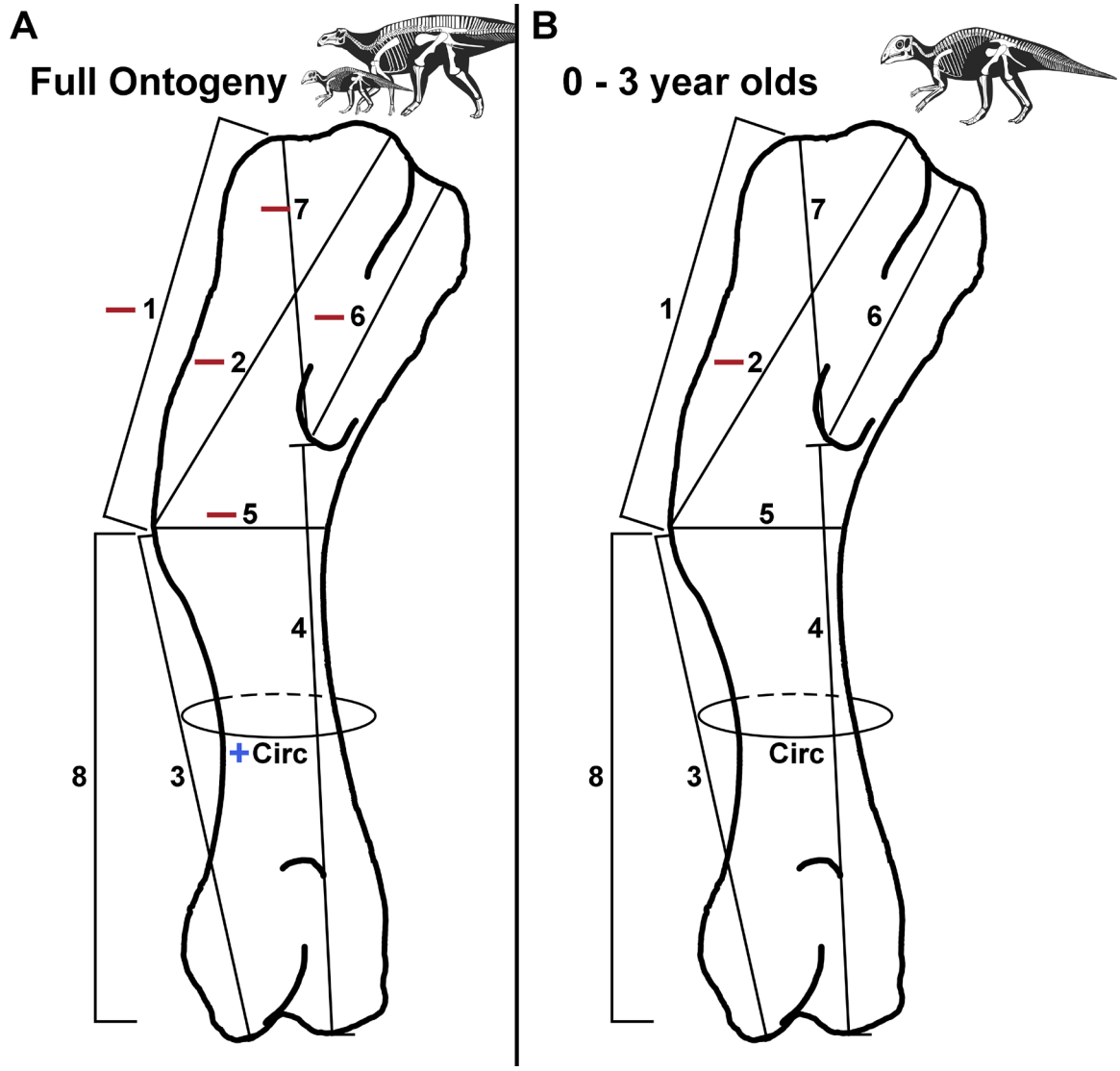

Figure 42. Visual representation of allometric trends in humerus morphology across (A) *Maiasaura* ontogeny and (B) within *Maiasaura* 0-3 years old. Red dash – negative allometry, blue plus – positive allometry, no symbol – isometry.

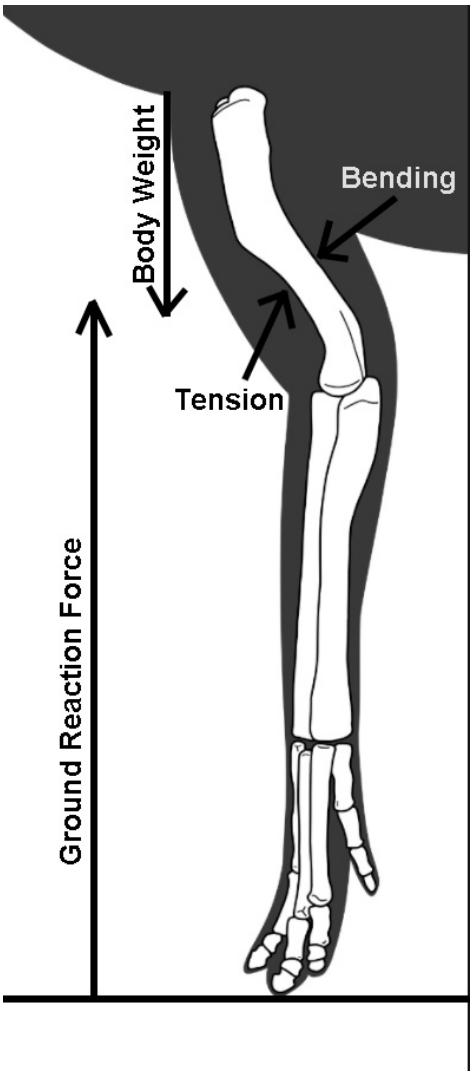

Figure 43. Shift to quadrupedal locomotion in *Maiasaura* would introduce ground reaction forces and mass loading on forelimbs. Loading imposes bending forces on the posterior side of humeri while tension occurs anteriorly.

Figure 44. Location of muscle attachment of *m. latissimus dorsi* on posterior aspect of humerus.

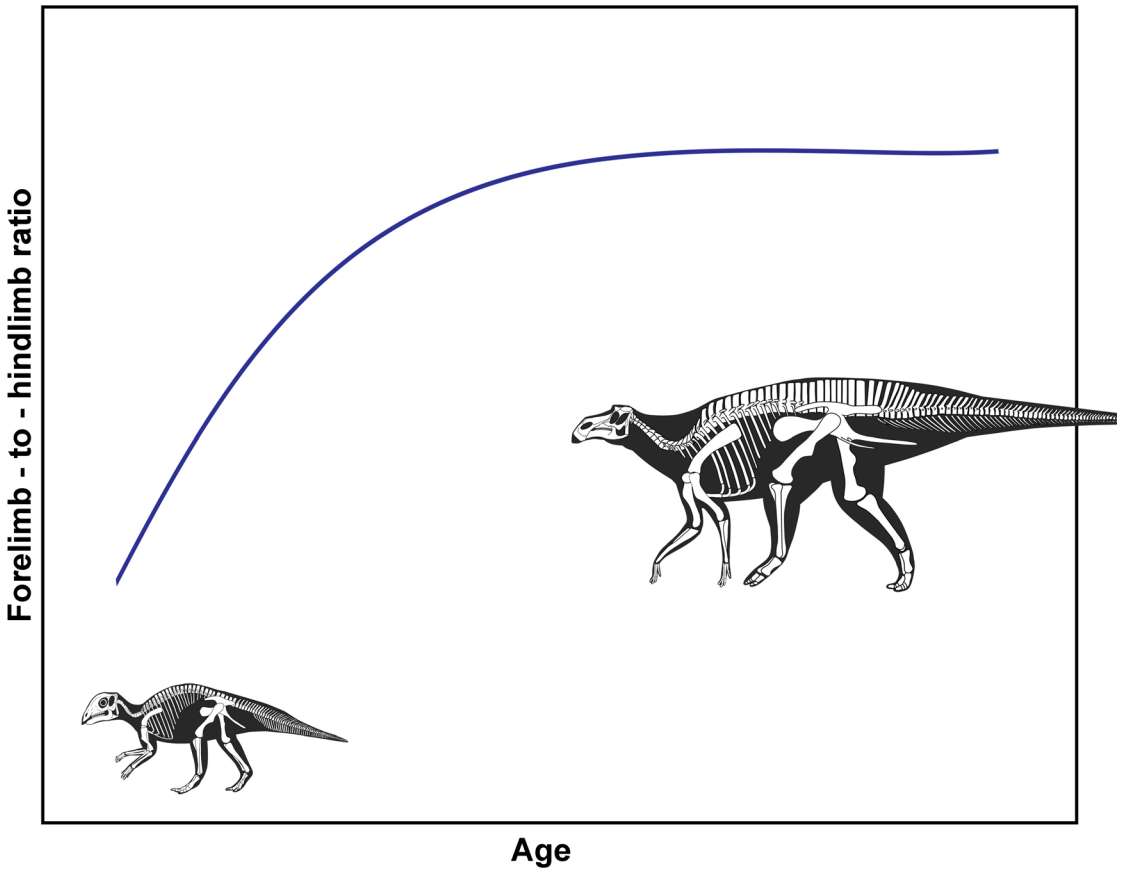

Figure 45. Hypothesized limb sacaling in an ontogenetic locomotor shift in which forelimbs grow at a faster rate than hindlimbs until quadrupedalism is achieved.

Tables

Table 10. Regression results of *Maiasaura* humerus measurements with (top) humerus length and (bottom) humerus circumference across ontogeny. Bold and italics indicate significance from isometry.

Humerus Length			Confidence Interval				
Variable	*n*	Slope (*m*)	Lower (95%)	Upper (95%)	R^2	*p-value*	Trend
1	24	***0.847***	0.708	0.986	0.874	*< 0.001*	neg
2	22	***0.762***	0.634	0.890	0.879	*< 0.001*	neg
3	31	0.982	0.908	1.056	0.961	*< 0.001*	iso
4	27	0.966	0.891	1.041	0.965	*< 0.001*	iso
5	28	***0.442***	0.242	0.642	0.432	*< 0.001*	neg
6	22	***0.701***	0.049	0.914	0.691	*< 0.001*	neg
7	19	***0.781***	0.619	0.942	0.851	*< 0.001*	neg
8	32	0.984	0.904	1.064	0.953	*< 0.001*	iso
Circumference	47	***1.026***	1.004	1.048	0.995	*< 0.001*	pos

Humerus Circumference							
Variable	*n*	Slope (*m*)	Lower (95%)	Upper (95%)	R^2	*p-value*	Trend
1	24	***0.814***	0.683	0.946	0.877	*< 0.001*	neg
2	22	***0.732***	0.623	0.853	0.884	*< 0.001*	neg
3	31	0.947	0.871	1.024	0.955	*< 0.001*	iso
4	27	0.925	0.845	1.005	0.956	*< 0.001*	iso
5	28	***0.426***	0.234	0.618	0.433	*< 0.001*	neg
6	22	***0.666***	0.462	0.871	0.685	*< 0.001*	neg
7	19	***0.744***	0.594	0.893	0.859	*< 0.001*	neg
8	32	0.950	0.868	1.033	0.947	*< 0.001*	iso
Length	47	***0.970***	0.949	0.991	0.995	*< 0.001*	pos

Table 11. Regression results of *Maiasaura* humerus measurements with (top) humerus length and (bottom) humerus circumference within 0-3 year-olds. Bold and italics indicate significance from isometry.

Humerus Length			Confidence Interval				
Variable	*n*	Slope (*m*)	Lower (95%)	Upper (95%)	R^2	*p-value*	Trend
1	12	*0.780*	0.441	1.119	0.724	*< 0.001*	Iso
2	10	***0.571***	0.293	0.848	0.738	*0.001*	Neg
3	18	0.926	0.791	1.060	0.930	*< 0.001*	Iso
4	14	0.944	0.770	1.118	0.921	*< 0.001*	Iso
5	14	*0.908*	0.610	1.207	0.786	*< 0.001*	Iso
6	11	*0.364*	-0.022	0.749	0.336	*0.062*	Iso
7	9	*0.668*	0.179	1.156	0.599	*0.014*	Iso
8	19	0.906	0.766	1.079	0.888	*< 0.001*	Iso
Circumference	25	*1.039*	0.999	1.079	0.992	*< 0.001*	iso

Humerus Circumference							
Variable	*n*	Slope (*m*)	Lower (95%)	Upper (95%)	R^2	*p-value*	Trend
1	12	*0.734*	0.420	1.048	0.730	*< 0.001*	Iso
2	10	***0.539***	0.288	0.790	0.755	*0.001*	Neg
3	18	0.878	0.747	1.010	0.926	*< 0.001*	Iso
4	14	0.889	0.723	1.055	0.919	*< 0.001*	Iso
5	14	*0.859*	0.584	1.135	0.794	*< 0.001*	Iso
6	11	*0.329*	-0.030	0.689	0.323	*0.068*	Iso
7	9	*0.618*	0.170	1.066	0.603	*0.014*	Iso
8	19	0.860	0.722	1.027	0.884	*< 0.001*	iso
Length	25	***0.955***	0.918	0.992	0.992	*< 0.001*	neg

Table 12. Limb scaling regression results between humeri and tibiae using data derived from the monomolecular growth model. Tibia data from Woodward et al. 2015. Bold and italics indicate significance from isometry. HC – humerus circumference, HL – humerus length, TC – tibia circumference, TL – tibia length.

Monomolecular

Variables	Slope (*m*)	Lower (95%)	Upper (95%)	R^2	*p-value*	Trend
HL:TL	***1.091***	1.020	1.162	0.989	*< 0.001*	pos
HL:TC	1.007	0.936	1.078	0.988	*< 0.001*	iso
HL:HC	***1.033***	1.028	1.037	1.000	*< 0.001*	pos
TL:TC	***0.924***	0.918	0.929	1.000	*< 0.001*	neg
TL:HC	0.936	0.871	1.001	0.988	*< 0.001*	iso
HC:TC	0.974	0.901	1.047	0.986	*< 0.001*	iso

Table 13. Limb scaling regression results using data derived from logarithmic modeling of (left) full *Maiasaura* ontogeny and (right) 0-3 year-old juvenile *Maiasaura*. Tibia data from Woodward et al. 2015. Bold and italics indicate significance from isometry. HC – humerus circumference, HL – humerus length, TC – tibia circumference, TL – tibia length.

Logarithmic					Juveniles Only				
Variables	Slope (*m*)	Lower (95%)	Upper (95%)	Trend	Variables	Slope (*m*)	Lower (95%)	Upper (95%)	Trend
HL:TL	***0.978***	0.977	0.979	neg	HL:TL	***0.973***	0.971	0.975	neg
HL:TC	***0.925***	0.921	0.929	neg	HL:TC	***1.020***	1.019	1.021	pos
HL:HC	***1.016***	1.015	1.017	pos	HL:HC	***0.908***	0.903	0.914	neg
TL:TC	***0.946***	0.943	0.949	neg	TL:TC	***0.934***	0.929	0.938	neg
TL:HC	***1.039***	1.037	1.041	pos	TL:HC	***1.048***	1.045	1.051	pos
HC:TC	***0.910***	0.905	0.915	neg	HC:TC	***0.890***	0.884	0.897	neg

CHAPTER VII

BONE FUNCTION ADAPTATION AND *MAIASAURA*: TESTING THE LOCOMOTOR SHIFT HYPOTHESIS USING HUMERUS CROSS-SECTIONAL GEOMETRY AND CORTICAL REMODELING

Introduction

Non-avian dinosaurs (hereafter, 'dinosaurs') were diverse in form, function, and ecology, and inhabited a wide array of environments and niches (Weishampel et al. 2004). Dinosaur evolution included changes in appendicular skeletal morphology resulting in various locomotor functions or habits (e.g. Barrett and Maidment 2017). Quadrupedal locomotion arose multiple times within Dinosauria from bipedal ancestral stock (Maidment and Barrett 2012, 2014, Barrett and Maidment 2017). Quadrupedal locomotion in Saurischia only arose within Sauropoda (e.g. McPhee et al. 2018), while multiple shifts to quadrupedalism occurred in Ornithischia (e.g. Barrett and Maidment 2017). Crown-group ceratopsians and thyrephorans were obligate quadrupeds, and derived ornithopods were at least facultative quadrupeds (e.g. Maidment et al. 2012, Maidment and Barrett 2012, 2014, Barrett and Maidment 2017). Phylogenetic shifts in locomotion were accompanied by morphological changes to the musculoskeletal system (Maidment and Barrett 2014).

In addition to phylogenetic locomotor shifts, several dinosaur taxa are hypothesized to transition between locomotor habits through ontogeny (Chapelle et al. 2019 and references therein). *Psittacosaurus lujiatunensis* and *Mussaurus patagonicus* shift from quadrupedal juveniles to bipedal adults (Zhao et al. 2013, Otero et al. 2019), while the Brachylophosaurine hadrosaur *Maiasaura peeblesorum* undergoes a shift from bipedal juveniles to quadrupedal adults (Dilkes 2000, 2001, but see Chapelle et al. 2019). This locomotor shift from bipedal juveniles to quadrupedal adults was suggested to be a shared trait among hadrosaurs (Horner et al. 2004), but recent analyses of limb scaling show no evidence of such an ontogenetic change occurring (Wosik et al. 2018, Chapelle et al. 2019, Heck Ch. VI). However, published results examining dinosaur ontogenetic locomotor shifts rely heavily on limb scaling, do not histologically age specimens, and lack large sample sizes. To further test the hypothesis of ontogenetic locomotor change independent of limb scaling requires examination of the biomechanical effects of such a change. This includes increased forelimb loading, center of mass moving cranially, and reduced loading in the hindlimb elements (Dilkes 2001, Barrett and Maidment 2017).

Generally, bone responds to increased loading by altering geometric shape through differential cortical apposition and resorption, also known as bone functional adaptation (Roux 1881, see Ruff et al. 2006 for review). Changes to bone geometry and limb position increase long bone ability to withstand ground reaction forces and loading, thus, maintaining structural safety limits (Biewener 1983, Biewener and Taylor 1986, Bertram and Biewener 1988, Carrano 2001, Main and Biewener 2007). For example, bone compaction (osteosclerosis) and cortical thickness increase in graviportal and aquatic tetrapods (Houssaye et al. 2016), humerus geometry reflects biomechanics in bats (López-Aguirre et al. 2021), trabecular anisotropy is greater in forelimbs of xenarthrans (Amson et al. 2017), and intracortical remodeling increases in response to introduced limb loading in sheep (Lieberman et al. 2003). Ontogenetic changes in dinosaur locomotion

introduce heavy loading to forelimb elements and, based on functional adaptation, changes in bone geometry should reflect the increased loading.

Here, we independently test the locomotor shift hypothesis in the dinosaur *Maiasaura peeblesorum* by analyzing changes in forelimb bone geometry and cortical remodeling through ontogeny with a large, histologically aged, sample. Hadrosaur dinosaurs are cursorial and, thus, limb bones are loaded as inclined beams (but see Carrano 1999). As such, a locomotor shift in *Maiasaura* would introduce axial compression perpendicular to the ground, compressive bending forces on the posterior aspect of humeri, and tension on the anterior side of the humerus (McGowan 1999; Fig. 46)). Humerus bone growth is expected to respond to these forces by 1) increase cortical area, 2) differential bone deposition on the axis of stress (anterior or posterior cortical thickening), and/or 3) increase bone remodeling (Fig. 47). As ontogenetic locomotor shifts are hypothesized for numerous dinosaur taxa (e.g. Zhao et al. 2013, Otero et al. 2019), here we use the large *Maiasaura* sample as a case study to examine the extent to which biological inferences can be derived from bone geometry and cortical remodeling.

Material and Methods

Materials

Maiasaura humeri were excavated from a single, monodominant, laterally expansive bonebed in Two Medicine Formation sediments of the Willow Creek Anticline in Teton County, Montana and accessioned at Museum of the Rockies (Bozeman, MT) under museum numbers MOR 005 and MOR 758. The bonebed is composed of thousands of disarticulated and disassociated *Maiasaura* materials, and is hypothesized as the result of multiple mass death episodes followed by a singular mass sediment flow transporting materials to the present locality (Schmitt et al. 2014). This mass death assemblage has been utilized to better understand *Maiasaura* growth (Horner et al. 2000, Kilbourne and Makovicky 2010, Woodward et al. 2015, Woodward 2019,

Heck Ch. VI), biomechanics (Dilkes 2000, 2001, Guenther 2014, Cubo et al. 2015), pathology (Cubo et al. 2015), taphonomy (Schmitt et al. 2014), and population dynamics (Varricchio and Horner 1993, Woodward et al. 2015, Heck Ch. V). Humeri were chosen for the present study to analyze a potential biomechanical response to locomotor change in addition to further expanding upon work done by Dilkes (2000, 2001) and Heck (Ch. VI).

A large sample of *Maiasaura* humeri (n=47) was histologically sectioned at the mid-diaphysis for a previous study examining humeri growth trends (Heck Ch. V). *Maiasaura* ontogeny is well-represented in the humerus sample by age (<1 – 19 years-old) and size (205mm – 580mm in length). The transverse sections were all removed from a standardized location at the minimum circumference of the humerus; humerus minimum circumference is located in the tubular portion of the humerus, distal to the delto-pectoral crest. Theoretically, *Maiasaura* humeral minimum circumference is exposed primarily to loading and ground reaction forces, and is only indirectly impacted by muscle actions resulting in bending forces. Heck (Ch. V) prepared the histological sections to quantify humerus cortical growth in addition to determining individual age at death by counting cortical growth marks (lines of arrested growth (LAGs)). The present study utilizes humeral histological sections to extract macro-morphological and micro-morphological data to analyze bone response to biomechanical forces through ontogeny.

Maximum humerus length was measured with fabric tape on complete specimens (n=17). Humerus circumference was measured from retrodeformed thin-section images (see Heck Ch. V) using the BoneJ plugin for ImageJ (Doube et al. 2010, Schneider et al. 2012, Domander et al. 2021). Humerus length in incomplete specimens (n=30) was interpolated using a linear regression of circumference and length derived from complete specimens (see Heck Ch. V). Unless stated otherwise, cortical measurements were performed using ImageJ (Schneider et al. 2012) and the BoneJ plugin for ImageJ (Doube et al. 2010, Domander et al. 2021).

Methods

Heck (Ch. VI) performed linear morphological measurements on humeri and found humerus diaphyseal circumference to increase with positive allometry relative to humerus length. Here, cortical area and medullary cavity area are measured to determine the factors driving robustness in the humerus diaphysis. Cortical area (CA) is defined as the total sum area of compact cortical bone and trabecular bone (Fig. 48A). CA measurements did not account for subperiosteal vascular spaces. Medullary cavity area (MA) is the area of open space within the medullary cavity and was measured as: *MA = total section area – CA* (Fig. 48A). Increasing cortical area should increase bone resistance to axial compression and tension, forces humeri encounter during quadrupedal locomotion (Biewener 1982, Langel and Bonnan in prep). CA and MA were measured using retrodeformed specimens (n=30). However, trabecular bone spanning the medullary cavity of *Maiasaura* humeri is often crushed from taphonomic processes (pers. obs.) and trabecular data is subsequently lost. Areas of trabecular crushing were replaced with uncrushed trabeculae by duplicating adjacent intact trabeculae in Adobe Photoshop to provide a more accurate estimation of CA and MA.

Long bones develop to accommodate a variety of forces during locomotion while minimizing mass. Bone functional adaptation suggests cortical bone responds to directional stresses such as those encountered during a shift in locomotion or function. For example, Hert et al. (1972) found increasing periosteal and endosteal apposition along loaded axes in rabbits in response to experimental loading. Similarly, Robling et al. (2002) experimentally loaded adult rat forelimbs and recorded, in response, increases in forelimb bone cortical thicknesses along the plane of bending. Cortical thickness was measured in *Maiasaura* humeri (n=42) to test for cortical response to introduced load bearing forces associated with a locomotor change from bipedalism to quadrupedalism. Cortical thickness (CT) was measured along four major anatomical axes in humeri: anterior, posterior, medial, lateral (Fig. 48B). Cortical thickness is defined as the single-

dimension, straight line width of compact bone. Unlike *Maiasaura* tibiae, *Maiasaura* humerus compact bone transitions to cancellous bone near the medullary cavity. The internal border of compact bone was estimated by the authors for cortical thickness measurements and linear measurements extended out to the periosteal surface aligned with the cross-section centroid.

Increases in bone loading and stress result in similar increases in cortical microcrack proliferation. Directional stress, such as those during parasagittal locomotion, should result in directional microcrack proliferation and microcrack repair (e.g. Bentolila et al. 1998). However, bone shape and cortical thickness can diffuse the relative area of cortical remodeling. Therefore, cortical remodeling is measured in *Maiasaura* humeri within 1mm thick transects along major and minor axes (Fig. 48C-D). Major axes extend out from the geometric centroid to the periosteal surface with the minor axis intersecting the centroid perpendicular to the major axis. A 1mm thick transect of cortical bone was examined along the two components of each axis resulting in a total of four transects (Fig. 48D). Secondary tissue area (ST) was summed along all four transects. Secondary tissue includes secondary osteons and secondarily deposited lamellar tissue along trabecular margins and resorption cavities.

Biomechanical strain and loading history is recorded in bone geometry and cortical remodeling according to bone functional adaptation. Bone signal strength of locomotor shifts occurring early in ontogeny may not be as strong in adult specimens. Juvenile bone is fast growing and experimental mechanical stimuli result in a more pronounced and recordable bone response (Forwood and Burr 1993, Turner et al. 2003). Heck (Ch. V) determined age at death for sampled *Maiasaura* humeri using cortical growth marks and growth curve modeling. Ordinary least squares (OLS) regressions were performed to explore the relationships between cortical measurements and humerus length and humerus circumference (Kilmer and Rodriguez 2017). Additionally, all four CT measurements were regressed using OLS, against CA. OLS regressions were also performed on two subsamples of the full ontogenetic sample to explore potentially

stronger biomechanical signals in juvenile *Maiasaura* relative to adults. *Maiasaura* growth curves estimate sexual maturity occurred at approximately 2-3 years old (Woodward et al. 2015, Heck Ch. V). Therefore, two subsamples of *Maiasaura* were regressed separately: ≤3 year-old and >3 year-old *Maiasaura*. All OLS regressions were performed in R version 4.1.0 and plotted with the ggplot2 and ggpubr packages (Wickham 2016, Alboukadel 2020, R Core Team 2021).

Results

Cross section geometry

Table 14 displays regression results for the entire *Maiasaura* ontogeny. *Maiasaura* humerus diaphyseal cortical area scales with isometry relative to both humerus length and humerus circumference ($b_{isometry}$=0.5, $b_{CA\text{-}L}$=0.49, $b_{CA\text{-}Circ}$=0.49) throughout ontogeny. Medullary cavity area scales with negative allometry to both humerus length ($b_{MC\text{-}L}$=0.30) and humerus circumference ($b_{MC\text{-}Circ}$=0.29) through *Maiasaura* ontogeny. Cortical area and medullary cavity area are both correlated with humerus length ($R^2_{CA\text{-}L}$=0.979, $R^2_{MC\text{-}L}$=0.728) and circumference ($R^2_{CA\text{-}Circ}$=0.985, $R^2_{MC\text{-}Circ}$=0.736) and returned significant p-values ($p<0.001$).

Anterior and lateral humeral cortical thickness scales with negative allometry to both humerus length ($b_{isometry}$=1.00, $b_{ACT\text{-}L}$=0.752, $b_{LCT\text{-}L}$= 0.784) and humerus circumference ($b_{ACT\text{-}Circ}$=0.737, $b_{LCT\text{-}Circ}$=0.865). Posterior and medial cortical thickness scales with isometry to both humerus length and humerus circumference (Table 1). Correlation is not as strong as cortical area between cortical thicknesses and humerus length (R^2 = 0.519 – 0.700) or humerus circumference (R^2=0.514 – 0.703).

Table 15 displays regression results of humerus measures in *Maiasaura* 0-3 years-old. Juvenile *Maiasaura* (≤3 year-olds) cortical area scale with isometry relative to humerus length ($b_{isometry}$=0.5, $b_{CA\text{-}L}$=0.525) and humerus circumference ($b_{CA\text{-}Circ}$=0.525). Medullary cavity area in juvenile *Maiasaura* scales with negative allometry to humerus length ($b_{MC\text{-}L}$=0.227) and humerus

circumference ($b_{MC\text{-}Circ}$=0.206). Correlation is high between cortical area and both length (R^2=0.947) and circumference (R^2=0.960), but correlation is low between medullary cavity area and humerus length (R^2=0.469) and circumference (R^2=0.425).

Anterior, Posterior, and lateral cortical thickness in juvenile *Maiasaura* scale with negative allometry relative to both humerus length and circumference, while medial cortical thickness scales with isometry to length and circumference. However, correlation is low between cortical thicknesses and humerus length (R^2=0.338 - 0.402) and humerus circumference (R^2=0.332 – 0.422) with significant p-values ($p<0.005$).

Table 16 displays regression results of humerus measures in *Maiasaura* over 3 years-old. *Maiasaura* >3 years old have lower sample sizes, less correlation, and higher p-values than juveniles. Cortical area scales with isometry to both humerus length ($b_{CA\text{-}L}$=0.402, CI=0.263-0.541) and humerus circumference ($b_{CA\text{-}Circ}$=0.395, CI=0.289-0.502); cortical area relationships are significant and have high correlation ($R^2_{CA\text{-}L}$=0.827, $R^2_{CA\text{-}Circ}$=0.887). Medullary cavity area has a highly negative allometric relationship with humerus length ($b_{MC\text{-}L}$=0.058) and humerus circumference ($b_{MC\text{-}Circ}$=0.083) in the older age bracket of *Maiasaura*, but correlation is low ($R^2_{MC\text{-}L}$=0.1203, $R^2_{MC\text{-}Circ}$=0.275) and the relationships are not statistically significant ($p_{MC\text{-}L}$=0.296, $p_{MC\text{-}Circ}$=0.0977).

Cortical thicknesses in >3 year-old *Maiasaura* are not well-correlated with humerus length (R^2=0.019 – 0.392) nor humerus circumference (R^2=0.007 – 0.381). All four cortical thicknesses display negative allometry relative to humerus length and humerus circumference (Table 3), but only anterior and posterior cortical thicknesses have a significant relationship with both humerus length and humerus circumference.

Cortical remodeling

Across the entire *Maiasaura* sample, average secondary tissue area scales with negative allometry with both humerus length (b=0.241) and humerus circumference (b=0.234), and relationships between secondary tissue area and both humerus length and circumference are highly correlated ($R^2_{ST\text{-}L}$=0.741, $R^2_{ST\text{-}Circ}$=0.746) and significant ($p<0.001$).

Average secondary tissue area in *Maiasaura* juveniles (≤3 years-old) scales with negative allometry to both humerus length (b=0.116) and humerus circumference (b=0.111); neither relationship is well-correlated ($R^2_{ST\text{-}L}$=-0.349, $R^2_{ST\text{-}Circ}$=0.356) though the relationships are significant ($p<0.05$). *Maiasaura* >3 years-old display negative allometry between average secondary tissue area and both humerus length (b=-0.034) and humerus circumference (b=-0.026), though the relationships are not correlated ($R^2_{ST\text{-}L}$=0.013, $R^2_{ST\text{-}Circ}$=0.008) or significant ($p_{ST\text{-}L}$=0.739, $p_{ST\text{-}Circ}$=0.792).

Discussion

Bone geometry

Bone is a complex tissue that serves a multitude of purposes for tetrapods including locomotion, protection, housing marrow, and as a calcium reservoir (Currey 2002, Hall 2015). Locomotion and function primarily drive bone shape and mineral density in tetrapod long bones within phylogenetic constraints (e.g. Bertram and Biewener 1992, Carrano 2001, Pearson and Lieberman 2004). Bone growth response to applied loads during locomotion and function has historically been recognized as a general definition of Wolff's Law, but the term 'bone functional adaptation' is more appropriate (Ruff et al. 2006). In bone functional adaptation, bone growth is directional and dependent on load orientation and type of applied loading (e.g. torsion, compression). Additionally, bone response to applied loads is constrained by available resources, calcium requirements, maintaining muscle attachments, stiffness requirements, epigenetic factors, and

ontogeny (Pearson and Lieberman 2004). Essentially. bone must maintain structural integrity while adapting to internal and external forces.

Cross-sectional cortical area reflects, in part, a long bone's ability to resist axial compression and tension (Currey 2002). However, cortical area does not necessarily reflect strength or resistance to non-axial loading (Davison et al. 2006). Signals of non-axial loading are better reflected in differential cortical thickness about the bone circumference. Second moment of area and polar moment of area are more accurate indicators of a bone's resistance to non-axial loading; both moment measurements are affected by cortical thickness and bone geometric shape.

Maiasaura humeral cortical area scales with isometry relative to humerus length and humerus circumference, while medullary cavity area scales with negative allometry to humerus length and circumference. Generally, long bone loading in juvenile tetrapods is more evident in adult cross-sectional geometry in comparison to loading regimes in adult bones (Pearson and Lieberman 2004). *Maiasaura* juvenile (0-3 years old) cortical indices have higher correlations and larger slopes, but the stronger signal is likely due to the limited adult *Maiasaura* sample size and not loading regime.

Modern Analogues

Maiasaura are hypothesized to undergo an ontogenetic locomotor shift from bipedal to quadrupedal locomotion (Dilkes 2001). This shift would introduce ground reaction forces, body mass loading, and extensive pectoral musculature tensions on forelimb long bones. Modern analogues for an ontogenetic bipedal to quadrupedal locomotor shift are absent, but ontogenetic changes in locomotion and limb bone function are present in modern taxa and are used here to evaluate *Maiasaura* cortical geometry.

Mallards (*Anas platyrhynchos*) hatch with precocial hindlimbs and altricial forelimbs. Hindlimbs are functional for locomotion the day of hatching, while forelimbs are able to power long distance

flight once adult size is reached (Nice 1962, Stark and Ricklefs 1998). Forelimb bone length and width scale with positive allometry in early mallard development and hindlimb dimensions typically scale with isometry (femur length, tarsometatarsus length, tibiotarsus width, tarsometatarsus width). Positive allometry in forelimbs is essential to meet the biomechanical demands of flight, a locomotor strategy introduced in late mallard ontogeny (Bennett 2008, Dial and Carrier 2012). On the other hand, humeral diameter in flightless paleognaths scale with negative allometry (Cubo and Casinos 1997) and hindlimb elements scale with negative allometry in pigeons (*Columba livia domestica*) (Wei and Zhang 2019). However, Wei and Zhang (2019) recorded general isometry in Japanese quail (*Coturnix coturnix japonica*) femoral geometry through ontogeny.

Alternatively, bone response to epigenetic factors has been tracked in human studies and experimentally loaded animal models. Kontulainen et al. (2002) measured forelimb bone geometry and mineral content in young and old female tennis and squash players. Forelimb bones in the dominant hand (arm primarily used in sport) were consistently thicker (cortical bone area) relative to non-dominant hands and functional cortical signals were more prominent in juvenile players. Similar changes in bone cortices were recorded in long jumpers (Heinonen et al. 2001) and weight lifters (Heinonen et al. 2002). Osteogenic responses are greater in rapid, dynamic loading rather than sustained, lower impact activities (Nordström et al. 1998, Kontulainen et al. 2002, Rector et al. 2008, Smith et al. 2021). Experimental loading in rats confirms bone response to mechanical stimuli is greater in response to dynamic loading in juveniles (e.g. Ruff et al. 2006). Therefore, cortical signals of limb use in sustained, static locomotion may not be recognized in adult individuals. When tested separately, juvenile *Maiasaura* humeri did not differ from scaling trends in the whole sample and, thus, do not support a sudden, ontogenetically early locomotor shift to quadrupedalism.

Bone adaptation to function is also apparent between taxa differing in ecology and limb function. Cortical compaction is higher in marine iguanas (*Amblyrhynchus cristatus*) compared to terrestrial iguanid relatives, likely a mechanism for buoyancy control (Hugi and Sanchez-Villagra 2012). Cortical area and cross section geometry in mustelids reflects the high specialization across the group: natatorial mustelids and fossorial mustelids have higher forelimb cortical values than scansorial and generalist mustelid taxa (Fabre et al. 2015, Botton-Divet et al. 2016, 2017, Kilbourne and Hutchinson 2019). Primates utilize a wide range of locomotor strategies and species utilizing quadrupedalism have lower femoral robustness relative to saltatorial taxa (Young et al. 2020, but see Demes et al. 1991, Demes and Jungers 1993).

Meers (2002) did not find correlations between humerus biomechanical variations and crocodilian locomotor behavior or habitat. Langel and Bonnan (in prep) recorded isometric growth in *Alligator mississippiensis* humeri cortical area despite changing locomotor capacities through alligator ontogeny. Predicting bone loading history and function from cross-sectional properties remains controversial due to the complex nature of internal and external factors impacting bone growth (Lieberman et al. 2004).

Unlike large bipeds, modern analogues of large bodied quadrupeds are prevalent, though forelimb posture and evolution may not be entirely convergent between non-avian dinosaurs and modern mammal taxa (Van Buren and Bonnan 2013). Long bones in modern quadrupedal taxa typically increase robustness relative to body mass across large-bodied mammalian groups (Christiansen 2007, Mallet et al. 2019, Etienne et al. 2020, 2021). *Maiasaura* humeral circumference increases with weak positive allometry (Heck Ch. VI), though humeral cortical area scales with isometry. Positive increases in *Maiasaura* humeral robustness would support a fully quadrupedal habit in which humeri scale in response to increasing body mass. However, cortical area does not scale with positive allometry and is more indicative of habitual bipedalism, similar to findings from Chapelle et al. (2019).

Dinosaur Bone Geometry

Studies of bone functional adaptation in modern species benefit from known ecology and behavior in studied taxa. Bone function inferences in extinct taxa is nearly entirely reliant on morphological data and limited sample sizes. Previous analyses studied limb scaling, muscle attachment site size, and external bone dimensions to infer behavior and locomotion in extinct dinosaurs (e.g. Wosik et al. 2018, Dilkes 2000, Heinrich 1993). Few dinosaur studies focus on internal bone geometry in predicting limb loading history. For example, Dumont et al. (2014) recorded isometric scaling between long bone geometry and length in a small sample of *Apatosaurus sp.* (n=4). A larger sample of neosauropods confirmed isometric scaling of cortical thickness in *Apatosaurus* and related taxa and imply limb-moving muscle mechanical advantage and limb range of movement decreased with size in neosauropods (Bonnan 2007). Farke and Alicea (2009) measured femora cross sectional geometry in extinct non-avian dinosaurs (n=4), flightless aves, and flighted aves (aves n=30). Femoral geometry did not reflect changing locomotor habits despite drastic shifts in femoral posture across Dinosauria.

The present study found humeral cortical area scales with isometry throughout *Maiasaura* ontogeny, while cortical thickness scaling is dependent on the measured axis. Anterior and lateral cortical thicknesses scale with negative allometry relative to humerus length and circumference. Forelimb transitions to load bearing in cursorial taxa should, theoretically, result in increased cortical area (resistance to axial compression) and/or increased osteogenesis along axes of bending and/or tension. Bone geometry in *Maiasaura* humeri does not support ontogenetic shifts from bipedalism to quadrupedalism, and further analyses are required to fully explore locomotor shifts in *Maiasaura*.

Cortical Remodeling and Bone Functional Adaptation

The present study marks the largest, single taxon evaluation of ontogenetic changes in cortical remodeling of an extinct species. Remodeling scaled with negative allometry relative to humerus circumference and length throughout ontogeny, and negative scaling trends were consistent in separate juvenile and adult *Maiasaura* sub-samples. Cortical remodeling also does not support an ontogenetic locomotor shift; increasing remodeling through ontogeny should reflect forelimb changes in function and loading.

However, several caveats must be addressed regarding sampling. Cortical remodeling was measured along major and minor axes. A more accurate measure of loading effects would be aligned along anatomical orientations (e.g. anterior, posterior, etc). Additionally, raw measures of cortical remodeling were evaluated in the present study. Proportion of cortical remodeling relative to total cortical bone should be explored in future research as this measure is less likely to be effected by cortical thickness.

Future Work and Alternative Hypotheses

Cortical area isometry, cortical thickness isometry and negative allometry, and medullary cavity area negative allometry implies medullary cavity area decreases due to an expansion of the *Maiasaura* humeral trabecular network. Trabecular density and orientation are correlated, in part, with principal stresses (Currey 2002), although trabeculae also serve non-mechanical biological roles (Kivell 2016 and references therein). The present study does not quantify trabecular area, despite the potential mechanical signal within. Future work should focus on quantifying humeral trabecular density, strut angulation, tissue composition, and changes in ontogeny to assess the presence of a mechanical signal.

Cortical geometry does not eliminate the possibility of a locomotor shift in *Maiasaura* from bipedal to quadrupedal. Forelimb geometry early in ontogeny may reflect growth trajectories of expected loads later in ontogeny after a possible shift to quadrupedalism (i.e. symmorphosis;

Weibel et al. 1991). Testing instances of cortical bone symmorphosis is difficult without direct behavioral observations and modern studies are extremely limited.

The locomotor shift hypothesis in *Maiasaura* was established by extensive studies on *Maiasuara* myology and long bone morphometrics (Dilkes 2000, 2001; Fig. 49A). Dilkes (2000) reported expansions of pectoral muscle attachment sites through *Maiasaura* ontogeny, and Dilkes (2001) recorded allometric increases in postural muscle attachments, lever arms of protractor muscles, and increased humeral robustness. Heck (Ch. VI) confirmed increases in *Maiasaura* humeral robustness with an expanded ontogenetic sample, but forelimb and hindlimb scaling did not support ontogenetic locomotor changes. Additionally, Chapelle et al. (2019) compared femoral and humeral robusticity and concluded, based on a small sample, *Maiasaura* did not transition to quadrupedalism and instead remained bipedal throughout ontogeny (Fig. 49B). Bipedal locomotion in *Maiasaura* is further supported by analyses of modern taxa (McPhee et al. 2018, Chapelle et al. 2019). *Maiasaura* femora have not been extensively sampled histologically despite the importance of femoral robustness in determining locomotor habit.

Slight increases in *Maiasaura* humeral robusticity and trabecular area do not support drastic changes in limb loading. Instead, positive allometry in robustness is consistent with increasing bone strength in conjunction with increased body mass in quadrupeds. Alternatively, *Maiasaura* may undergo slight changes in forelimb function; functions that may not result in strong cortical signals. Numerous *Maiasaura* nests are reported from separate facies of the Willow Creek Anticline. *Maiasaura* nests are bowl shaped depressions in which eggs may have been laid and covered with vegetation (Horner and Gorman 1988). Forelimbs may serve an essential role in nest building, similar to hindlimb use in ratite and megapode nest building (e.g. Jolly 1989, Carpenter 1999).

Regardless, the results here and Chapter VI do not support a locomotor shift in *Maiasaura* ontogeny. Cortical signals in forelimb bone growth and geometry do not necessarily confirm hypotheses of full quadrupedalism or bipedalism. *Maiasaura* may have been a facultative biped through ontogeny - utilizing quadrupedalism during slow movement and foraging, but resorting to bipedal locomotion during escape and running (e.g. Horner et al. 2004; Fig. 49C). Further tests comparing femora with humeri and examining humeri cross sectional polar moments, secondary moments, and cranial-caudal remodeling would aid in locomotor clarification.

Figures

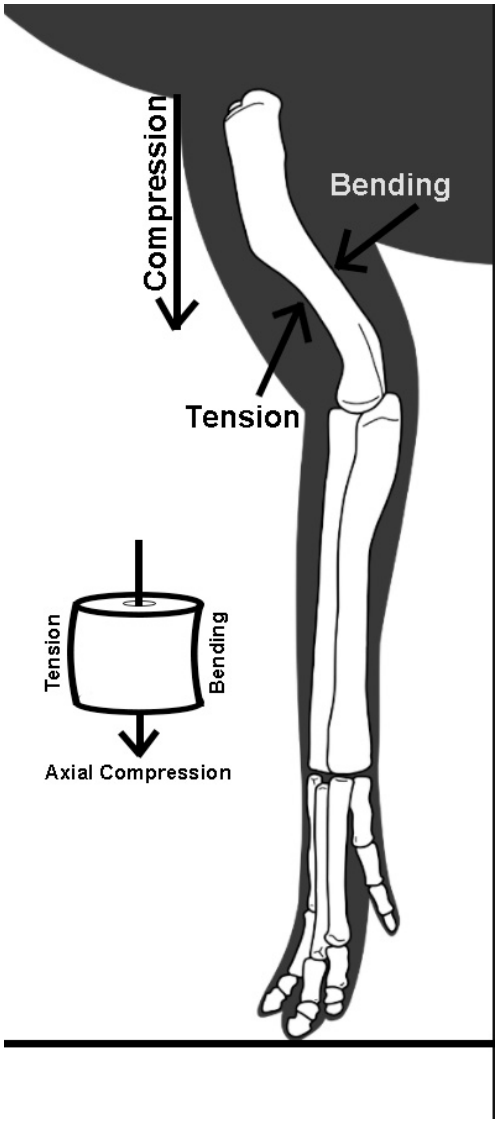

Figure 46. Forces acting on forelimbs during quadrupedal locomotion.

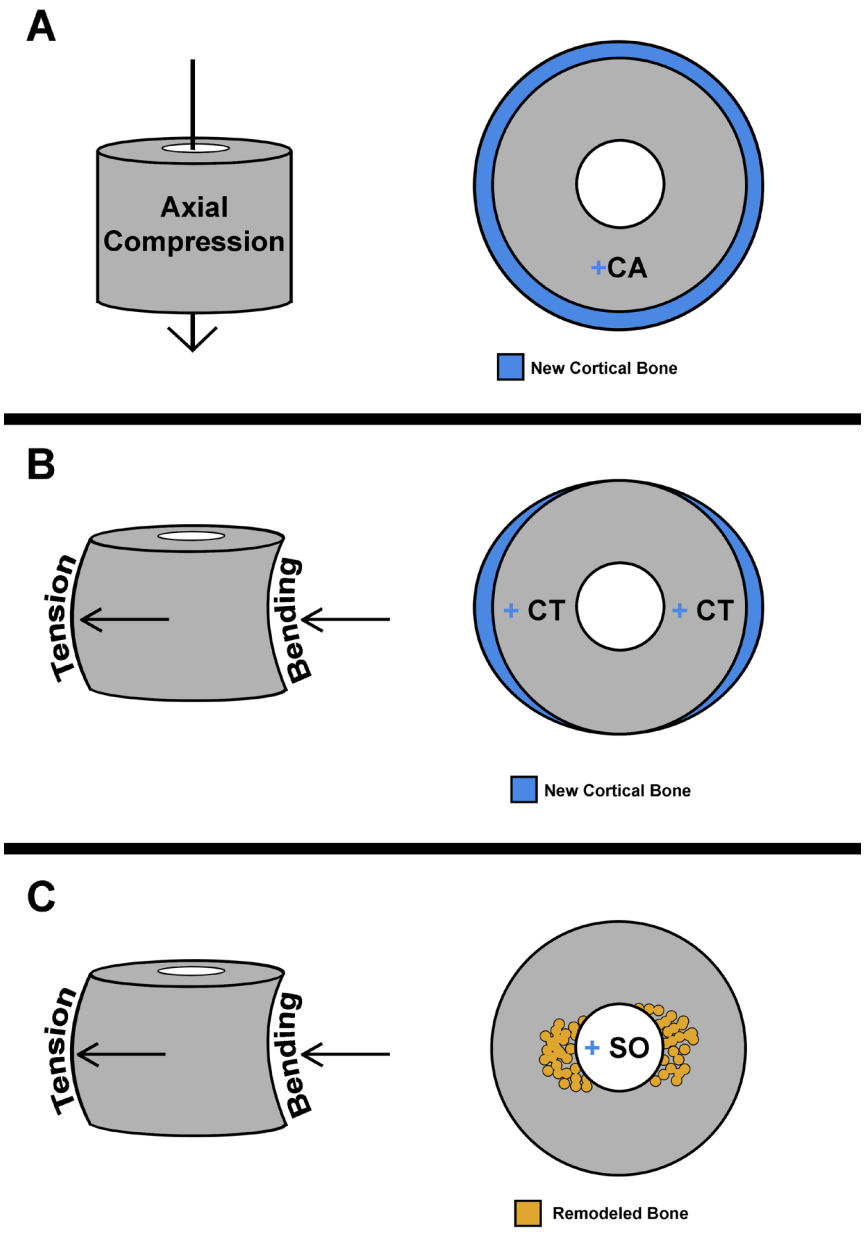

Figure 47. Visual hypothesis of bone growth response to introduced loading in an ontogenetic locomotor shift to quadrupedalism. (A) Cortical area increases to account for axial compression. (B) Differential cortical growth increases resistance to cranial-caudal bending and tension. (C) Increase loading and directional bending results in microcracks, which bone remodels during repair.

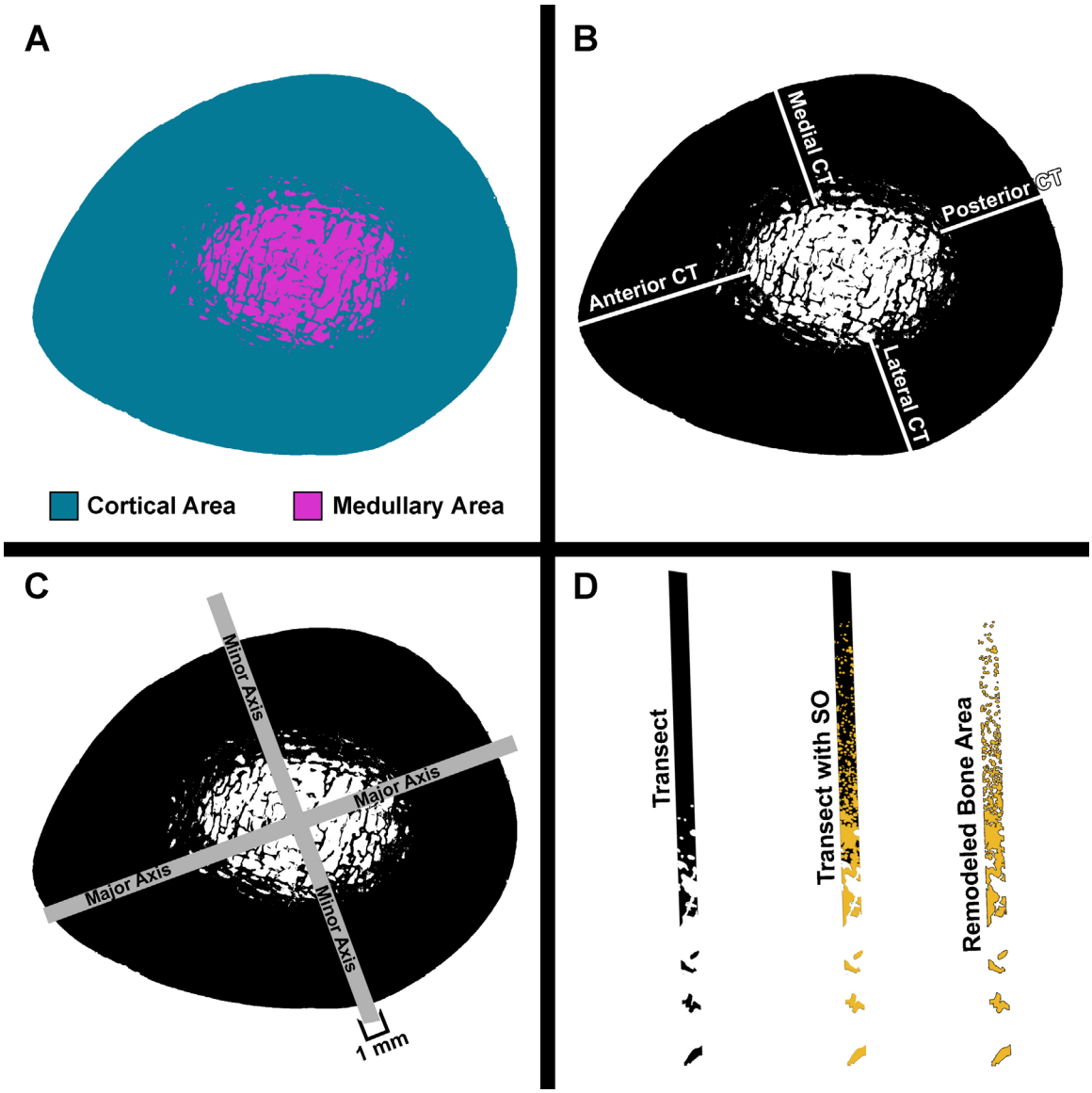

Figure 48. Measurements used to evaluate *Maiasaura* humerus geometry and bone functional adaptation. (A) Cortical area and medullary cavity area were measured from whole cross-sections. (B) Cortical thickness was measured along a straight line from inner border of compact bone outward to periosteal surface. (C) Four 1mm wide transects were evaluated for cortical remodeling along the major and minor axis. (D) Secondary tissue area was measured within each transect and summed across all four transects for each humerus.

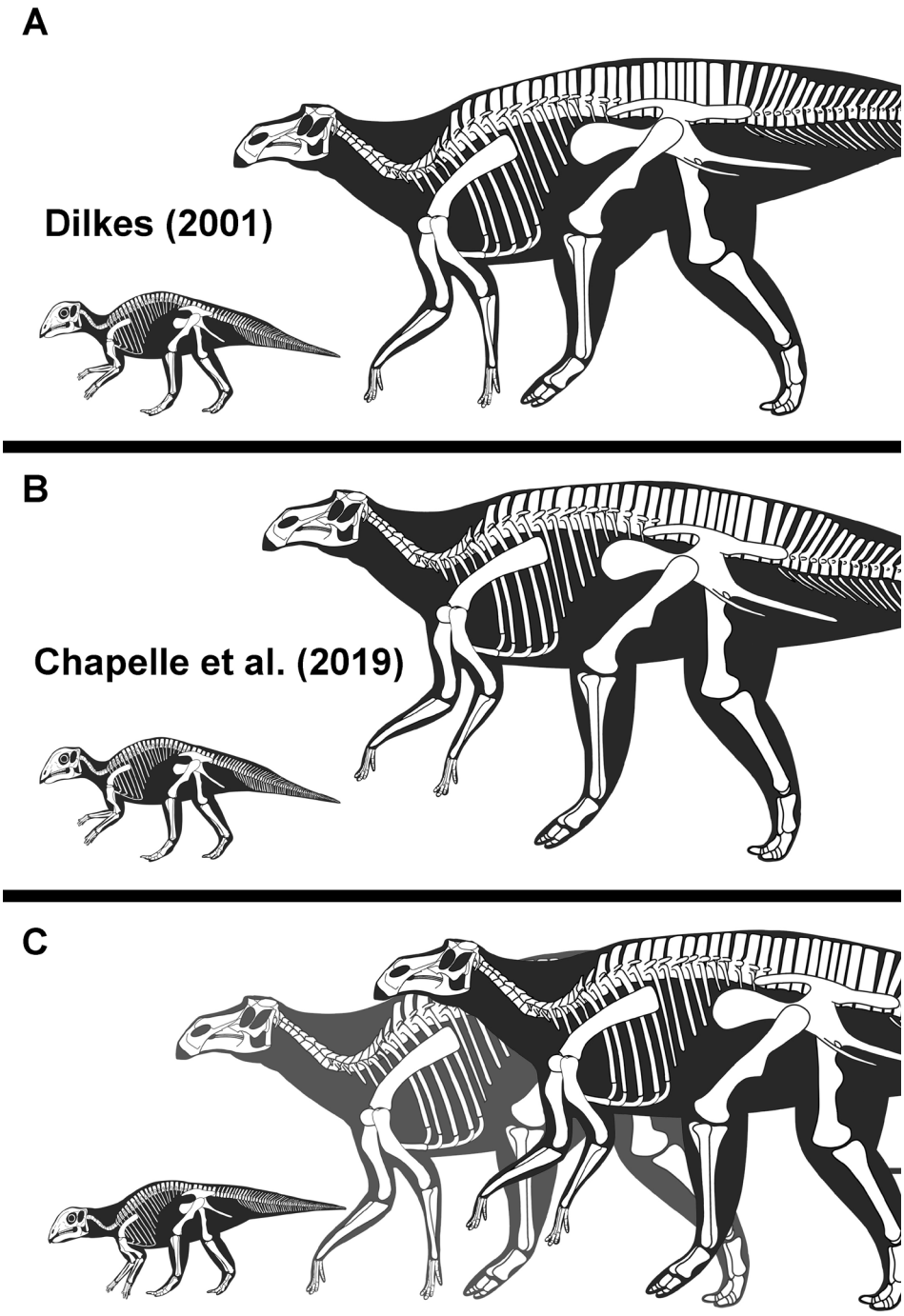

Figure 49. Ontogenetic locomotion in *Maiasaura*. (A) Dilkes (2001) proposed a bipedal juvenile to quadrupedal adult shift. (B) Chapelle et al. (2019) used femora and humeri robustness to suggest a fully bipedal *Maiasaura*. (C) Facultative bipedalism is suggested for other hadrosaurs and, in the current study, *Maiasaura.*

Tables

Table 14. OLS regression results from entire ontogenetic sample. Bold and italics indicate slopes significantly different from isometry.

Comparison with Length	n	Slope (b)	Lower CI (95%)	Upper CI (95%)	R^2	p-value	Trend
Cortical Area	30	0.491	0.463	0.518	0.979	<0.0001	Iso
Medullary Cavity Area	30	***0.296***	0.226	0.366	0.728	<0.0001	Neg
Anterior CT	42	***0.752***	0.579	0.924	0.660	<0.0001	Neg
Posterior CT	42	0.814	0.563	1.064	0.519	<0.0001	Iso
Medial CT	42	0.909	0.718	1.099	0.700	<0.0001	Iso
Lateral CT	42	***0.784***	0.610	0.958	0.674	<0.0001	Neg
Comparison with Circumference							
Cortical Area	30	0.477	0.455	0.500	0.985	<0.0001	Iso
Medullary Cavity Area	30	***0.289***	0.222	0.356	0.736	<0.0001	Neg
Anterior CT	42	***0.737***	0.572	0.903	0.669	<0.0001	Neg
Posterior CT	42	0.789	0.544	1.034	0.514	<0.0001	Iso
Medial CT	42	0.887	0.702	1.071	0.703	<0.0001	Iso
Lateral CT	42	***0.865***	0.597	0.934	0.678	<0.0001	neg

Table 15. OLS regression results in specimens 0-3 years-old. Bold and italics indicate slopes significantly different from isometry. Upper and lower confidence limits for 95%.

Comparison with Length	**n**	**Slope (b)**	**Lower CI**	**Upper CI**	**R^2**	**p-value**	**Trend**
Cortical Area	19	0.525	0.462	0.589	0.947	<0.0001	Iso
Medullary Cavity Area	19	***0.227***	0.103	0.351	0.469	0.001	Neg
Anterior CT	24	***0.491***	0.222	0.760	0.394	0.001	Neg
Posterior CT	24	***0.562***	0.214	0.909	0.519	0.003	Neg
Medial CT	24	0.680	0.313	1.047	0.402	<0.001	Iso
Lateral CT	24	***0.481***	0.196	0.766	0.358	0.002	Neg
Comparison with Circumference							
Cortical Area	19	0.503	0.450	0.556	0.960	<0.0001	Iso
Medullary Cavity Area	19	***0.206***	0.083	0.328	0.425	0.002	Neg
Anterior CT	24	***0.487***	0.235	0.739	0.422	<0.001	Neg
Posterior CT	24	***0.534***	0.199	0.868	0.514	0.003	Neg
Medial CT	24	0.662	0.314	1.010	0.414	<0.001	Iso
Lateral CT	24	***0.471***	0.201	0.740	0.373	0.002	neg

Table 16. OLS regression results in specimens ≥ 4 years-old. Bold and italics indicate slopes significantly different from isometry. Upper and lower confidence limits for 95%.

Comparison with Length	**n**	**Slope (b)**	**Lower CI**	**Upper CI**	**R^2**	**p-value**	**Trend**
Cortical Area	11	0.402	0.263	0.541	0.827	0.0001	Iso
Medullary Cavity Area	11	0.058	-0.060	0.176	0.120	0.296	Iso
Anterior CT	18	***0.234***	0.056	0.412	0.328	0.013	Neg
Posterior CT	18	0.127	-0.071	0.326	0.104	0.192	Iso
Medial CT	18	***0.283***	0.096	0.469	0.392	0.005	Neg
Lateral CT	18	0.086	-0.239	0.411	0.019	0.584	Iso
Comparison with Circumference							
Cortical Area	11	0.395	0.289	0.502	0.887	<0.0001	Iso
Medullary Cavity Area	11	0.083	-0.019	0.185	0.275	0.097	Iso
Anterior CT	18	***0.219***	0.050	0.388	0.320	0.015	Neg
Posterior CT	18	0.114	-0.074	0.302	0.093	0.218	Iso
Medial CT	18	***0.263***	0.085	0.441	0.381	0.006	Neg
Lateral CT	18	0.048	-0.261	0.357	0.007	0.746	Iso

REFERENCES

Ahmed, W. U. & Voort, G. V. (2000). Petrographic examination methods. Tech Notes, 3(5): 1-5.

Ahmed, W. U. & Voort, G. V. (2003). Specimen preparation of bones, tissues and other similar materials. Tech Notes, 3(8): 1-5.

Alboukadel, K. (2020). ggpubr: 'ggplot2' based publication ready plots. Retrieved from https://CRAN.R-project.org/package=ggpubr.

Alonso, J. C., Magana, M., Alonso, J. A., Palacin, C., Martin, C. A. & Martin, B. (2009). The most extreme sexual size dimorphism among birds: allometry, selection, and early juvenile development in the Great Bustard (*Otis tarda*). The Auk 126(3): 657-665.

Amprino, R. (1947). La structure du tissu osseux envisagée comme expression de différrences dans la vitesse de l'accroissement. Archives de Biologie 58: 315-330.

Amson, E., Arnold, P., van Heteren, A. H., Canoville, A. & Nyakatura, J. A. (2017). Trabecular architecture in the forelimb epiphyses of extant xenarthrans (Mammalia). Frontiers in Zoology 14(1): 52.

Andersson, M. B. (1994). Sexual Selection. Princeton: Princeton University Press.

Atterholt, J. & Woodward, H. N. (2021). A histological survey of avian post-natal skeletal ontogeny. PeerJ 9: e12160. doi:10.7717/peerj.12160.

Avrahami, H. M., Makovicky, P. & Zanno, L. E. (2019). Paleohistology of a new orodromine from the Upper Cretaceous (Cenomanian) Mussentuchit Member of the Cedar Mountain Formation, Utah; histological implications for burrowing behavior. Journal of Vertebrate Paleontology, Programs and Abstracts 2019: 56.

Bader, C., Böhmer, C., Abou, M., & Houssaye, A. (2022). How does bone microanatomy and musculature covary? An investigation in the forelimb of two species of martens (*Martes foina*, *Martes martes*). Journal of Anatomy doi:https://doi.org/10.1111/joa.13645.

Bailleul, A. M., O'Connor, J. & Schweitzer, M. H. (2019). Dinosaur paleohistology: review, trends and new avenues of investigation. PeerJ 7: e7764. doi:10.7717/peerj.7764.

Barrett, P. M. & Maidment, S. C. R. (2017). The evolution of ornithischian quadrupedality. Journal of Iber Geology doi:10.1007/s41513-017-0036-0.

Beale, G. (1985). A radiological study of the kiwi (*Apteryx australis mantelli*). J. R. Soc. N. Z. 15: 187-200.

Beale, G. (1991). The maturation of the skeleton of a kiwi (*Apteryx australis mantelli*) - a ten-year radiological study. J. R. Soc. N. Z. 21: 219-220.

Behrensmeyer, A. K., Western, D., & Boaz, D. E. D. (1979). New perspectives in vertebrate paleoecology from a recent bone assemblage. Paleobiology 5(1): 12-21.

Bennett, M. B. (2008). Post-hatching growth and development of the pectoral and pelvic limbs in the black noddy, *Anous minutus*. Comparative Biochemistry and Physiology 150: 159-168.

Bentolila, V., Boyce, T. M., Fyhrie, D. P., Drumb, R., Skerry, T. M., & Schaffler, M. B. (1998). Intracortical remodeling in adult rat long bones after fatigue loading. Bone 23(3): 275-281.

Bertozzo, F. (2017). The Venice specimen of *Ouranosaurus nigeriensis* (Dinosauria, Ornithopoda). PeerJ 5: e3403. doi:10.7717/peerj.3403.

Bertram, J. E. A., & Biewener, A. A. (1988). Bone curvature: sacrificing strenth for load predictability? Journal of Theoretical Biology 131: 75-92.

Bertram, J. E. A., & Biewener, A. A. (1992). Allometry and curvature in the long bones of quadrupedal mammals. Journal of Zoological Society of London 226: 455-467.

Biewener, A. A. (1982). Bone strength in small mammals and bipedal birds: do safety factors change with body size? Journal of Experimental Biology 98: 289-301.

Biewener, A. A. (1983). Allometry of quadrupedal locomotion: the scaling of duty factor, bone curvature and limb orientation to body size. Journal of Experimental Biology 105: 147-171.

Biewener, A. A. (1989). Scaling body support in mammals: limb posture and muscle mechanics. Science 245: 45-48.

Biewener, A. A. (2005). Biomechanical consequences of scaling. Journal of Experimental Biology 208: 1665-1676.

Biewener, A. A., & Taylor, C. R. (1986). Bone strain: a determinant of gait and speed. Journal of Experimental Biology 123: 383-400.

Bishop, P. J., Bates, K. T., Allen, V. R., Henderson, D. M., Randau, M., & Hutchinson, J. R. (2020). Relationships of mass properties and body proportions to locomotor habit in terrestrial Archosauria. Paleobiology 46(6): 550-568.

Bonnan, M. F. (2007). Linear and geometric morphometric analysis of long bone scaling patterns in Jurassic neosauropod dinosaurs: their functional and paleobiological implications. The Anatomical Record 290: 1089-1111.

Botfalvai, G., Prondvai, E., & Osi, A. (2021). Living alone or moving in herds? A holistic approach highlights complexity in the social lifestyle of Cretaceous ankylosaurs. Cretaceous Research 118: 104633.

Botha-Brink, J., Codron, D., Huttenlocker, A. K., Angielczyk, K. D., & Ruta, M. (2016). Breeding young as a survival strategy during earth's greatest mass extinction. Scientific Reports 6: 24053. doi:https://doi.org/10.1038/srep24053.

Botton-Divet, L., Cornette, R., Fabre, A.-C., Herrel, A., & Houssaye, A. (2016). Morphological analysis of long bones in semi-aquatic mustelids and terrestrial relatives. Integrative and Comparative Biology 56: 1298-1309.

Botton-Divet, L., Cornette, R., Houssaye, A., Fabre, A.-C., & Herrel, A. (2017). Swimming and running: a study of the convergence in long bone morphology among semi-aquatic mustelids (Carnivora: Mustelidae). Biological Journal of the Linnean Society 121: 38-49.

Bourdon, E., Castanet, J., des Ricqlès, A., Scofield, P., Tennyson, A., Lamrous, H., & Cubo, J. (2009). Bone growth marks reveal protracted growth in New Zealand kiwi (Aves, Apterygidae). Biology Letters 5: 639-642. doi:10.1098/rsbl.2009.0310

Brinkman, D. B. (2014). The size-frequency distribution of hadrosaurs from the Dinosaur Park Formation of Alberta, Canada. In D. A. Eberth & D. C. Evans (Eds.), Hadrosaurs (pp. 524-531). Bloomington: Indiana University Press.

Broughton, J. M., Rampton, D., & Holanda, K. (2002). A test of an osteologically based age determination technique in the Double-crested Cormorant *Phalacrocorax auritus*. Ibis 144: 143-146.

Brown, C. M., & Vavrek, M. J. (2015). Small sample sizes in the study of ontogenetic allometry; implications for paleobiology. PeerJ 3: e818.

Bruce, R. C., & Castanet, J. (2006). Application of skeletochronology in aging larvae of the salamanders Gyrinophilus porphyriticus and Pseudotriton ruber. Journal of Herpetology 40: 85-90.

Bryant, H. N., & Seymour, K. L. (1990). Obsrvations and comments on the reliability of muscle reconstruction in fossil vertebrates. Journal of Morphology 206: 109-117.

Burbridge, M., Colbourne, R., Roberson, H., & Baker, A. (2003). Molecular and other biological evidence supports the recognition of at least three species of brown kiwi. Conservation Genetics 4: 167-177.

Burr, D. B., Martin, R. B., Schaffler, M. B., & Radin, E. L. (1985). Bone remodeling in response to in vivo fatigue microdamage. Journal of Biomechanics 18: 189-200.

Butler, R. J., & Barrett, P. M. (2012). Ornithopods. In M. K. Brett-Surman, T. R. Holtz, & J. O. Farlow (Eds.), The Complete Dinosaur (2 ed., pp. 551-566). Bloomington: University of Indiana Press.

Bybee, P. J., Lee, A. H., & Lamm, E.-T. (2006). Sizing the Jurassic theropod dinosaur Allosaurus: assessing growth strategy and evolution of ontogenetic scaling of limbs. Journal of Morphology 267: 347-359. doi:10.1002/jmor.10406.

Calderón, T., DeMiguel, D., Arnold, W., Stalder, G., & Köhler, M. (2019). Calibration of life history traits with epiphyseal closure, dental eruption and bone histology in captive and wild red deer. Journal of Anatomy 235: 205-216. doi:10.1111/joa.13016.

Campione, N. E., & Evans, D. C. (2012). A universal scaling relationship between body mass and proximal limb bone dimensions in quadrupedal terrestrial tetrapods. BMC Biology 10: doi:https://doi.org/10.1186/1741-7007-10-60

Canoville, A., Schweitzer, M. H., & Zanno, L. E. (2019). Identifying medullary bone in extinct avemetatarsalians: challenges, implications and perspectives. Philisophical Transactions of the Royal Society B. 375: 20190133. doi:http://dx.doi.org/10.1098/rstb.2019.0133.

Canoville, A., Schweitzer, M. H., & Zanno, L. E. (2019). Systemic distribution of medullary bone in the avian skeleton: ground truthing criteria for the identification of reproductive tissues in extinct Avemetatarsalia. BMC Evolutionary Biology 19: 71. doi:https://doi.org/10.1186/s12862-019-1402-7.

Capaldo, S. D., & Peters, C. R. (1995). Skeletal inventories from Wildebeest drownings at lakes Masek and Ndutu in the Serengeti ecosystem of Tanzania. Journal of Archaeological Science 22: 385-408.

Carpenter, K. (1999). Eggs, Nests, and Baby Dinosaurs. Bloomington: Indiana University Press.

Carrano, M. T. (1998). Locomotion in non-avian dinosaurs: integrating data from hindlimb kinematics, in vivo strains, and bone morphology. Paleobiology 24: 450-469.

Carrano, M. T. (1999). What, if anything, is a cursor? Categories versus continua for determining locomotor habit in mammals and dinosaurs. Journal of Zoological Society of London 247: 29-42.

Carrano, M. T. (2001). Implications of limb bone scaling, curvature and eccentricity in mammals and non-avian dinosaurs. Journal of Zoological Society of London 254: 41-55.

Castanet, J., Croci, S., Aujard, F., Perret, M., Cubo, J., & de Margerie, E. (2004). Lines of arrested growth in bone and age estimation in a small primate: Microcebus murinus. J. Zool. Lond. 263: 31-39. doi:10.1017/S0952836904004844

Castanet, J., Francillon-Vieillot, H., Meunier, P., & de Ricqlés, A. (1993). Bone and individual aging. In B. K. Hall (Ed.), Bone (pp. 245-283). London: CRC Press.

Castanet, J., Grandin, A., Abourachid, A., & de Ricqlés, A. (1996). Expression de la dynamique de croissance dans la structure de l'os periostique chez *Anas plathyrhynchos*. Comptes Rendus de l'Academie des Sciences - Series III - Sciences de la Vie 319: 301-308.

Castanet, J., Rogers, K. C., Cubo, J., & Boisard, J-J. (2000). Periosteal bone growth rates in extant ratites (ostriche and emu). Implications for assessing growth in dinosaurs. . Comptes Rendus de l'Academie des Sciences - Series III - Sciences de la Vie 323(6): 543-550.

Cerda, I. A., Tambussi, C. P., & Degrange, F. J. (2015). Unexpected microanatomical variation among Eocene Antarctic stem penguins (Aves: Sphenisciformes). Historical Biology 27(5): 549-557.

Chang-Fu, Z., Ke-Qin, G., & Fox, R. C. (2010). Morphology and histology of lattice-like ossified epaxial tendons in *Psittacosaurus* (Dinosauria: Ceratopsia). Acta Geologica Sinica 84(3): 463-471.

Chapelle, K. E. J., Benson, R. B. J., Stiegler, J., Otero, A., Zhao, Q., & Choiniere, J. N. (2019). A quantitative method for inferring locomotory shifts in amniotes during ontogeny, its application to dinosaurs and its bearing on the evolution of posture. Palaeontology 63(2): 229-242.

Chinsamy, A. (1993). Image analysis and the physiological implications of the vascularisation of femora in archosaurs. Modern Geology 19(1): 101-108.

Chinsamy, A., Chiappe, L. M., & Dodson, P. (1995). Mesozoic avian bone microstructure: physiological implications. Paleobiology, 21(4), 561-574.

Chinsamy, A., Martin, L. D., & P., D. (1998). Bone microstructure of the diving Hesperornis and the voltant Ichthyornis from the Niobrara Chalk of western Kansas. Cretaceous Research, 19, 225-233.

Chinsamy, A., & Raath, M. A. (1992). Preparation of fossil bone for histological examination. Palaeontologia africans 29: 39-44.

Christiansen, P. (2007). Long bone geometry in columnar-limbed animals: allometry of the proboscidean appendicular skeleton. Zoological Journal of the Linnean Society 149: 423-436.

Cooper, L. N., Lee, A. H., Taper, M. L., & Horner, J. R. (2008). Relative growth rates of predator and prey dinosaurs reflect effects of predation. . Proceedings of the Royal Society B - Biological Sciences 275: 2609-2615.

Cubo, J., & Casinos, A. (1997). Flightlessness and long bone allometry in palaeognathiformes and sphenisciformes. Netherlands Journal of Zoology 47(2): 209-226.

Cubo, J., Legendre, P., de Ricqlés, A., Montes, L., de Margerie, E., Castanet, J., & Desdevises, Y. (2008). Phylogenetic, functional, and structural components of variation in bone growth rate of amniotes. Evolution and Development 10(2): 217-227.

Cubo, J., Woodward, H. N., Wolff, E., & Horner, J. R. (2015). First reported cases of biomechanically adaptive bone modeling in non-avian dinosaurs. PLOS One 10(7): e0131131.

Cullen, T. M., Canale, J. I., Apesteguía, S., Smith, N. D., Hu, D., & Makovicky, P. (2020). Osteohistological analyses reveal diverse strategies of theropod dinosaur body-size evolution: diverse strategies of theropod gigantism. Proceedings of the Royal Society B, 287(1939), 20202258.

Cullen, T. M., Evans, D. C., Ryan, M. J., Currie, P. J., & Kobayashi, Y. (2014). Osteohistological variation in growth marks and osteocyte lacunar density in a theropod dinosaur (Coelurosauria: Ornithomimidae). BMC Evolutionary Biology 14(231).

Cullen, T. M., Simon, D. J., Benner, E. K. C., & Evans, D. C. (2020). Morphology and osteohistology of a large-bodied caenagnathid (Theropoda, Oviraptorosauria) from the Hell Creek Formation (Montana): implications for size-based classifications and growth reconstruction in theropods. Papers in Paleontology 2020: 1-17. doi:10.1002/spp2.1302.

Currey, J. D. (2002). Bones: structure and mechanics. Princeton: Princeton University Press.

Currey, J. D. (2014). The mechanical adaptations of bones. Princeton: Princeton University Press.

Currie, P. J. (1985). Cranial anatomy of *Stenonychosaurus inequalis* (Saurischia, Theropoda) and its bearing on the origin of birds. Canadian Journal of Earth Sciences 22(11): 1643-1658.

Curry-Rogers, K., & Kulik, Z. (2018). Osteohistology of *Rapetosaurus krausei* (Sauropoda: Titanosauria) from the Upper Cretaceous of Madagascar. Journal of Vertebrate Paleontology 38(4): 1-24.

Curtin, A. J., Macdowell, A. A., Shaible, E. G., & Roth, V. L. (2012). Noninvasive histological comparison of bone growth patterns among fossil and extant neonatal elephantids using synchrotron radiation x-ray microtomography. Journal of Vertebrate Paleontology 32(4): 939-955.

Dacke, C. G., Elsey, R. M., Trosclair III, P. L., Sugiyama, T., Nevarez, J. G., & Schweitzer, M. H. (2015). Alligator osteoderms as a source of labile calcium for eggshell formation. Journal of Zoology 297: 255-264. doi:10.1111/jzo.12272.

Davison, K. S., Siminoski, K., Adachi, J. D., Hanley, D. A., Goltzman, D., Hodsman, A. B., Josse, R., Kaiser, S., Olszynski, W.P., Papaioannou, A., Ste-Marie, L.-G., Brown, J. P. (2006). Bone strength: the whole is greater than the sum of its parts. Seminars in Arthritis and Rheumatism 36(1): 22-31.

de Buffrénil, V., & Francillon-Vieillot, H. (2001). Ontogenetic changes in bone compactness in male and female Nile Monitors (*Varanus niloticus*). Journal of Zoology 254: 539-546.

de Buffrénil, V., Laurin, M., & Jouve, S. (2021). Archosauromorpha: The Crocodylomorpha. In V. de Buffrénil, A. de Ricqlès, L. Zylberberg, & K. Padian (Eds.), Vertebrate Skeletal Histology and Paleohistology (pp. 486-510). Boca Raton: CRC Press.

de Buffrénil, V., & Quilhac, A. (2021). Bone Remodeling. In V. de Buffrénil, A. de Ricqlès, L. Zylberberg, & K. Padian (Eds.), Vertebrate Skeletal Histology and Paleohistology (pp. 229-246). London: CRC Press.

de Buffrénil, V., Quilhac, A., & Castanet, J. (2021). Cyclical Growth and Skeletochronology. In V. de Buffrénil, A. de Ricqlès, L. Zylberberg, & K. Padian (Eds.), Vertebrate Skeletal Histology and Paleohistology. London: CRC Press.

de Buffrénil, V., Quilhac, A., & Cubo, J. (2021). Accretion rate and histological features of bone. In V. de Buffrénil, A. de Ricqlès, L. Zylberberg, & K. Padian (Eds.), Vertebrate Skeletal Histology and Paleohistology (pp. 221-228). London: CRC Press.

de Margerie, E. (2006). Biomechanical function of bone microstructure in birds. Comptes Rendus - Paleovol 5: 619-628.

de Margerie, E., Cubo, J., & Castanet, J. (2002). Bone typology and growth rate: testing and quantifying 'Amprino's rule' in the mallard (*Anas platyhynchos*). Comptes Rendus Biologies 325: 221-230.

de Margerie, E., Robin, J.-P., Verrier, D., Cubo, J., Groscolas, R., & Castanet, J. (2004). Assessing a relationship between bone microstructure and growth rate: a fluorescent labelling study in the king penguin chick (*Aptenodytes patagonicus*). The Journal of Experimental Biology 207: 869-879.

de Ricqlès, A. (1980). Tissue structure of dinosaur bone: functional significance and possible relations to dinosaur physiology. In E. C. Olson & R. D. K. Thomas (Eds.), A cold look at the warm-blooded dinosaurs. (pp. 103-139). Boulder: Westview.

de Ricqlès, A., Bourdon, E., Legendre, L., & Cubo, J. (2016). Preliminary assessment of bone histology in the extinct elephant bird *Aepyornis* (Aves, Palaeognathae) from Madagascar. Comptes Rendus Palevol 15: 197-208. doi:10.1016/j.crpv.2015.01.003.

de Ricqlès, A., Padian, K., & Horner, J. R. (2001). The bone histology of basal birds in phylogenetic and ontogenetic perspectives. In J. Gauthier & L. Gall (Eds.), New Perspectives on the origin and early evolution of birds. (pp. 411-426). New Haven: Yale University Press.

Deevey, E. S. (1947). Life tables for natural populations of animals. The Quarterly Review of Biology 22: 283-314.

Demes, B., & Jungers, W. L. (1993). Long bone cross-sectional dimensions, locomotor adaptations and body size in prosimian primates. Journal of Human Evolution 25(1): 57-74.

Demes, B., Jungers, W. L., & Selpien, K. (1991). Body size, locomotion, and long bone cross-sectional geometry in Indriid primates. American Journal of Physical Antropology 86: 537-547.

Deymier-Black, A. C., Pasteris, J. D., Genin, G. M., & Thomopoulos, S. (2015). Allometry of the tendon enthesis: mechanisms of load transfer between tendon and bone. Journal of Biomechanical Engineering 137(11): e111005.

Dial, T. R., & Carrier, D. R. (2012). Precocial hindlimbs and altricial forelimbs: partitioning ontogenetic strategies in mallards (*Anas platyrhynchos*). Journal of Experimental Biology 215: 3703-3710.

Dilkes, D. W. (2000). Appendicular myology of the hadrosaurian dinosaur *Maiasaura peeblesorum* from the Late Cretaceous (Campanian) of Montana. Transactions of the Royal Society of Edinburgh: Earth Sciences 90: 87-125.

Dilkes, D. W. (2001). An ontogenetic perspective on locomotion in the Late Cretaceous dinosaur *Maiasaura peeblesorum* (Ornithischia: Hadrosauridae). Canadian Journal of Earth Sciences 38: 1205-1227.

Domander, R., Felder, A. A., & Doube, M. (2021). BoneJ2 - refactoring established research software. Wellcome Open Research 6: 37. doi:10.12688/wellcomeopenres.16619.2.

Doube, M., Klosowski, M. M., Arganda-Carreras, I., Cordelières, F., Dougherty, R. P., Jackson, J., Schmid, B., Hutchinson, J.R., Shefelbine, S. J. (2010). BoneJ: free and extensible bone image analysis in ImageJ. Bone 47: 1076-1079.

Dumont, M., Borbely, A., Kaysser-Pyzalla, A., & Sander, M. P. (2014). Long bone cortices in a growth series of *Apatosaurus* sp. (Dinosauria: Diplodocidae): geometry, body mass, and crystallite orientation of giant animals. Biological Journal of the Linnean Society 112: 782-798.

Early, C. M., Morhardt, A. C., Cleland, T. P., Milensky, C. M., Kavich, G. M., & James, H. F. (2020). Chemical effects of diceCT staining protocols on fluid-preserved avian specimens. PLOS One e0238783.

Edgren, R. A. (1960). A seasonal change in bone density in female musk turtles, *Sternothaerus odoratus* (Latreille). Comparative Biochemistry and Physiology 1: 213-217.

Elsey, R. M., Joanen, T., McNease, L., & Kinler, N. (1992). Growth rates and body condition factors of *Alligator mississippiensis* in coastal Louisiana wetlands: a comparison of wild and farm-released juveniles. Comparative Biochemistry and Physiology Part A: Physiology 103(4): 667-672.

Elsey, R. M., & Wink, C. S. (1986). The effects of estradiol on plasma calcium and femoral bone structure in alligators (*Alligator mississippiensis*). Comparative Biochemistry and Physiology Part A: Molecular and Integrative Physiology 84A(1): 107-110.

Enlow, D. H. (1963). Principles of bone remodeling: an account of post-natal growth and remodeling processes in the long bones and the mandible. Springfield: Charles C. Thomas.

Erickson, G. M. (2005). Assessing dinosaur growth patterns: a microscopic revolution. TRENDS in Ecology and Evolution 20: 677-684.

Erickson, G. M., Currie, P. J., Inouye, B. D., & Winn, A. A. (2006). Tyrannosaur life tables: an example of nonavian dinosaur population biology. Science 313: 213-217.

Erickson, G. M., Currie, P. J., Inouye, B. D., & Winn, A. A. (2010). A revised life table and survivorship curve for *Albertosaurus sarcophagus* based on the Dry Island mass death assemblage. Canadian Journal of Earth Sciences 47: 1269-1275.

Erickson, G.M., & Druckenmiller, P.S. (2011). Longevity and growth rate estimates for a polar dinosaur: a *Pachyrhinosaurus* (Dinosauria: Neoceratopsia) specimen from the North Slope of Alaska showing a complete developmental record. Historical Biology 23: 327-334.

Erickson, G.M., Makovicky, P., Currie, P.J., Norell, M.A., Yerby, S.A., Brochu, C.A. (2004). Gigantism and comparative life-history parameters of tyrannosaurid dinosaurs. Nature 430: 772-775.

Erickson, G. M., Makovicky, P., Inouye, B. D., Zhou, C. F., & Gao, K. Q. (2009). A life table for Psittacosaurus lujiatunensis: initial insights into ornithischian dinosaur population biology. Anatomical Record (Hoboken) 292: 1514-1521.

Erickson, G.M., Rogers, K.C., Varricchio, D.J., Norell, M.A., Xu, X. (2007). Growth patterns in brooding dinosaurs reveals the timing of sexual maturity in non-avian dinosaurs and genesis of the avian condition. Biology Letters 3: 558-561.

Erickson, G. M., Rogers, K. C., & Yerby, S. A. (2001). Dinosaurian growth patterns and rapid avian growth rates. Nature 412: 429-432.

Erickson, G. M., & Tumanova, T. A. (2000). Growth curve of *Psittacosaurus mongoliensis* Osborn (Ceratopsia: Psittacosauridae) inferred from long bone histolgy. Zoological Journal of the Linnean Society 130: 551-566.

Etienne, C., Filippo, A., Cornette, R., & Houssaye, A. (2020). Effect of mass and habitat on the shape of limb long bones: a morpho-functional investigation on Bovidae (Mammalia: Cetartiodactyla). Journal of Anatomy 238: 886-904.

Etienne, C., Houssaye, A., & Hutchinson, J. R. (2021). Limb myology and muscle architecture of the Indian rhinoceros *Rhinoceros unicornis* and the white rhinoceros *Ceratotherium simum* (Mammalia: Rhinocertidae). PeerJ 9: e11314.

Fabre, A.-C., Cornette, R., Goswami, A., & Peigné, S. (2015). Do constraints associated with the locomotor habitat drive the evolution of forelimb shape? Journal of Anatomy 226: 596-610.

Fariña, R. A., & Vizcaíno, S. F. (1997). Allometry of the bones of living and extinct armadillos (Xenarthra, Dasypoda). Zeitschrift fur Saugetierkunde 62(2): 65-70.

Farlow, J. O., & Britton, A. R. C. (2000). Size and body proportions in *Alligator mississippiensis*: implcations for archosaurian ichnology. Paleontological Society of Korea Special Publication 4: 189-206.

Farlow, J. O., Hurlburt, G. R., Elsey, R. M., Britton, A. R. C., & Langston Jr., W. (2005). Femoral dimensions and body size of *Alligator mississippiensis* estimating the size of extinct mesoeucrocodylians. Journal of Vertebrate Paleontology 25(2): 354-369.

Faure-Brac, M. G., Pelissier, F., & Cubo, J. (2019). The influence of plane of section on the identification of bone tissue types in amniotes with implications for paleophysiological inferences. Journal of Morphology 280: 1282-1291. doi:10.1002/jmor.21030.

Fearon, J. L., & Varricchio, D. J. (2016). Reconstruction of the forelimb musculature of the Cretaceous ornithopod dinosaur *Oryctodromeus cubicularis*: implications for digging. . Journal of Vertebrate Paleontology 36(2): e1078341.

Fondevilla, V., Vecchia, F. M. D., Gaete, R., Galobart, A., Moncunill-Sole, B., & Köhler, M. (2018). Ontogeny and taxonomy of the hadrosaur (Dinosauria, Ornithopoda) remains from Basturs Poble bonebed (late early Maastrichtian, Tremp Suncline, Spain). PLOS One 13(10): e0206287. doi:10.1371/journal.pone.0206287.

Forwood, M. R., & Burr, D. B. (1993). Physical activity and bone mass: exercises in futility? Bone and Mineral 21(2): 89-112.

Fowler, E. A. F., & Horner, J. R. (2015). A new Brachylophosaurin Hadrosaur (Dinosauria: Ornithischia) with an intermediate nasal crest from the Campanian Judith River Formation of Northcentral Montana. PLOS One 10(11): e0141304. doi:10.1371/journal.pone.0141304.

Francillon-Vieillot, H., de Buffrénil, V., Castanet, J., Geraudie, J., Meunier, F. J., Sire, J. Y., . . . De Ricqlès, A. (1990). Microstructure and mineralization of vertebrate skeletal tissues. In J. Carter (Ed.), Skeletal biomineralization patterns, processes and evolutionary trends. (pp. 471-548). New York: Van Nostrand Reinhold.

Frylestam, B., & Schantz, T. v. (1977). Age determination of European hares based on periosteal growth lines. Mammal Review 7(3): 151-154.

Garcia-Martínez, R., Marín-Moratella, N., Jordana, X., & Köhler, M. (2011). The ontogeny of bone growth in two species of dormice: reconstructing life history traits. Comptes Rendus Palevol 10: 489-498.

Garrone, M. C., Cerda, I. A., & Tomassini, R. L. (2019). Ontogenetic variability in the limb bones histology of plains vizcacha (*Lagostomus maximus*, Chinchillidae, Rodentia): implications for life history reconstruction of fossil representatives. Historical Biology. doi.org/10.1080/08912963.2019.1648450.

Gatesy, S. M., & Biewener, A. A. (1991). Bipedal locomotion: effects of speed, size and limb posture in birds and humans. Journal of Zoological Society of London 224: 127-147.

Geist, N. R., & Jones, T. D. (1996). Juvenile skeletal structure and the reproductive habits of dinosaurs. Science 272(5262): 712-714.

Graveland, J., & Berends, A. E. (1997). Timing of the calcium intake and effect of calcium deficiency on behaviour and egg laying in captive great tits, Parus major. Physiological Zoology 70(1): 74-84.

Graveland, J., & Drent, R. H. (1997). Calcium availability limits breeding success of Passerines on poor soils. Journal of Animal Ecology 66(2): 279-288.

Griebeler, E. M. (2021). Dinosaurian survivorship schedules revisited: new insights from an age-structured population model. Palaeontology 1-16. doi:10.1111/pala.12576.

Griebeler, E.M., Klein, N., Sander, P.M. (2013). Aging, maturation and growth of sauropodomorph dinosaurs as deduced from the growth curves using long bone histological data. PLOS One 8: e67012.

Griffin, C. T., Stocker, M. R., Colleary, C., Stefanie, C. M., Lessner, E. J., Riegler, M., Formoso, K., Koeller, K., Nesbitt, S. J. (2021). Assessing ontogenetic maturity in extinct saurian reptiles. Biological Reviews 96: 470-525.

Gross, T., Edward, J., McLeod, K., & Rubin, C. (1997). Strain gradients correlate with sites of periosteal bone formation. Journal of Bone and Mineral Research 12: 982-988.

Guenther, M. F. (2009). Influence of sequence heterochrony on Hadrosaurid dinosaur postcranial development. The Anatomical Record 292(9): 1427-1441.

Guenther, M. F. (2014). Comparative ontogenies (appendicular skeleton) for three hadrosaurids and a basal Iguanodontian: divergent developmental pathways in Hadrosaurinae and Lambeosaurinae. In D. A. Eberth & D. C. Evans (Eds.), Hadrosaurs (pp. 398-415). Bloomington: Indiana University Press.

Haines, R. W. (1942). The evolution of epiphyses and of enchondral bone. Biological Reviews of the Cambridge Philosophical Society 174: 267-292.

Hall, B. K. (2015). Bones and cartilage: developmental and evolutionary skeletal biology. (2 ed.). New York: Academic Press.

Hancox, N. M. (1972). Biology of Bone. Cambridge: Cambridge University Press.

Heck, C. T., Varricchio, D. J., Gaudin, T. J., Woodward, H. N., & Horner, J. R. (2019). Ontogenetic changes in the long bone microstructure in the nine-banded armadillo (*Dasypus novemcinctus*). PLOS One 14(4): e0215655. doi:10.1371/journal.pone.0215655.

Heck, C. T., Volkmann, G., & Woodward, H. N. (2020). Polyester or epoxy: assessing embedding product efficacy in paleohistological methods. PeerJ 8: e10495.

Heck, C. T., & Woodward, H. N. (2021). Intraskeletal bone growth patterns in the North Island Brown Kiwi (*Apteryx mantelli*): growth mark discrepancy and implications for extinct taxa. Journal of Anatomy 239(5): 1075-1095.

Heinonen, A., Sievänen, H., Kannus, P., Oja, P., & vuori, I. (2002). Site-specific skeletal response to long-term weight training seems to be attributable to principal loading modality: a pQCT study of female weightlifters. Calcified Tissue International 70: 469-474.

Heinonen, A., Sievänen, H., Kyröläinen, H., Perttunen, J., & Kannus, P. (2001). Mineral mass, size, and estimated mechanical strength of triple jumpers' lower limbs. Bone 29: 279-285.

Heinrich, R. E., Ruff, C. B., & Weishampel, D. B. (1993). Femoral ontogeny and locomotor biomechanics of *Dryosaurus littowverbecki* (Dinosauria, Iguanodontia). Zoological Journal of the Linnean Society 108: 179-196.

Henderson, B. A., & Bowen, H. M. (1979). A short note: estimating the age of European rabbit, *Oryctolagus cuniculus*, by counting the adhesion lines in the periosteal zone of the lower mandible. Journal of Applied Ecology 16: 393-396.

Hert, J., Pribylová, E., & Lisková, M. (1972). Reaction of bone to mechanical stimuli. Cells Tissues Organs 8(2): 218-230.

Hill, R. W., Sleboda, D. A., & Millar, J. J. (2021). Youth in the study of comparative physiology: insights from demography in the wild. Journal of Comparative Physiology B 191: 1-16.

Hirsch, K. F., & Quinn, B. (1990). Eggs and eggshell fragments from the Upper Cretaceous Two Medicine Formation of Montana. Journal of Vertebrate Paleontology 10(4): 491-511.

Holdaway, R. N., Worthy, T. H., & Tennyson, A. (2001). A working list of breeding bird species of the New Zealand region at first human contact. New Zealand Journal of Zoology 28: 119-187.

Holland, B., Bell, P. R., Fanti, F., Hamilton, S. M., Larson, D. W., Sissons, R., Sullivan, C., Vavrek, M.J., Wang, Y., Campione, N. E. (2021). Taphonomy and taxonomy of a juvenile lambeosaurine (Ornithischia: Hadrosauridae) bonebed from the late Campian Wapiti Formation of northwestern Alberta, Canada. PeerJ 9: e11290.

Hone, D. W., & Mallon, J. C. (2017). Protracted growth impedes the detection of sexual dimorphism in non-avian dinosaurs. Palaeontology 60: 535-545. doi:10.1111/pala.12298.

Horner, J. R. (1982). Evidence of colonial nesting and 'site fidelity' among ornithischian dinosaurs. Nature 297(5868): 675-676.

Horner, J. R. (1983). Cranial osteology and morphology of the type specimen of *Maiasaura peeblesorum* (Ornithischia: Hadrosauridae), with discussion of its phylogenetic position. Journal of Vertebrate Paleontology 3(1): 29-38.

Horner, J. R. (1984). The nesting behavior of dinosaurs. Scientific American 250: 130-137.

Horner, J. R., & Gorman, J. (1988). Diggin Dinosaurs: the search that unraveled the mystery of baby dinosaurs. New York: Workman Publishing.

Horner, J. R., & Makela, R. (1979). Nest of juveniles provides evidence of family structure among dinosaurs. Nature 282(5736): 296-298.

Horner, J. R., de Ricqlès, A., & Padian, K. (1999). Variation in dinosaur skeletochronology indicators: implications for age assessment and physiology. Paleobiology 25: 295-304.

Horner, J. R., de Ricqlès, A., & Padian, K. (2000). Long bone histology of the hadrosaurid dinosaur *Maiasaura peeblesorum*: growth dynamics and physiology based on an ontogenetic series of skeletal elements. Journal of Vertebrate Paleontology 20(1): 115-129.

Horner, J. R., & Weishampel, D. B. (1988). A comparative embryological study of two ornithischian dinosaurs. Nature 332: 256-257.

Horner, J. R., Weishampel, D. B., & Forster, C. A. (2004). Hadrosauridae. In D. B. Weishampel, P. Dodson, & H. Osmolska (Eds.), The Dinosauria (pp. 438-463). Berkeley: University of California Press.

Horner, J. R., Woodward, H. N., & Bailleul, A. M. (2016). Mineralized tissues in dinosaurs interpreted as having formed through metaplasia: a preliminary evaluation. Comptes Rendus Palevol 15: 176-196.

Houssaye, A. (2013). Palaeoecological and morphofunctional interpretation of bone mass increase: an example in Late Cretaceous shallow marine squamates. Biological Reviews 88: 117-139. doi:10.1111/j.1469-185X.2012.00243.x

Houssaye, A. (2014). Advances in vertebrate palaeohistology: recent progress, discoveries, and new approaches. Biological Journal of the Linnean Society 112: 645-648.

Houssaye, A., Waskow, K., Hayashi, S., Cornette, R., Lee, A. H., & Hutchinson, J. R. (2016). Biomechanical evolution of solid bones in large animals: a microanatomical investigation. Biological Journal of the Linnean Society 117: 350-371.

Hübner, T. R. (2012). Bone histology in *Dysalotosaurus lettowvorbecki* (Ornithischia: Iguanodontia) - variation, growth, and implications. PLOS One 7: e22958.

Hugi, J., & Sanchez-Villagra, M. R. (2012). Life history and skeletal adaptations in the galapagos marine iguana (*Amblyrhynchus cristatus*) as reconstructed with bone histological data - a comparative study of iguanines. Journal of Herpetology 46: 312-324.

Hutchinson, J. R. (2021). The evolutionary biomechanics of locomotor function in giant land animals. Journal of Experimental Biology 224(11): jeb217463.

Huttenlocker, A. K., Woodward, H. N., & Hall, B. K. (2013). The biology of bone. In K. Padian & E.-T. Lamm (Eds.), Bone Histology of fossil tetrapods: advancing methods, analysis, and interpretation. (pp. 13-34). Berkeley, CA: University of California Press.

Ibrahim, N., Sereno, P. C., Dal Sasso, C., Maganuco, S., Fabbri, M., Martill, D. M., Martill, D.M., Zouhri, S., Myhrvold, N., Iurino, D. A. (2014). Semiaquatic adaptations in a giant predatory dinosaur. Science 345: 1613-1616.

Iijima, M., & Kubo, T. (2019). Allometric growth of limb and body proportions in crocodylians. Journal of Zoology 309(3): 200-211.

Jentgen-Ceschino, B., Stein, K., & Fischer, V. (2020). Case study of radial fibrolamellar bone tissues in the outer cortex of basal sauropods. Philisophical Transactions of the Royal Society B. 375(1793): 20190143.

Jetz, W., Sekercioglu, C. H., & Böhning-Gaese, K. (2008). The Worldwide variation in avian clutch size across species and space. PLoS Biology 6(12): e303.

Joanen, T., & McNease, L. (1975). Notes on the reproductive biology and captive propogation of the American alligator. Proceedings of the Annual Conference of Southeast Association of the Game and Fish Commission 25: 252-275.

Joanen, T., & McNease, L. (1987). Alligator farming research in Louisiana, USA. In J. W. Grahame, S. Webb, C. Manolis, & P. J. Whitehead (Eds.), Wildilife management: crocodiles and alligators. (pp. 329-340). Chipping Norton, NSW, AUS: Surrey Beatty and Sons.

Joanen, T., & McNease, L. (1989). Ecology and physiology of nesting and early development of the American alligator. American Zoologist 29: 987-998.

Jolly, J. N. (1989). A field study of the breeding biology of the little spotted kiwi (*Apteryx owenii*) with emphasis on the causes of nest failures. Journal of the Royal Society of New Zealand 19(4): 433-448.

Kalmey, J. K., & Lovejoy, C. O. (2002). Collagen fiber orientation in the femoral necks of apes and humans: do their histological structures reflect differences in locomotor loading? Bone 31(2): 327-332.

Kastschenko, M. (1881). Uber die Genese und Architektur der Batrachier Knochen. Archiv fur Mikroskopische Anatomie 19: 1-52.

Kautz, T. M., Belant, J. L., Beyer Jr., D. E., Strickland, B. K., & Duquette, J. F. (2020). Influence of body mass and environmental conditions on winter mortality risk of a northern ungulate: evidence for a late-winter survival bottleneck. Ecology and Evolution 10(3): 1666-1677.

Keklikoglu, N., & Akinci, S. (2013). Comparison of three different techniques for histological tooth preperation. Folia Histochimica ET Cytobiologica 51(4): 286-291.

Kerschnitzki, M., Zander, T., Zaslansky, P., Fratzl, P., Shahar, R., & Wagermaier, W. (2014). Rapid alterations of avian medullary bone material during the daily egg-laying cycle. Bone 69: 109-117.

Kilbourne, B. M., & Hutchinson, J. R. (2019). Morphological diversification of biomechanical traits: mustelid locomotor specializations and the macroevolution of long bone cross-sectional morphology. BMC Evolutionary Biology 19: 37.

Kilbourne, B. M., & Makovicky, P. (2010). Limb bone allometry during postnatal ontogeny in non-avian dinosaurs. Journal of Anatomy 217: 135-152.

Kilmer, J. T., & Rodriguez, R. L. (2017). Ordinary least squares regression is indicated for studies of allometry. Journal of Evolutionary Biology 30: 4-12.

Kivell, T. L. (2016). A review of trabecular bone functional adaptation: what have we learned from trabecular analyses in extant hominoids and what can we apply to fossils? Journal of Anatomy 228: 569-594.

Klein, N., & Sander, M. P. (2007). Bone histology and growth of the prosauropod dinosaur *Plateosaurus engelhardti von meyer*, 1837 from the Norian bonebeds of Trossingen (Germany) and Frick (Switzerland). Special Papers in Palaeontology 77: 169-206.

Klein, N., Scheyer, T. M., & Tütken, T. (2009). Skeletochronology and isotopic analysis of a captive individual of *Alligator mississippiensis* Daudin, 1802. Fossil Record 12(2): 121-131.

Klein, N., Verrière, A., Sartorelli, H., Wintrich, T., & Fröbisch, J. (2019). Microanatomy and growth of the mesosaurs *Stereosternum tumidum* and *Brazilosaurus sanpauloensis* (Reptilia, Parareptilia). Fossil Record 22: 91-110.

Klevezal, G. A. (1996). Recording structures of mammals: determination of age and reconstruction of life history. Brookfield: A.A. Balkema Publishers.

Klevezal, G. A., & Fedyk, A. (1978). Adhesion lines pattern as an indicator of age in Voles. Acta Theriologica 23(27): 413-422.

Klinkhamer, A. J., Mallison, H., Poropat, S. F., Sinapius, G. H. K., & Wroe, S. (2018). Three-dimensional musculoskeletal modeling of the sauropodomorph hind limb: the effect of postural change on muscle leverage. The Anatomical Record 301(12): 2145-2163.

Klomp, N. I., & Furness, R. W. (1992). A technique which may allow accurate determination of the age of adult birds. Ibis 134: 245-249.

Köhler, M., Marín-Moratalla, N., Jordana, X., & Aanes, R. (2012). Seasonal bone growth and physiology in endotherms shed light on dinosaur physiology. Nature 487: 358-361. doi:10.1002/mmng.200900002.

Kolb, C., Scheyer, T. M., Veitschegger, K., Forasiepi, A. M., Amson, E., Geer, A. A. E. V. d., Hoek Ostende, L.W. v. d., Hayashi, S., Sánchez-Villagra, M. R. (2015). Mammalian bone palaeohistology: a survey and new data with emphasis on island forms. PeerJ 3: e1358. doi:10.7717/peerj.1358

Kontulainen, S., Sievänen, H., Kannus, P., Pasanen, M., & Vuori, I. (2002). Effect of long-term impact-loading on mass, size, and estimated strength of humerus and radius of femal racquet-sports players: a peripheral quantitative computed tomography study between young and old starters and controls. Journal of Bone and Mineral Research 17: 2281-2289.

Kuehn, A. L., Lee, A. H., Main, R. P., & Simons, E. L. R. (2019). The effects of growth rate and biomechanical loading on bone laminarity within the emu skeleton. PeerJ 7:e7616. doi:https://doi.org/10.7717/peerj.7616.

Lamm, E.-T. (2013). Preparation and sectioning of specimens. In K. Padian & E.-T. Lamm (Eds.), Bone Histology of Fossil Tetrapods: Advancing methods, analysis, and interpretation. (pp. 55-160). Berkely: University of California Press.

Lammers, A. R., & German, R. Z. (2002). Ontogenetic allometry in the locomotor skeleton of specialized half-bounding mammals. Journal of Zoological Society of London 258: 485-495.

Lance, V. A. (2003). Alligator physiology and life history: the importance of temperature. Experimental Gerontology 38(7): 801-805.

Langel, C., & Bonnan, M. F. (In Prep). Ontogenetic changes in the cross-sectional geometry and deltopectoral crest of the humerus in *Alligator mississippiensis*.

Lanyon, L. E. (1996). Using functional loading to influence bone mass and architecture: objectives, mechanisms, and relationship with estrogen of the mechanically adaptive process in bone. Bone 18: S37-S43.

Lee, A. H., & O'Connor, P. M. (2013). Bone histology confirms determinate growth and small body size in the noasaurid theropod *Masiakosaurus knopfleri*. Journal of Vertebrate Paleontology 33: 865-876.

Lee, A. H., & Werning, S. (2008). Sexual maturity in growing dinosaurs does not fit reptilian growth models. PNAS 105(2): 582-587. doi:10.1073/pnas.0708903105

Lee, D. E., Lee, W. G., & Mortimer, N. (2001). Where and why have all the flowers gone? Depletion and turnover int eh New Zealand Cenozoic angiosperm flora in relation to palaeogeography and climate. Australian Journal of Botany 49: 341-356.

Legendre, L., Bourdon, E., Scofield, R. P., Tennyson, A. J. D., Lamrous, H., de Ricqlès, A., & Cubo, J. (2014). Bone histology, phylogeny, and palaeognathous birds (Aves: Palaeognathae). Biological Journal of the Linnean Society 112: 688-700.

Legendre, L. J., & Botha-Brink, J. (2018). Digging the compromise: investigating the link between limb bone histology and fossoriality in the aardvark (*Orycteropus afer*). PeerJ 6:e5216 doi:10.7717/peerj.5216.

Lehman, T.M. & Woodward, H.N. (2008). Modeling growth rates for sauropod dinosaurs. Paleobiology 34: 264-281.

Lemnell, P.A. (1974). Age determination in red squirrels (*Sciurus vulgaris*). XIth International Congress of Game and Biology of Stockholm 1973: 573-580.

Lieberman, D. E., Devlin, M. J., & Pearson, O. M. (2001). Articular responses to mechanical loading: effects of exercise, age, and skeletal locomotion. American Journal of Physical Antropology 116: 266-277.

Lieberman, D. E., Pearson, O. M., Polk, J. D., Demes, B., & Crompton, A. W. (2003). Optimization of bone growth and remodeling in response to loading in tapered mammalian limbs. Journal of Experimental Biology 206: 3125-3138.

Lieberman, D. E., Polk, J. D., & Demes, B. (2004). Predicting long bone loading from cross-sectional geometry. American Journal of Physical Antropology 123: 156-171.

Livingston, V. J., Bonnan, M. F., Elsey, R. M., Sandrik, J. L., & Wilhite, D. R. (2009). Differential limb scaling in the American alligator (*Alligator mississippiensis*) and its implications for archosaur locomotor evolution. Anatomical Record 292(6): 787-797.

López-Aguirre, C., Wilson, L. A. B., Koyabu, D., Tu, V. T., & Hand, S. J. (2021). Variation in cross-sectional shape and biomechanical properties of the bat humerus under Wolff's law. The Anatomical Record 304: 1937-1952.

Lorenz, J. C., & Gavin, W. (1984). Geology of the Two Medicine Formation and the sedimentology of a dinosaur nesting ground. In J. D. McBane & P. B. Garrison (Eds.), Northwestern Montana Guidebook, 1984 Field Conference (pp. 172-186). Billings, Montana: Montana Geological Society.

Maidment, S. C. R., & Barrett, P. M. (2011). The locomotor musculature of basal ornithischian dinosaurs. Journal of Vertebrate Paleontology 31(6): 1265-1291.

Maidment, S. C. R., & Barrett, P. M. (2012). Does morphological convergence imply functional similarity? A test using the evolution of quadrupedalism in ornithischian dinosaurs. Proceedings of the Royal Society B 279: 3765-3771. doi:10.1098/rspb.2012.1040.

Maidment, S. C. R., & Barrett, P. M. (2014). Osteological correlates for quadrupedality in ornithischian dinosaurs. Acta Palaeontologica Polonica 59(1): 53-70.

Maidment, S. C. R., Henderson, D. M., & Barrett, P. M. (2014). What drove reversions to quadrapedality in ornithischian dinosaurs? Testing hypotheses using centre of mass modelling. Naturwissenschaften 101: 989-1001. doi:10.1007/s00114-014-1239-2.

Maidment, S. C. R., Linton, D. H., Upchurch, P., & Barrett, P. M. (2012). Limb-bone scaling indicates diverse stance and gait in quadrupedal ornithischian dinosaurs. PLOS One 7(5): e36904.

Main, R. P., & Biewener, A. A. (2007). Skeletal strain patterns and growth in the emu hindlimb during ontogeny. Journal of Experimental Biology 210: 2676-2690.

Mallet, C., Cornette, R., Billet, G., & Houssaye, A. (2019). Interspecific variation in the limb long bones among modern rhinoceroses - extent and drivers. PeerJ 7: e7647.

Mallon, J. C. (2017). Recognizing sexual dimorphism in the fossil record: lessons from nonavian dinosaurs. Paleobiology 43(3): 495-507.

Marean, C. W., Spencer, L. M., Blumenschine, R. J., & Capaldo, S. D. (1992). Captive hyaena bone choice and destruction, the Schlepp effect and olduvai archaeofaunas. Journal of Archaeological Science 19(1): 101-121.

Marín-Moratalla, N., Cubo, J., Jordana, X., Moncunill-Solé, B., & Köhler, M. (2014). Correlation of quantitative bone histology data with life history and climate: a phylogenetic approach. Biological Journal of the Linnean Society 112: 678-687.

Marín-Moratalla, N., Jordana, X., & Köhler, M. (2013). Bone histology as an approach to providing data on certain key life history traits in mammals: implications for conservation biology. Mammalian Biology 78: 422-429.

Marsà, J. A. G., Agnolín, F. L., & Novas, F. (2019). Bone microstructure of *Vegavis iaai* (Aves, Anseriformes) from the Upper Cretaceous of Vega Island, Antarctic Peninsula. Historical Biology 31(2): 163-167.

McFeeters, B., Evans, D. C., & Maddin, H. C. (2021). Ontogeny and variation in the skull roof and braincase of the hadrosaurid dinosaur *Maiasaura peeblesorum* from the Upper Cretaceous of Montana, USA. Acta Palaeontologica Polonica 66. doi:https://doi.org/10.4202/app.00698.2019.

McFeeters, B., Evans, D. C., Ryan, J. M., & Maddin, H. C. (2021). First occurrence of *Maiasaura* (Dinosauria, hadrosauridae) from the Upper Cretaceous Oldman Formation of southern Alberta, Canada. Canadian Journal of Earth Sciences 58(3): 286-296.

McGee-Lawrence, M., Buckendahl, P., Carpenter, C., Henriksen, K., Vaughan, M., & Donahue, S. (2015). Suppressed bone remodeling in black bears conserves energy and bone mass during hibernation. The Journal of Experimental Biology 218: 2067-2074.

McGowan, C. (1979). The hind limb musculature of the brown kiwi, *Apteryx australis mantelli*. Journal of Morphology 160: 33-74.

McGowan, C. (1999). A practical guide to verebrate mechanics. Cambridge: Cambridge University Press.

McLennan, J. A., Dew, L., Miles, J., Gillingham, N., & Waiwai, R. (2004). Size matters: predation risk and juvenile growth in North Island brown kiwi (*Apteryx mantelli*). New Zealand Journal of Ecology 28(2): 241-250.

McLennan, J. A., Potter, M. A., Robertson, H. A., Wake, G. C., Colbourne, R., Dew, L., Joyce, L., McCann, A.J., Miles, J., Miller, P.J., Reid, J. (1996). Role of predation in the decline of kiwi, *Apteryx* spp., in New Zealand. New Zealand Journal of Ecology 20: 27-35.

McNab, B. K. (1994). Energy conservation and the evolution of flightlessness in birds. American Naturalist 144(4): 628-642.

McPhee, B. W., Benson, R. B. J., Botha-Brink, J., Bordy, E. M., & Choiniere, J. N. (2018). A giant dinosaur from the earliest Jurassic of South Africa and the transition to quadrupedality in early sauropodomorphs. Current Biology 28: 3143-3151.

Meers, M. D. (2002). Cross-sectional geometric properties of the crocodylian humerus: an exception to Wolff's Law? Journal of Zoological Society of London 258: 405-418.

Meister, W. W. Changes in histological structure of the long bones of white-tailed deer (*Odocoileus virginianus*) during the growth of the antlers. Anatomical Record 124: 709-721.

Mikhailov, K. E. (1994). Eggs of sauropod and ornithopod dinosaurs from the Cretaceous deposits of Mongolia. Journal of Paleontology 28(3): 141-159.

Mikhailov, K. E. (1997). Fossil and recent eggshell in amniotic verebrates: fine structure, comparative morphology and classification. Special Papers in Palaeontology 56: 1-76.

Montes, L., Le Roy, N., Perret, M., de Buffrénil, V., Castanet, J., & Cubo, J. (2007). Relationships between bone growth rate, body mass and resting metabolic rate in growing amniotes: a phylogenetic approach. Biological Journal of the Linnean Society 92: 63-76.

Montoya-Sanhueza, G., Bennett, N. C., Oosthuizen, M. K., Dengler-Crish, C. M., & Chinsamy, A. (2021). Bone remodeling in the longest living rodent, the naked mole-rat: interelement variation and the effects of reproduction. Journal of Anatomy 239(1): 81-90.

Montoya-Sanhueza, G., & Chinsamy, A. (2017). Long bone histology of the subterranean rodent *Bathyergus suillus* (Bathyergidae): ontogenetic pattern of cortical bone thickening. Journal of Anatomy 230(2): 203-233. doi:https://doi.org/10.1111/joa.12547.

Morris, P. A. (1970). A method for determining absolute age in the hedgehog. Journal of Zoology 161: 277-280.

Morschhauser, E. M., You, H., Li, D., & Dodson, P. (2018). Postcranial morphology of the neoceratopsian (Ornithischia: Ceratopsia) *Auroraceratops rugosus* from the Early Cretaceous (Aptian-Albian) of northwestrn Gansu Province, China. Journal of Vertebrate Paleontology 38: 75-116.

Nacarino-Meneses, C., Jordana, X., & Köhler, M. (2016). First approach to bone histology and skeletochronology of *Equus hemionus*. Comptes Rendus Palevol 15: 267-277. doi:10.1016/j.crpv.2015.02.005.

Nacarino-Meneses, C., & Köhler, M. (2018). Limb bone histology records birth in mammals. PLOS One 13(6): e0198511. doi:https://doi.org/10.1371/journal.pone.0198511.

Neenan, J. M., Chapelle, K. E. J., Fernandez, V., & Choiniere, J. N. (2018). Ontogeny of the *Massospondylus* labyrinth: implications for locomotory shifts in a basal sauropodomorph dinosaur. Palaeontology 62(2): 255-265. doi:10.1111/pala.12400.

Nice, M. M. (1962). Development of behavior in precocial birds. Transactions of the Linnean Society of New York 8: 1-211.

Nordström, P., Pettersson, U., & Lorentzon, R. (1998). Type of physical activity, muscle strength, and pubertal stage as determinants of bone mineral density and bone area in adolescent boys. Journal of Bone and Mineral Research 13: 1141-1148.

Norell, M. A., Wiemann, J., Fabbri, M., Yu, C., Marsicano, C. A., Moore-Nall, A., Varricchio, D.J., Pol, D., Zelenitsky, D. K. (2020). The first dinosaur egg was soft. Nature 583: 406-410.

Norman, D. B. (1980). On the ornithischian dinosaur *Iguanodon bernissartensis* from the Lower Cretaceous of Bernissart (Belgium). Institut Royal des Sciences Naturelles de Belgique, Memoires 178: 1-103.

O'Donnel, C. F. J., Weston, K. A., & Monks, J. M. (2017). Impacts of introduced mammalian predators on New Zealand's alpine fauna. New Zealand Journal of Ecology 41(1): 1-22. doi:10.20417/nzjecol.41.18.

Olivier, C., Houssaye, A., Jalil, N.-E., & Cubo, J. (2017). First palaeohistological inference of resting metabolic rate in an extinct synapsid, *Moghreberia nmachouensis* (Therapsida: Anomodontia). Biological Journal of the Linnean Society 121: 409-419.

Olsen, R. A., Womble, M. D., Thomas, D. R., Glenn, Z. D., & Butcher, M. T. (2016). Functional morphology of the forelimb of the nine-banded armadillo (*Dasypus novemcinctus*): comparative perspectives on the myology of Dasypodidae. Journal of Mammal Evolution 23: 49-69. doi:10.1007/s10914-015-9299-4.

Otero, A., Allen, V. R., Pol, D., & Hutchinson, J. R. (2017). Forelimb muscle and joint actions in Archosauria: insights from *Crocodylus johnstoni* (Pseudosuchia) and *Mussaurus patagonicus* (Sauropodomorpha). PeerJ 5: e3976.

Otero, A., Allen, V. R., Sumner-Rooney, L., Pol, D., & Hutchinson, J. R. (2019). Ontogenetic changes in the body plan of the sauropodomorph dinosaur *Mussaurus patagonicus* reveal shifts of locomotor stance during growth. Scientific Reports 9: 7614.

Packard, M. J., & Packard, G. C. (1989). Mobilization of calcium, phosphorus and magnesium by embryonic alligators (*Alligator mississippiensis*). American Journal of Physiology 257: 1541-1547.

Padian, K. (2013). Why study the bone microstructure of fossil tetrapods? In K. Padian & E.-T. Lamm (Eds.), Bone histology of fossil tetrapods: advancing methods, analysis, and interpretation. Berkeley: University of California Press.

Padian, K., Lamm, E-T. (2013). Bone histology of fossil tetrapods: advancing methods, analysis, and interpretation. Berkeley: University of California Press.

Padian, K., de Ricqlès, A., & Horner, J. R. (2001). Dinosaurian growth rates and bird origins. Nature 412: 405-408.

Padian, K., Lamm, E.-T., & Werning, S. (2013). Selection of Specimens. In K. Padian & E.-T. Lamm (Eds.), Bone Histology of fossil tetrapods: advancing methods, analysis, and interpretation. (pp. 35-54). Berkeley: University of California Press.

Padian, K., & Stein, K. (2013). Evolution of growth rates and their implications. In K. Padian & E.-T. Lamm (Eds.), Bone histology: advancing methods, analysis, and interpretation. (pp. 253-264). Berkeley: University of California Press.

Padian, K., Werning, S., & Horner, J. R. (2016). A hypothesis of differential secondary bone formation in dinosaurs. Comptes Rendus Palevol 15: 40-48.

Padian, K., & Woodward, H. N. (2021). Archosauromorpha: Avemetatarsalia - Dinosaurs and their relatives. In V. de Buffrénil, A. de Ricqlès, L. Zylberberg, & K. Padian (Eds.), Vertebrate Skeletal Histology and Paleohistology. (pp. 511-549). Boca Rotan: CRC Press.

Pawlina, W., & Ross, M. H. (2018). Histology: a text and atlas: with correlated cell and molecular biology. (8 ed.): Wolters Kluwer Health.

Peabody, F.E. (1996). Annual growth zones in living and fossil vertebrates. Journal of Morphology 108: 11-62.

Pearson, O. M., & Lieberman, D. E. (2004). The aging of Wolff's "Law": ontogeny and responses to mechanical loading in cortical bone. Yearbook of Physical Anthropology 47: 63-99.

Petrtýl, M., Hert, J., & Fiala, P. (1996). Spatial organization of the Haversian bone in man. Journal of Biomechanics 29(2): 161-169.

Pol, D., Mancuso, A. C., Smith, R. M. H., Marsicano, C. A., Ramezani, J., Cerda, I. A., Otero, A., Fernandez, V. (2021). Earliest evidence of herd-living and age segregation amongst dinosaurs. Scientific Reports 11: 20023.

Ponton, F., Elzanowski, A., Castanet, J., Chinsamy, A., de Margerie, E., de Ricqlès, A., & Cubo, J. (2004). Variation of the outer circumferential layer in the limb bones of birds. Acta Ornithologica 39: 137-140.

Potter, M. A., Fordham, R. A., & McLennan, J. A. (1996). Reproductive biology of the kiwi. In D. C. Deeming (Ed.), Improving our Understanding of Ratites in a Farming Environment (pp. 161-162). Oxfordshire, UK: Ratite Conference.

Prier, E. A., Gartrell, B. D., Potter, M. A., Lopez-Villalobos, N., & McLennan, J. (2013). Characterization of hatch-size and growth rates of captive and wild-reared brown kiwi (*Apteryx mantelli*) chicks. Zoo Biology 32: 541-548. doi:10.1002/zoo.21088.

Prieto-Marquez, A., Gignac, P. M., & Joshi, S. (2007). Neontological evaluation of pelvic skeletal attributes purported to reflect sex in extinct non-avian archosaurs. Journal of Vertebrate Paleontology 27: 603-609.

Prieto-Marquez, A., & Guenther, M. F. (2018). Perinatal specimens of *Maiasaura* from the Upper Cretaceous of Montana (USA): insights into the early ontogeny of saurolophine hadrosaurid dinosaurs. PeerJ 6: e4734. doi:10.7717/peerj.4734.

Prinzinger, R., & Dietz, V. (2002). Pre- and postnatal energetics of the North Island brown kiwi (*Apteryx mantelli*). Comparative Biochemistry and Physiology Part A: Molecular and Integrative Physiology 131(4): 725-732.

Prondvai, E., Godefroit, P., Adriaens, D., & Hu, D.-Y. (2018). Intraskeletal histovariability, allometric growth patterns, and their functional implications in bird-like dinosaurs. Scientific Reports 8: 258. doi:10.1038/s41598-017-18218-9.

Prondvai, E., Stein, K., Osi, A., & Sander, M. P. (2012). Life history of *Rhamphorhynchus* inferred from bone histology and the diversity of Pterosaurian growth strategies. PLOS One 7(2): e31392. doi:10.1371/journal.pone.0031392.

Prondvai, E., Stein, K. H. W., de Ricqlès, A., & Cubo, J. (2014). Development-based revision of bone tissue classification: the importance of semantics for science. Biological Journal of the Linnean Society 112: 799-816.

Prosser, R. L., & Suzuki, H. K. (1968). The effects of estradiol valerate on the serum and bone of hatchling and juvenile caiman crocodiles (*Caiman sclerops*). Comparative Biochemistry and Physiology 25: 529-534.

Putman, R. J., Langbein, J., Hewison, A. J. M., & Sharma, S. K. (1996). Relative roles of density-dependent and density-independent factors in population dynamics of British deer. Mammal Review 26: 81-101.

Quemeneur, S., de Buffrénil, V., & Laurin, M. (2013). Microanatomy of the amniote femur and inference of lifestyle in limbed vertebrates. Biological Journal of the Linnean Society 109: 644-655.

Rainwater, T. R., Woodward, H. N., Woodward, A. R., & Wilkinson, P. M. (2021). Evidence of determinate growth in an American alligator (*Alligator mississippiensis*) based on long-term recapture and osteohistological confirmation. The Anatomical Record.

Rector, R. S., Rogers, R., Ruebel, M., & Hinton, P. S. (2008). Participation in road cycling vs running is associated with lower bone mineral density in men. Metabolism 57(2): 226-232.

Reisz, R. R., Evans, D. C., Sues, H.-D., & Scott, D. (2010). Embryonic skeletal anatomy of the sauropodomorph dinosaur *Massospondylus* from the Lower Jurassic of South Africa. Journal of Vertebrate Paleontology 30: 1653-1665.

Reisz, R. R., Scott, D., Sues, H.-D., Evans, D. C., & Raath, M. A. (2005). Embryos of an Early Jurassic prosauropod dinosaur and their evolutionary significcance. Science 309: 761-764.

Roach, H. I., Mehta, G., Oreffo, R. O. C., Clarke, N. M. P., & Cooper, C. (2003). Temporal analysis of rat growth plates: cessation of growth with age despite presence of a physis. The Journal of Histochemistry and Cytochemistry 51(3): 373-383.

Robertson, H. A., Colbourne, R. M., Graham, P. J., Miller, P. J., & Pierce, R. J. (2011). Experimental management of Brown Kiwi *Apteryx mantelli* in central Northland, New Zealand. Bird Conservation International 21: 207-220. doi:10.1017/S0959270910000444.

Robling, A. G., Hinant, F. M., Burr, D. B., & Turner, C. H. (2002). Improved bone structure and strength after long-term mechancial loading is greatest if loading is separated into short bouts. Journal of Bone and Mineral Research 17: 1545-1554.

Rogers, K. C., Whitney, M. R., D'Emic, M., & Bagley, B. (2016). Precocity in a tiny titanosaur from the Cretaceous of Madagascar. Science 352(6284): 450-453.

Romanoff, A. L., & Romanoff, A. J. (1949). The Avian Egg. New York: John WIley.

Roux, W. (1881). Der zuchtende Kampf der Teile, oder die "Teilauslee" im Organismus (Theorie der "funktionellen Anpassung"). Leipzig: Wilhelm Engelmann.

Ruff, C., Holt, B., & Trinkhaus, E. (2006). Who's afraid of the big bad Wolff?: "Wolff's law" and bone functional adaptation. American Journal of Physical Antropology 129(4): 484-498.

Russell, D., & Tucker, W. (1971). Supernovae and the extinction of the dinosaurs. Nature 229(5286): 553-554.

Saitta, E. T., Stockdale, M. T., Longrich, N. R., Bonhomme, V., Benton, M. J., Cuthill, I. C., & Makovicky, P. J. (2020). An effect size statistical framework for investigating sexual dimorphism in non-avian dinosaurs and other extinct taxa. Biological Journal of the Linnean Society 131: 231-273.

Sala, N., & Arsuaga, J. L. (2018). Regarding beasts and humans: a review of taphonomic works with living carnivores. Quaternary International 466: 131-140.

Sales, J. (2005). The endangered kiwi: a review. Folia Zoologica 54: 1-20.

Salgado, L., Coria, R. A., & Calvo, J. O. (1997). Evolution of titanosaurid sauropods. I: Phylogenetic analysis based on the postcranial evidence. Ameghiniana 34: 3-32.

Samuels, J. X., & Van Valkenburgh, B. (2008). Skeletal indicators of locomotor adaptations in living and extinct rodents. Journal of Morphology 269(11): 1387-1411.

Sander, P. M., & Andrassy, P. (2006). Lines of arrested growth and long bone histology in Pleistocene large mammals from Germany: What do they tell us about dinosaur physiology? Palaeontographica Abt. A 277: 143-159.

Schmitt, J. G., Jackson, F. D., & Hanna, R. R. (2014). Debris flow origin of an unusual late Cretaceous hadrosaur bonebed in the Two Medicine Formation of western Montana. In D. A. Eberth & D. C. Evans (Eds.), Hadrosaurs. Bloomington: Indiana Press.

Schneider, C. A., Rasband, W. S., & Eliceiri, K. W. (2012). NIH image to imagej: 25 years of image analysis. Nature Methods 9(7): 671-675. doi:10.1038/nmeth.2089.

Schucht, P. J., Klein, N., & Lambertz, M. (2021). What's my age again? On the ambiguity of histology-based skeletochronology. Proceedings of the Royal Society B 288(1955): 20211166. doi:10.1098/rspb.2021.1166.

Schweitzer, M. H., Elsey, R. M., Dacke, C. G., Horner, J. R., & Lamm, E.-T. (2007). Do egg-laying crocodilian (*Alligator mississippiensis*) archosaurs form medullary bone? Bone 40: 1152-1158.

Schweitzer, M. H., Wittmeyer, J., & Horner, J. R. (2005). Gender-specific reproductive tissue in ratites and *Tyrannosaurus rex*. Science 308(5727): 1456-1460.

Schweitzer, M. H., Zheng, W., Zanno, L. E., Werning, S., & Sugiyama, T. (2016). Chemistry supports the identification of gender-specific reproductive tissue in *Tyrannosaurus rex*. Scientific Reports 6: 23099.

Shelton, C. D., Chinsamy, A., & Rothschild, B. M. (2017). Osteomyelitis in a 265-million-year-old titanosuchid (Dinocephalia, Therapsida). Historical Biology 31: 1093-1096.

Shine, R. (1989). Ecological causes for the evolution of sexual dimorphism: a review of the evidence. The Quaterly Review of Biology 64: 419-456.

Skedros, J. G., & Doutré, M. S. (2019). Collagen fiber orientation pattern, osteon morphology and distribution, and presence of laminar histology do not distinguish torsion from bending in bat and pigeon wing bones. Journal of Anatomy 234(6): 748-763.

Skedros, J. G., Mendenhall, S. D., Kiser, C. J., & Winet, H. (2009). Interpreting cortical bone adaptation and load history by quantifying osteon morphotypes in circularly polarized light images. Bone 44(3): 392-403.

Skedros, J. G., Sybrowsky, C. L., Anderson, W. E., & Chow, F. (2011). Relationships between in vivo microdamage and the regional material and strain heterogeneity of cortical bone of adult deer, elk, sheep and horse calcanei. Journal of Anatomy 219(6): 722-733.

Skedros, J. G., Sybrowsky, C. L., Parry, T. R., & Bloebaum, R. D. (2003). Regional differences in cortical bone organization and microdamage prevalence in Rocky Mountain mule deer. The Anatomical Record Part A 274A: 837-850.

Slowiak, J., Tereshchenko, V. S., & Fostowicz-Frelik, L. (2019). Appendicular skeleton of *Protoceratops andrewsi* (Dinosauria, Ornithischia): comparative morphology, ontogenetic stages, and the implications for non-ceratopsian locomotion. PeerJ 7:e7324.

Smith, C., Tacey, A., Mesinovic, J., Scott, D., Lin, X., Brennan-Speranza, T. C., Lewis, J.R., Duque, G., Levinger, I. (2021). The effects of acute exercise on bone turnover markers in middle-aged and older adults: a systematic review. Bone 143: 115766.

Smith, D. K. (2021). Hind limb muscle reconstruction in the incipiently opisthopubic large therizinosaur *Nothronychus* (Theropoda; Maniraptora). Journal of Anatomy 238(6): 1404-1424.

Smith, N. A., & Clarke, J. A. (2014). Osteological histology of the Pan-Alcidae (Aves, Charadriiformes): correlates of wing-propelled diving and flightlessness. The Anatomical Record 297: 188-199.

Snyder, K., McLain, M., Wood, J., & Chadwick, A. (2020). Over 13,000 elements from a single bonebed help elucidate disarticulation and transport of an *Edmontosaurus thanatocoenosis*. PLOS One 15(5): e0233182. doi:10.1371/journal.pone.0233182.

Song, H., Polk, J. D., & Kersh, M. E. (2019). Rat bone properties and their relationship to gait during growth. Journal of Experimental Biology 222: jeb203554.

Starck, J. M., & Chinsamy, A. (2002). Bone microstructure and developmental plasticity in birds and other dinosaurs. Journal of Morphology 254: 232-246.

Stearns, S. C. (1992). The Evolution of Life Histories. Oxford: Oxford University Press.

Stein, K., & Prondvai, E. (2014). Rethinking the nature of fibrolamellar bone: an integrative biological revision of sauropod plexiform bone formation. Biological Reviews 89: 24-47. doi:10.1111/brv.12041.

Stein, K., & Sander, M. P. (2009). Histological core drilling: a less destructive method for studying bone histology. In M. Brown & W. Parker (Eds.), Fossil preperation: proceedings of the first annual fossil preperation and collections symposium. (pp. 69-80).

Steinsaltz, D., & Orzack, S. H. (2011). Statistical methods for paleodemography on fossil assemblages having small numbers of specimens: an investigation of dinosaur survival rates. Paleobiology 37(1): 113-125.

Straehl, F. R., Scheyer, T. M., Forasiepi, A. M., MacPhee, R. D., & Sánchez-Villagra, M. R. (2013). Evolutionary patterns of bone histology and bone compactness in xenarthran mammal long bones. PLOS One 8(7): e69275. doi:10.1371/journal.pone.0069275.

Sturkie, P. D. (1965). Avian Physiology. London: Bailliere, Tindall and Cassell.

R Coding Team (2021). R: A language and environment for statistical computing. Vienna, Austria: R Foundation for Statistical Compuing. Retrieved from https://www.R-project.org/

Thorbjarnarson, J. B. (1996). Reproductive characteristics of the order Crocodylia. Herpetologica 52(1): 8-24.

Thulborn, R. A. (1982). Speeds and gaits of dinosaurs. Palaeogeography, Palaeoclimatology, Palaeoecology 38: 227-256.

Torres, D. A., Freitas, M. B., & Goncalves, R. V. (2017). Changes in bone turnover and calcium homeostasis during pregnancy and lactation in mammals: a meta-analysis. Reproduction, Fertility and Development 30: 681-688.

Tumarkin-Deratzian, A. R. (2007). Fibrolamellar bone in wild adult *Alligator mississippiensis*. Journal of Herpetology 41: 341-345.

Turbill, C., Bieber, C., & Ruf, T. (2011). Hibernation is associated with increased survival and the evolution of slow life histories among mammals. Proceedings of the Royal Society B 278: 3355-3363.

Turner, C. H. (1998). Three rules of bone adaptation to mechanical stimuli. Bone 23(5): 399-407.

Turner, C. H., Sun, Q., Schriefer, J., Pitner, N., Price, R., Bouxsein, M. L., Rosen, C.J., Donahue, L.R., Shultz, K.L., Beamer, W. G. (2003). Congenic mice reveal sex-specific genetic regulation of femoral structure and strength. Calcified Tissue International 73: 297-303.

Turvey, S. T., Green, O. R., & Holdaway, R. N. (2005). Cortical growth marks reveal extended juvenile development in New Zealand moa. Nature Letters 435: 940-943. doi:10.1038/nature03635.

van Sittert, S., Skinner, J., & Mitchell, G. (2015). Scaling of the appendicular skeleton of the Giraffe (*Giraffa camelopardalis*). Journal of Morphology 276: 503-516.

VanBuren, C. S., & Bonnan, M. (2013). Forearm posture and mobility in quadrupedal dinosaurs. PLOS One 8: e74842.

Varricchio, D. J., & Horner, J. R. (1993). Hadrosaurid and lambeosaurid bone beds from the Upper Cretaceous Two Medicine Formation of Montana: taphonomic and biologic implications. Canadian Journal of Earth Sciences 30: 997-1006.

Veitschegger, K., Kolb, C., Amson, E., Scheyer, T. M., & Sánchez-Villagra, M. R. (2018). Palaeohistology and life history evolution in cave bears, *Ursus spelaeus* sensu lato. PLOS One 13(11): e0206791. doi:10.1371/journal.pone.0206791.

Walker, M. M., Louys, J., Herries, A. I. R., Price, G. J., & Miszkiewicz, J. J. (2020). Humerus midshaft histology in a modern and fossil wombat. Australian Mammalogy 43: 30-39.

Wei, X., & Zhang, Z. (2019). Ontogenetic changes of geometrical and mechanical characteristics of the avian femur: a comparison between precocial and altricial birds. Journal of Anatomy 235: 903-911.

Weibel, E. R., Taylor, C. R., & Hoppeler, H. (1991). The concept of symmorphosis: a testable hypothesis of structure-function relationship. Proceedings of the National Academy of Sciences 88: 10357-10361.

Weigele, J., & Franz-Odendaal, T. A. (2016). Functional bone histology of zebrafish reveals two types of endochondral ossification, different types of osteoblast clusters and a new bone type. Journal of Anatomy 229: 92-103. doi:10.1111/joa.12480.

Weir, J. T., Haddrath, O., Robertson, H. A., Colbourne, R. M., & Baker, A. J. (2016). Explosive ice age diversification of kiwi. PNAS 113(38): E5580-E5587.

Weishampel, D.B., Dodson, P., Osmólska, H. (Eds.). (2004).The Dinosauria. Berkeley: University of California Press.

Weon, B. M. (2015). Tyrannosaurs as long-lived species. Scientific Reports, 6, 19554.

Werning, S. (2012). The ontogenetic osteohistology of *Tenontosaurus tilletti*. PLOS One 7(3): e33539. doi:10.1371/journal.pone.0033539.

Werning, S. (2018). Medullary bone is phylogenetically widespread and its skeletal distribution varies by taxon. Journal of Ornithology 159: 527-543.

Whitehead, C. C. (2004). Overview of bone biology in the egg-laying hen. Poultry Science 83: 193-199.

Whitehead, C. C., & Fleming, R. H. (2000). Osteoporosis in cage layers. Poultry Science 79:1033-1041.

Whitney, M. R., Tse, Y. T., & Sidor, C. A. (2019). Histological evidence of trauma in tusks of southern African dicynodonts. Palaeontologia africana 53: 75-80.

Wickham, H. (2016). ggplot2: elegant graphics for data analysis. New York: Springer-Verlag.

Wiemann, J., Yang, T.-R., & Norell, M. A. (2018). Dinosaur egg colour had a single evolutionary origin. Nature 563(7732): 355-354.

Wilkinson, P. M., & Rhodes, W. E. (1997). Growth rates of American alligators in coastal South Carolina. Journal of Wildlife Management 61: 397-402.

Wilson, J. P., Woodruff, D. C., Gardner, J. D., Flora, H. M., Horner, J. R., & Organ, C. L. (2016). Vertebral adaptationsto large body size in theropod dinosaurs. PLOS One 11(7): e0158962. doi:10.1371/journal.pone.0158962.

Wilson, L. E., & Chin, K. (2014). Comparative osteohistology of *Hesperornis* with reference to pygoscelid penguins: the effecs of climate and behavior on avian bone microstructure. Royal Society Open Science 1: 140245.

Wink, C. S., & Elsey, R. M. (1986). Changes in femoral morphology during egg-laying in *Alligator mississippiensis*. Journal of Morphology 189(2): 183-188.

Wink, C. S., Elsey, R. M., & Hill, E. M. (1987). Changes in femoral robusticity and porosity during the reproductive cycle of the female alligator (*Alligator mississippiensis*). Journal of Morphology 193(3): 317-321.

Witmer, L. M. (1995). The extant phylogenetic bracket and the importance of reconstructing soft tissues in fossils. In J. J. Thomason (Ed.), Functional morphology in vertebrate paleontology. (pp. 19-33). Cambridge: Cambridge University Press.

Wood, J. R., & de Pietri, V. L. (2015). Next-generation paleornithology: technological and methodological advances allow new insights into the evolutionary and ecological histories of living birds. Auk 132: 486-506.

Woodruff, C. D., Fowler, D. W., & Horner, J. R. (2017). A new multi-faceted framework for deciphering diplodocid ontogeny. Palaeontologia Electronica 20: 1-53.

Woodruff, C. D., Goodwin, M. B., Lyson, T. R., & Evans, D. C. (2021). Ontogeny and variation of the pachycephalosaurine dinosaur *Sphaerotholus buchholtzae*, and its systematics within the genus. Zoological Journal of the Linnean Society 193(2): 563-601.

Woodward, H. N. (2019). *Maiasaura* (Dinosauria: Hadrosauridae) tibia osteohistology reveals non-annual cortical vascular rings in young of the year. Frontiers in Earth Science 7: 1-50. doi:https://www.frontiersin.org/article/10.3389/feart.2019.00050

Woodward, H. N., Freedman Fowler, E. A., Farlow, J. O., & Horner, J. R. (2015). *Maiasaura*, a model organism for extinct vertebrate population biology: a large sample statistical assessment of growth dynamics and survivorship. Paleobiology 41(4): 503-527. doi:10.1017/pab.2015.19.

Woodward, H. N., Horner, J. R., & Farlow, J. O. (2011). Osteohistological evidence for determinate growth in the American Alligator. Journal of Herpetology 45(3): 339-342.

Woodward, H. N., Horner, J. R., & Farlow, J. O. (2014). Quantification of intraskeletal histovariability in *Alligator mississippiensis* and implications for vertebrate osteohistology. PeerJ 2: e422. doi:10.7717/peerj.422.

Woodward, H. N., Padian, K., & Lee, A. H. (2013). Skeletochronology. In K. Padian & E.-T. Lamm (Eds.), Bone histology of fossil tetrapods: advancing methods, analysis, and interpretation. (pp. 195-215). Berkeley: University of California Press.

Woodward, H. N., Rich, T. H., Chinsamy, A., & Vickers-Rich, P. (2011). Growth dynamics of Australia's polar dinosaurs. PLOS One 6(8): e23339. doi:10.1371/journal.pone.0023339.

Woodward, H. N., Rich, T. H., & Vickers-Rich, P. (2018). The bone microstructure of polar "hypsilophodontid" dinosaurs from Victoria, Australia. Scientific Reports 2018(8): 1162. doi:10.1038/s41598-018-19362-6.

Woodward, H. N., Tremaine, K., Williams, S. A., Zanno, L. E., Horner, J. R., & Myhrvold, N. (2020). Growing up *Tyrannosaurus rex*: osteohistology refutes the pygmy "Nanotyrannus" and supports ontogenetic niche partitioning in juvenile Tyrannosaurus. Science Advances 6(1): eaax6250. doi:10.1126/sciadv.aax6250.

Wosik, M., Chiba, K., Therrien, F., & Evans, D. C. (2020). Testing size-frequency distributions as a method of ontogenetic aging: a life-history assessment of hadrosaurid dinosaurs from the Dinosaur Park Formation of Alberta, Canada, with implications for hadrosaurid paleoecology. Paleobiology 46(3): 379-404. doi:10.1017/pab.2020.2.

Wosik, M., Goodwin, M. B., & Evans, D. C. (2018). A nestling-sized skeleton of *Edmontosaurus* (Ornithischia, Hadrosauridae) from the Hell Creek Formation of northeastern Montana, U.S.A., with an analysis of ontogenetic limb allometry. Journal of Vertebrate Paleontology 37: e1398168. doi:10.1080/02724634.2017.1398168.

Yoon, H. S., Lee, Y.-N., Jung, S.-H., Kong, D.-Y., Kim, S.-H., & Son, M. (2021). A juvenile ornithopod tracksite from the Lower Cretaceous Haman Formation, South Korea. Cretaceous Research 125: 104877.

Young, J. W., Fernández, D., & Fleagle, J. G. (2020). Ontogeny of long bone geometry in capuchin monkeys (*Cebus albifrons* and *Cebus apella*): implications for locomotor development and life history. Biology Letters 6(2): 197-200.

Zelenitsky, D. K., & Hills, L. V. (1997). Normal and pathological eggshells of *Spheroolithus albertensis*, oosp. nov. from the Oldman Formation (Judith River Group, late Campanian), southern Alberta. Journal of Vertebrate Paleontology 17(1): 167-171.

Zhao, Q., Benton, M. J., Sullivan, C., Sander, M. P., & Xu, X. (2013). Histology and postural change during the growth of the ceratopsian dinosaur *Psittacosaurus lujiatunensis*. Nature Communications 4: 2079.

Zhu, X., Wang, Q., & Wang, X. (2022). Restudy of the original and new materials of *Stromatoolithus pinglingensis* and discussion on some Spheroolithidae eggs. Historical Biology 34(2): 283-297.

APPENDICES

APPENDIX A

Supplemental File 1. DiceCT processing methods.

Diffusible iodine-based contrast-enhanced CT (diceCT) leverages the radiopacity of Lugol's iodine (iodine-potassium iodide, I_2KI) along with the relatively low cost and high spatial resolution of micro-computed tomography (μCT) imaging to visualize soft tissues. During osmosis lipids and sugars present within soft structures hold aqueous polymers of triiodide (I_3^-). Various soft tissues contain varying amounts of fats and carbohydrates, causing triiodide to binds in tissue-specific ways. Although bone and connective tissues are do not stain well, muscle tissue, epithelia, glands, and neurons neurons readily take in iodine, and, thus, become radiodense. This allows for soft-tissue anatomy to visualized using X-ray technologies like computed tomography imaging. DiceCT has been repeatedly used to image avian soft tissues.

Here a captive adult male (14.3 years old) *Apteryx australis* housed in a German[US?] zoological collection was imaged to capture skeletal and soft-tissue anatomy in 3D. The specimen was frozen after necropsy, which included thoracoabdominal organ removal. Upon thawing it was immediately fixed in 10% neutral buffered formalin for 28 days. Following fixation, the the head was removed from the body at the third cervical vertebra. Head and body imaging and preparation were treated separately.

The specimen was first μCT scanned to image skeletal anatomy at DENTSPLY R&D in Tulsa, OK on a 2013 Nikon 225 XT H microcomputed tomography system (Nikon Corp., Shinagawa,

Tokyo, JPN). For all scans the samples were double-wrapped in heat-sealed polyethylene bags to prevent dehydration during scanning and physically stabilized using polyethylene foam within a plastic mounting unit. The skull was scanned at 80.06 microns resolution (isometric voxels), using 150 kilovolts (kV), 61 micro-amperages (μA), 708 millisecond (ms) exposure timing, no multi-frame averaging, without a filter, and on a tungsten reflection target for 37 minutes. The post-cranial skeleton was scanned at 107.9 microns resolution (isometric voxels), using 150 kilovolts (kV), 61 micro-amperages (μA), 708 millisecond (ms) exposure timing, no multi-frame averaging, without a filter, and on a tungsten reflection target for 74 minutes in two sections. The two resulting TIFF image stacks were fused, using the "3D Stitching" feature of ImageJ (National Institutes of Health, Bethesda, Maryland, USA).

Subsequently, both head and body were fully submerged in I_2KI for staining. The head was stained in a 5% weight-by-volume (w/v) solution of I_2KI for 21 days (refreshed once), followed by a 3% w/v solution for 28 days (not refreshed). Fast scans were undertaken during the staining period to evaluate stain uptake. Two final CT dataset (following staining completion) were captured at the MicroCT Imaging Consortium for Research and Outreach (MICRO, Fayetteville, Arkansas, USA) on a 2018 Nikon 225 XT H microcomputed tomography system. The first included the entire head at 59.99 microns resolution (isometric voxels), using 201 kV, 310 μA, 267 ms exposure timing, four-times multi-frame averaging, with a 0.125 mm copper filter, and on a tungsten rotating target for 113 minutes in two sections. The pair of TIFF stacks were fused using ImageJ. The second diceCT cranial dataset focused on the brain and roots of the cranial nerves. It was captured at 32.32 microns resolution (isometric voxels), using 200 kV, 400 μA, 354 ms exposure timing, eight-times multi-frame averaging, with a 0.125 mm copper filter, and on a tungsten rotating target for 150 minutes.

The body was stained in a 5% (w/v) solution of I_2KI for 42 days (one refresh). Fast scans were undertaken during the staining period to evaluate stain uptake. The final dataset (following

staining completion) was captured at MICRO at 121.14 microns resolution (isometric voxels), using 165 kV, 300 μA, 354 ms exposure timing, four-times multi-frame averaging, with a 0.125 mm copper filter, and on tungsten reflection target for 221 minutes in two sections. The pair of TIFF stacks were fused using ImageJ.

Following successful diceCT imaging, the head and body were destained using alternating baths of of 1% w/v solutions of sodium thiosulfate and de-ionized water until tissues returned to normal coloration (approximately 12 weeks).

APPENDIX B

Table S1. Gross morphological data of alligator specimens sampled.

Alligator #	Sex	Habitat	Femur Length (mm)	Total Length (mm)	Body Mass (kg)
1	Female	Captive	191.1	2819	NA
2	Female	Captive	179.8	2572	85.8
3	Female	Captive	186.5	2769	79.9
6	Female	Captive	194.9	2845	113.5
7	Female	Captive	185.9	2807	103.1
8	Female	Captive	186.2	2743	80.8
9	Female	Captive	190.2	2845	73.5
10	Female	Captive	185.6	2769	83.1
15	Female	Captive	185.1	2769	96.2
20	Female	Captive	184	2667	72.4
28	Female	Captive	189.3	2769	91.3
30	Female	Captive	184.7	2515	79
32	Female	Captive	189.8	2794	90.6
33	Female	Captive	184.3	2686	89.2
35	Female	Captive	190.4	2705	86.3
36	Female	Captive	192.1	2946	98.1
37	Female	Captive	187.3	2857	97.6
38	Female	Captive	192.3	2857	85.4
40	Female	Captive	144.4	2045	34.5
4	Male	Captive	266.9	3823	279.2
13	Male	Captive	211.5	3759	237.9
29	Male	Captive	259.5	3873	268.3
31	Male	Captive	242.3	3607	232.9
39	Male	Captive	239	3518	209.7
41	Male	Captive	166.9	2584	59.2
44	Male	Captive	245.6	3670	202
45	Male	Captive	260.4	3785	270.1
49	Male	Captive	245.5	3581	245.2
50	Male	Captive	266.1	3810	286

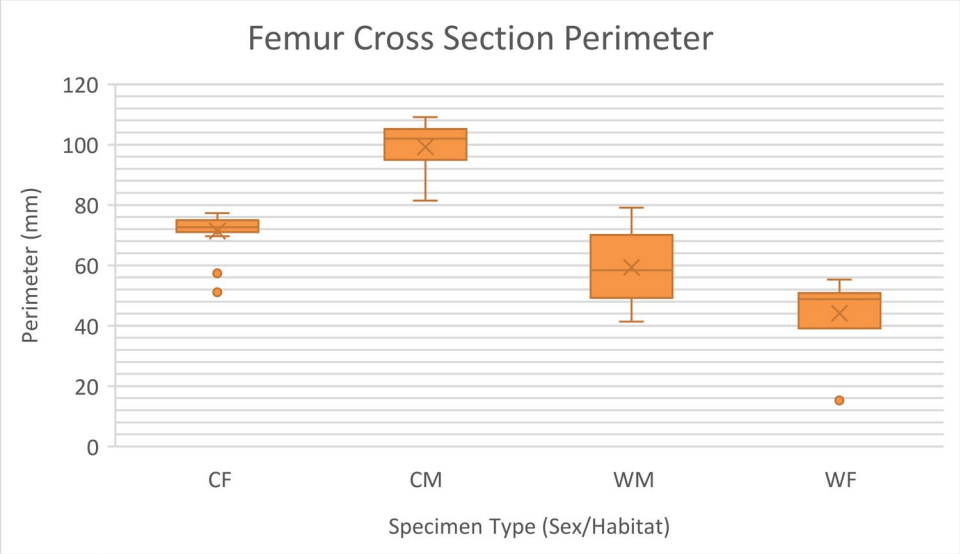

Figure S1. Femora cross-section perimeter (mm) in captive females (CF), captive males (CM), wild males (WM), and wild females (WF).

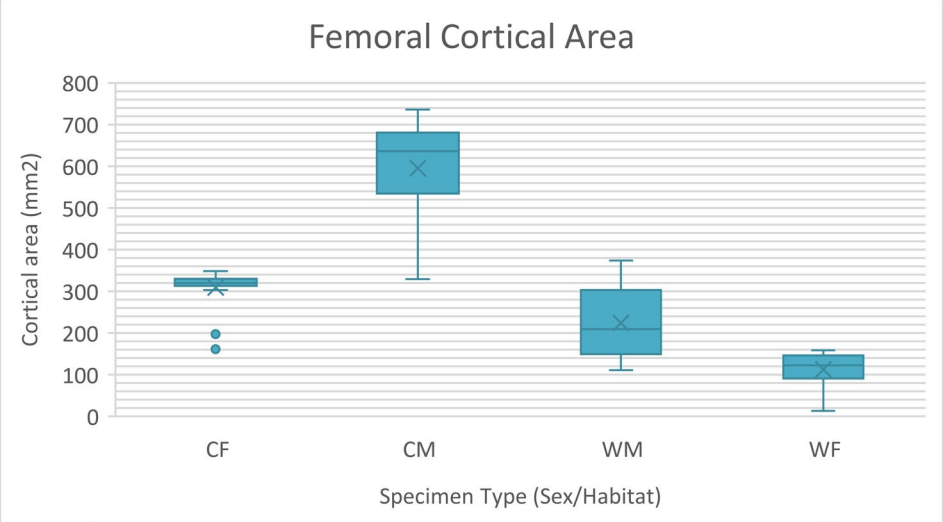

Figure S2. Femoral cross-section cortical area (mm^2) in captive females (CF), captive males (CM), wild males (WM), and wild females (WF).

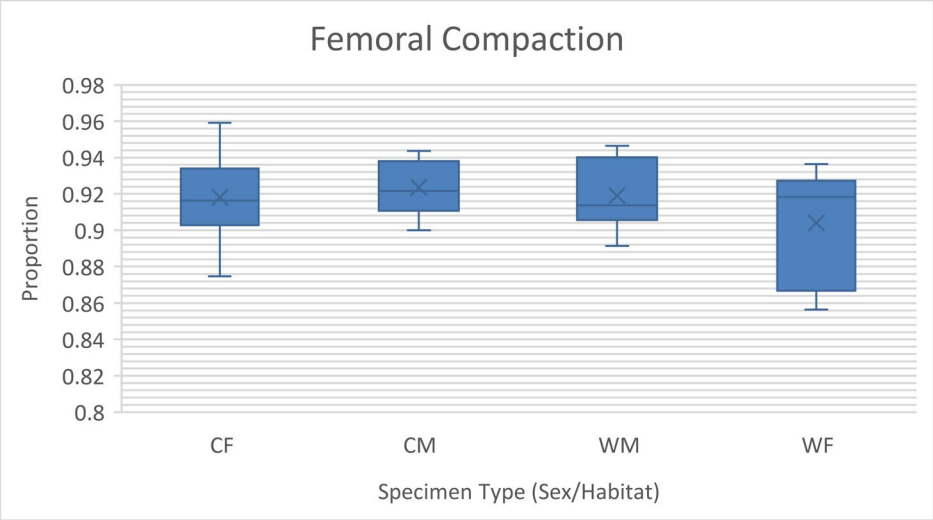

Figure S3. Femoral compaction in captive females (CF), captive males (CM), wild males (WM), and wild females (WF).

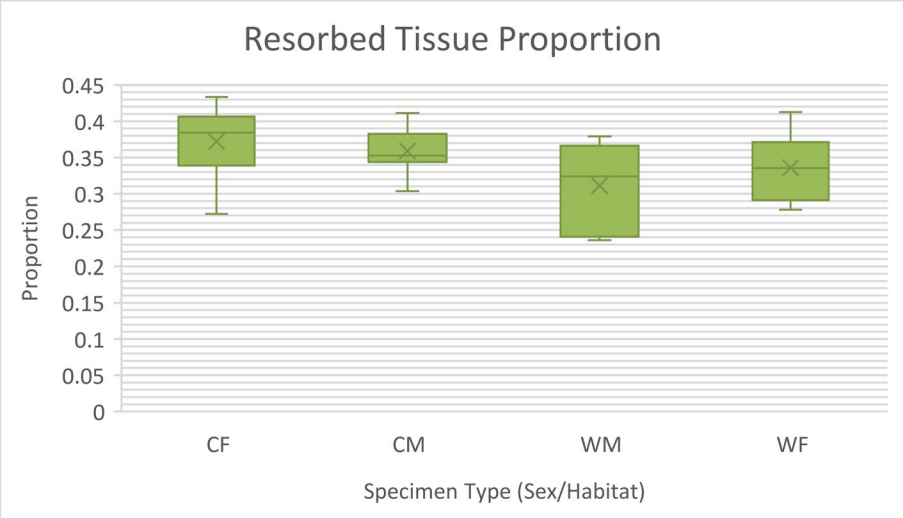

Figure S4. Proportion of resorbed tissue in femoral transects in captive females (CF), captive males (CM), wild males (WM), and wild females (WF).

APPENDIX C

Table S2. Humerus circumference and length for histologically sampled specimens. Bold – length used to develop regressions for estimating lengths based on cross-section circumferences. Italics – lengths estimated using regression analysis.

Specimen Code	Circumference (mm)	Length (mm)
H1	82	**205**
H2	81	*210*
H3	91	**235**
H4	97	*253*
H5	90	*234*
H6	91	*237*
H7	92	**226**
H8	93	*242*
H9	103	*269*
H10	105	*274*
H11	98	**265**
H12	116	*303*
H13	109	*285*
H14	131	**334**
H15	134	*351*
H16	144	*378*
H17	137	*359*
H18	134	*351*
H19	148	*388*
H20	155	**407**
H21	161	**426**
H22	147	*386*
H23	127	**350**
H24	145	*380*

H25	171	**443**
H26	174	**454**
H27	176	*463*
H28	179	**460**
H29	187	*492*
H30	192	**473**
H31	189	*498*
H32	192	*505*
H33	197	*519*
H34	203	*535*
H35	173	**465**
H36	207	*545*
H37	203	*535*
H38	205	**575**
H39	210	**549**
H40	198	**565**
H41	202	*532*
H42	209	**542**
H43	218	*575*
H44	220	*580*
H45	89	*231*
H46	113	*295*
H47	211	*556*

VITA

Christian Thomas Heck

Candidate for the Degree of

Doctor of Philosophy

Dissertation: IDENTIFYING LIFE HISTORY TRAITS IN MODERN AND EXTINCT ARCHOSAURS UTILIZING OSTEOHISTOLOGY

Major Field: Biomedical Sciences

Biographical:

Education:

Completed the requirements for the Doctor of Philosophy in Biomedical Sciences at Oklahoma State University, Stillwater, Oklahoma in May, 2022.

Completed the requirements for the Bachelor of Science in Ecology at Montana State University, Bozeman, Montana in 2014.

Completed the requirements for the Bachelor of Arts in Telecommunications at Michigan State University, East Lansing, Michigan in 2008.

Experience:
Graduate Teaching Assistant for Clinical Anatomy at Oklahoma State University Center for Health Sciences from 2017-2018.
Graduate Teaching Assistant for Paleohistology at Oklahoma State University Center for Health Sciences from 2015-2019.
Graduate Teaching Assistant for Neuroanatomy at Oklahoma State University Center for Health Sciences in 2021.

Professional Memberships:
Sigma Xi, Society of Vertebrate Paleontology, Society for the Advancement of Chicanos/Hispanics and Native Americans in Science, Society for Integrative and Comparative Biology, American Society of Mammalogists, American Microscopy Society